INFORMATION TO USERS

This manuscript has been reproduced from the microfilm master. UMI films the text directly from the original or copy submitted. Thus, some thesis and dissertation copies are in typewriter face, while others may be from any type of computer printer.

The quality of this reproduction is dependent upon the quality of the copy submitted. Broken or indistinct print, colored or poor quality illustrations and photographs, print bleedthrough, substandard margins, and improper alignment can adversely affect reproduction.

In the unlikely event that the author did not send UMI a complete manuscript and there are missing pages, these will be noted. Also, if unauthorized copyright material had to be removed, a note will indicate the deletion.

Oversize materials (e.g., maps, drawings, charts) are reproduced by sectioning the original, beginning at the upper left-hand corner and continuing from left to right in equal sections with small overlaps.

Photographs included in the original manuscript have been reproduced xerographically in this copy. Higher quality 6" x 9" black and white photographic prints are available for any photographs or illustrations appearing in this copy for an additional charge. Contact UMI directly to order.

ProQuest Information and Learning
300 North Zeeb Road, Ann Arbor, MI 48106-1346 USA
800-521-0600

Université d'Ottawa • University of Ottawa

Endothelium–derived hyperpolarizing factor (EDHF) in rat mesenteric artery

Ethan Williams BURNETTE

Department of Cellular and Molecular Medicine
Pharmacology Graduate Program
Faculty of Medicine
University of Ottawa
Ottawa, Ontario, CANADA

A thesis submitted in conformity with the requirements of the
Doctor of Philosophy Degree at the University of Ottawa

ABSTRACT

The endothelium, a critical modulator of vascular resistance and blood pressure, can release at least three factors that relax vascular smooth muscle, including nitric oxide (NO), prostacyclin (prostaglandin I_2, PGI_2), and endothelium–derived hyperpolarizing factor (EDHF). EDHF–induced relaxation is correlated with a strong hyperpolarization and may activate vascular smooth muscle cell (VSMC) K–channels. The identity of EDHF is unknown, though it may be a cytochrome P–450 metabolite of arachidonic acid or an endogenous cannabinoid related to anandamide. The research presented studied ACh–induced EDHF release from rat tail artery (TA) and superior mesenteric artery (SMA). Calcium–activated potassium (K_{Ca}) channels in the rat mesenteric resistance artery (MRA), putative targets of EDHF, were characterized.

ACh–induced EDHF release from rat TA or SMA hyperpolarized target single TA VSMCs current–clamped with the nystatin perforated patch technique. In the absence of donor tissue, ACh induced depolarization. Hyperpolarization persisted in the presence of a nitric oxide synthase inhibitor. Hyperpolarization was absent in target TA VSMCs far (> 1.8 mm) from the donor tissue, which suggests that EDHF is short–lived and/or released in small quanta. Hyperpolarization was blocked by tetraethylammonium ions, which suggests that K–channels are targets of EDHF. These results confirm that an inducible, transferable EDHF was released from rat TA and SMA.

TA and MRA VSMCs were patch clamped in the whole–cell configuration and macroscopic K–currents were elicited by depolarizing pulses.

Calcium–activated (K_{Ca}) and voltage–dependent (K_{dr}) potassium currents were observed in both TA and MRA VSMCs. Apamin (300 nM) significantly inhibited MRA (79% of control at +50 mV) but not TA whole–cell K_{Ca} current. Iberiotoxin (IbTX) or charybdotoxin (ChTX) (150 nM) abolished K_{Ca} current in TA and MRA VSMCs. 4–aminopyridine (4–AP) (2 mM) completely blocked MRA K_{dr} current but had no effect on MRA K_{Ca}. In contrast, previous research found that 4–AP (2 mM) partially inhibited K_{Ca} current and incompletely inhibited K_{dr} current in rat TA (Bolzon, 1992). These observations suggest that the K_{dr} and K_{Ca} channels in rat MRA and TA VSMCs are pharmacologically distinct.

Single rat MRA VSMCs were patch clamped using the inside–out technique. Four K_{Ca} channels were observed and named: BK, IK, SK, and miniK (big, intermediate, small, and mini K_{Ca} channels). In symmetrical potassium (150 mM), the single channel conductances were linear (BK, 197; IK, 94; SK, 50; miniK, 31 pS) and similar to those observed in rat TA. MRA K_{Ca} channels were calcium–dependent at +40 mV ($[Ca^{2+}]_i$ = 0 to 500 nM), but only the miniK and SK channels were calcium–dependent at –40 mV. BK, IK, and SK were voltage–dependent at positive voltages and inactivated at negative voltages. In contrast, the miniK channel was voltage–dependent at positive and negative voltages.

ChTX (150 nM) completely blocked the BK, IK, and miniK channels, and dramatically inhibited the SK channel (inside–out, +40 mV, $[Ca^{2+}]_i$ = 500 nM). IbTX (150 nM) completely blocked all MRA K_{Ca} channels. 4–AP (2 mM) completely blocked the BK and IK channels, partially blocked the SK channel,

and dramatically inhibited the miniK channel. Apamin (300 nM) selectively blocked the BK channel.

It is concluded that rat TA and SMA donor tissue released an ACh–induced, transferable NO–independent EDHF. Four rat MRA VSMC K_{Ca} channels were characterized and their role in the regulation of resting membrane potential and repolarization investigated. The MRA VSMC has a unique apamin–sensitive K_{Ca} current and BK channel which is involved in EDHF dependent hyperpolarization and relaxation.

ACKNOWLEDGEMENTS

The current work was completed by the author with the continued support of friends and family.

TABLE OF CONTENTS

	Page
Abstract	i
Acknowledgements	iii
Table of Contents	iv
List of Figures	ix
List of Tables	xi
List of Abbreviations	xiii
INTRODUCTION	1
PART I. Endothelium–dependent Factors	3
I. Endothelium	3
II. EDRF (NO)	5
III. Prostacyclin / Prostaglandins	8
IV. EDHF	9
V. Cytochrome P–450 Metabolites	12
VI. P–450 Metabolites: Application and Inhibition	14
VII. P–450 Induction and Depletion	16
VIII. Anandamide	18

PART II. VSMC Ion Channel Mediated Hyperpolarization and Relaxation..... 22

I. Ca^{2+}–channel Mediated Hyperpolarization and Relaxation 22

II. K–channel Mediated Hyperpolarization and Relaxation 23

PART III. Ion Channels and Physiological Functions in VSM 26

I. Calcium Channels 26

II. Chloride Channels 28

III. Potassium Channels 29

i. K_v channels 30

ii. K_{ir} channels 35

iii. K_{ATP} channels 38

iv. K_{Ca} channels 41

BACKGROUND 48

HYPOTHESIS 48

OBJECTIVES 48

METHODS 49

I. Cell Isolation 49

II. Recording Technique 50

III. Solutions and Chemicals 52

IV. Data Acquisition 55

V. Data Analysis 56

VI. Experimental Protocol 57

PART I. Endothelium–dependent Hyperpolarization 57

PART II. Properties of Mesenteric Resistance Artery VSMC 62

PART III. Properties of 4 Types of MRA VSMC K–Channel — Linear Method 65

PART IV. Properties of 4 Types of MRA VSMC K–Channel — Non–Linear Method 72

PART V. Single Channel Activity of 4 MRA VSMC K–Channels 77

RESULTS 81

PART I. Endothelium–dependent Hyperpolarization 81

PART II. Properties of Mesenteric Resistance Artery VSMC 90

II.1 morphological properties 90

II.2 passive membrane properties 92

II.3 whole–cell current density 92

II.4 whole–cell pharmacology of MRA VSMCs 97

PART III. Properties of 4 Types of MRA VSMC K–Channel – Linear Method 105

III.1 MRA VSMCs exhibited 4 types of K–channel 105

III.2 linear method 108

III.3 reversal potential analysis (Nernst and K_{rev}) 111

III.4 maximum conductance (g_{max} and $K_{1/2}$) 113

PART IV. Properties of 4 Types of MRA VSMC K–Channel –

Non–Linear Method 114

IV.1 permeability constants 114

IV.2 GHK equations 114

IV.3 instantaneous conductance 117

IV.4 physiological conductance 118

IV.5 maximum conductance (g_{max} and $K_{1/2}$) 119

IV.6 MRA VSMC K–channel ion selectivity 121

PART V. Single Channel Activity of 4 MRA VSMC K–Channels 123

V.1 Ca^{2+}–dependent NP_o of 4 MRA VSMC K–channels (+40 mV) 123

V.2 Ca^{2+}–dependent NP_o of 4 MRA VSMC K–channels (–40 mV) 127

V.3 Voltage–dependent NP_o of 4 MRA VSMC K–channels 129

V.4 percentage contribution of 4 MRA VSMC K–channels 133

V.5 pharmacology of 4 MRA VSMC K–channels 135

DISCUSSION 137

PART I. Endothelium–dependent Hyperpolarization 138

PART II. Properties of Mesenteric Resistance Artery VSMC 145

PART III, IV. Properties of 4 Types of MRA VSMC K–Channel — Linear and Non–Linear Methods 151

PART V. Single Channel Activity of 4 MRA VSMC K–Channels 154

BK 156

IK 158

SK 159

miniK 160

CONCLUSION 168

FUTURE STUDIES 171

APPENDIX I 174

APPENDIX II 194

APPENDIX III 202

REFERENCES 205

LIST OF FIGURES

Page

Figure I–1. P–450 Metabolism of Arachidonic Acid 13

Figure M–1. Diagram of Three Endothelium Donor Tissue Techniques 59

Figure RI–1. ACh–induced Endothelium–dependent Hyperpolarization 82

Figure RI–2. Inverted Rings in Pipette Tip (SMA–IRPT) 84

Figure RI–3. EDH was a Function of Donor–target Distance (SMA–PIT) 86

Figure RI–4. Internal Perfusion of Tail Artery (TA–IP) 87

Figure RI–5. Internal Perfusion of SMA (SMA–IP)..... 88

Figure RII–1. MRA VSMC Length and Diameter 91

Figure RII–2. MRA VSMC Capacitance 93

Figure RII–3. Whole–cell Current in MRA and TA VSMCs 95

Figure RII–4. MRA and TA VSMC Current Density 96

Figure RII–5. Apamin Inhibited MRA VSMC Whole–cell Current 100

Figure RII–6. Current–voltage Relationship of Apamin on MRA and TA VSMCs .. 101

Figure RII–7. Pharmacology of MRA VSMC Whole–cell Major Currents 103

Figure RII–8. Current–voltage Relationship of IbTX and 4–AP on MRA VSMCs .. 104

Figure RIII–1. Examples of 4 MRA VSMC K–channels 106

Figure RIII–2. Examples of 4 TA VSMC K–channels 107

Figures RIII–3, 4, 5, and 6. Linear Analysis of Unitary Current 110

Figure RIII–7. Linear Analysis of TA VSMC K–channels 112

Figures RIV–1, 2, 3, and 4. Non–linear Analysis of Unitary Current 115

Figures RV–1, 2, 3, and 4. Examples of Ca^{2+}–dependent Activity of 4 MRA

VSMC K–channels (+40mV) 124

Figures RV–5. Ca^{2+}–dependent Activity of 4 MRA VSMC K–channels (+40mV) .. 125

Figures RV–6. Ca^{2+}–dependent Activity of 4 MRA VSMC K–channels (–40mV) ... 128

Figure RV–7. Voltage–dependent Activity of 4 MRA VSMC K–channels 130

Figure RV–8. Voltage–dependent NP_o of 4 MRA VSMC K–channels (500nM $Ca^{2+}]_i$) 131

Figure RV–9. Relative Contribution of 4 MRA VSMC K–channels 134

Figure AI–1. Effect of clotrimazole (30μM) on whole–cell Ca^{2+}–acivated K^+ channel currents in single vascular cell from the rat tail artery 188

Figure AI–2. Modulation of whole–cell Ca^{2+}–activated K^+ channel currents by different concentrations of clotrimazole, metyrapone, and proadifen 189

Figure AI–3. Single Ca^{2+}–activated K^+ channel activities recorded from an outside–out patch 190

Figure AI–4. Effects of metyrapone and proadifen on whole–cell outward currents elicited by depolarizing pulses of –80 to +80 mV (holding potential –80 mV) 191

Figure AI–5. Effects of clotrimazole and metyrapone on whole–cell delayed rectifier currents 192

Figure AI–6. Effects of P–450 induction / depletion and clotrimazole on whole–cell current 193

LIST OF TABLES

Page

Table M–1. Solutions 54

Table M–2. Fabiato Calculation of Free Calcium 54

Table M–3. Reversal Potentials From the Nernst Equation 69

Table M–4. Potassium Channel Antagonists and their Targets 80

Table RIII–1. Linear Conductance of 4 MRA VSMC K–channels 108

Table RIII–2. Linear Conductance of 4 TA VSMC K–channels..... 111

Table RIII–3. Linear g_{max} and $K_{1/2}$ for MRA VSMC K–channels..... 113

Table RIV–1. MRA VSMC K–channel Permeability Constants 114

Table RIV–2. GHK Conductance for 4 MRA VSMC K–channels 116

Table RIV–3. Estimated Physiological Conductance of 4 MRA VSMC K–channels 118

Table RIV–4. Non–linear g_{max} and $K_{1/2}$ for MRA VSMC K–channels 120

Table RV–1. NP_o of 4 K–channel Types from Inside–out Patches for TA and MRA VSMCs at +40 mV 126

Table RV–2. NP_o of 4 K–channel Types from Inside–out Patches for TA and MRA VSMCs at –40 mV 127

Table RV–3. Comparison of NP_o (–40 and +40 mV) for 4 MRA VSMC K–channels 132

Table RV–4. Comparison of NP_o for 4 MRA VSMC K–channels (–40 and +40mV) 133

Table RV–5. Pharmacology of 4 MRA VSMC K–channels 136

Table D1. Properties of Rat TA and MRA VSMCs 146

Table D2. Properties of 4 MRA K–channel Types 154

Table D3. Selectivity of Antagonists for MRA and TA K–channels 162

Table A2–1. Summary of EDHF and P–450 in various tissues 195

Table A2–2. Literature summary of EDHF and P–450 in various tissues 196

Table A3–1. Properties of K–channels in the Literature 203

LIST OF ABBREVIATIONS

3–MC	3–methylcholanthrene
4–AP	4–aminopyridine
AA	arachidonic acid
ACh	acetylcholine
AHP	afterhyperpolarization
A_m	electrical surface area
ATP	adenosine triphosphate
BK/BK_{Ca}	large conductance calcium–dependent K–channel
β–NF	β–naphthoflavone
C_{50}	$[Ca^{2+}]_i$ required to activate K–channels to ½ maximum NP_o (500 nM)
$[Ca^{2+}]_i$	concentration of calcium in intracellular solution
$[Ca^{2+}]_o$	concentration of calcium in extracellular solution
$CB_{1/1A}$,CB_2	cannabinoid receptors
CHO	Chinese hamster ovary
ChTX	charybdotoxin
C_m	cell membrane capacitance
$CoCl_2$	cobalt chloride
DHP	dihydropyridine
DHT	dihydroxy– epoxyeicosatrienoic acid
DMSO	dimethylsulfoxide
DTT	dithiothreitol
DTX	dendrotoxin
E	voltage
EDCF	endothelium–derived contracting factor
EDH	endothelium–dependent hyperpolarization
EDHF	endothelium–derived hyperpolarizing factor
EDR	endothelium– dependent relaxation
EDRF	endothelium–derived relaxing factor
EET	epoxyeicosatrienoic acid

EGTA	ethyleneglycol tetraacetic acid
F	Faraday's constant
g	conductance
GHK	Goldman–Hodgkin–Katz constant field equations
g_{max}	maximum conductance under high intracellular and extracellular potassium
Hb	hemoglobin
HEPES	hydroxyethyl piperazine ethane sulphonic acid
HETE	hydroxyeicosatetraenoic acid
HPIS	high potassium intracellular solution
IbTX	iberiotoxin
I_K	single channel unitary current
IK	intermediate conductance potassium channel
IP	internal perfusion technique, SMA or TA donor
IRPT	inverted rings in pipette tip technique, SMA donor
I–V	current–voltage
$K_{1/2}$	$[K^+]_o$ at which $g = ½ (g_{max})$
K_{ATP}	ATP–dependent potassium channel
K_{Ca}	calcium–dependent potassium channel
K_{dr}	delayed rectifier potassium channel
$[K^+]_{eq}$	concentration of potassium under symmetrical conditions
$[K^+]_i$	concentration of potassium in intracellular solution
K_i	one–half inhibition constant for ion channel antagonists
K_{ir}	inward rectifier potassium channel
$[K^+]_o$	concentration of potassium in extracellular solution
K_{rev}	reversal potential
K_{to}	transient outward potassium channel
K_v	voltage–dependent potassium channel
L–NNA	L–nitro–N^{ω}–arginine
MB	methylene blue
MCA	middle cerebral artery
miniK	very small (mini) conductance potassium channel

MRA	mesenteric resistance artery
$[Na^+]_i$	concentration of sodium in intracellular solution
$[Na^+]_o$	concentration of sodium in extracellular solution
NE	norepinephrine
NO	nitric oxide
NOS	nitric oxide synthase
NP_o	open probability
P	probability 2 sets of numbers are randomly different (Student's t–test)
PIT	pinned inverted tubes technique, SMA donor
P_K	permeability constant of potassium
P_{Na}	permeability constant of sodium
PTX	pertussis toxin
R	universal gas constant
RMP	resting membrane potential
R_s	series resistance
SK	small conductance potassium channel
SK_{Ca}	small conductance calcium–dependent potassium channel
SMA	superior mesenteric artery
SMC	smooth muscle cell
SR141716A	(*N*–piperidino–5–(4–chlorophenyl)–1–(2,–dichlorophenyl)–4–methyl–3–pyrazole–carboxamide
T	temperature in Kelvins
TA	tail artery
TEA	tetraethyl ammonium
VSM	vascular smooth muscle
VSMC	vascular smooth muscle cell

INTRODUCTION

EDHF donors – conducting versus resistance arteries

The arterial circulatory system is comprised of large elastic or *conducting arteries* which branch from the heart and small branches of muscular *resistance arteries* which supply the organs. The large *conducting arteries* are high–pressure vessels composed of more elastic fibres and less smooth muscle than smaller arteries. The muscular *resistance arteries* branch from the conducting arteries and have a thick wall to lumen ratio. It is the smaller resistance arteries which are believed to regulate blood pressure (Nelson and Quayle, 1995; Brayden, 1996; Urakami–Harasawa *et al.*, 1997).

Conducting arteries (~ 400 – 1 000+ μm) have been the principal tissues used in organ bath experiments since resistance arteries (~ ≤ 200 μm) are usually too small to canulate (Garland *et al.*, 1995). Hence, resistance arteries have been poorly characterized compared to conductance arteries. Conducting arteries have been pharmacologically induced to release a number of endothelium–dependent factors, including NO, prostaglandins, and EDHF (Félétou and Vanhoutte, 1996; Mombouli and Vanhoutte, 1997). Rat superior mesenteric artery (SMA) and tail artery (TA), conducting arteries that branch from the aorta, were used as donor tissues to release EDHF since both were previously studied in our laboratory and have similar diameter though different function (Chen and Cheung, 1997; Bolzon and Cheung, 1989).

Rat SMA (~ 600 μm) has numerous very small branches of mesenteric resistance arteries (MRAs, 100 – 150 μm) along its surface, and branches into

smaller second and third order arteries (~ 300 μm), all of which supply the GI. Rat TA has no branches along the first proximal 1/3, then has very regular branches of smaller arteries that are involved in temperature regulation (Wu *et al.*, 1995). Previous studies have shown that SMA can release EDHF, but have failed to conclusively demonstrate that EDHF is a diffusible factor (Chen and Cheung, 1997), and it has not been demonstrated that TA can release an EDHF.

TA VSMC isolation was an established practice and TA K–channels have been well characterized in our laboratory (Bolzon, 1992; Bolzon and Cheung, 1989). Thus, TA VSMCs were targets for donor tissue (TA and SMA) EDHF. However, since TA and SMA are both conducting arteries, a novel procedure was developed to isolate and characterize VSMCs from the mesenteric resistance artery (MRA) and their K–channels, since resistance artery K–channels are putative targets of EDHF (Waldron and Cole, 1999). MRA and TA VSMCs were compared, and their K–channels characterized.

PART I. Endothelium–dependent Factors

I. Endothelium

function and regulation

A single squamous cell layer of endothelium lines the lumen of blood vessels. Endothelial cells are activated by a number of physiological stimuli, including shear stress, intramural pressure, and hypoxia. Chemical modulators of endothelium–mediated relaxation include amines (catecholamines, serotonin, histamine), cytokines, fatty acids (arachidonic acids and P–450 metabolites), growth factors, nucleotides (adenosine, ATP, ADP, UTP), peptides (bradykinin, substance P, endothelin, vasopressin, vasoactive intestinal peptide), and proteases (thrombin, trypsin) (Vanhoutte and Mombouli, 1996; Neylon, 1999).

Many endothelial receptors are linked to G proteins, some of which are sensitive to pertussis toxin (PTX; α_2 adrenergic receptor activated, serotonin, thrombin) while others are PTX–insensitive (bradykinin, ADP) (Vanhoutte, 1997). Activation of some G proteins (G_i and G_q) results in elevation of intracellular calcium, both from extracellular calcium entry and inositol trisphosphate (IP_3)–dependent calcium release from the sarcoplasmic reticulum (Boulanger and Vanhoutte, 1997). The potent vasoconstrictor endothelin (ET–1) binds to two endothelial receptors, ET(A) and ET(B), both of which are coupled with G proteins (G_s and G_i) (Douglas and Ohlstein, 1997). Intracellular calcium activates calmodulin, and the calcium–calmodulin complex putatively increases NO and EDHF synthesis (Nilius, 1991; Boulanger and Vanhoutte, 1997).

The role of the endothelium in acetylcholine–induced relaxation of isolated arteries was observed 20 years ago (Furchott and Zawadski, 1980). In the traditional organ bath technique, endothelial–derived vasomediators (prostaglandins, EDRF, and EDHF) are elicited from endothelium–intact donor vascular smooth muscle (VSM) tissue using muscarinic agonists (acetylcholine / ACh, carbachol) and the responses (hyperpolarization / relaxation) are compared to endothelium–free (denuded, damaged) tissue. Antagonists to these vasomediators (indomethacin / PGI_2, NOS inhibitors / EDRF) are used to select for EDHF.

The sandwich preparation is the principal technique used to demonstrate that an endothelium–intact donor tissue preparation can release a transferable factor(s) which can modulate the function of another preparation. The endothelium–intact donor tissue is placed in close proximity to the endothelium–free target smooth muscle preparation. Agonist–induced endothelium–dependent relaxation (EDR) is often restored (Gruetter and Lemke, 1986).

The experiments presented (Methods) demonstrate novel techniques that distinctly separate donor tissue (SMA and TA) and target TA VSMCs, unlike the traditional sandwich preparation. This separation of donor endothelium and target VSMC allows for comparison of different donor–target couples and distances. Two novel techniques presented (SMA/TA–IP, SMA–IRPT) allowed for separation of donor and target bathing solution, which allowed for isolation of pharmacological reagents (agonists and antagonists).

Endothelium–dependent hyperpolarization and relaxation of VSM is mediated by many factors, including endothelium–derived relaxing factor (EDRF), prostaglandins, and endothelium–derived hyperpolarizing factor(s) (EDHFs) (Vanhoutte and Mombouli, 1996; Mombouli and Vanhoutte, 1997).

II. EDRF (NO)

identitiy, function, and regulation

Endothelium–derived relaxing factor (EDRF) is generally accepted to be nitric oxide (NO) or a NO–like nitrosyl compound (Ignarro *et al.*, 1987; Palmer *et al.*, 1987). Nitric oxide is a small lipophilic molecule that is only partially soluble in aqueous solution. Nitric oxide has a very short half–life (~ 5 seconds) that limits duration and spatial localization of the effect. The vascular system contains two types of nitric oxide synthase (NOS): constitutive NOS (cNOS) and inducible NOS (iNOS). Constitutive NOS produces small amounts of NO continuously, and is induced by calcium, shear stress (Ranjan *et al.*, 1995), and receptor agonists such as angiotensin II (Saito *et al.*, 1996). Protein kinase C inhibits activation of cNOS, while cytokines inhibit production and expression of cNOS (Geng, *et al.*, 1994). Inducible NOS (iNOS) is a calcium–independent enzyme activated by cytokines (interleukin–1 beta, IL–1β, and tumor necrosis factor alpha, TNF_{α}) and endotoxin (lipopolysaccharide, LPS), which suggests a role in inflammatory responses (Liu *et al.*, 1993; Vane *et al.*, 1994). Corticosteroids (dexamethasone) inhibit iNOS synthesis, as do inhibitors of DNA transcription

(tumor growth factor beta – 1, $TGF_{\beta-1}$) and mRNA translation (TGF_{β}) (Cetkovic–Cvrlje *et al.*, 1993; Vodovotz *et al.*, 1993; Perrella *et al.*, 1994).

EDRF produces vasodilation via activation of soluble guanylate cyclase (GC) in the smooth muscle cell (Moncada and Higgs, 1993). NO also inhibits smooth muscle proliferation (Garg and Hassid, 1989), platelet adhesion and aggregation (Siney and Lewis, 1992), monocyte adhesion (Gaboury *et al.*, 1993; Lefer *et al.*, 1993), and oxidation of low density lipoprotein (Jacobs *et al.*, 1990).

In physiological solution, NO is a poorly reactive species that has a high affinity for heme groups. Soluble guanylate cyclase has a heme moiety that readily binds NO to form the activated GC complex. The binding of NO increases enzyme activity 50–fold, converting magnesium guanosine 5'–triphosphate (MgGTP) substrate to guanosine 3',5'–monophosphate (cyclic GMP, cGMP). Cyclic GMP initiates a cascade of phosphorylation / dephosphorylation that results in the dephosphorylation of myosin light chain and relaxation. The NO–GC interaction represents a signal transduction system that links extracellular stimuli with intracellular second messengers (Ignarro, 1990).

NO synthesis is linked to L–arginine synthesis and availability in endothelial cells (Bogle *et al.*, 1996). Nitric oxide synthesis is inhibited by the false substrates N^{G}–methyl–L–arginine (L–NMA), N^{ω}–nitro–L–arginine methyl ester (L–NAME), and N^{ω}–nitro–L–arginine (L–NNA). Heme containing molecules bind NO readily, and hemoglobin (Hb) and oxyhemoglobin act as NO scavengers. Methylene blue (MB) blocks soluble guanylate cyclase and metabolizes NO (Garland *et al.*, 1995).

NO and conducting vs. resistance arteries

In many tissues, NO appears to be the predominant EDRF (human, rat, and guinea pig uterine artery, Jovanović *et al.*, 1995; Jovanović *et al.*, 1998; Jain *et al.*, 1999; rat femoral artery, intrarenal artery, and aorta, Zygmunt and Högestätt, 1995; rat aorta, pulmonary artery, and iliac artery, Nagao *et al.*, 1992; human small coronary artery, Kemp and Cocks, 1997; sheep pulmonary artery and vein, Kemp *et al.*, 1995).

In human gastroepiploic artery, another conducting artery, ACh–induced relaxation and bradykinin–induced hyperpolarization and relaxation were significantly reduced by indomethacin (10 μM) plus L–NNA (100 μM), suggesting that NO is the predominant EDHF (Urakami–Harasawa *et al.*, 1997). By comparison, in distal resistance microvessels (100 – 150 μM), the EDHF–mediated hyperpolarization and relaxation was inhibited by elevated $[K^+]_o$, indicating modulation via K–channels (Urakami–Harasawa *et al.*, 1997).

In rat SMA (~ 650 μm, unstretched diameter), ACh–induced endothelium–dependent relaxation was abolished by hemoglobin (10 μM), methylene blue (10 μM), and L–NMMA (1 mM), which suggests that NO is the principal relaxing factor in rat SMA (Hwa *et al.*, 1994). Similarly, in rat SMA, ACh–induced NO–dependent relaxation and expression of eNOS (immunostaining and immunoblotting) were significantly greater in proximal versus distal segments (Shimokawa *et al.*, 1996).

In rat small SMA, ACh–induced hyperpolarization / relaxation is poorly inhibited by NOS inhibitors (diameter: ~325 μm, 100 μM L-NAME, relaxation

89% reduced to 68%, maximum hyperpolarization unchanged, Waldron and Garland, 1994; ~200 μm, 10 μM Hb, 1 mM L–NMMA, 10 μM MB, relaxation not significantly reduced, Hwa *et al.*, 1994). These results suggest that **NO is the principal relaxing factor in large SMA** and other conducting arteries whereas **NO and EDHF are both involved in the small SMA**. It was this difference in EDHF sensitivity which prompted the investigation of the MRA VSMCs and their K–channels.

III. Prostacyclin / Prostaglandins

identity, function, and regulation

Prostacyclin (prostaglandin I_2, PGI_2) is the principal product of cyclo–oxygenase in the vascular endothelium, but prostaglandin D_2 and E_2 (PGD_2 and PGE_2) may be the dominant product in some vascular beds (Vane *et al.*, 1982; Vanhoutte and Mombouli, 1996). Other prostaglandins are enhanced in disease states, including prostaglandin $F_{2\alpha}$ ($PGF_{2\alpha}$), prostaglandin H_2 (PGH_2), and thromboxane A_2 (TXA_2). Prostaglandins are synthesized by cyclo–oxygenase from arachidonic acid (AA) liberated form the cell membrane by phospholipase A_2. AA is processed by PGGH synthase which yields PGG_2 (cyclo–oxygenase activity) or $PGGH_2$ (peroxidase activity), the precursor for all prostanoids. Prostacyclin induces vascular smooth muscle relaxation via activation of adenylyl cyclase, which synthesizes 3',5'–cyclic monophosphate (cAMP) from ATP.

PGI_2 and conducting vs. resistance arteries

The involvement of PGI_2 in endothelium–dependent relaxation is tissue and species specific (Triggle *et al.*, 1999). In rabbit MCA and guinea pig mesenteric arteriole, the cyclo–oxygenase inhibitor indomethacin is required to completely suppress ACh–induced relaxation (Triggle *et al.*, 1999). In contrast, in other arteries like rat SMA (Garland and McPherson, 1992; Shimokawa *et al.*, 1996; Fukao *et al.*, 1997b; McCulloch *et al.*, 1997) and MRA (Clark and Fuchs, 1997), ACh– or carbachol–induced hyperpolarization / relaxation was not significantly inhibited by indomethacin. Similarly, ACh–induced relaxation in rabbit mesenteric artery was unaffected by glybenclamide (Khan *et al.*, 1993).

In tissues where prostanoids do contribute to hyperpolarization and relaxation, responses are nearly abolished by the K_{ATP}–channel inhibitor glybenclamide (1 μM) (rat TA, Schubert *et al.*, 1997; guinea pig coronary artery and mammary artery, Tare *et al.*, 2000). In the presence of indomethacin or glybenclamide, there is **no significant prostanoid component of endothelium–dependent hyperpolarization / relaxation in rat SMA or TA**. The prostanoid component of EDR in small resistance arteries (MRA) has yet to be determined and should not be discounted.

IV. EDHF

identity, function, and regulation

The identity of endothelium–derived hyperpolarizing factor (EDHF) is currently not known. EDHF is defined as a non–NO, non–PGI_2 endothelium–derived relaxing and hyperpolarizing factor. Endothelium–dependent relaxation

induced by muscarinic agonists has been associated with a NO–independent hyperpolarization (Chen *et al.*, 1988; Taylor and Weston, 1988). There is strong evidence that EDHF may be an AA derivative of P–450 metabolism or an endocannabinoid related to anandamide (Félétou and Vanhoutte, 1996; Mombouli and Vanhoutte, 1997; Resende *et al.*, 1998).

ACh–induced endothelium–dependent hyperpolarization / relaxation are inhibited or abolished when the endothelium is intentionally damaged (denuded through abrasion or damaged with hypoxia / hyperoxia) or in aged / hypertensive rat MRA (Fujii *et al.*, 1992; Fujii *et al.*, 1993; Lüscher *et al.*, 1992). EDHF has been proposed to be a transferable factor, even though chemically unrelated factors may exist in different tissue (Chen *et al.*, 1991; Triggle *et al.*, 1999). The current definition of EDHF is an inducible and transferable non–NO/PGI_2 endothelium–derived hyperpolarizing factor. This definition allows for the possibility of a family of factors including a cytochrome P–450 metabolite of AA or an endogenous cannabinoid (Triggle *et al.*, 1999).

In rabbit mesenteric artery ring segments but not sandwich preparations, ACh–induced non–NO/PGI_2 relaxation was inhibited by the gap junction inhibitor Gap 27 (300 μM). However, the calcium ionophore A23187–mediated relaxation was unaffected by Gap 27. This suggests that ACh–induced EDHF may be a transferable factor that is transported from the endothelium to smooth muscle via gap junctions (Hutcheson *et al.*, 1999). Gap 27 and other gap junction inhibitors also abolished ACh–induced NO–independent relaxation in rabbit aorta and iliac artery (Chaytor *et al.*, 1998; Taylor *et al.*, 1998). The disparity between tissues,

species, and agonists suggest that different EDHFs may be released or that alternate sites of release are possible. The involvement of gap junctions in EDHF–mediated relaxation is unknown and has not been addressed by this study.

EDHF and conducting vs. resistance arteries

In guinea pig sandwich preparation, ACh induced the release of a transferable factor from endothelium–intact carotid artery (donor tissue) which relaxed and hyperpolarized endothelium–denuded coronary artery (target tissue) (Chen *et al.*, 1991). The hyperpolarization was not inhibited by L–NNA or indomethacin, which suggests the release of a transferable, non–NO/PGI_2 EDHF (Chen *et al.*, 1991).

In rat aorta, pulmonary artery, and iliac artery, ACh–induced EDR was blocked by L–NNA, which suggests that NO is the principal EDRF in these tissues (Nagao *et al.*, 1992). In many rat tissues (mesenteric, femoral, and renal arteries, Nagao *et al.*, 1992; mesenteric and hepatic arteries, Zygmunt *et al.*, 1995), ACh–induced EDR was partially inhibited by L–NNA, which suggests a role for both EDHF and NO in these tissues. In porcine coronary artery, bradykinin–induced EDR was only slightly blocked by L–NNA, which suggests that EDHF is the principal endothelium derived factor in this tissue (Nagao and Vanhoutte, 1992a; Nagao and Vanhoutte, 1992b; Kauser and Rubanyi, 1996). Thus, EDHF is a major relaxing agent in some conducting arteries (porcine coronary), a component of relaxation in others (rat mesenteric, femoral, and renal arteries), or not involved (rat aorta, pulmonary artery, and iliac artery). These

examples indicate that EDHF is more involved in the relaxation of smaller resistance vessels rather than larger conductance vessels, despite differences in tissue and experimental protocol.

V. Cytochrome P–450 Metabolites

function and regulation

There is strong evidence that EDHF may be a cytochrome P–450 derivative of AA (Campbell *et al.*, 1996; Chen and Cheung, 1996; Popp *et al.*, 1996). AA can be metabolized by one of three pathways: cyclo–oxygenase, lipoxygenase, or cytochrome P–450 dependent mono–oxygenase (Schwartzman, 1990; McGiff, 1991). The cytochrome P–450 system is a broad and diverse family of enzymes which are responsible for the metabolism of cholesterol, bile acids, vitamins, steroids, and many xenobiotics (McGiff, 1991).

The cytochrome P–450 metabolism of AA can follow three oxidative pathways – epoxidation, allylic oxidation and omega (ω) and omega–1 (ω–1) hydroxylation – all of which require O_2 and NADPH (1:1):

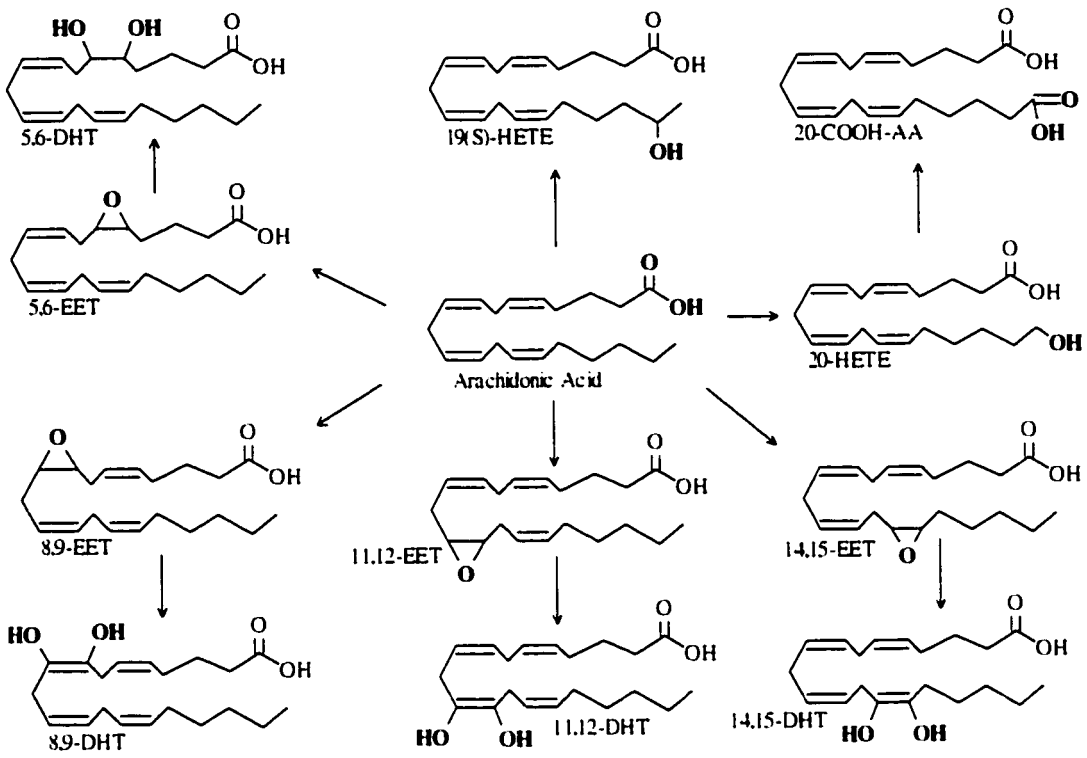

Figure I–1. P–450 Metabolism of Arachidonic Acid.

(i). The epoxidation of AA can occur at any of the four double bonds to produce four epoxides: 5,6–, 8,9–, 11,12–, or 14,15– epoxyeicosatrienoic acid (EET). These four epoxides can be converted by epoxide hydrolase to four corresponding dihydroxyeicosatrienoic acids (DHTs). (ii). The allylic oxidation of AA results in hydroxyeicosatetraenoic acids (HETEs) at the double bonds to form 5–, 8–, 9–, 11–, 12–, and 15– HETE. (iii). Omega and omega–1 hydroxylation of AA produce 20–HETE and 19–HETE, respectively. 17–octadecynoic acid (17–ODYA) is a specific suicide substrate inhibitor of ω–hydroxylation by P–450 enzymes and prevents formation of 19– and/or 20–

HETE. P–450 mono–oxygenase is inhibited by the P–450 inhibitors clotrimazole, proadifen, metyrapone, and the AA false substrate 7–ethoxyresorufin (7–ER).

VI. P–450 Metabolites: Application and Inhibition

P–450 metabolites and conducting vs. resistance arteries

In rat SMA, clotrimazole significantly inhibited muscarinic–induced EDHF responses (Chen and Cheung, 1996; Fukao *et al.*, 1997a; McCulloch *et al.*, 1997). Though ACh–induced EDH was also inhibited by proadifen, metyrapone, 17–ODYA, ETYA, or AA were without effect (Fukao *et al.*, 1997a). Though there is evidence that supports the notion that rat SMA ACh–induced EDHF is a P–450 metabolite, the evidence against it is equally strong. Similarly, in rabbit SMA, ACh–induced EDR was inhibited by clotrimazole, proadifen, TEA, ChTX, and 4–AP, but was unaffected by 17–ODYA or direct application of all four EETs (Fujimoto *et al.*, 1999).

In sharp contrast, in guinea pig mesenteric artery, ACh–induced EDR was unaffected by clotrimazole or 7–ER, but 17–ODYA (3 μM), ChTX (100 nM), or apamin (300 nM) plus IbTX (100 nM) partially inhibited relaxation (Triggle *et al.*, 1999). These results indicate the involvement of K–channels but refute the idea that EDR is mediated through P–450 metabolites and supports the notion that clotrimazole directly inhibits K_{Ca} channels (human RBCs and rat thymocytes, Alvarez *et al.*, 1992).

These examples demonstrate that the involvement of P–450 metabolites in agonist–induced EDHF release has not been clearly determined in mesenteric

artery. Though it is unknown whether a P–450 metabolite(s) is an EDHF, there is evidence that vascular smooth muscle is modulated by P–450 metabolites of AA (see Appendices I and II).

P–450 metabolites and K–channel targets

Although the mechanism of action of EDHF has not been determined, VSMC K–channels have been proposed as potential sites of action (Waldron and Cole, 1999). All four EETs (5,6–; 8,9–; 11,12–; and 14,15–EET) increase BK_{Ca} single channel activity in cell–attached patches from rabbit portal vein, rat caudal artery, guinea pig aorta, and porcine coronary arteries with similar potencies (0.1 – 3 μM) and only when applied to the extracellular surface, implying a receptor–mediated mechanism of action (Hu and Kim, 1993).

Similarly, EETs (8,9–; 11,12–; and 5,6–EET) activate a BK_{Ca} channel (98 pS, K_o = 145 mM) in cell–attached patches from cat cerebral microvessels (Gebremedhin *et al.*, 1992). Cat cerebral microvessels incubated with ^{14}C–AA showed that the predominant metabolite (20–HETE) was probably of the 4A family, based on its molecular mass and binding affinity to polyclonal antibodies (Harder *et al.*, 1994). Exogenous 20–HETE constricted cat cerebral microvessels and inhibited a BK channel (217 pS, TEA–sensitive) in cell–attached mode, and 17–ODYA inhibited 20–HETE synthesis and increased BK activity (Harder *et al.*, 1994). These examples demonstrate that BK channels are modulated by P–450 metabolites of AA (20–HETE, EETs) and thus are possible targets of EDHF. The

use of classical inhibitors of cytochrome P–450 was examined in our laboratory using rat TA single VSMC K–channel currents (K_{Ca} and K_{dr}) as targets.

In our laboratory, we examined the effects of three cytochrome P–450 inhibitors (clotrimazole, metyrapone, and proadifen) and found that all three had variable effects on rat TA VSMC whole–cell K–channel currents (K_{Ca} and K_{dr}) (Appendix I).

These examples focus on the release or application of P–450 metabolites (EETs / DHTs, HETEs), or their inhibition by antagonists (clotrimazole, metyrapone, proadifen, 17–ODYA). Another way to study the activity of the P–450 mono–oxygenase pathway is to use induction or depletion agents.

VII. P–450 Induction and Depletion

function and regulation

The P–450 mono–oxygenase system of enzymes is metabolically controlled and subject to modulation. In rat hepatic microsomes, treatment with β–naphthoflavone (β–NF) has been shown to increase the production 19– and 20–HETEs and concomitantly decrease the production of EETs (McGiff, 1991). As well, phenobarbital has been used to increase the production of EETs, even though it altered the ratio of stereospecific isomers: 11(S)–, 12(R)–EET became dominant after induction whereas 11(R)–, 12(S)–EET was initially the principal product (McGiff, 1991). 3–methylcholanthrene (3–MC) and β–naphthoflavone (β–NF) are agents known to induce P–450 activity whereas cobalt chloride ($CoCl_2$) is a known inhibitor of P–450 enzymes.

P–450 induction and EDR / EDH

In rat SMA, P–450 induction (3–MC / β–NF) enhanced ACh–induced EDHF–mediated hyperpolarization but not relaxation, whereas P–450 depletion ($CoCl_2$) reduced both the hyperpolarization and relaxation responses (Chen and Cheung, 1996). In canine coronary artery rings, P–450 induction (3–MC / β–NF) enhanced AA–induced EDR and P–450 depletion ($CoCl_2$) diminished AA–induced relaxation (Pinto *et al.*, 1987). Similarly, in porcine coronary artery, bradykinin–induced EDHF release was enhanced by β–NF (Popp *et al.*, 1996). These examples enforce the notion that vascular tone is regulated by P–450 metabolites and refute the idea that P–450 inhibitors like clotrimazole act exclusively through direct modulation of K–channels.

P–450 induction / depletion and K–channel targets

In our laboratory, rat TA VSMC K–channels were studied as potential targets of P–450 metabolites. P–450 activity was induced (3–MC / β–NF) or depleted ($CoCl_2$) and the basal whole–cell outward current (K_{Ca} and K_{dr}) and BK_{Ca} NP_o of inside-out patches observed in the presence or absence of the P–450 inhibitors (unpublished observations, see Appendix I). Though P–450 induction / depletion did not change basal activity, responses to clotrimazole supported the notion that rat TA VSMCs are regulated by cytochrome P–450 enzymes and metabolites (Appendix I).

VIII. Anandamide

function and regulation

Although controversial, some propose that an endogenous cannabinoid, like anandamide, may be an EDHF that affects K–channels (Randall *et al.*, 1996; Randall and Kendall, 1998). Anandamide is proposed to be an endogenous cannabinoid receptor ligand (Randall *et al.*, 1996). Three currently identified cannabinoid receptors (CB_1, CB_{1A}, and CB_2) activate pertussis toxin (PTX)–sensitive G–proteins and cause adenylyl cyclase inhibition (Felder *et al.*, 1995; Rinaldi–Carmona *et al.*, 1996a). In vitro studies have provided functional evidence of cannabinoid CB_1 receptors in human ileum longitudinal smooth muscle (Croci *et al.*, 1998) and rodent brain (Rinaldi–Carmona *et al.*, 1994). CB_2 receptors have been isolated and cloned from human, rat, and mouse spleen (Rinaldi–Carmona *et al.*, 1998a).

Functional tests of the effectiveness of cannabinoid ligands have focused on their ability to modulate forskolin–stimulated adenylyl cyclase activity. Cannabinoid agonists (CP 55,940, WIN 55212–2, Δ^9–THC) inhibit forskolin–stimulated adenylyl cyclase activity, which is reversed in the presence of a selective cannabinoid antagonist.

The diarylpyrazole SR 141716A (*N*–piperidino– 5–(4–chlorophenyl)– 1–(2,–dichlorophenyl)– 4–methyl– 3–pyrazole–carboxamide) is a highly potent and selective inverse agonist for the CB_1 receptor in rat neurons (Rinaldi–Carmona *et al.*, 1994; Rinaldi–Carmona *et al.*, 1995). An amino–truncated and –modified CB_1 receptor isoform, CB_{1A}, exhibited the properties of CB_1 but was less sensitive

to ligand binding. The rank order of potency of rodent brain CB_1 receptor ligands was SR 141716A > CP 55,940 > WIN 55212–2 = Δ^9–THC > anandamide, illustrating the high affinity of SR 141716A for the CB_1 receptor (Rinaldi–Carmona *et al.*, 1996b). SR 141716A had a 10–fold higher binding affinity for the CB_1 receptor than CB_{1A}, whereas the cannabinoid ligands CP 55,940, WIN 55212–2, and Δ^9–THC had a three–fold higher binding affinity for the CB_1 receptor (Rinaldi–Carmona, 1996a; Rinaldi–Carmona, 1996b). In contrast, anandamide had a similar binding affinity for both CB_1 and CB_{1A} receptors.

Following long–term exposure (72 hours) to the cannabinoid agonist CP 55,940, CB_1 receptors on the surface of CHO cells were internalized (Rinaldi–Carmona *et al.*, 1998b). In contrast, SR 141716A promoted the externalization of the CB_1 receptor. These results imply that the modulation of the number of cell surface receptors may regulate cannabinoid sensitivity.

SR 144528 is a potent and selective inverse agonist of mouse, rat, and human CB_2 cannabinoid receptors (Rinaldi–Carmona *et al.*, 1998a; Portier *et al.*, 1999). SR 144528 has a 700 fold lower affinity for the rat brain and human CB_1 receptor and even less affinity for 70 other receptors, ion channels, or enzymes in a broad based screen (Rinaldi–Carmona *et al.*, 1998a).

anandamide and EDHF

In order to determine whether anandamide represents EDHF, muscarinic– and anandamide–induced relaxations were compared pharmacologically using various K–channel antagonists. Toxin–derived antagonists (ChTX, IbTX) did not

inhibit muscarinic–induced relaxation (Randall and Kendall, 1998; Plane *et al.*, 1997; White and Hiley, 1997), and most researchers found anandamide–induced relaxation was unaffected by IbTX (White and Hiley, 1997) or ChTX (Randall and Kendall, 1998). However, other researchers observed that anandamide–induced relaxation was inhibited (IbTX) or abolished (ChTX) by toxin–derived antagonists (Plane *et al.*, 1997). In rat SMA, Randall and Kendall (1998) found that the combination of ChTX plus apamin abolished both muscarinic– and anandamide–induced relaxation, whereas White and Hiley (1997) observed that the ChTX / apamin combination only blocked muscarinic–induced relaxation. The question as to whether anandamide is EDHF or one of many EDH factors remains unresolved.

In rat small SMA, the CB_1 cannabinoid receptor antagonist SR 141716A (1 μM) blocked carbachol–induced EDHF–mediated relaxation, but anandamide–induced relaxation was parallel shifted tenfold without changing the maximum relaxation (White and Hiley, 1997). In contrast, SR 141716A (5 μM) had no effect on rat small SMA ACh– or anandamide–induced EDHF–mediated relaxation (Plane *et al.*, 1997). These results suggest that SR 141716A is not specific for the SMA CB receptor, or that EDHF is sensitive to small differences in experimental protocol.

The work of White and Hiley (1997) and Waldron and Garland (Plane *et al.*, 1997) suggests that there are some fundamental differences between anandamide and endogenous EDHF. However, the work of Randall and Kendall

(1997, 1998) suggests that, in some tissue, anandamide or an endogenous cannabinoid may be an EDHF.

The regulation of membrane potential and smooth muscle contraction through the three major pathways, NO, PGI_2, and EDHF, is multifaceted and is modulated by a number of complex interactions. However, in rat SMA, NO– and EDHF–mediated components are dominant, while the prostanoid component appears to be minimal (McCulloch *et al.*, 1997).

PART II. VSMC Ion Channel Mediated Hyperpolarization and Relaxation

The cholinergic–induced hyperpolarization and relaxation response may involve NO, prostacyclin, and/or EDHF. Endothelium derived products act through many different mechanisms, including the modulation of ion channel activity (Nagao and Vanhoutte, 1993). The VSMC Ca^{2+}– and K^{+}–channels are common targets of pharmacological investigation since their activation or inhibition modulates endothelium dependent hyperpolarization and relaxation (Félétou and Vanhoutte, 1996).

I. Ca^{2+}–channel Mediated Hyperpolarization and Relaxation

In rat mesenteric artery, ACh–induced EDHF mediated hyperpolarization was unaffected by indomethacin (10 μM), L—NOARG (300 μM), or oxyhemoglobin (10 μM) (Fukao *et al.*, 1997b). Fukao *et al.* (1997b) found that two sources of calcium contribute to two types of hyperpolarization, which supports the idea that EDHF mediated hyperpolarization is a calcium–dependent process. The transient hyperpolarization was inhibited by the endoplasmic reticulum Ca^{2+}–ATPase inhibitors thapsigargin (100 nM) and cyclopiazonic acid (3 μM) and is $[Ca^{2+}]_o$–independent, whereas the sustained hyperpolarization is $[Ca^{2+}]_o$–dependent and inhibited by the non–selective Ca^{2+}–channel inhibitors Ni^{+} (5 mM) and Mn^{2+} (3 mM), but not by the L–type Ca^{2+}–channel antagonist nifedipine (1 μM) (Fukao *et al.*, 1997b). This suggests that L—type Ca^{2+}–channels are not involved in EDHF mediated hyperpolarization, at least in rat SMA.

Similarly, in bovine coronary artery, nifedipine (1 μM) did not inhibit bradykinin–induced EDHF mediated relaxation (indomethacin 3μM + L—NOARG 100 μM + oxyhemoglobin 10 μM) (Drummond and Cocks, 1996). **In rat SMA** (and bovine coronary artery), **nifedipine did not block non—NO/PGI_2 mediated hyperpolarization** (and relaxation), **which implies that L–type Ca^{2+}–channels are not involved in EDHF–mediated hyperpolarization and relaxation**. The investigation of resistance vessel (rat MRA) ion channels was therefore limited to K–channels as functional targets of EDHF.

II. K–channel Mediated Hyperpolarization and Relaxation

Endothelium–derived relaxing factors (NO, PGI_2, EDHF) act via numerous mechanisms, including the activation of VSMC K–channels (Félétou and Vanhoutte, 1996; Waldron and Cole, 1999). Experiments using selective K–channel antagonists or elevated $[K^+]_o$ have been used to demonstrate K–channel involvement.

In rat MRA (Hwa *et al.*, 1994) and SMA (Chen and Cheung, 1997; Adeagbo and Triggle, 1993), ACh–induced EDHF–mediated hyperpolarization and relaxation were inhibited by apamin or ChTX, and abolished by the combination, but unaffected by glybenclamide, suggesting a role for BK_{Ca} and/or IK_{Ca} channels, but not K_{ATP} channels. In rat SMA with physiological $[K^+]_o$ (4.7 mM), the EDHF–mediated relaxation accounted for most (~80 %) of the total relaxation response (Adeagbo and Triggle, 1993). However, when the $[K^+]_o$ was raised (25 – 60 mM), the EDHF–mediated relaxation was significantly reduced (Adeagbo and Triggle,

1993; Waldron and Garland, 1994; Randall *et al.*, 1997; McCulloch *et al.*, 1997). **In the rat SMA, a conductance vessel, EDHF–mediated relaxation was highly dependent upon apamin–sensitive K–channels (possibly SK_{Ca}), somewhat dependent upon ChTX–sensitive K–channels (possibly BK_{Ca} / IK_{Ca}), but not dependent upon glybenclamide–sensitive K_{ATP} channels.**

In rabbit SMA, ACh–induced EDHF–mediated hyperpolarization was blocked by apamin (1 nM) and other inhibitors of apamin–sensitive K–channels (scyallatoxin, 10 nM; d–tubocurarine, 100 μM; gallamine, 300 μM), but not by IbTX (10 nM), glybenclamide (5 μM), TEA (1 mM), or 4–AP (500 μM), which suggests that apamin–sensitive channels are responsible for EDHF hyperpolarization in rabbit SMA (Murphy and Brayden, 1995).

In other tissues, agonist induced EDHF–dependent relaxation was blocked by elevated $[K^+]_o$ (porcine coronary artery, He *et al.*, 1996; human cerebral artery, Petersson *et al.*, 1996), TEA (1 mM) (porcine coronary artery, He *et al.*, 1996; rabbit renal artery, Kitagawa *et al.*, 1994), or the combination of ChTX (100 nM) plus apamin (100 nM) (porcine coronary artery, Ge *et al.*, 2000; rat hepatic artery, Zygmunt and Högestätt, 1996; guinea pig cerebral artery, Petersson *et al.*, 1997; guinea pig submucosal artery, Hashitani and Suzuki, 1997; guinea pig carotid artery, Corriu *et al.*, 1996b). These observations suggest that K_{Ca} channels are involved, but the general ineffectiveness of ChTX, IbTX, or apamin alone suggests that a novel K–channel is involved which is only inhibited by the dual combination of ChTX and apamin and is IbTX–insensitive, or that a compensation mechanism exists that is uncovered when one channel is blocked.

Agonist induced EDHF–dependent relaxation was not blocked by glybenclamide (3 μM) (He *et al.*, 1996; Yamakawa *et al.*, 1997), which suggests that K_{ATP} channels are not involved.

These observations indicate that K_{Ca} channels play a major role in EDHF relaxation in multiple tissue types. However, experiments in the rat hepatic artery imply that neither classical K_v nor K_{Ca} channels are involved in EDHF–mediated relaxation (Zygmunt *et al.*, 1997). The ACh–induced relaxation was inhibited by the K_v inhibitor ciclazindol (10 μM) and abolished by ciclazindol plus apamin, but not by other K_v inhibitors (agitoxin–2, kaliotoxin, β–dendrotoxin, dofetilide, or terikalant) (Zygmunt *et al.*, 1997). ChTX plus apamin blocked relaxation but were ineffective when used alone (Zygmunt *et al.*, 1997; also in guinea pig carotid artery, Corriu *et al.*, 1996b). IbTX (Kitazono *et al.*, 1997) or apamin (García–Pascual *et al.*, 1995) alone rarely inhibited ACh–induced EDHF dependent relaxation, even though IbTX has been shown to be more selective than ChTX for BK_{Ca} channels (Giangiacomo *et al.*, 1992). ChTX has been observed to also block K_v channels (Kaczorowski *et al.*, 1996; Nelson and Quayle, 1995). This implies that the target of EDHF in the rat hepatic artery is neither a K_v nor a K_{Ca} channel in the classical sense (Zygmunt *et al.*, 1997). The synergistic effect of apamin plus ChTX, but not apamin plus IbTX, suggests that IbTX may not be selective for all K_{Ca} channels, or that a novel K–channel exists. However, the existence of a novel ChTX– and apamin–sensitive K–channel has yet to be characterized.

PART III. Ion Channels and Physiological Functions in Vascular Smooth Muscle

Vascular smooth muscle contraction and relaxation is modulated by the activity of numerous membrane ion channels. Though sodium channels play a dominant role in the action potential of neurons, they are seldom found in VSM and are poorly characterized (rat neonatal portal vein, Sturek and Hermsmeyer, 1986; rabbit aorta, Bkaily, 1991). In contrast, there has been a great deal of research on calcium, chloride, and potassium channels found in VSM.

I. Calcium Channels

Three major classes of neuronal voltage–dependent Ca^{2+}–channels (T, L, and N) have been characterized, and a fourth type (P) has been found in cerebral Purkinje cells (Nowycky *et al.*, 1985; Llinas *et al.*, 1989). However, only T– and L–type Ca^{2+}–channels have been observed in cardiac tissue and VSM (Reuter *et al.*, 1982; Benham *et al.*, 1987). Voltage–dependent Ca^{2+}–channels in vascular preparations are activated when depolarized from the resting membrane potential to the threshold range (–50 to –30 mV), resulting in slow and maintained contraction (Droogmans *et al.*, 1977; Bolton *et al.*, 1984).

T–type Ca^{2+}–channels (6 – 10 pS) have rapid inactivation kinetics with more negative activation / inactivation ranges compared to L–type Ca^{2+}–channels (Caffrey *et al.*, 1986; Benham *et al.*, 1987). Although the role of T–type Ca^{2+}–channels in VSM is uncertain, it is suggested that they mediate pacemaker activity (Sturek and Hermsmeyer, 1986; Hagiwara *et al.*, 1988). T–type Ca^{2+}–channels

contribute to excitatory junction potentials in muscular arteries (Benham *et al.*, 1987) and are prominent in embryonic skeletal and smooth muscle cells (Beam and Knudson, 1988; Sturek and Hermsmeyer, 1986), which has led to the speculation that they play a developmental role (Bean, 1989). Due to the lack of selective antagonists, the role of T–type channels in the control of vascular function is still largely unknown.

L–type Ca^{2+}–channels (15 – 25 pS) comprise the sustained Ca^{2+}–dependent current in VSM (Aaronson *et al.*, 1986; Benham *et al.*, 1987). Dihydropyridine (DHP) antagonists are partially selective for L–type Ca^{2+}–channels. Although L–type currents predominate in VSM (Benham *et al.*, 1987), both T– and L– type currents were found in preparations from rat aorta (Toro and Stefani, 1987), guinea pig aorta (Caffrey *et al.*, 1986), rabbit mesenteric and ear artery (Aaronson *et al.*, 1986; Benham *et al.*, 1987), neonatal rat portal vein (Sturek and Hermsmeyer, 1986), and canine saphenous vein (Yatani *et al.*, 1987).

The molecular structure of L–type Ca^{2+}–channels is composed of five subunits, α_1, α_2, β, δ, and γ (Catteral, 1988; Spedding and Paoletti, 1992). The α_1 subunit contains the DHP binding site and phosphorylation sites for many protein kinases (PKA, PKG, PKC, and Ca^{2+}–calmodulin kinase) (Nastainczyk *et al.*, 1987; Rohrkasten *et al.*, 1988; Hosey and Lazdunski, 1988; Tuana and Murphy, 1990). The β subunit (54 kD) contains phosphorylation sites for PKA, PKG, and PKC (Catteral, 1988; Ruth *et al.*, 1989).

Functional Ca^{2+}–channels are expressed through microinjection of cDNA or mRNA into *Xenopus* oocytes (Biel *et al.*, 1991) or Chinese hamster ovaries

(Bosse *et al.*, 1992). The α_1 subunit cDNA is sufficient for the expression of stable Ca^{2+}–channels (Bosse *et al.*, 1992), and co–expression of the α_1 and β subunits shifts channel gating kinetics and increases DHP sensitivity (Singer *et al.*, 1991; Varadi *et al.*, 1991; Wei *et al.*, 1991). L–type Ca^{2+}–channels are modulated by phosphorylation (α_1 and β subunits). The degree of phosphorylation correlates with the rate of ^{45}Ca flux and the number of functional channels in reconstituted phospholipid, which suggests that phosphorylation is an important regulator of Ca^{2+}–channel activity (Miller and Fox, 1990).

II. Chloride Channels

Chloride (Cl^-–) channels have been observed in vascular smooth muscle from rat aorta (Kokubun *et al.*, 1991), rat and rabbit portal vein (Byrne and Large, 1988; Pacaud *et al.*, 1989), and rabbit ear artery (Amedee *et al.*, 1990; Wang and Large, 1991). Cl^-–channel opening results in membrane depolarization for VSMCs, which usually have a resting potential (~ –30 to –50 mV) more negative than the Cl^- equilibrium potential (~ –30 mV) (Kuriyama *et al.*, 1971). In rat portal vein, Cl^-–channels were found to be Ca^{2+}–dependent (Pacaud *et al.*, 1989), which suggests that Cl^- conductance is an important factor in Ca^{2+}–dependent action potentials, at least in this tissue preparation. In rabbit portal vein and guinea pig mesenteric vein, Cl^- currents were activated by noradrenaline (Byrne and Large, 1988; van Helden, 1988).

Papaverine, which modulates caffeine sensitive $[Ca^{2+}]_i$ stores, also affects noradrenaline induced Cl^- current in rabbit ear artery (Wang and Large, 1991). In

rat aorta, large conductance Cl^-–channels were selectively blocked by disulphonic stilbene derivatives 4,4'–diisothiocyanostilbene–2,2'–disulphonic acid (DIDS) and 4–acetamido–4–isothiocyanostilbene–2,2'–disulphonic acid (SITS) (Kokubun *et al.*, 1991). VSMC Cl^-–channels share characteristics (voltage dependence and unitary channel conductance, ~ 300 pS) with those found in skeletal– and cardiac–muscle cells (Blatz and Magleby, 1983; Coulombe *et al.*, 1987).

III. Potassium Channels

Potassium channels comprise the most diverse class of ion channels in the membranes of mammalian cells. The functions and activity of K–channels in modulating cellular processes is extensive. K–channels found in vascular smooth muscle are classified in three genetic families: voltage–dependent K–channels (K_v channels), inward rectifier K–channels (K_{ir} channels, K_{ATP} channels), and calcium–dependent K–channels (K_{Ca} channels) (Waldron and Cole, 1999).

Endothelium–dependent relaxing and hyperpolarizing factors directly affect specific K–channels. NO has been linked to large conductance K_{Ca} channels (bovine coronary artery), K_v channels (bovine coronary, rat pulmonary), and K_{ATP} channels (guinea pig carotid, rabbit mesenteric). Prostacyclin has been linked to BK_{Ca} channels (rat tail), K_v channels (rabbit cerebral, bovine coronary), and K_{ATP} channels (guinea pig carotid, rabbit mesenteric). EDHF has been linked to BK_{Ca} channels (porcine / bovine coronary), SK_{Ca} channels (guinea pig carotid, rat hepatic, porcine mesenteric, bovine coronary), K_v channels (rat hepatic, bovine / guinea pig coronary), and K_{ATP} channels (rabbit cerebral, porcine coronary). In

some cases, multiple conductances of the same family (channel type) have been affected by the same relaxing factor. The molecular diversity of potassium channels necessitates the use of selective antagonists to determine the endothelium derived relaxing and hyperpolarizing factor channel targets (Waldron and Cole, 1999).

i. K_v channels

Voltage–dependent K–channels (K_v channels) have been found in all VSMCs investigated, including human mesenteric artery (Smirnov and Aaronson, 1992), cat and rat cerebral artery (Bonnet *et al.*, 1991; Hirst *et al.*, 1986), rabbit pulmonary artery (Clapp and Gurney, 1991), rabbit coronary artery (Volk *et al.*, 1991; Volk and Shibata, 1993; Ishikawa *et al.*, 1993; LeBlanc *et al.*, 1994), canine renal artery (Gelband and Hume, 1992), and canine coronary artery (Wilde and Lee, 1989).

Subtypes of the voltage–dependent K–channel include the delayed rectifier potassium channel (K_{dr} channel) (Hodgkin and Huxley, 1952) and the transient outward potassium channel (K_{to} channel) (Beech and Bolton, 1989b; Clapp and Gurney, 1991).

There is mounting evidence that multiple subtypes of K_v channel are expressed in VSMCs. This evidence consists of differences in voltage dependence of activation and inactivation, pharmacological sensitivity, and single channel conductance. One member of the K_v channel family, $K_v1.5$, has been found to be expressed in VSMCs (Roberds and Tamkun, 1991; Roberds *et al.*,

1993; Overturf *et al.*, 1994). When expressed in *Xenopus* oocytes, $K_v1.5$ was activated by depolarizing current, inhibited by 4–AP (K_i = 211 μM), and had a single channel conductance of 8.3 pS ($K_{i/o}$ = 140 mM) (Overturf *et al.*, 1994).

The unitary conductance of K_v channels is divided into two groups. Small conductance K_v channels (K_o = 4 – 6 mM, cell attached configuration) have been found in rabbit portal vein (5 and 8 pS, Beech and Bolton, 1989c), rabbit basilar artery (5.5 pS, Robertson and Nelson, 1994), and porcine coronary artery (7.3 pS, Volk and Shibata, 1993). Intermediate conductance K_v channels have been reported in rabbit coronary artery (70 pS, $K_{i/o}$ = 140 mM, Ishikawa *et al.*, 1993) and canine renal artery (57 pS, K_o = 5.4 mM, cell attached, Gelband and Hume, 1992). The K_{dr} channel has a small unitary conductance (5 – 20 pS). In nerve and skeletal muscle, the current through the K_{dr} channel is activated after a brief delay following depolarization (Hille, 1992). The time course of K_{dr} current development is modeled by a fourth order exponential (Hodgkin and Huxley, 1952). This time course occurs with faster kinetics with increasing depolarization, and is believed to model four closed state transitions that have voltage–dependent rate constants. K_v channels are rapidly activated by membrane depolarization, and most slowly inactivate, which results in a time–dependent increase in peak current, followed by a slow decline (Nelson and Quayle, 1995).

Under sustained depolarization, the K_{dr} channel slowly inactivates, and decay of outward current occurs over a period of several seconds (Nelson and Quayle, 1995). Differences in single channel kinetics amongst tissues suggests that K_{dr} channels do not comprise a homogeneous population of channels

(Dubois, 1981). Michelakis *et al.* (1997) found that K–channel diversity wasn't limited to tissue or species differences. Individual cells were also found to exhibit differences in channel populations. In pulmonary arteries, K_{Ca} channels were more common in proximal conduit arteries whereas K_{dr} channels were more common in distal resistance vessels (Michelakis *et al.*, 1997).

The transient outward current (K_{to}) or A current was first observed in molluscan neurons (Connor and Stevens, 1971). K_{to} currents are voltage–dependent but have a rapid decay constant such that peak current declines even under sustained depolarization. Inactivated K_{to} currents are voltage–dependently activated by more negative hyperpolarizing pulses. The K_{to} current is normally inhibited at the resting potential of most cells but can be elicited by hyperpolarizing pulses, such as occur during the afterhyperpolarization of an action potential. It is believed that the K_{to} current may play a pacemaker role by slowing subsequent depolarization spikes (Connor and Stevens, 1971).

The K_{to} current has been observed in the rat TA (Bolzon, 1992), rabbit portal vein (Hume and Leblanc, 1989; Beech and Bolton, 1989b), and guinea pig ureter (Lang, 1989). The inactivation range of smooth muscle K_{to} currents is significantly higher than in neural tissue. The rat TA K_{to} current had a half maximal inactivation constant of –45 mV, similar to the K_{dr} current constant (–42 mV) (Bolzon, 1992). It has been suggested that the significantly higher inactivation range of K_{to} current in smooth muscle would allow the current to modulate resting membrane potential, and may account for the difficulty in eliciting action potentials in smooth muscle preparations. A Ca^{2+}–sensitive 85 pS

K–channel associated with the K_{to} current was observed in rat TA isolated VSMCs (Bolzon, 1992).

The pharmacology of K_v channels are poorly characterized by toxins relative to K_{Ca} and K_{ATP}. The most selective inhibitor of K_v channels in VSM is 4–aminopyridine (4–AP). The one–half inhibition constant (K_i) for 4–AP is ~1.1 mM in human mesenteric artery (Smirnov and Aaronson, 1992), 0.3 mM in rabbit pulmonary artery (Okabe *et al.*, 1987), and 0.7 mM in canine renal artery (Gelband and Hume, 1992). At this concentration range (0.2 – 1.1 mM), 4–AP does not usually inhibit K_{Ca} or K_{ir} channels, but may inhibit K_{ATP} channels (Beech and Bolton, 1989a; Quayle *et al.*, 1993; Nelson and Quayle, 1995). 4–AP preferentially inhibits rapidly inactivating currents, which makes it more selective for K_{to} rather than K_{dr} channels (Pfründer and Kreye, 1992).

K_v channels are less selectively blocked by phencyclidine (K_i = 30 μM) (Beech and Bolton, 1989a), tedisamil (K_i = 2.9 μM) (Pfründer and Kreye, 1992), and quinidine (K_i = 30 μM) (Beech and Bolton, 1989a). The K_{dr} channel was blocked by proadifen (10 μM) in rat portal vein (Edwards *et al.*, 1996) and guinea pig coronary artery (Yamanaka *et al.*, 1998).

The principal function of K_v channels in neurons and cardiac cells is to repolarize the cell following action potential depolarization (Beech and Bolton, 1989c; Hille, 1992). However, most arterial smooth muscle preparations exhibit a variable degree of contractility that is unlikely to be modulated by K_v channels through action potential repolarization.

The principal function of K_v channels in arterial smooth muscle is to regulate membrane potential (Knot and Nelson, 1995). Depolarization due to calcium entry and / or contraction activates K_v channels, thereby acting as a feedback inhibition mechanism (Nelson and Quayle, 1995). K_v channels are likely to be active at resting membrane potentials since 4–AP depolarizes and contracts guinea pig smooth muscle tissues (Hara *et al.*, 1980) and rabbit cerebral artery (Knot and Nelson, 1995).

Knot and Nelson (1995) found that 4–AP (1 mM) and 3,4–diaminopyridine (3,4–DAP) (1 mM) depolarized pressurized small cerebral arteries (100 – 300 μm diameter) by ~ 20 mV and constricted them significantly (Knot and Nelson, 1995). The weak K_v channel inhibitor 3–aminopyridine (3–AP) (1 mM) was only able to depolarize the artery by 1 mV and had no significant effect on artery diameter (Knot and Nelson, 1995).

The effects of 4–AP and 3,4–DAP on membrane potential and diameter were not prevented by inhibitors of Ca^{2+}–channels, K_{Ca} channels, K_{ATP} channels, K_{ir} channels, blockers of adrenergic, serotonergic, muscarinic, and histaminergic receptors, or by removal of the endothelium (Knot and Nelson, 1995). These results suggest that voltage–dependent K–channels are involved in the regulation of membrane potential and artery contraction.

Vascular responses to hypoxia are varied. Small systemic arteries usually vasodilate when hypoxic, which is believed to involve the opening of K_{ATP} channels. In contrast, pulmonary arteries constrict and depolarize when hypoxic, and inhibitors of K_v channels (TEA, 4–AP) constrict pulmonary arteries (Nelson

and Quayle, 1995). These observations suggest that voltage–dependent K–channels regulate membrane potential in pulmonary arteries as well as in systemic arteries.

ii. K_{ir} channels

The K_{ir} channel or current has been observed in rat TA (Bolzon *et al.*, 1993), guinea pig mesenteric arteriole (Edwards and Hirst, 1988), rat coronary artery (Bonev and Nelson, 1993), rat cerebral arteriole (Edwards *et al.*, 1988; Hirst *et al.*, 1986), and rat cerebral artery (Quayle *et al.*, 1993). The activity of K_{ir} channels is voltage– and potassium–dependent ($[K^+]_o$). K_{ir} channels conduct current into the cell when the membrane potential drops below the potassium reversal potential (E_K usually= –84 mV), but conduct little current out of the cell when the potential is above the E_K. When the channel is conducting current inward, activity increases as voltage decreases. When the $[K^+]_o$ is increased, the E_K shifts from ~ –84 mV to more positive potentials. This shifts the voltage threshold for K_{ir} opening from negative to more positive potentials. The $[K^+]_o$–dependent activity of the K_{ir} channel is unique to this channel type. Changes in $[K^+]_o$ shift the reversal potential of K_{Ca} and K_v channels but the voltage activation range is unaffected (Nelson and Quayle, 1995).

K_{ir} channels have been cloned from mouse macrophage, rat heart / brain, and human heart / brain (Kubo *et al.* 1993a; Kubo *et al.* 1993b; Tang and Yang, 1994). The rat heart clone (rKir3.1) is muscarinic–activated via a G–protein (Kubo *et al.* 1993b). The proposed structure of the K_{ir} channel has two membrane

spanning domains that form the pore, but lacks the S1 – S4 transmembrane domains found in K_v channels (Kubo *et al.* 1993a). The assembly of K_{ir} sub–units into functional channels has not been elucidated. However, in atrial VSMCs, K_{ir} channels are a heteromultimer composed of two inwardly–rectifying proteins (rKir3.1 + rKir3.4, Krapivinsky *et al.*, 1995). Combinations of monomers confirms that heteromultimers carry up to 10 fold more current than monomultimers (Velimirovic *et al.*, 1996), and expression of rKir3.1and hKir3.4 monomers in *Xenopus* oocytes suggests a tetramer composed of two dimers ($(rKir3.1)_2 + (hKir3.4)_2$, Silverman *et al.*, 1996).

There are no selective inhibitors of the K_{ir} channel. Barium ions (Ba^{2+}) have proven to be the most selective inhibitor of K_{ir} channels in arterial preparations, with half–inhibition in the micromolar range (K_i = 2 μM) in rat cerebral artery at –60 mV (Quayle *et al.*, 1993). Barium blockade is voltage–dependent and can be expressed as an exponential function of membrane potential. In rat cerebral artery, the dissociation constant of Ba^{2+} decreased *e*–fold for each 24 mV hyperpolarization. The K_i decreased from 8 μM at –40 mV to 0.6 μM at –100 mV (Quayle *et al.*, 1993). The voltage–dependent block of the K_{ir} channel by barium is associated with the blocking and not the unblocking rate constant (Quayle *et al.*, 1993). Barium inhibits K_{ATP} channels in guinea pig urinary bladder (K_i = 100 μM) (Bonev and Nelson, 1993), K_v channels in guinea pig portal vein (K_i > 1 mM) (Pfründer and Kreye, 1992), but has no effect on K_{Ca} channels in guinea pig mesenteric artery (K_i > 10 mM) (Benham *et al.*, 1985).

Compared to the other K–channels, K_{ir} channels are relatively selectively blocked by barium ions in the low micromolar range.

Intracellular magnesium ions (Mg^{2+}) blocked K_{ir} channels in starfish eggs, tunicate eggs, and guinea pig cardiac myocytes (Hagiwara *et al.*, 1975; Ohmori, 1978, Ishihara *et al.*, 1989). Physiological concentrations of Mg^{2+} are sufficient to minimize outward current. This mechanism of block is completely reversed and K_{ir} currents are near linear and voltage–dependent in magnesium free solutions (Ishihara *et al.*, 1989).

K_{ir} channels may modulate resting membrane potential. When Na^+–K^+–ATPase has been highly active, the membrane potential of a cell is lowered, which may trigger the opening of K_{ir} channels to prevent excessive hyperpolarization (Nelson and Quayle, 1995).

K^+ released from neurons has been proposed to regulate neuronal artery diameter (Nelson and Quayle, 1995). Elevated $[K^+]_o$ (>10 mM) has been observed during ischemic and hypoxic events and lower concentrations (~3 mM) have been observed during normal physiological function (Silberberg and van Breemen, 1992). $[K^+]_o$ may dilate cerebral arteries by activation of K_{ir} channels. When $[K^+]_o$ was raised (from 5–6 to 10–16 mM), rat cerebral arteries were hyperpolarized and dilated (Edwards *et al.*, 1988; Knot *et al.*, 1994; Knot *et al.*, 1996). This response was blocked by Ba^+ (<10 μM), but was not reversed by other K–channel antagonists, receptor antagonists, or the removal of the endothelium (Edwards *et al.*, 1988; Knot *et al.*, 1994; Knot *et al.*, 1996). Rat and canine coronary arteries have also been dilated by $[K^+]_o$, which has led to the

suggestion that $[K^+]_o$ may be an EDHF in the cerebral vasculature (Nelson and Quayle, 1995).

The role of K_{ir} channels in disease has not been fully explored. However, if the underlying disease resulted in cell lysing, the elevated $[K^+]_o$ would trigger neighboring cells to increase potassium uptake by the Na^+–K^+–ATPase pump and K_{ir} channels. This might prevent the elevated $[K^+]_o$ from depolarizing neighboring cells, which could possibly initiate a kindling event.

iii. K_{ATP} channels

The K_{ATP} channel was first isolated in cardiac muscle (Noma, 1983). Since then, K_{ATP} channels have been observed in rabbit mesenteric artery (Quayle *et al.*, 1994), rabbit pulmonary artery (Clapp and Gurney, 1991), porcine and canine coronary artery (Dart and Standen, 1993; Xu and Lee, 1994), rat, rabbit and guinea pig portal vein (Noack *et al.*, 1992; Beech *et al.*, 1993; Pfründer *et al.*, 1993), guinea pig urinary bladder (Bonev and Nelson, 1993), and guinea pig gallbladder (Zhang *et al.*, 1994).

The K_{ATP} channel was cloned from rat kidney and human brain (Stoffel *et al.*, 1995; Krishnan *et al.*, 1995). The structure of the K_{ATP} channel suggests that it is a member of the K_{ir} family and is composed of two transmembrane domains (Nelson and Quayle, 1995). K_{ATP} channels are a heteromultimer composed of a K_{ATP} protein of the K_{ir} family coupled with a member of the sulfonylurea receptor (SUR) family (Inagaki *et al.*, 1996). The stoichiometry suggests a tetramer of coupled dimers ($(Kir/SUR)_4$) (Inagaki *et al.*, 1997; Shyng and Nichols, 1997). A

K_{ATP} clone (73 pS) with mRNA expressed in brain, skeletal muscle, cardiac muscle, and pancreatic beta–cells was blocked by external barium, tolbutamide, quinine and by internal ATP (Sakura *et al.*, 1995).

K_{ATP} single channel conductance is divided into two classes, small–intermediate and large. Small–intermediate conductance K_{ATP} channels (15 – 50 pS, $K_{i/o}$ = high and symmetrical) have been observed in single VSMCs from rat and rabbit portal vein and guinea pig urinary bladder. A small–intermediate K_{ATP} channel (35 pS, $K_{i/o}$ = 143 mM) was observed in pig coronary artery VSMCs (Dart and Standen, 1993). Large conductance K_{ATP} channels (130 – 260 pS, $K_{i/o}$ = high and symmetrical) have been observed in rat and rabbit mesenteric artery (Standen *et al.*, 1989), porcine coronary artery (Inoue *et al.*, 1989), rabbit renal afferent arteriole (Lorenz *et al.*, 1992), and canine aorta (Nelson and Quayle, 1995). In rat portal vein, a large K_{ATP} channel (50 pS, $K_{i/o}$ = 130/60 mM) was inhibited by ATP (K_i = 11 – 23 μM) whereas a small K–channel (22 pS) was activated by ATP (Zhang and Bolton, 1996). Though both K–channels were inhibited by glybenclamide, only the small channel was activated by the potassium channel openers levcromakalim and pinacidil. These results suggest the existence of multiple K_{ATP} channel sub–types.

K_{ATP} channels show little or no voltage–dependence. Intracellular ATP inhibits K_{ATP} currents with a half–inhibition (K_i) ranging from 30 – 350 μM, depending upon tissue type (Nelson and Quayle, 1995). Conversely, intracellular ADP and other diphosphates increase K_{ATP} single channel activity in rabbit (Beech *et al.*, 1993) and guinea pig (Pfründer *et al.*, 1993) portal vein cells.

Glybenclamide inhibits K_{ATP} channels selectively in the nanomolar range (K_i = 20 – 100 nM) in rabbit portal vein (Beech *et al.*, 1993) and canine coronary artery (Xu and Lee, 1994). Glybenclamide (10 μM) has no effect on the other K–channels found in arterial smooth muscle cells (Nelson and Quayle, 1995). 4–Morpholinecarboximidine–1–adamantyl–*N'*–cyclohexylhydrochloride (U – 37883) inhibits K_{ATP} channels with a half inhibition constant (K_i) of 0.8 μM. Barium and TEA are non–selective for K_{ATP} channels and have half inhibition constants (K_i) of 100 μM and 7 mM, respectively (Nelson and Quayle, 1995).

Many antihypertensive drugs – including minoxidil sulfate, diazoxide, pinacidil, nicorandil, and cromakalim – vasodilate by opening K_{ATP} channels. Glybenclamide reverses the vasodilation of all potassium channel openers. Cromakalim and pinacidil directly activate K_{ATP} channels in porcine coronary artery (Dart and Standen, 1993), canine coronary artery (Xu and Lee, 1994), rabbit mesenteric artery (Quayle *et al.*, 1994), rabbit pulmonary artery (Clapp and Gurney, 1991), rabbit portal vein (Beech *et al.*, 1993), and guinea pig urinary bladder (Bonev and Nelson, 1993).

K_{ATP} channels have been implicated in the metabolic regulation of blood flow. Under hypoxic conditions, intracellular ATP decreases while ADP increases, and K_{ATP} channels are activated. The opening of K_{ATP} channels results in glybenclamide–sensitive dilation in coronary, cerebral, renal, and skeletal muscle blood vessels (Nelson and Quayle, 1995). It is believed that blood vessel dilation increases circulation to the hypoxic region to prevent tissue necrosis. Adenosine is a potent vasodilator and membrane hyperpolarizing agent released

from cardiac myocytes. Dart and Standen (1993) observed that adenosine can act at a specific receptor (A_1) to induce glybenclamide–sensitive dilations in porcine coronary artery smooth muscle cells.

K_{ATP} channels are implicated in the modulation of resting membrane potential in rat mesenteric artery (Garland and McPherson, 1992). There is also evidence for K_{ATP} modulation of resting tone in coronary circulation (Nelson and Quayle, 1995). Glybenclamide depolarizes and constricts mesenteric, coronary, and hamster cheek pouch arterioles. However, glybenclamide has no effect on resting tone in cerebral, pulmonary, or renal arteries (Nelson and Quayle, 1995).

Reactive hyperemia, or increased blood flow, occurs in arteries following occlusion. In coronary and skeletal muscles, reactive hyperemia is attenuated by glybenclamide, which suggests a K_{ATP} –dependent vasodilation. Glybenclamide also disrupts coronary and cerebral artery auto–regulation in response to changes in perfusion pressure (Nelson and Quayle, 1995).

iv. *K_{Ca} channels*

Calcium–dependent potassium (K_{Ca}) channels form the broadest class of K–channels. Membrane depolarization and intracellular calcium activate K_{Ca} channels. K_{Ca} channels have been observed in rat TA (Bolzon *et al.*, 1993), and in almost every type of smooth muscle, including rabbit portal vein (Beech and Bolton, 1989a; Beech and Bolton, 1989b) and guinea pig mesenteric artery (Benham *et al.*, 1986).

K_{Ca} single channels are divided into three principal classes of unitary conductance, small K–channels (SK_{Ca}, 10 – 15 pS), intermediate K–channels (IK, 20 – 60 pS), and large K–channels (BK_{Ca}, 200 – 300 pS) (Brayden, 1996). BK_{Ca} channels are commonly observed in many tissue types, including most mammalian smooth muscle preparations (Nelson and Quayle, 1995). BK_{Ca} channels have also been found in non–mammalian VSMCs, such as the stomach muscularis of the toad *Bufo marinus* (Singer and Walsh, 1986).

A gating kinetics model proposes that calcium binding to the closed K_{Ca} channel is the rate determining step in the activation pathway, and that calcium unbinding is the rate limiting step in the deactivation process (DiChiara and Reinhart, 1995). This suggests that calcium and not voltage is the principal modulator of K_{Ca} channel activity.

K_{Ca} channels are comprised of two subunits, α and β (Kaczorowski *et al.*, 1996). The α subunit (pore) is a member of the **slo** K_{Ca}–channel family and forms the ion conducting pore. The β subunit (tail) is a membrane–spanning protein that contributes to channel gating and pharmacology (Kaczorowski *et al.*, 1996).

Atkinson *et al.* (1991) cloned the first K_{Ca} channel from the *Drosophila slo* gene (*dslo*). K_{Ca} channels have six hydrophobic regions, S1 through S6. H5, the putative pore region, is found between S5 and S6. The hydrophobic domains (S1 – S6) were compared with previously cloned K_v channels to examine the degree of conservation between families of channels. The degree of conservation within the family of *Drosophila* K_v channels (Shaker, Shab, Shal, and Shaw) is ~ 40% (Wei *et al.*, 1990; Salkoff *et al.*, 1992). There is a high degree of conservation between

species. For example, when *Drosophila* and mice K_v channels are compared, the degree of conservation is at least 55% (Shaw, mouse and fly) and often higher (Shaker, 70%; Shab, 75%; Shal, 82%) (Salkoff *et al.*, 1992). Overall, *dslo* shares only 20% identity with other *Drosophila* K–channels (Salkoff *et al.*, 1992). This suggests that K_{Ca} channels comprise a family that is distinct from K_v channels. The initial cloning of the *Drosophila slo* gene (Atkinson *et al.*, 1991) was followed by the cloning of alternative splice variants and channel characterization (Adelman *et al.*, 1992).

To explore the function of the *dslo* gene transcripts, Adelman *et al.* (1992) patch clamped *Xenopus* oocytes that had been injected with *dslo* RNA transcribed from cDNA. A functional K_{Ca} channel was expressed with an intermediate single channel conductance (123 pS; $K_{i/o}$ = 120 mM), a linear current–voltage relationship, and a reversal potential of 0 mV (Adelman *et al.*, 1992). The channel exhibited marked calcium–dependence and was blocked by TEA, but not by ChTX or apamin (Adelman *et al.*, 1992). Various splice variants were compared, and all had the same unitary conductance but different kinetic and calcium binding properties (Adelman *et al.*, 1992). This variability between alternatively spliced variants may account for the differences in function in different cell types. Further variability may also be introduced through post–translational modification of the *slo* transcript, such as phosphorylation, which does not occur in the *Xenopus* oocyte.

Wei and Salkoff isolated the first mammalian gene coding for a K_{Ca} channel (Butler *et al.*, 1993). This gene, derived from mouse brain and skeletal muscle, was named mouse *Slo* (*mSlo*), and shares >60% amino acid identity with *dslo* (Adelman

et al., 1992; Butler *et al.*, 1993). Channel properties were characterized by injecting *mSlo* RNA derived from mouse brain cDNA into *Xenopus* oocytes. Inside–out patches revealed a K–channel with a large single channel conductance (272 pS; $K_{i/o}$ = 156 mM) that exhibited a linear current–voltage relationship and a reversal potential of ~ 0 mV (Butler *et al.*, 1993). The channel was Ca^{2+}–dependent, and much more sensitive to intracellular calcium than the channel derived from *dslo*. Unlike **dslo**, **mSlo** was blocked by ChTX, IbTX, and TEA (Butler *et al.*, 1993).

Wei and Salkoff observed that *dslo* and *mSlo* share a high degree of conservation in the core region (S1 – S6) and in the tail region (S7 – S10) but that there was a highly disparate region between S8 and S9 (Wei *et al.*, 1994). Wei and Salkoff hypothesized that the injection of tail or core regions as separate material could still produce functional cRNAs from each half (Wei *et al.*, 1994). Co–injection of mouse and fly crossovers (*mSlo* core and *dslo* tail; or *mSlo* tail and *dslo* core) resulted in functional channels different from same–same injections. It was observed that the **mSlo** tail is much more sensitive to calcium than the **dslo** tail, which is strong evidence that the tail region contained a calcium–binding site (Wei *et al.*, 1994). A number of functional channels can be created through splice variation. Many similar but distinct channels can be encoded by a single gene, which makes efficient use of genetic material.

BK_{Ca} channels are selectively blocked by TEA (K_i = 200 μM), ChTX (K_i = 10 nM), and IbTX (K_i < 10 nM) (Brayden, 1996). Though TEA non–selectively blocks other K–channels at high concentrations, most BK_{Ca} channels are blocked by sub–millimolar concentrations. SK_{Ca} channels are effectively

inhibited by apamin (K_i = 0.3 nM) (Garcia *et al.*, 1991). Tedisamil is a non–selective inhibitor of both K_{dr} and K_{Ca} channels in guinea pig portal vein (Pfründer and Kreye, 1991; Pfründer and Kreye, 1992).

K_{Ca} channels have been implicated in the regulation of myogenic tone. Myogenic tone refers to the spontaneous constriction observed when intravascular pressure depolarizes smooth muscle cells in resistance vessels. The depolarization and increase in $[Ca^{2+}]_i$ associated with constriction are capable of activating K_{Ca} channels. K_{Ca} channel opening would increase potassium efflux and re–polarize the cell. TEA, ChTX, and IbTX depolarized and constricted resting cerebral and coronary arteries, which suggests that K_{Ca} channels are intrinsically involved in the regulation of membrane potential (Brayden and Nelson, 1992; Rusch *et al.*, 1996).

Endogenous activators of K_{Ca} channels play a fundamental role in the modulation of arterial tone. Nitric oxide, which is believed to be the principal EDRF, directly activated BK_{Ca} channels from rabbit aorta (Bolotina, *et al.*, 1994) and cultured porcine coronary artery VSMCs (Miyoshi and Nakaya, 1994). K_{Ca} channels have been activated by adenosine in coronary artery (Cabell, *et al.*, 1994), PKA in coronary artery (Scornik *et al.*, 1993), and cGMP in cerebral and canine coronary arteries (Robertson *et al.*, 1993; Taniguchi *et al.*, 1993).

SK_{Ca} channels may play a significant role in EDR. Apamin blocks a NO–independent, acetylcholine–induced hyperpolarization and relaxation in rat mesenteric (Chen and Cheung, 1997; Adeagbo and Triggle, 1993) and rabbit mesenteric artery (Murphy and Brayden, 1995).

In neuronal cells, activation of BK_{Ca} channels contributes to action–potential repolarization, while SK_{Ca} channels are thought to underlie the afterhyperpolarization (AHP) (Sah, 1996). AHPs in neurons are divided into two distinct types that are separated by kinetic and pharmacological criteria. One type of AHP can be explained by activation of SK_{Ca} channels while a novel type of K_{Ca}–channel is believed to account for the other (Sah, 1996). Current research suggests that the kinetic differences between apamin–sensitive and apamin–insensitive slow AHPs are not attributable to intrinsic gating differences between the two subtypes (Vergara *et al.*, 1998).

K_{Ca} channels regulate neuronal excitability, and modulate interspike interval and spike frequency adaptation (Vergara *et al*, 1998). Neuronal K_{Ca} channels were activated by calcium via specific and co–localized Ca^{2+}–channels (Marrion and Tavalin, 1998). In hippocampal neurons, BK channels were activated by N–type Ca^{2+}–channels whereas SK channels were activated by L–type Ca^{2+}–channels. The delay between the opening of L–type Ca^{2+}–channels and SK channels suggested that these channels were 50 – 150 nm apart. P/Q–type Ca^{2+}–channels did not couple to either BK or SK channels (Marrion and Tavalin, 1998).

limitations of current knowledge

The regulation of VSMC contractility is modulated by the activity of calcium, chloride, and potassium channels. Activation of K–channels in VSMCs can result in vasodilation that increases blood flow and decreases blood pressure.

The modulation of K–channels by vasoactive signals is critical to the regulation of arterial tone. The literature suggests that EDHF may be an inducible factor. The current work investigated the hypothesis that EDHF is an inducible non–NO transferable factor which can be released from conducting arteries such as the rat TA and SMA.

The targets and identity of EDHF are currently unknown. However, EDHF–mediated hyperpolarization involves K–channels, even if they are not direct targets. Resistance arteries have been poorly characterized in whole tissue experiments due to canulation difficulty. However, resistance arteries are important regulators of blood pressure, which suggests that resistance artery K–channels are logical targets of EDHF.

The current work investigated the notion that EDHF is an inducible and transferable factor released from the endothelium of conducting arteries (TA and SMA) that can modulate the activity of target TA VSMCs. As well, the properties of novel K_{Ca} channels in single VSMCs from rat mesenteric resistance artery (MRA) were characterized.

BACKGROUND

ACh–induced release of EDHF in rat superior mesenteric artery (SMA) (+LNNA) was partially blocked by the large–conductance K_{Ca}–channel blocker ChTX and was blocked more by the small–conductance K_{Ca}–channel blocker apamin. The combination of apamin plus ChTX abolished ACh–induced endothelium–dependent hyperpolarization (Chen and Cheung, 1997).

HYPOTHESIS

Endothelium–dependent hyperpolarizing factor is an inducible and transferable factor that activates potassium (ion) channels to effect hyperpolarization of vascular smooth muscle cells (VSMCs).

OBJECTIVES

Patch clamp techniques were employed *i.* to demonstrate that SMA and TA donor tissue can release an ACh–induced, transferable EDHF, and *ii.* to identify and characterize the novel K–channels in freshly isolated VSMCs from rat mesenteric resistance artery (MRA), the putative targets of EDHF. The following objectives were pursued:

i. To characterize ACh–induced release of donor TA or SMA EDHF on TA VSMC membrane potential.

ii. To characterize the K–channel pharmacology of TA and MRA potassium currents.

iii. To characterize the biophysical properties of the novel MRA VSMC K–channels.

METHODS

I. Cell Isolation

The experiments performed were conducted using freshly isolated vascular smooth muscle cells (VSMCs) from the rat tail artery (TA), and the mesenteric resistance arteries (MRA) (~ 100 – 150 μm diameter) that branch from the superior mesenteric artery (SMA) (~ 600 μm). TA digestion followed a technique developed in our laboratory (Bolzon and Cheung, 1989). Briefly, 0.5 – 1 cm long TA segments from male Wistar rats (10 – 12 weeks, Charles River Labs, Inc., Wilmington, MA) were excised and suspended in a heated organ chamber. Arteries were tied with silk sutures to polyethylene tubing (PE–10) that was infused by a syringe pump (model 22, Harvard Apparatus).

Tail arteries were internally perfused with a Ca^{2+}– and Mg^{2+}–free HEPES buffer solution (CMF Hanks) at 37°C for 30 – 40 minutes (0.2 ml/min,). Enzyme perfusion followed with CMF Hanks containing collagenase (0.02%, type II, Sigma, 150 U/ml), dithiothreitol (DTT, 0.025%, Sigma), and papain (0.12%, BDH, 20 U/ml) for 50 – 60 minutes (0.1 ml/min).

Mesenteric resistance artery (MRA) VSMCs were enzymatically digested with collagenase, dithiothreitol (DTT), and papain in CMF Hanks using a protocol adapted from Bolzon *et al.* (1989). Superior mesenteric arteries were excised and cleaned of fat and connective tissue. Small regular resistance arteries (MRA) branched frequently along the SMA. MRAs were gently cut from the SMA and opened with fine forceps and scissors to expose the luminal surface. Digestion was performed at 37° C for 100 – 120 minutes in CMF Hanks with

collagenase (0.01%, type II, Sigma, 150 U/ml), dithiothreitol (DTT, 0.0125%, Sigma), and papain (0.06%, BDH, 20 U/ml). Single cells were obtained by gentle trituration of the digested tissue onto 35 mm round culture dishes. Cell viability, determined from visual inspection of population cell length and rate of spontaneous contraction over time or to electrode contact, was similar to TA VSMCs and all experiments were performed with fresh cells at room temperature (20 – 22° C) in a 3 – 5 hour period following digestion. Typically, 1 to 4 cells / patches could be recorded each day, but viable cells were not obtained every day.

II. Recording Technique

All experiments were performed within 3 – 5 hours following digestion and cell isolation. Culture dishes containing harvested cells were mounted on the stage of an inverted phase microscope (Olympus) and constantly perfused with bathing solution at a rate of 1 – 2 ml/min. Experiments were performed at room temperature (20 – 22 °C) using the tight seal patch clamp technique (Hamill *et al.*, 1981). Electrodes were pulled from borosilicate glass tubing (o.d. 1.5 mm, i.d. 0.8 mm, A–M Systems, Everett, WA) with a Flaming Brown P–80 pipette puller (Sutter Instruments, Novato, CA). Electrode tips were fire–polished prior to use with a heated platinum wire coated with glass. Pipette resistance was 2 – 5 MΩ when filled with CMF Hanks solution. Electrodes were positioned using a Starrett vernier manipulator (Newport Corp., Fountain Valley, CA) and cells were patched using a Burleigh PCS250 piezo–electric micromanipulator. Prior to

forming a seal, the null potential was manually zeroed. The pipette–membrane seal was in the range of 1 – 10 GΩ.

For measurement of cellular membrane potential, the nystatin perforated patch technique was employed. Nystatin (Sigma, 200 μg/ml) was included in the pipette tip to perforate the cell membrane with pores so that the membrane potential could be regulated without loss of cellular material. Following seal formation, the membranes were slowly perforated (~ 2 – 3 minutes). In tracking mode (I = 0 pA), the seal was monitored by applying a 5 mV oscillating pulse (line frequency, 50 – 60 Hz).

Cell capacitance was calculated to determine the membrane surface area (~ cell size) and was used to normalize whole cell current populations from cells of different size (current / unit area). Cell capacitance was obtained by integrating the area under the curve (formed by the capacitive spike) by the voltage step (± 2.5 mV). The capacitive time constant was obtained by fitting a single exponential to the decay curve of the capacitive spike. The series resistance was calculated by dividing the capacitive decay time constant by the cell capacitance. The formation of a nystatin perforated patch was indicated by a decrease in the series resistance, approximately 80% of which was compensated. Leak current was negligible and was not subtracted.

For whole–cell recording, the patch membrane was disrupted by increased suction after formation of a gigaohm seal. For inside–out patch clamp recording, the cell membrane was sealed with light suction and the pipette was withdrawn to remove a patch of membrane.

In current clamp mode, current injection was required to stabilize VSMCs at a membrane potential near the RMP, which would otherwise slowly spontaneously depolarize and contract. However, accurate control of membrane potential while in current clamp mode was not possible with the amplifier used (Axopatch 200). The Axopatch 200 was designed for voltage clamp and only coarse increments of current injection (mA range) were available. As such, the smallest increments in current resulted in wide ranges of membrane potential and only a few cells that were maintained within physiological ranges could be used. The current was adjusted to maintain a stable membrane potential (± 2 mV, 2 – 5 minutes) for each VSMC that varied between –45 mV and –70 mV. A superior amplifier designed for current clamp (pA range current injection) would have maintained the membrane potential of all VSMCs near the RMP (~ –50 mV).

III. Solutions and Chemicals

L–NNA (30 μM) was used to inhibit NO synthesis. Previous experiments demonstrated that 30 μM L–NNA was sufficient for the inhibition of NO synthesis in SMA and that higher concentrations or the further addition of S–methyl–L–thiocitrulline (10 μM) were no more effective (Chen and Cheung, 1997). Atropine (1 μM) was used to prevent direct ACh–induced depolarization of VSMCs. Glybenclamide (300 nM) was added to the extracellular solution and ATP (1 mM) to the intracellular solution to inhibit K_{ATP} channels. Nifedipine (1 μM) was included to inhibit L–type Ca^{2+} channels. The solutions used for each different protocol are in the following list:

i. solutions for cell isolation

CMF Hanks

CMF Hanks + collagenase + DTT + papain

ii. solutions for recording membrane potential (Results I)

internal perfusion (SMA–IP, TA–IP)
pipette: HPIS + nystatin (200 μg/ml)
bath line: Hanks + atropine (1 μM)
artery line: Hanks + L–nitro–N^{ω}–arginine (L–NNA, 30 μM)

pinned inverted tubes (SMA–PIT)
pipette: HPIS + nystatin (200 μg/ml)
bath line: Ringers + L–NNA (30 μM)

inverted rings in plastic pipette tip (SMA–IRPT)
pipette: HPIS + nystatin (200 μg/ml)
bath line: Hanks + atropine (10 μM) + nifedipine (1 μM)
artery line (plastic pipette): Hanks ± L–NNA (30 μM)

iii. whole–cell recording (current density, pharmacology)

pipette: HPIS (500nM $[Ca^{2+}]_i$) + ATP (1 mM)
bath line: Hanks + nifedipine (1 μM) + glybenclamide (300 nM)

iv. inside–out recording

single channel amplitude
pipette: K–Hanks, 100 mM $[K^+]_o$, 50 mM $[K^+]_o$, or 5.5 mM $[K^+]_o$;
+ nifedipine (1 μM) + glybenclamide (300 nM)
bath line: HPIS + ATP (1 mM)

open probability (NP_o)
pipette: K–Hanks + nifedipine (1 μM) + glybenclamide (300 nM)
bath line: HPIS + ATP (1mM)

The solutions named above are defined in the following table:

Table M–1. Solutions.

species	extracellular solutions (mM)							intracellular solution (mM)
	Ringers	CMF Hanks	Hanks	K–Hanks[1]				high–potassium (HPIS)
				150	100	50	5.5	
NaCl	120	137	137	0	48.7	95.4	137	
KCl	5	5.5	5.5	150	100	50	5.5	150
KH_2PO_4		0.4	0.4	0.8				
NaH_2PO_4	1	0.4	0.4					
$NaHCO_3$	25	4.2	4.2	4.2				
glucose	11	5.6	5.6	5.6				
HEPES		10	10	10				10
$MgCl_2$			1	1				1
$MgSO_4$	1							
EGTA								5
$CaCl_2$	2		2	2				variable[2]
pH (adjusted with)	~7.4 (5%CO_2–95%O_2)	7.4 (NaOH, 10mM)	7.4 (NaOH, 10mM)	7.4 (KOH, 1mM)				7.3 (TRIS)

Notes: *1.* If the external potassium concentration ($[K^+]_o$) of K–Hanks is not mentioned, it is assumed to be 150 mM (symmetrical solutions).

2. The free calcium is determined from the Fabiato program (Fabiato, 1988) and is displayed in the following table:

Table M–2. Fabiato Calculation of Free Calcium.

total calcium (bound and free)	free calcium[1]
0 mM	0 nM
1.64	50
3.00	155
3.72	300
4.15	500
4.40	750
4.54	1000

Notes: *1.* The free calcium calculation takes into account all interacting species, not just Ca^{2+}–EGTA, as well as temperature and pH.

All salts in Table M–1 (NaCl, KCl, KH_2PO_4, NaH_2PO_4, $MgCl_2$, $MgSO_4$, and $CaCl_2$, BDH Chemicals, Fisher Sales; EGTA, Sigma) were made into stock

solutions of 10x and replaced each week. Final solutions were made every second day or every day by diluting the concentrated salt solution with the unstable compounds ($NaHCO_3$, glucose, HEPES, BDH Chemicals, Fisher Sales; Na_2ATP, Sigma). All water used was double distilled and de–ionized (Milli–Q water system, Millipore); pH adjustment was done with NaOH (Sigma), KOH (Fisher Scientific), or TRIS (BDH).

Nifedipine and glybenclamide were made into 1000x stock solutions (1 mM and 300 μM, Sigma) in DMSO. The final concentration of DMSO in the bath is less than 0.1%, which has been shown to have no effect on smooth muscle membrane currents (Xiong *et al.*, 1995). Charybdotoxin (ChTX) (Alomone Lab., Jerusalem, Israel) and iberiotoxin (IbTX) (Alomone) were made into stock solutions of 5 μM in water. Tetraethylammonium (TEA) (Sigma) was prepared as 1 M stock solution in water. Apamin (Sigma) was prepared as a 0.3 mM stock solution in water. 4–aminopyridine (4–AP) (Sigma) was prepared as a 1 M stock solution in water. All solutions were stored frozen (–20°C) except TEA and 4–AP (22°C). All other chemicals were obtained from Sigma and were dissolved directly into the solutions.

IV. Data Acquisition

Data was collected using a low noise amplifier (Axopatch 200, CV 201 headstage, Axon Instruments, Foster City, CA) and converted to a digital signal (Labmaster TL–1 analog–to–digital interface) for recording to a personal computer (Acer 486–DX 33MHz with Ocean V 256 MB magnetic optical SCSI–2

storage device). Data acquisition and analysis was performed using pClamp6.1.1 software (Axon Instruments). Currents were recorded and filtered at 2 kHz (low–pass filter, 8–pole Bessel). Whole cell currents were electronically compensated (Axopatch 200) to minimize the series resistance (electrode resistance), the fraction of command voltage that drops across the electrode and is not seen by then cell. This was maximized by a tight GΩ seal and, following suction induced disruption of the membrane, a reduction in the membrane time constant coupled with an increase in cell capacitance (measured by an increased current under small depolarizing pulses).

Current clamp experiments were used to measure the membrane potential of single TA VSMCs. The type of amplifier used disallowed fine control of current injection. Injected current was adjusted to maintain a membrane potential near the RMP (~ –50 mV), while the range of stable membrane potentials for different VSMCs varied (–45 to –70 mV). The potential of individual cells was stable within a 1 – 2 mV range for several minutes (2 – 5 minutes).

V. Data Analysis

Figures and curve fitting were performed by SigmaPlot 5.00 (DOS, Jandel Scientific, San Rafael, CA). Data generated by linear regression and non–linear fitting (SigmaPlot 5.00) are presented as means ± standard deviation (SD) (SigmaPlot standard output). Linear regression used the method of least squares. Non–linear curve fitting employed user–entered functions with multiple

parameters (variables) with small Markov steps to ensure convergence (>1000 iterations).

Channel open probability was calculated from extended segments of continuous recording (~ 5 minutes, ≥2000 events, pClamp6.6.2). Open probability was calculated as the fraction of open time to the total time (NP_o).

Data from multiple experiments (NP_o, membrane potential, etc.) are presented as means ± standard error of mean (s.e.m.). The MRA NP_o data ($\Delta[Ca^{2+}]_i$, ΔV) were reduced from the initial set by eliminating values outside one standard deviation. The remaining set is presented as mean ± standard error of mean (s.e.m.).

Student's t–test was used for statistical comparison and $P<0.05$ was considered significant ($P<0.05$, *; $P<0.01$, **; $P<0.001$, ***).

VI. Experimental Protocol

PART I. Endothelium–dependent Hyperpolarization

To determine the effects of endothelium derived factors on TA VSMCs, experiments were designed which included TA or SMA as donor tissue. Three types of experiments were performed using donor tissue: *i.* internal perfusion (SMA/TA–IP), *ii.* pinned inverted tubes (SMA–PIT), and *iii.* inverted rings in pipette tip (SMA–IRPT).

I.1 The *internal perfusion* (SMA–IP or TA–IP, Figure M–1A; SMA–IP, RI–1B) technique was used to determine if an intact endothelium could release ACh–

induced hyperpolarizing factor(s). The SMA/TA–IP technique had two flow systems. The *artery line* was slowly perfused (0.022 ml/min, continuous pump, model 375A, SAGE Instruments, Orion Research Inc., Cambridge, MA) through an excised artery (6 – 9 mm) sutured with silk to a small length of polyethylene tubing (4 – 5 mm, PE–10) which flowed into the culture dish. The artery was kept moist through slow leak through the artery wall or through leak through small cut arterioles. Artery branches were tied with silk sutures. The slow flow through the artery prevented damage due to high pressure or flow rate – no distension or collapse of artery lumen was observed. This separate flow system allowed agents to be introduced in small quantities in the artery line. L–NNA (30 μM) was included in the artery line to inhibit NO synthesis. The *bath line* was perfused 9 fold faster (0.192 ml/min) and oxygenated to maintain single cell viability. The bath line was also perfused with atropine (1 μM) to prevent acetylcholine from directly depolarizing the cells.

The target TA VSMCs were patch clamped using the nystatin perforated patch technique. The recording pipette contained HPIS (500 nM $[Ca^{2+}]_i$) plus nystatin (200 μg/ml). In current–clamp mode, the membrane potential was maintained at approximately the resting potential (–45 to –75 mV). ACh (0.1 μM) was added to the artery line when the TA VSMC membrane potential was stable.

Figure M–1. Diagram of Three Endothelium Donor Tissue Techniques.

Panel A. internal perfusion (SMA/TA–IP): An excised section of superior mesenteric artery (SMA) or tail artery (TA) (6 – 9 mm) was tied off at either end by silk sutures to polyethylene tubing connected to a continuous micropump (0.022 ml/min). The bath line (0.192 ml/min) washed the 35 mm dish, modified by the addition of silicon gel which reduced the total fluid volume (~ 185 – 200 µl) and provided a trench to support the donor artery. The artery was kept moist by slight leak through severed arterioles. Freshly isolated single VSMCs from rat TA were patch clamped near the mouth of the PE tubing. TA and SMA were used as donor tissues, and donor–dependent responses were compared.

Panel B. pinned inverted tubes (SMA–PIT): Two to three short lengths of SMA (4 – 6 mm) were inverted and gently pinned with tungsten wire staples to the sides of a modified 35 mm culture dish. The custom dish was lined with inert silicone gel to reduce bath volume (~ 185 – 200 µl) and provide a footing for the staples. The artery was constantly perfused by a single bath line (0.192 ml/min) positioned directly above. This technique lacked the advantage of the separate artery– and bath–lines of the perfusion technique but was superior in maintaining artery viability. TA VSMCs were patch clamped close (≤0.2 mm) or far (≥1.8 mm) from the nearest edge of exposed endothelium.

Panel C. inverted rings in pipette tip (SMA–IRPT): Small rings (3–5 rings, 2–4 mm) of SMA were inverted and placed in a modified plastic pipette tip. The severed tip of a 10 ml plastic pipette was crimped to prevent the washout of artery rings but permitted the flow of solution. The pipette tip was sealed at the apex with a section of tubing connected to the artery perfusion line (0.022 ml/min). The tip was held by a stereotaxic manipulator, which allowed placement of the artery rings directly above the patch clamped TA VSMC. Bath perfusion (0.192 ml/min, bath volume: ~ 185–200 µl) washed the 35 mm dish, modified by the inclusion of a milled plastic insert.

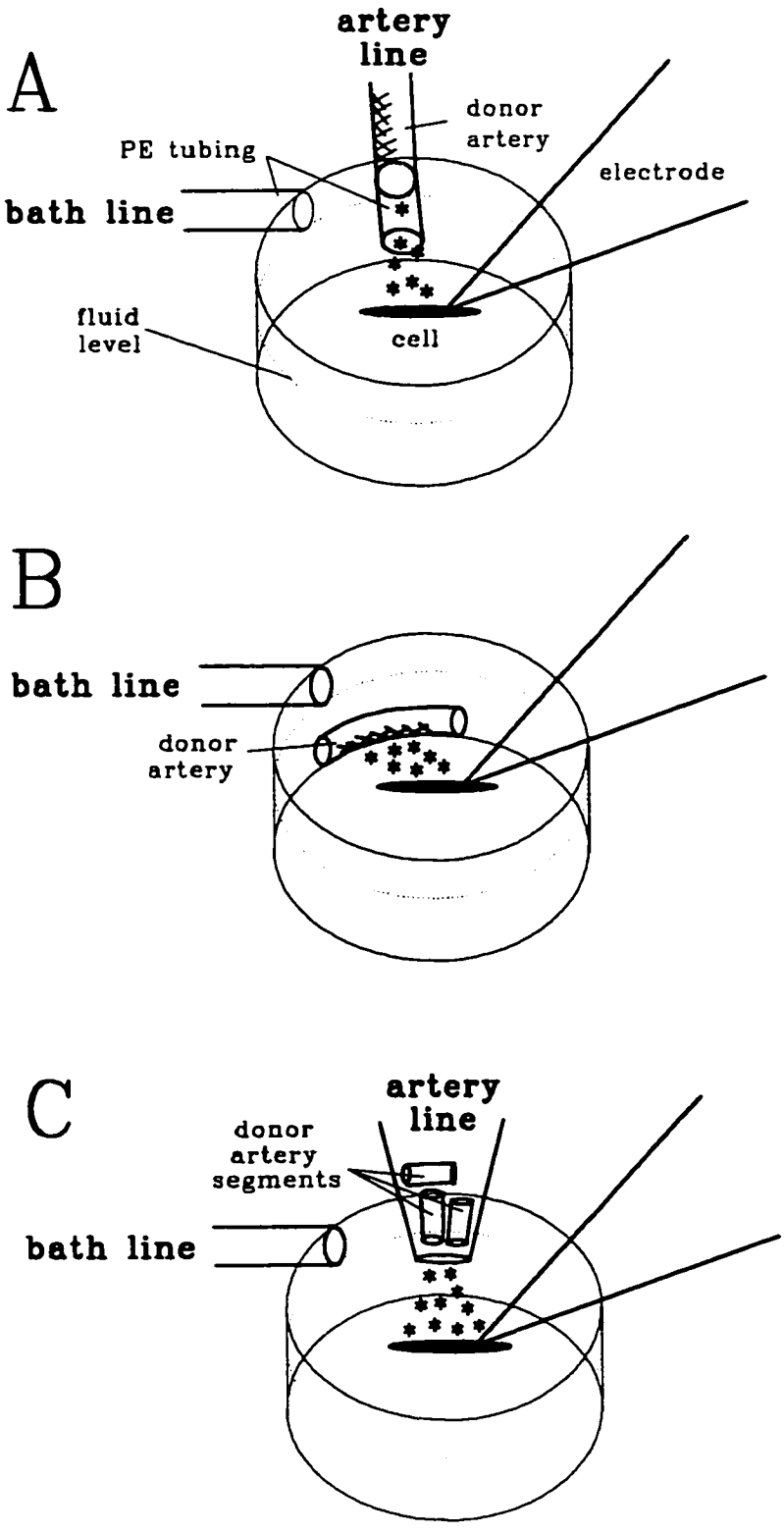
A
artery line
donor artery
PE tubing
electrode
bath line
fluid level
cell
B
bath line
donor artery
C
artery line
donor artery segments
bath line

I.2 The *inverted rings in pipette tip* technique (SMA–IRPT, Figure M–1C, RI–2) was used to determine if ACh–induced endothelium–dependent hyperpolarization was NO–independent. Small rings (3 – 5 rings, 2 – 4 mm) of SMA were inverted and placed in a modified plastic pipette tip. The severed tip of a 10 ml plastic pipette was crimped to prevent the washout of artery rings but permitted the flow of solution. The plastic pipette tip was sealed at the apex with a section of tubing connected to the artery line. The tip was held by a stereotaxic manipulator, which allowed placement of the artery segments directly above the cell studied.

The bath line was washed by Hanks solution with atropine (1.0 μM) to prevent ACh–induced depolarization of VSMCs and with nifedipine (1.0 μM) to block L–type Ca^{2+}–channels. The artery line was perfused with Hanks (control) or with Hanks plus L–NNA (30 μM) to inhibit NO synthesis.

The target TA VSMCs were patch clamped using the nystatin perforated patch technique. The recording pipette contained HPIS (500 nM $[Ca^{2+}]_i$) plus nystatin (200 μg/ml). In current–clamp mode, the membrane potential was maintained at approximately the resting potential (–45 to –75 mV). ACh (control, Hanks: 1, 10 nM; Hanks + L–NNA (30 μM): 0.1, 1 μM) was added to the artery line when the TA VSMC membrane potential was stable.

I.3 The *pinned inverted tubes* technique (SMA–PIT, Figure M–1B, RI–3) was used to determine if ACh–induced EDHF(s) were stable. Two to three short lengths of SMA (4 – 6 mm) were inverted and gently pinned with tungsten wire

staples to the sides of a modified 35 mm culture dish. The custom dish was lined with inert silicone gel to reduce bath volume and provide a footing for the staples. A single bath line positioned directly above the artery provided continuous perfusion. This technique lacked the advantage of the separate artery– and bath–lines of the perfusion technique but was superior in maintaining artery viability. Inversion of short artery tubes required both rapidity and delicacy to prevent endothelium removal due to stretch / shear, physical abrasion, and hypoxia. This technique provided viable tissue with an intact endothelium that was able to release inducible and transferable relaxing and hyperpolarizing factors.

In this configuration, there was no separate bath and artery perfusion. The bath solution flowed over the tissue and washed the TA VSMC. Ringers solution was used to maximize tissue longevity plus L–NNA (30 μM) to inhibit NO synthesis.

The target TA VSMCs were patch clamped using the nystatin perforated patch technique. The recording pipette contained HPIS (500 nM $[Ca^{2+}]_i$) plus nystatin (200 μg/ml). The donor–target distance was measured using the microscope vernier positioning table from the donor endothelium leading edge closest to the target TA VSMC. ACh (1 nM – 1 μM) was added to the bath line when the TA VSMC membrane potential was stable.

1.4/5 The *internal perfusion* technique (TA–IP, RI–4; SMA–IP, RI–5) was used to determine if both TA and SMA can release EDHF. The TA had no branches and was perfused as per the SMA. Regardless of donor, the artery line was

perfused with Hanks plus L–NNA (30 μM) and the bath with Hanks plus atropine (1 μM). The target TA VSMCs were patch clamped using the nystatin perforated patch technique. The recording pipette contained HPIS (500 nM $[Ca^{2+}]_i$) plus nystatin (200 μg/ml). ACh (0.1, 1 μM) was added to the artery line when the TA VSMC membrane potential was stable.

I.6 The SMA–IRPT technique was used with voltage–clamped TA VSMCs (RI–1C) to determine if ACh–induced EDHF could affect whole–cell K–channel spiking currents.

The SMA donor tissue (IRPT) was constantly perfused by Hanks solution. The bath was washed by Hanks solution plus atropine (1.0 μM) to prevent ACh depolarization and nifedipine (1.0 μM) to block L–type calcium channels. The recording pipette contained HPIS (500 nM $[Ca^{2+}]_i$) plus nystatin (200 μg/ml). The TA VSMC membrane potential was held at –50 mV and ACh (10, 100 nM) was added when spiking currents were stable. When the ACh–induced effect was stable, TEA (5 mM) was added.

PART II. Properties of Mesenteric Resistance Artery VSMC

II.1 Single MRA and TA VSMCs were resolved under reverse phase light microscopy and their length and diameter measured. The technique used to digest MRA tissue to obtain single VSMCs is described in Methods I. Cell Isolation.

II.2 Single MRA and TA VSMCs were patch clamped to determine their passive membrane properties. MRA and TA VSMCs were patch clamped using the whole–cell technique. The bath was perfused with Hanks plus nifedipine (1 μM) plus glybenclamide (300 nM). The recording pipette contained high potassium (500 nM $[Ca^{2+}]_i$) plus ATP (1 mM).

Cell size can be approximated from the capacitance of a cell. In the whole–cell configuration, VSMCs were voltage clamped at a holding potential of –50 mV, near the resting membrane potential of rat SMA VSMCs (Chen and Cheung, 1997). When the membrane was depolarized by 5 mV, only passive capacitive current was elicited. The capacitance was calculated by integrating the area under the curve of a small transient depolarizing spike. The capacitance decay time constant was calculated by fitting a single exponential to the decay curve of the capacitance spike. The series resistance was calculated by dividing the time constant by the capacitance (Hille, 1992).

II.3 Single MRA VSMCs were patch clamped using the whole–cell technique to determine whole–cell current density.

Whole–cell current density was used to compare the total current relative to the cell size which was derived from the capacitance. Single MRA VSMCs were patch clamped in the whole–cell configuration. Cells were bathed in Hanks plus nifedipine (1 μm) plus glybenclamide (300 nM). The recording pipette contained high potassium (500 nM $[Ca^{2+}]_i$) plus ATP (1 mM). Membrane potential was clamped at –50 mV to approximate the resting membrane potential

and depolarized to +50 mV in 10 mV increments for 500 ms. The current–voltage relationship was derived by normalizing the whole–cell current to the cell size. The current density was derived by dividing the average current in the plateau region (300 – 500 ms after step trigger) by the cell capacitance.

II.4 Single MRA VSMCs were patch clamped using the whole–cell technique to determine whole–cell pharmacology.

Whole–cell pharmacology of MRA VSMCs was used to determine the effect of K–channel antagonists (apamin, IbTX, 4–AP) on whole–cell current, and the responses compared to TA VSMCs. Single MRA and TA VSMCs were patch clamped using the whole–cell technique. Cells were bathed in Hanks plus nifedipine (1 μm) plus glybenclamide (300 nM). The recording pipette contained high potassium (500 nM $[Ca^{2+}]_i$) plus ATP (1 mM).

Whole–cell pharmacology of MRA and TA VSMCs focused on the effect of apamin, which has been shown to be an important blocker of endothelium dependent hyperpolarization in SMA (Chen and Cheung, 1997). Previously, apamin was found to have little or no effect on TA VSMC whole–cell current in our laboratory. When the MRA or TA whole–cell current was stable, apamin (0.3 μm) was added to the bath.

When patch clamped using the whole–cell technique, TA VSMCs exhibited two components of time–dependent outward current (Bolzon *et al.*, 1993). Cells maintained at a holding potential of –80 mV were depolarized to +60 mV (10 mV increments, 500 ms). In this configuration, both components of

outward current were elicited. Starting at –40 mV, small regular currents were elicited which corresponded to the delayed rectifier current (K_{dr}). At potentials above +30 mV, large and noisy currents became dominant. The larger component of outward current corresponded to the calcium–dependent potassium channel current (K_{Ca}). When the holding potential was increased from –80 mV to –40 mV, the K_{dr} component was not observed and only the K_{Ca} current remained. In TA VSMCs, ChTX was selective for K_{Ca} current and 4–AP was selective for K_{dr} current (Bolzon *et al.*, 1993).

MRA and TA VSMCs were patch clamped in the whole–cell configuration and held at –80 mV to elicit K_{Ca} and K_{dr} current, or at –40 mV to elicit K_{Ca} current. The K–channel antagonist IbTX (150 nM) was added to the bath when the currents were stable. When the current stabilized in the presence of IbTX, 4–AP (2 mM) was also added.

PART III. Properties of 4 Types of MRA VSMC K–Channel — Linear Method

III.1 MRA and TA VSMCs were patch clamped using the inside–out technique to determine what types of K–channels were present.

VSMCs were bathed with HPIS containing 155 nM $[Ca^{2+}]_i$. ATP (1 mM) was included in the bath to block ATP–dependent potassium channels (K_{ATP}). The pipette contained K–Hanks solution ($[Ca^{2+}]_o$ = 2 mM) plus glybenclamide (300 nM) to block K_{ATP}–channels and nifedipine (1 μ M) to block L–type Ca^{2+}–channels. In K–Hanks solution, potassium replaced sodium so that symmetrical potassium solutions ($[K]_i$ = $[K]_o$ = 150 mM) would bathe the intracellular and

extracellular sides of an isolated patch. The membrane potential was held at +40 mV to activate K–channels.

III.2 linear method

MRA and TA VSMCs were patch clamped using the inside–out technique under variable membrane potential (–60, –40, –20, 0, +20, +40, +60 mV) to determine the linear conductance of the K–channels. MRA VSMCs were also patch clamped using the inside–out technique under varying external potassium concentration ($[K^+]_o$ = 5.5, 50, 100, 150 mM) to determine the linear conductance of the K–channels.

VSMCs were bathed with HPIS containing 155 nM $[Ca^{2+}]_i$. ATP (1 mM) was included in the bath to block ATP–dependent potassium channels (K_{ATP}). The TA pipette contained K–Hanks ($[K^+]_o$ = 150 mM; $[Ca^{2+}]_o$ = 2 mM) whereas the MRA pipette contained K–Hanks ($[K^+]_o$ = 5.5, 50, 100, or 150 mM; $[Ca^{2+}]_o$ = 2 mM), both with glybenclamide (300 nM) to block K_{ATP}–channels and nifedipine (1 μ M) to block L–type Ca^{2+}–channels. The average recording was at least 2 minutes in length and most were 3 – 5 minutes. In most cases, more than 5000 events were recorded where one event is a change in level which represents a single channel opening or closing.

The constant field equations as derived by Goldman–Hodgkin–Katz predict that, in symmetrical potassium solutions, true K–channels exhibit a linear voltage–dependent change in amplitude. At positive voltages, K–channels open and allow current to flow outward. At negative voltages, current flows inward.

At zero holding potential, no current should be observed. The voltage at which no current flows inward or outward is the reversal potential (K_{rev}).

The cut–off criterion normally applied to measure the opening of a channel is 50%. This means that any opening greater than half the amplitude of the channel is considered an open channel, until the signal drops below the cut–off again. The amplitude of a channel is measured from midpoint in the closed noise signal to midpoint in the open channel noise signal.

The analysis of data from inside–out patches from the MRA VSMC used 75% cut–off criterion. This means that the current of a single channel had to exceed 75% of the open amplitude to be counted as open. It was necessary to deviate from normal practice because the four channel types were similar in amplitude. The four most common channel types – miniK, SK, IK, and BK – had single channel amplitudes that would have necessitated the inclusion of smaller or larger channels in their opening if 50% cut–off had been used. For example, if 50% cut–off had been applied to the data when counting IK openings, SK openings and BK openings would have been included as IK events. 75% cut–off criterion was applied to the open probability analysis of all inside–out data.

Protocols other than the standard 50% cut–off have been used before. Benham *et al.* (1986) used 75% cut–off for openings and 50% cut–off for closings to measure open probability in smooth muscle cell membranes from rabbit jejunum or guinea pig mesenteric artery.

The average open amplitude for the four channel types at different voltages was measured from long openings where the channel remained at the

first open level for more than 50 ms. This ensured that brief openings would not contribute to a lower average open amplitude. Brief openings were included in open time data analysis.

III.3 reversal potential analysis (Nernst and K_{rev})

The reversal potential (K_{rev}) for each K–channel was determined from the voltage intercept at zero current from the linear fit of unitary current versus voltage. The linear calculated K_{rev} was compared to the theoretical expected K_{rev} (Nernst equation). The $[K^+]_o$ = 5.5 mM data were not plotted because they were not linear.

The Nernst equation for channels predicts that the reversal potential is a function of the driving force of potassium across the membrane. The driving force is a function of the voltage and the ratio of potassium ions across the membrane. The $[K^+]_o$ was varied from physiological (5.5 mM) to symmetrical (50 mM, 100 mM, and 150 mM (symmetrical)). The intracellular solution potassium concentration was not altered. According to the Nernst equation, the reversal potential at any potassium concentration is:

$$K_{rev} = (RT/F) \ln ([K^+]_o / [K^+]_i)$$

where:

K_{rev} is the reversal potential

R is the universal gas constant

T is the temperature in Kelvins

F is the Faraday constant

$[K^+]_o$ is the external potassium concentration

$[K^+]_i$ is the internal potassium concentration

At room temperature, RT/F is a constant ($RT/F_{22°C}$ = 25.43 mV). The reversal potentials as predicted by the Nernst equation are in Table M–3:

Table M–3. Reversal Potentials From the Nernst Equation.

$[K^+]_o$ (mM)	K_{rev} (mV)
150	0
100	–10
50	–28
5.5	–84

III.4 maximum conductance (g_{max} and $K_{1/2}$)

The maximum conductance (g_{max}) of K–channels was calculated by plotting the linear unitary conductance versus the $[K^+]_o$ and extrapolating a fitted Michaelis–Menten function to saturation. The concentration of external potassium ($K_{1/2}$) at half maximum conductance ($1/2*g_{max}$) was also calculated. The $[K^+]_o$ = 5.5 mM data were not plotted because they were not linear.

saturation theory

The flux of ions through a K–channel was dependent upon the driving force acting on either side of the membrane. When the $[K^+]_o$ was decreased from symmetrical (150 mM) to physiological (5.5 mM), the driving force across the membrane changed. At negative voltages in symmetrical solutions, current was forced from the extracellular to the intracellular side of the membrane. When the $[K^+]_o$ was reduced from 150 mM to 5.5 mM, potassium was pushing against a concentration gradient to cross the membrane from a region of low concentration

(exterior side) to a region of high concentration (interior side). This resulted in the non–linearity of the flux in this region.

When the voltage was positive, current was forced from the intracellular to the extracellular side of the membrane. The constant field equation predicted that a lower $[K^+]_o$ (5.5 mM) increased outward flux relative to the symmetrical high concentration condition (150 mM). The linear region from which the conductance was measured confirmed this hypothesis. As the $[K^+]_o$ was decreased, the unitary current increased. However, as the voltage moved from positive values towards zero, the driving force was reduced due to the difference in potassium concentration across the membrane and the slope or conductance decreased.

If the theory supporting the constant field equation were followed, then reducing the $[K^+]_o$ would have resulted in reduced conductance. A linear conductance was measured from the approximately linear section of data (positive voltage region) to confirm this hypothesis.

Saturation theory predicted that, under symmetrical conditions, the conductance of a channel would increase non–linearly with increasing concentration of permeant ions. This non–linear increase could be described by Michaelis–Menten kinetics. As the concentration of permeant ion increased through physiological ranges (0 to 150 mM), the conductance increased. Beyond physiological ranges, the conductance of the channels increased more slowly until a maximal conductance is reached. At this point the channels were **saturated** and no further increase in permeant ions could produce increases in channel flux.

Channel saturation is believed to be due to the rate limitation imposed by the binding–unbinding steps involved in ion permeation (Hille, 1992). The form of the Michaelis–Menten function is:

$$g = g_{max} / (1 + K_{1/2} / [K^+])$$

where:

g is the conductance of the channel at any symmetrical $[K^+]$

g_{max} is the maximum conductance of the channel

$K_{1/2}$ is the $[K^+]$ at which $g = ½ * g_{max}$

$[K^+]$ is the concentration of potassium

This equation was used to determine the maximum conductance (g_{max}) of a channel under conditions where the concentration of potassium was altered on both sides of the membrane. It assumed that symmetrical solutions were always used. However, in the experiments performed, only the $[K^+]_o$ was varied ($[K^+]_o$ = 150, 100, and 50 mM) while the internal concentration remained fixed ($[K^+]_i$ = 150 mM). The estimations of the conductance under non–symmetrical conditions ($[K^+]_o$ = 100 and 50 mM) are still used in the fitting of the function since it was found that no method of weighting could be applied to correct for the different ratio of internal and external concentrations of potassium.

To verify the quality of the fit, a 1% tolerance was allowed. The known values were weighted 100 times the value of the predicted values. In this condition, the conductance at $[K^+]_o$ = 0 and 150 mM were weighted 100 times the conductance at $[K^+]_o$ = 100 and 50 mM. Under these conditions, the fit was biased in favor of the values known to be correct, the zero permeation condition (0 mM) and the symmetrical condition (150 mM). It was found that the maximal

conductance (g_{max}) and the concentration of potassium at half maximal conductance ($K_{1/2}$) were unchanged when the 0 and 150 mM data were weighted one hundred fold. The curve fit was statistically the same. In the figures presented, each conductance at different $[K^+]_o$ is equally weighted.

PART IV. Properties of 4 Types of MRA VSMC K–Channel — Non–Linear Method

The single channel amplitude data were expected to be less linear as the $[K^+]_o$ was decreased from symmetrical (150 mM) to physiological (5.5 mM) and it was expected that the data could be fitted best with the constant field equations of Goldman–Hodgkin–Katz. These equations are regularly used to describe the conductance and reversal potential of channels in non–symmetrical solutions. These equations were derived to describe the movement of ions by simple diffusion and are not perfect at predicting channel properties.

IV.1 permeability constants

The permeability constants of the MRA VSMC K–channels were derived from the conductance under symmetrical external potassium.

The permeability of ion channels is a selective process. The channel allows the passage of some but not all ions. Without this selectivity, channels would not be able to regulate the concentration of ions across the membrane and the cellular processes that they affect. The channels studied in the MRA VSMC

preparation were all selective for potassium. This selectivity will be demonstrated later when it has been shown that the GHK equation can be used to fit the data.

The permeability constant of a channel describes how readily the channel can be permeated by a selective ion. The unitary current of a channel can be described by the following equation:

$$I_K = P_K * E * F^2/RT * [K^+]$$

where:

I_K is the unitary current of a K–channel at a specific voltage

P_K is the permeability constant

E is the voltage

F is the Faraday constant

R is the universal gas constant

T is the temperature in Kelvins

$[K^+]$ is the concentration of potassium under symmetrical conditions

This equation can be re–written to isolate the permeability constant in the form:

$$P_K = I_K/E * {}^{RT}/_F * {}^{1}/_F * 1/[K^+]$$

In this form, I_K/E is the conductance of the channel under symmetrical potassium concentrations, RT/F and 1/F are known constants and the concentration of potassium is 150 mM. This equation was used to calculate the permeability constant for each of the four MRA VSMCs.

IV.2 GHK equations

The GHK equations were fitted to the unitary current–voltage data (same as *III.2*) to determine the conductance. It was expected that the GHK equations would better fit the data than linear functions.

The form of the GHK equation used to isolate the permeability constant did not take into account changes in potassium concentration. A more comprehensive equation was needed. The full GHK equation is as follows:

$$I_K = P_K * E * F * {}^{F}/_{RT} * \frac{([K^+]_o - [K^+]_i * \exp(E * {}^{F}/_{RT}))}{(1 - \exp(E * {}^{F}/_{RT}))}$$

The simplified equation used previously demonstrated that the permeability constant was a function of the conductance of the channel under symmetrical conditions. The full GHK equation can be simplified to the following:

$$I_K = g/10^3 * 1/[K^+]_{eq} * E * \frac{([K^+]_o - [K^+]_i * \exp(E * {}^{F}/_{RT}))}{(1 - \exp(E * {}^{F}/_{RT}))}$$

where:

I_K is the unitary current

g is the conductance in pS

$[K^+]_{eq}$ is the concentration of potassium under symmetrical conditions

E is the voltage

$[K^+]_o$ is the external concentration of potassium

$[K^+]_i$ is the internal concentration of potassium

F, R, and T have already been defined

This equation was fit to the unitary current–voltage data for each of four MRA VSMC K–channels.

IV.3 instantaneous conductance

The instantaneous conductance of the four MRA VSMCs was calculated for varying voltage (–60, –40, –20, 0, +20, +40, +60 mV) and external potassium ($[K^+]_o$ = 5.5, 50, 100, 150 mM).

The instantaneous conductance is the conductance calculated under a specific voltage and $[K^+]_o$. This derivation includes the unitary current and the driving force in the form:

$$g(E) = I_K / (E - K_{rev})$$

where:

g(E) is the instantaneous conductance at a voltage E

I_K is the unitary current

$(E - K_{rev})$ is the driving force

E is the voltage

K_{rev} is the reversal potential

This function was used to calculate the instantaneous conductance which was plotted against the holding potential.

IV.4 physiological conductance

The physiological conductance was extrapolated from the $[K^+]_o$ = 5.5 mM data. The true physiological condition was not studied. However, intact SMA VSMCs had a resting membrane potential of –50 to – 51 mV (Chen and Cheung, 1997). A linear function was fit to the most physiological data ($[K^+]_o$ = 5.5 mM) and extrapolated to the expected membrane potential range (–60 mV to –40 mV).

The physiological conductance was estimated from the $[K^+]_o$ = 5.5 mM data at – 50 mV.

IV.5 maximum conductance (g_{max} and $K_{1/2}$)

The maximum conductance (g_{max}) and concentration of potassium at ½* g_{max} ($K_{1/2}$) were derived from the Michaelis–Menten equation which was fit to the instantaneous conductance data at +40 mV.

The Michaelis–Menten equation was fit to two sets of data, one which included the $[K^+]_o$ = 5.5 mM data and one which excluded it. It was expected that the data set which included the $[K^+]_o$ = 5.5 mM data would be a poor fit due to channel saturation under asymmetrical solutions.

IV.6 MRA VSMC K-Channel ion selectivity

The essential characteristic of ion channels is to regulate the flux of ions. To this end, the channel must be selective as to which ions are allowed to pass through the pore. Though no channel is perfectly selective, most are at least partially selective. The degree of selectivity is dependent upon the permeability ratio of the channel for ions that are allowed to pass. Potassium channels often allow some degree of permeation by sodium ions. Since sodium was the only major permeant ion other than potassium that was included in the solutions bathing the mesenteric patches, only sodium permeability was calculated.

The selectivity of the MRA VSMC K–channels for potassium can be calculated using a modified Nernst equation in the form:

$$K_{rev} = RT/F * \ln \frac{P_K*[K^+]_o + P_{Na}*[Na^+]_o}{P_K*[K^+]_i + P_{Na}*[Na^+]_i}$$

where:

K_{rev} is the reversal potential

R, T, and F have their usual meanings

P_K is the permeability quotient of potassium

P_{Na} is the permeability quotient of sodium

$[Na^+]_i$ / $[Na^+]_o$ are the concentration of sodium inside/outside

$[K^+]_i$ / $[K^+]_o$ are the concentration of potassium inside/outside

This function was used to determine if the four MRA VSMC K–channels were selective for potassium.

PART V. Single Channel Activity of 4 MRA VSMC K–Channels

The single channel activity (NP_o) of the four MRA VSMC K–channels was studied to determine calcium–dependence, voltage–dependence, and pharmacology.

V.1 Ca^{2+}–dependent NP_0 of 4 MRA VSMC K–channels (+40 mV)

To determine whether the four MRA VSMC K–channels were calcium–dependent at positive holding potentials, the single channel activity (NP_o) was studied at +40 mV under varying intracellular calcium concentration ($[Ca^{2+}]_i$ = 0, 50, 155, 300, 500, 750 nM).

MRA and TA VSMCs were patch clamped using the inside–out technique at +40 mV and bathed with HPIS plus ATP (1 mM). The pipette contained K–

Hanks plus nifedipine (1 μM) plus glybenclamide (300 nM). Long patches were recorded (~ 5 minutes, ≥ 2000 events) and analyzed using 75% cut–off criterion for channel opening. MRA and TA VSMC K–channel NP_o were compared.

V.2 Ca^{2+}–dependent NP_o of 4 MRA VSMC K–channels (–40 mV)

To determine whether the four MRA VSMC K–channels were calcium–dependent at negative holding potentials, the single channel activity (NP_o) was studied at –40 mV under varying intracellular calcium concentration ($[Ca^{2+}]_i$ = 0, 50, 155, 500, 750 nM).

MRA and TA VSMCs were patch clamped using the inside–out technique at –40 mV and bathed with HPIS plus ATP (1 mM). The pipette contained K–Hanks plus nifedipine (1 μM) plus glybenclamide (300 nM). Long patches were recorded (~ 5 minutes, ≥ 2000 events) and analyzed using 75% cut–off criterion for channel opening. MRA and TA VSMC K–channel NP_o were compared.

V.3 Voltage–dependent NP_o of Four MRA VSMC K–channels

To determine whether the four MRA VSMC K–channels were voltage–dependent, the single channel activity (NP_o) was studied at $[Ca^{2+}]_i$ = 500 nM under varying voltage (–40, –20, 0, +20, +40 mV). MRA VSMC K–channel NP_o at +40 and –40 mV was maximized at $[Ca^{2+}]_i$ = 500 nM so this concentration was fixed.

MRA VSMCs were patch clamped using the inside–out technique and bathed with HPIS plus ATP (1 mM) plus 500 nM Ca^{2+}. The pipette contained K–

Hanks plus nifedipine (1 μM) plus glybenclamide (300 nM). Long patches were recorded (~ 5 minutes, ≥ 2000 events) and analyzed using 75% cut–off criterion for channel opening. MRA VSMC K–channel NP_o were compared.

V.4 percentage contribution of 4 MRA VSMC K–channels

The percentage contribution of the four MRA VSMC K–channels to the total calcium–dependent K–channel activity of the cell was determined.

The contribution of activity of each of the four MRA VSMC K–channels to total activity cannot be calculated since the activity of other channels was not a part of this study. However, SMA VSMCs are known to be modulated by K_{Ca} channels (Chen and Cheung, 1997).

The four MRA VSMC K–channels were compared according to single channel conductance and voltage–dependent single channel activity. A comparison of channel activity was made by taking the product of single channel conductance and open probability ($g*NP_o$) at each voltage step (–40, –20, 0, +20, +40 mV) at fixed calcium ($[Ca^{2+}]_i$ = 500 nM). The units of relative activity are omitted because they hold no conventional value and are used only for channel comparison.

V.5 pharmacology of 4 MRA VSMC K–channels

MRA VSMC K–channel pharmacology was studied using the inside–out technique. Inside–out patches were held at +40 mV and recorded for ~5 minutes. The intracellular surface was bathed in HPIS (150 mM $[K^+]_i$) containing 500 nM

$[Ca^{2+}]_i$ to activate the four MRA VSMC K–channels and ATP (1 mM) to inhibit K_{ATP}–channels. The extracellular surface (pipette solution) was bathed with K–Hanks containing glybenclamide (300 nM) to inhibit K_{ATP}–channels and nifedipine (1 μM) to block L–type Ca^{2+}–channels.

The K–channel blockers studied were included in the pipette solution because they were only effective from the extracellular side. The K–channel blockers studied and their specific targets are listed in the following table:

Table M–4. Potassium Channel Antagonists and their Targets.

K–channel blocker		[antagonist]	selective K–channel
charybdotoxin	(ChTX)	10 – 100 nM[1]	BK_{Ca}
iberiotoxin	(IbTX)	5 – 100 nM[2]	BK_{Ca}
apamin		100 – 1000 nM[3]	SK_{Ca}
4–aminopyridine	(4–AP)	1 – 2 mM[4]	K_{dr}

References:
1. (Brayden, 1996; Nelson and Quayle, 1995; Bolzon, 1992; Miller *et al.*, 1985)
2. (Brayden, 1996; Nelson and Quayle, 1995; Galvez *et al.*, 1990)
3. (Brayden, 1996; Nelson and Quayle, 1995; Blatz and Magleby, 1986)
4. (Brayden, 1996; Nelson and Quayle, 1995; Bolzon, 1992)

The open probability of the four MRA VSMC K–channels was calculated in the presence or absence of one of the four K–channel antagonists.

RESULTS

PART I. Endothelium–dependent Hyperpolarization

I.1

acetylcholine depolarized TA VSMCs

Figure RI–1A is an example of the effect of ACh on TA VSMCs. The TA VSMC was bathed in Hanks solution and patch–clamped using the nystatin perforated patch technique. The TA VSMC was current clamped such that the membrane potential was approximately –68 mV. When perfused with ACh (0.1 μM), the TA VSMC depolarized to approximately –56 mV. The response was maintained for five minutes in the continuous presence of ACh. TA VSMCs depolarized with ACh contracted and the depolarization response could not be washed out.

In the absence of an endothelium donor, ACh depolarized TA VSMCs. In the presence of ACh 0.1 μM, the average depolarization was 7.3 ± 0.88 mV (n=3); in 1μ M ACh, ~ 15.0 mV (n=2).

endothelium–dependent ACh–induced hyperpolarization

Figure RI–1B is an example of the effect of ACh–induced hyperpolarization. The target TA VSMC was current–clamped to maintain a membrane potential of approximately –49 mV.

Figure RI–1. ACh–induced Endothelium–dependent Hyperpolarization.

Panel A. ACh (100 nM) depolarized a TA VSMC. The cell was bathed in Hanks solution and current clamped to maintain a membrane potential of approximately –68 mV. When perfused with ACh (100 nM), the cell depolarized to approximately –56 mV. The response was maintained for five minutes in the continuous presence of ACh. (The cell was clamped in current–clamp mode and the current adjusted to maintain a membrane potential as close as possible to the resting potential of –50 mV. However, the Axopatch 200 amplifier was not designed for current clamp and fine control of current was not possible.)

Panel B. ACh (100 nM) hyperpolarized a TA VSMC in the presence of an endothelium–intact donor. The cell was bathed in Hanks solution with atropine (1 μM) to block direct ACh depolarization. The donor tissue, a 4 – 6 mm section of SMA, was internally perfused (SMA–IP) with Hanks and the perfusate washed the target TA VSMC. L–NNA (30 μM) was included in the artery perfusate to inhibit nitric oxide synthesis.

The TA VSMC was current–clamped to maintain a membrane potential of approximately –49 mV. When the SMA was perfused with ACh (100 nM), the perfusate hyperpolarized the TA VSMC to ~ –64 mV. The response was sustained for five minutes under continuous ACh perfusion.

Panel C. ACh–induced outward currents were blocked by TEA. The voltage–clamped TA VSMC was held at a membrane potential of –50 mV. The donor tissue consisted of a number of SMA rings (3 – 5, each ~ 2 – 4 mm) held in a plastic pipette (SMA–IRPT). The donor tissue was constantly perfused by Hanks solution. The bath was washed by Hanks solution with atropine (10 μM) to prevent ACh depolarization and with nifedipine (1 μM) to block L–type Ca^{2+}–channels. In the resting condition, outward spiking currents were observed. These spiking currents increased in amplitude and frequency in the presence of ACh (10 and 100 nM) and were blocked by TEA (5 mM).

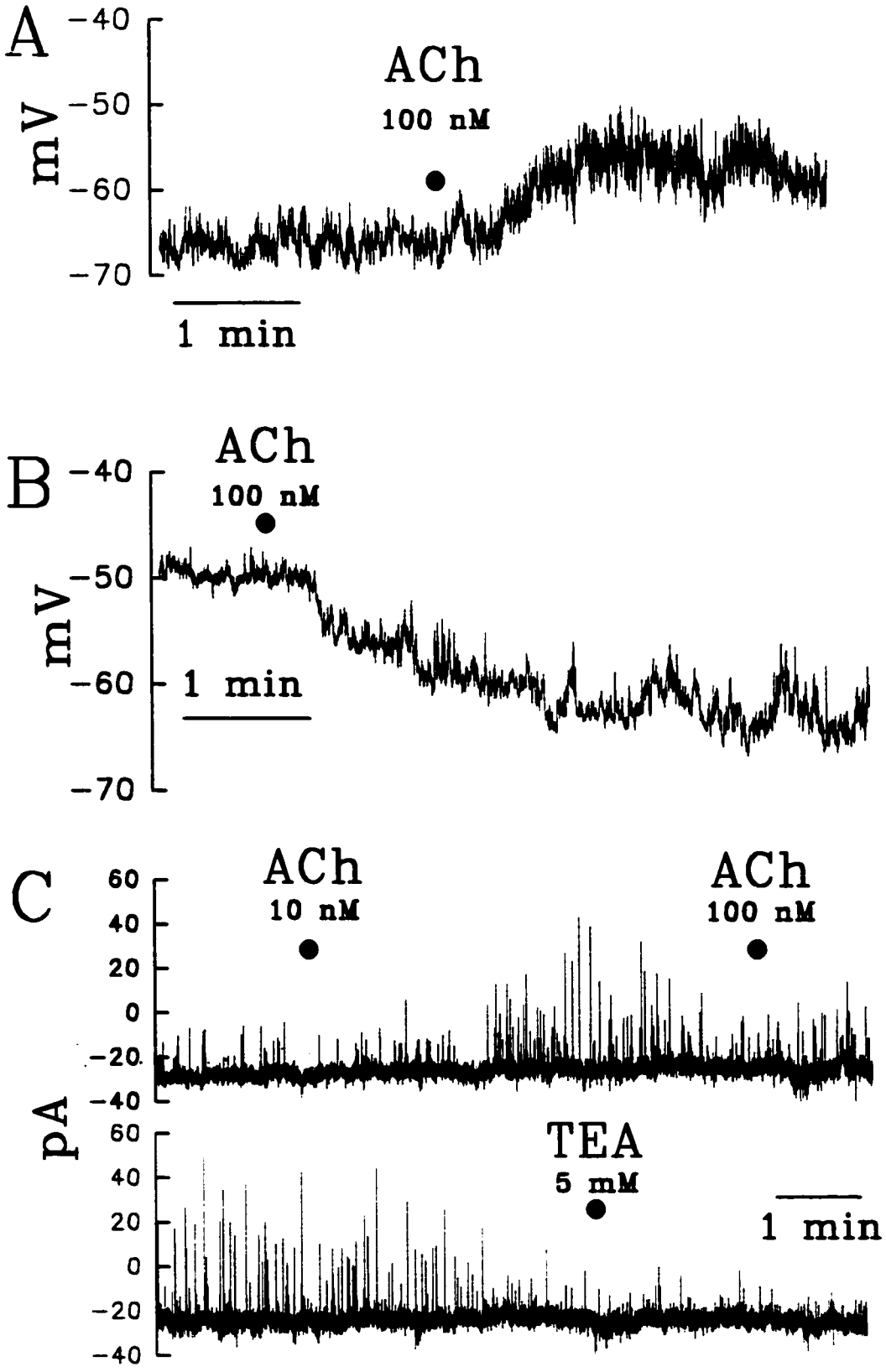
A
-40
-50
-60
-70
mV
ACh
100 nM
1 min
B
-40
-50
-60
-70
mV
ACh
100 nM
1 min
C
60
40
20
0
-20
-40
pA
ACh
10 nM
ACh
100 nM
TEA
5 mM
1 min

When the donor artery was perfused with ACh (0.1 μM), the perfusate hyperpolarized the TA VSMC to approximately –64 mV. The response was sustained for five minutes under continuous ACh perfusion. When the donor endothelium was damaged, the hyperpolarization response was reduced or reversed to a depolarization, indicating incomplete blockade by atropine. The extent of endothelium damage determined the degree of reversal but was not part of this study. The ACh–induced endothelium–dependent hyperpolarization is consistent with the idea that EDHF is a transferable and diffusible factor.

I.2 In Figure RI–2, the SMA–IRPT technique was used to demonstrate that ACh–induced EDH has a NO–independent component. ACh–induced hyperpolarization in the absence of L–NNA was robust, but hyperpolarization was maintained even when NO synthesis was inhibited (ACh (10 nM): –10.5 ± 1.9 mV (n=4); L–NNA (30 μM) + ACh (1 μM): ~ –5.5 mV (n=2)).

The *internal perfusion (IP)* and *pinned inverted tubes (PIT)* techniques were found to be superior to the *inverted rings in pipette tip (IRPT)* technique. It was found that atropine back washed into the pipette tip and blocked ACh–induced release of EDHF. This was due to the nature of the pump apparatus, which was not perfectly continuous, and to capillary action since the IRPT technique's crimped pipette tip was smaller than the open tubing used in the IP technique. The length and diameter of tubing at the distal end in the IP technique prevented bath solution from entering the donor tissue lumen.

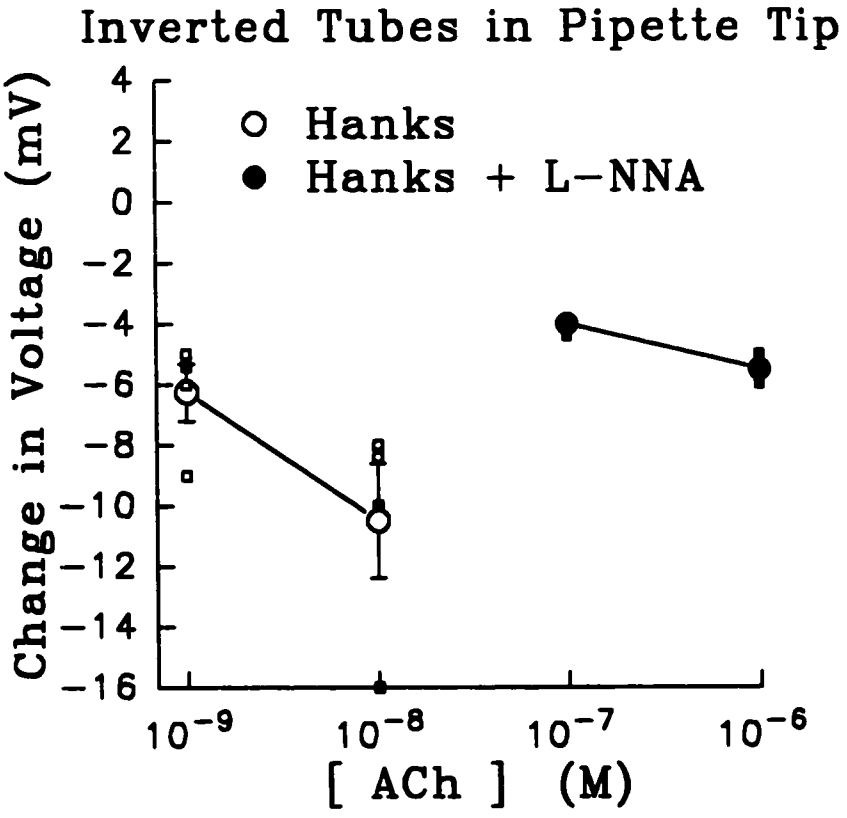

Figure RI–2. Inverted Rings in Pipette Tip (SMA–IRPT).

SMA donor tissue was cut into short rings (3 – 5, each ~ 2 – 4 mm) held in a modified plastic pipette tip. The rings were inverted to expose the endothelium to the perfusing solution. The pipette was retained in a stereotaxic device that could be moved close to any cell in the bath. The donor tissue was constantly perfused by Hanks solution. The bath was washed by Hanks solution with atropine (1 μM) to prevent ACh depolarization and with nifedipine (1 μM) to block L–type Ca^{2+}–channels. Small squares denote individual results whereas circles denote the average response (± s.e.m. if n≥3). ACh hyperpolarized the target TA VSMCs. ACh–induced hyperpolarization in the absence of L–NNA was robust, but hyperpolarization was maintained even when NO synthesis was inhibited by L–NNA (30 μM) (Hanks, n=4, 4; Hanks + L–NNA, n=2, 2).

I.3 In Figure RI–3, the SMA–PIT technique was used to demonstrate that ACh–induced endothelium–dependent hyperpolarization was a function of the distance between the donor tissue and the target cell.

Target TA VSMCs close to the donor tissue (≤0.2 mm) were hyperpolarized by ACh. Hyperpolarization was induced by nanomolar range concentrations of ACh with an average change in membrane potential of -10.3 ± 0.88 mV (n=3) at 0.3 μM ACh. Target TA VSMCs far (≥1.8 mm) from the donor tissue were not hyperpolarized.

I.4/5 ACh–induced EDH can be achieved with different donor tissues. Tail artery (TA) and superior mesenteric artery (SMA) can both produce endothelium–derived hyperpolarizing factors. These donor tissues were internally perfused with Hanks solution in the presence of L–NNA (30 μM) to inhibit NO synthesis. The bath was washed with Hanks solution plus atropine (1.0 μM) to prevent ACh–dependent depolarization. Figure RI–4 and Figure RI–5 demonstrate that ACh hyperpolarized TA VSMCs when tail and mesenteric arteries were used as donor tissue, respectively. The peak hyperpolarization in the presence of 1 μM ACh was -10.0 ± 1.4 mV (n=5) and -8.0 ± 1.7 mV (n=4) for tail and mesenteric arteries.

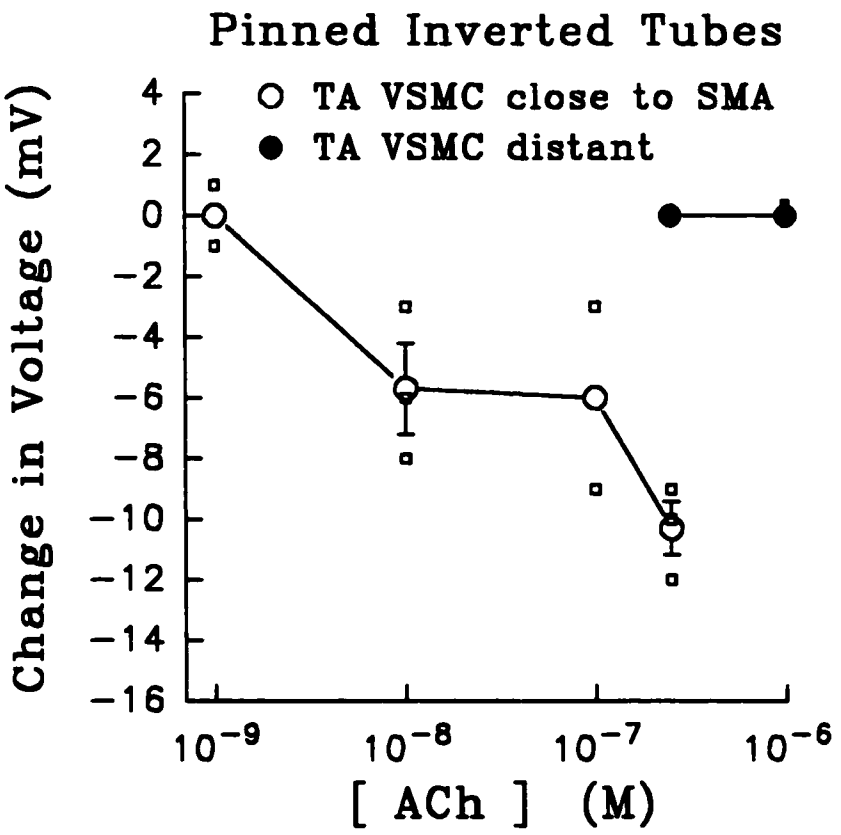

Figure RI-3. Endothelium-dependent Hyperpolarization was a Function of Donor-target Distance (SMA-PIT).

SMA donor tissue was cut into short tubes (~ 4 – 6 mm), inverted to expose the endothelium, and pinned to the side of the 35 mm dish (SMA-PIT). In this configuration, there was no separate bath and artery perfusion. The bath solution flowed over the tissue and washed the TA VSMCs. Ringers solution was used to maximize tissue longevity and L-NNA (30 μM) was included to inhibit NO synthesis.

Small squares denote individual results whereas circles denote the average response (± s.e.m. if n≥3). Target TA VSMCs close (≤0.2 mm) to the donor tissue were hyperpolarized by ACh (n=2, 3, 2, 3). Target TA VSMCs far (≥1.8 mm) from the donor tissue were not hyperpolarized (n=1, 2).

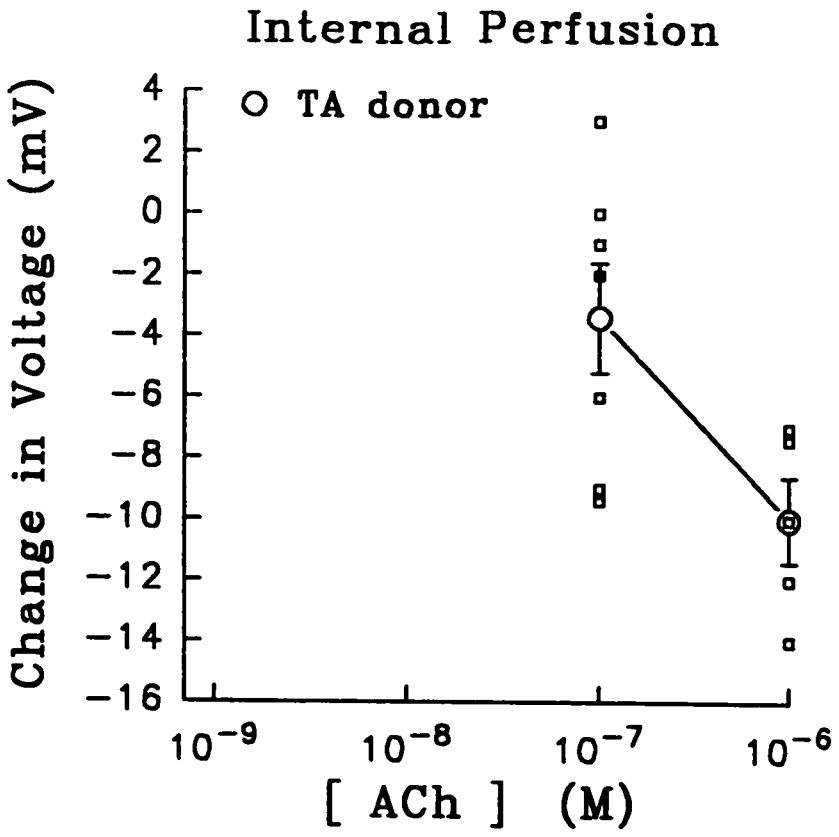

Figure RI–4. Internal Perfusion of Tail Artery (TA–IP).

The TA donor tissue was internally perfused with Hanks solution in the presence of L–NNA (30 μM) to inhibit NO synthesis. The bath was washed with Hanks solution plus atropine (1 μM) to prevent ACh–induced depolarization. Small squares denote individual results whereas circles denote the average response (± s.e.m. if n≥3). ACh hyperpolarized the target TA VSMCs (n=7, 5).

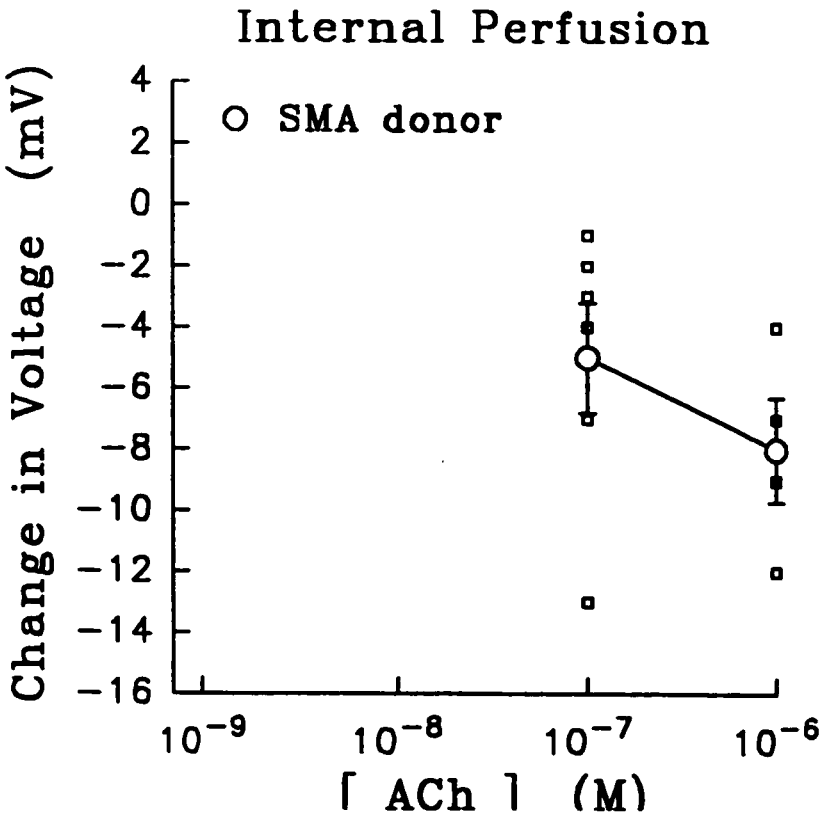

Figure RI–5. Internal Perfusion of SMA (SMA–IP).

The SMA donor tissue was internally perfused with Hanks solution in the presence of L–NNA (30 μM) to inhibit NO synthesis. The bath was washed with Hanks solution plus atropine (1 μM) to prevent ACh–dependent depolarization. Small squares denote individual results whereas circles denote the average response (± s.e.m. if n≥3). ACh hyperpolarized the target TA VSMCs (n=6, 4).

I.6 Figure RI–1C is an example of a TA VSMC in the voltage clamp configuration. The TA VSMC was held at a membrane potential of –50 mV. The donor tissue consisted of a number of inverted SMA rings (3 – 5, each ~ 2 – 4 mm) held in pipette tip (SMA–IRPT). In the resting condition, outward spiking currents were observed. These spiking currents were increased by ACh (0.01 and 0.10 μM) and blocked by tetraethylammonium ions (TEA, 5 mM). The ACh–induced spiking currents were delayed ~1 minute, even though the perfusion transit time was <30 seconds. As well, the effect of ACh persisted during continuous perfusion but the spike maximum declined over time. This suggests that EDHF production / release is transient. Since TEA (<5 mM) is a non–specific potassium channel blocker, it was suggested that the outward spikes were potassium currents. This suggests that potassium channels were responsible for ACh–induced endothelium–dependent hyperpolarization.

PART II. Properties of Mesenteric Resistance Artery VSMC

II.1 morphological properties

Single MRA VSMCs were resolved under reverse phase light microscopy. The average cell shape was an elongated spindle with small surface invaginations. MRA and TA VSMCs spontaneously contracted in Hanks solution ($[Ca^{2+}]_o$ = 2 mM) within 45 – 60 minutes of plating on 35 mm culture dishes. New dishes were then plated for further experiments. Only healthy cells exhibiting a bright distinct outline under phase microscopy were used.

Cell viability as measured by percentage of cells excluding 0.2% trypan blue uptake or agonist–dependent contraction (NA, $[K^+]_o$, $[Ca^{2+}]_o$, Bay K 8644) was not a part of this study (Bolzon and Cheung, 1989). Cell viability was determined daily by observing *i.* cell shape (cell length and diameter, clarity of cell membrane outline, texture and shading), *ii.* contractility to electrode touch (neither too sensitive nor insensitive), and *iii.* current measured (neither overly active nor inactive and stable over time).

Figure RII–1A is a comparison of the average cell length of MRA and TA VSMCs. MRA VSMCs were significantly shorter than TA VSMCs (MRA: 72.2 ± 4.2 μm, n=22; TA: 131.7 ± 4.4 μm, n=25; ***, $p<0.001$). Figure RII–1B is a comparison of the average cell diameter of MRA and TA VSMCs. MRA VSMCs were significantly more narrow than TA VSMCs. (MRA: 7.7 ± 0.3 μm, n=22; TA: 11.0 ± 0.4 μm, n=25; ***, $p<0.001$).

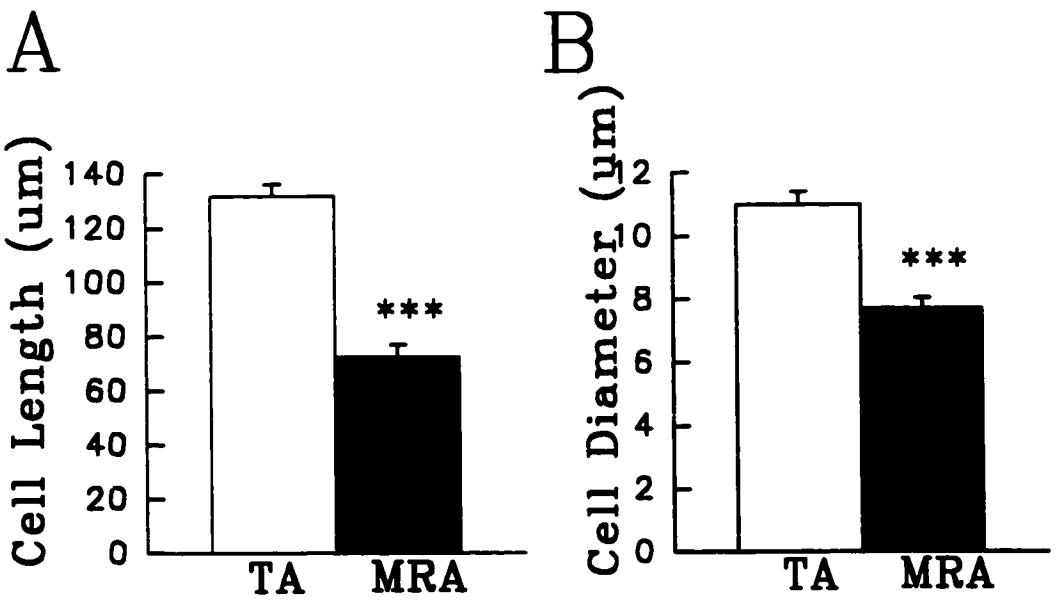

Figure RII–1. MRA VSMC Length and Diameter.

Panel A. A comparison of the average cell length of MRA and TA VSMCs. MRA VSMCs were significantly shorter than TA VSMCs (MRA: 72.2 ± 4.2 µm, n=22; TA: 131.7 ± 4.4 µm, n=25; ***, $p<0.001$).

Panel B. A comparison of the average cell diameter of MRA VSMCs and TA VSMCs. MRA VSMCs were significantly more narrow than TA VSMCs (MRA: 7.7 ± 0.3 µm, n=22; TA: 11.0 ± 0.4 µm, n=25; ***, $p<0.001$).

II.2 passive membrane properties

Figure RII–2A is a comparison of the capacitance of MRA and TA VSMCs. MRA VSMCs have a significantly lower capacitance than TA VSMCs (MRA: 12.2 ± 1.0 pF, n=8; TA: 31.1 ± 1.4 pF, n=5; ***, p<0.001). The electrical surface area of a cell can be calculated by assuming that the specific membrane capacitance is 1 $\mu F/cm^2$ (Hille, 1992). The electrical surface area of MRA VSMCs was significantly smaller than that of TA VSMCs (MRA: $1.2 \pm 0.10 \times 10^{-5}$ cm^2, n=8; TA: $3.1 \pm 0.14 \times 10^{-5}$ cm^2, n=5; ***, p<0.001). The smaller size of the MRA VSMCs compared to the TA VSMCs suggests that MRA myocytes have contractile responses that respond more rapidly to stimuli due to the proximity of neighbor cells and the smaller cell volume.

The series resistance of MRA VSMCs was not significantly different from TA VSMCs (MRA: 9.35 ± 0.86 MΩ, n=8; TA: 9.09 ± 1.60 MΩ, n=5; p=0.88). Due to the properties of the amplifier (Axopatch 200), it was not possible to inject accurate square current pulses to measure the input resistance, or to then calculate the specific membrane resistance.

II.3 whole–cell current density

Single MRA VSMCs were patch clamped in the whole–cell configuration. Membrane potential was clamped at –50 mV to approximate the RMP of excised SMA VSMCs (Chen and Cheung, 1997). Cells were step depolarized to +50 mV in 10 mV increments. Figure RII–3 is an example of the currents elicited in TA and MRA VSMCs. The average current was similar for both cell types even

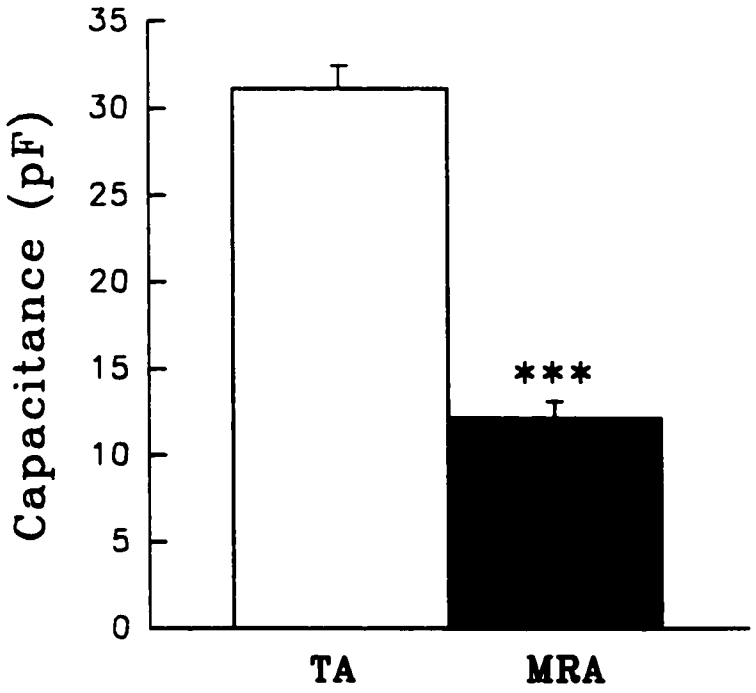

Figure RII–2. MRA VSMC Capacitance.

A comparison of capacitance between MRA and TA VSMCs. MRA VSMCs had a significantly lower capacitance than TA VSMCs (MRA: 12.2 ± 1.0 pF, n=8; TA: 31.1 ± 1.4 pF, n=5; ***, $p<0.001$)

though their cell sizes differed. The higher current density of MRA versus TA VSMCs suggests that MRA myocytes have twice the channel density of TA myocytes. However, MRA K–channels may be twice as active. This discrepancy was not a part of this study.

The current–voltage relationship for cells of different sizes was derived by normalizing the whole–cell current to the cell size. The current density was derived by dividing the average current in the plateau region (300–500 ms after step trigger) by the cell capacitance. Figure RII–4 is the average current density of MRA VSMCs and TA VSMCs. MRA VSMCs had a significantly larger current density than TA VSMCs. At +50 mV the SMA current density was more than twice that of TA VSMCs (MRA: 34.75 ± 3.09 pA/pF, n=4; TA: 15.28 ± 1.38 pA/pF, n=4; **, $p<0.01$).

There was a greater statistical difference between TA and MRA current in the negative membrane potential region (–30 to –10 mV) rather than the positive membrane potential region (+10 to +50 mV). The K_{dr} channel carries most of the K–current in the negative membrane potential region whereas the K_{Ca} channel carries most of the current in the positive region. This suggests that MRA myocytes are regulated more by voltage (and voltage dependent K–channels, K_{dr}) and less by calcium (and K_{Ca}) **relative to** TA myocytes.

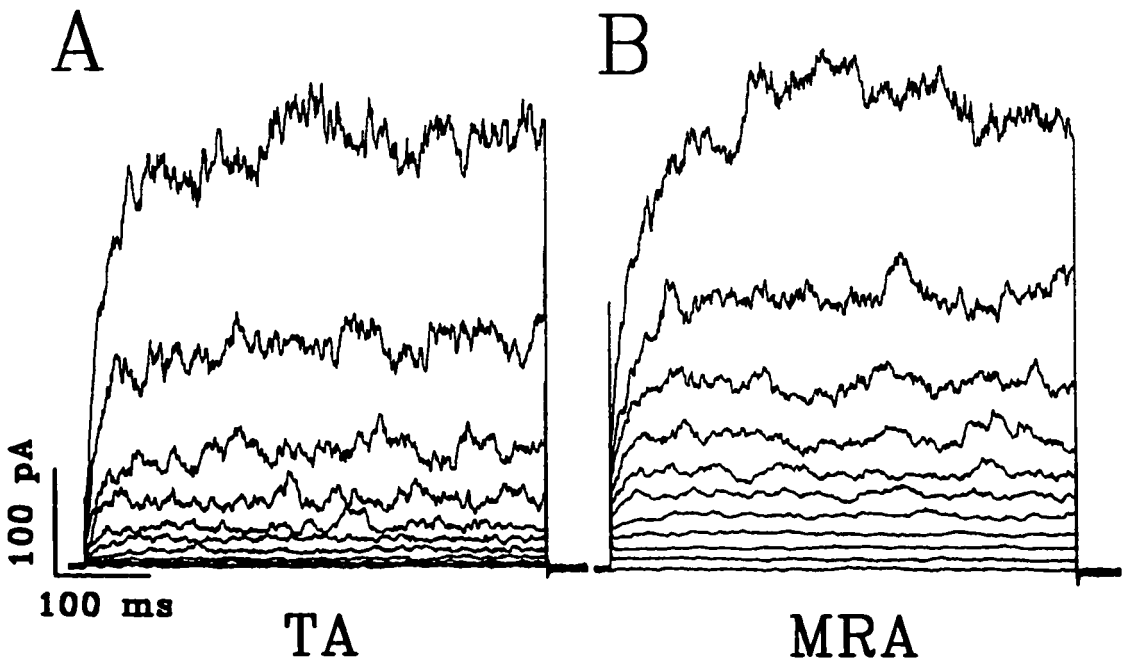

Figure RII–3. Whole–cell Current in MRA and TA VSMCs.

Panel A. Single TA VSMCs were patch clamped in the whole–cell configuration. Membrane potential was clamped at –50 mV to approximate the resting potential of *in vivo* cells. Cells were step depolarized to +50 mV in 10 mV increments. This trace is an average of 6 sweeps.

Panel B. Single MRA VSMCs were patch clamped as per *Panel A.* Currents elicited were similar in magnitude to those in TA VSMCs. This trace is an average of 10 sweeps, which makes it smoother than *Panel A.*

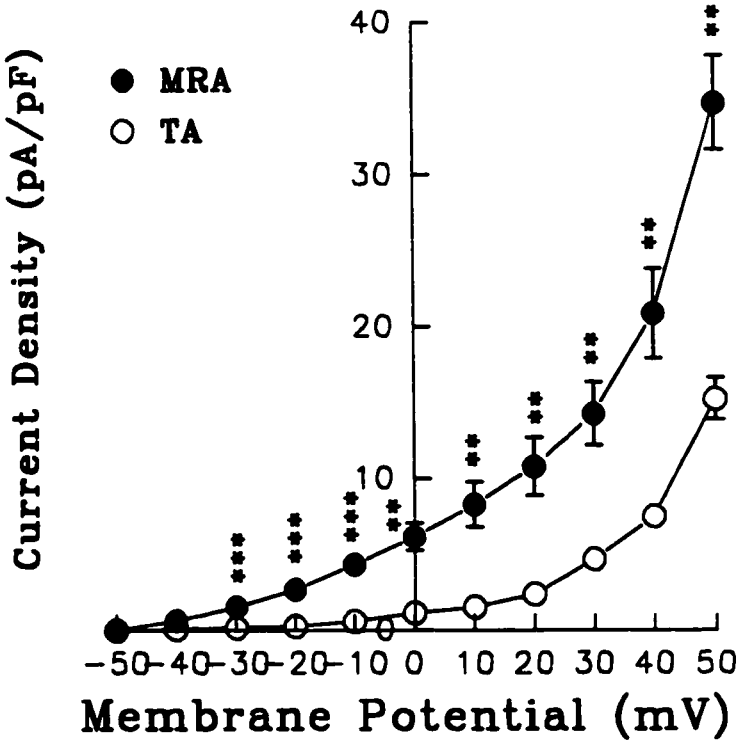

Figure RII–4. MRA and TA VSMC Current Density.

A comparison of MRA and TA VSMC whole–cell current density. MRA VSMCs had a significantly higher current density than TA VSMCs at all test voltages where current was elicited. The cells were held at –50 mV and step depolarized to +50 mV by 10 mV increments (MRA, TA: n=4; **, $p<0.01$; ***, $p<0.001$).

II.4 whole–cell pharmacology of MRA VSMCs

MRA VSMCs were patch clamped using the nystatin perforated patch technique. Cells were bathed in Hanks solution and perfused with apamin. MRA VSMC whole–cell current was inhibited by 0.3 μM apamin. This concentration has been shown to inhibit ACh–induced endothelium–dependent hyperpolarization in intact tissue studies using SMA (Chen and Cheung, 1997). Figure RII–5A is an example of the effect of apamin (0.3 μM) on a single MRA VSMC. The apamin–dependent current was derived by subtracting the current in the presence of apamin from the control current. Figure RII–6A is the current voltage relationship for MRA VSMCs in the presence of apamin. At +50 mV the whole–cell current was inhibited 21% (MRA: control: 34.75 ± 3.09 pA/pF, n=4; apamin: 27.60 ± 4.25 pA/pF, n=4; *, $p<0.05$).

The greater statistical difference between apamin and control at –10 mV is likely due to the stability of the K_{dr} current compared to the oscillatory nature of the K_{Ca} current at positive potentials. Figure RII–6B is an enlarged scale figure of the apamin–sensitive current.

TA VSMCs patch clamped as per MRA VSMCs were not inhibited by 0.3 μM apamin. Figure RII–5B is an example of a TA VSMC exposed to apamin. Figure RII–6A is the current voltage relationship for TA VSMCs in the presence of apamin (0.3 μM). No significant reduction in current was observed at any test potential (n=4). Figure RII–6B is an enlargement of the apamin–insensitive current.

Apamin has been shown to be an important blocker of endothelium–dependent hyperpolarization in whole tissue studies using SMA in our laboratory (Chen and Cheung, 1997). **Because apamin inhibited whole–cell currents in MRA VSMCs but not in TA VSMCs, MRA VSMC properties became the focus of this investigation** and were compared to TA VSMCs (presented observations; Bolzon, 1992).

When patch clamped using the whole–cell technique, TA VSMCs exhibited two components of time–dependent outward current (Bolzon *et al.*, 1993). MRA VSMCs patch clamped under the same conditions demonstrated the same two components of outward current. Cells maintained at a holding potential of –80 mV were depolarized to +60 mV (by 10 mV increments for 500 ms). In this configuration, both components of outward current were elicited. Starting at –40 mV, small regular currents are elicited which corresponded to the delayed rectifier current (K_{dr}). At potentials above +30 mV, large and noisy currents became dominant. The larger component of outward current corresponded to the calcium–dependent potassium channel current (K_{Ca}). When the holding potential was increased from –80 mV to –40 mV, the delayed rectifier component was not observed and only the calcium–dependent potassium channel current remained.

The pharmacology of whole–cell currents was investigated using well–characterized potassium channel blockers. Figure RII–7 is an example of a MRA VSMC in the whole–cell configuration. The cell was bathed in Hanks solution and the pipette contained high–potassium solution. In Figure RII–7A, the MRA VSMC was maintained at a holding potential of –80 mV and both components of

whole–cell current (K_{dr} and K_{Ca}) were observed. When IbTX (150 nM) was perfused into the bath, the K_{Ca}–dependent current was significantly inhibited. However, the K_{dr}–dependent current was unaffected. Further addition of 4–aminopyridine (4–AP, 2 mM) to the bath blocked the remaining K_{dr}–dependent current.

Figure RII–5. Apamin Inhibited MRA VSMC Whole–cell Current.

Panel A. An example of a MRA VSMC patch clamped in the whole–cell configuration. Cells were clamped at –50 mV and step depolarized to +50 mV by 10 mV increments. Apamin (300 nM) inhibited the whole–cell current, and the difference current is depicted in the third trace. This figure is the average of 7 – 10 sweeps.

Panel B. An example of a TA VSMC in the same configuration as *Panel A.* Apamin (300 nM) did not inhibit the TA VSMC whole–cell current. This figure is the average of 5 – 8 sweeps. The scale is the same for both panels.

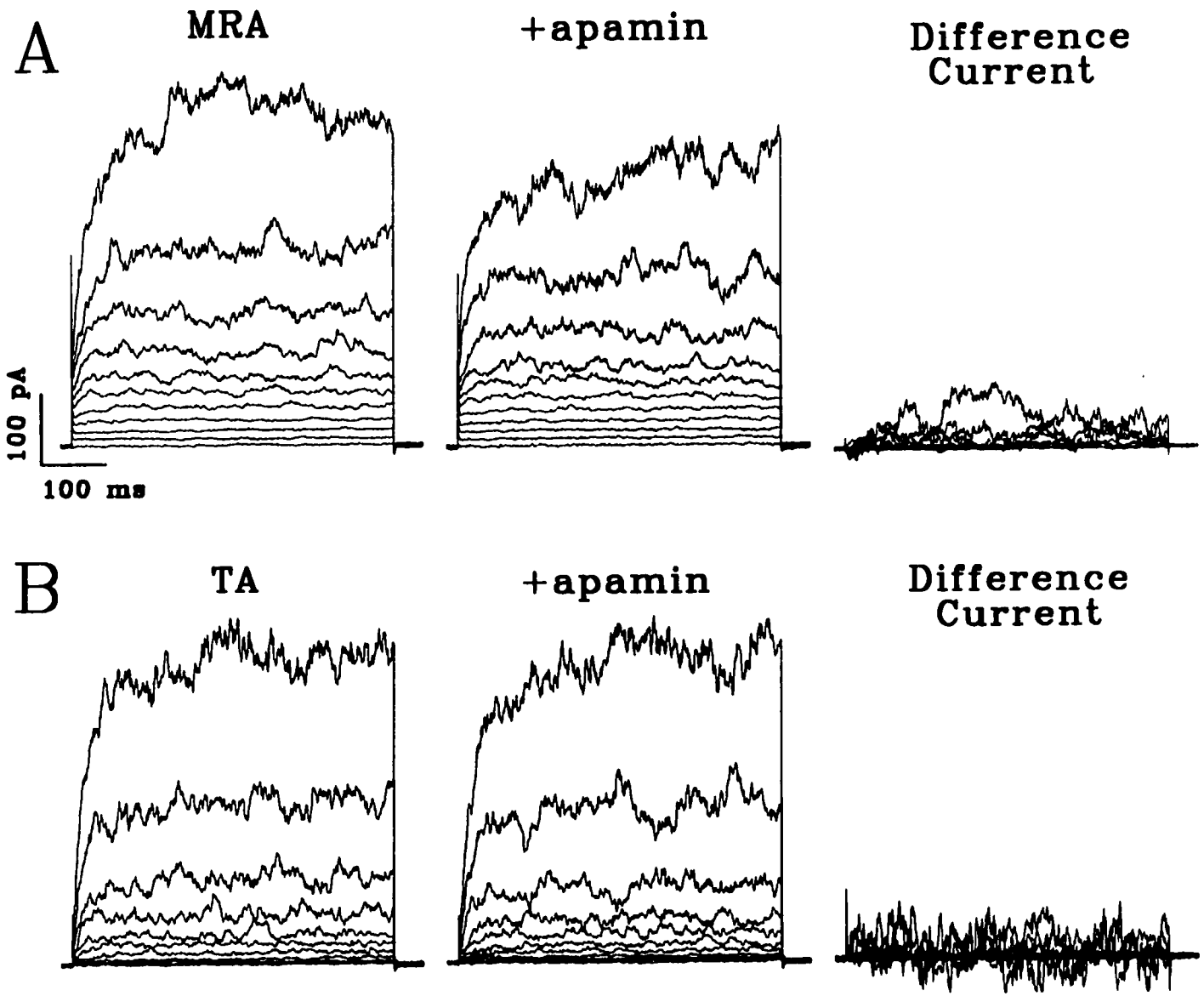
A
MRA
+apamin
Difference
Current
100 pA
100 ms
B
TA
+apamin
Difference
Current

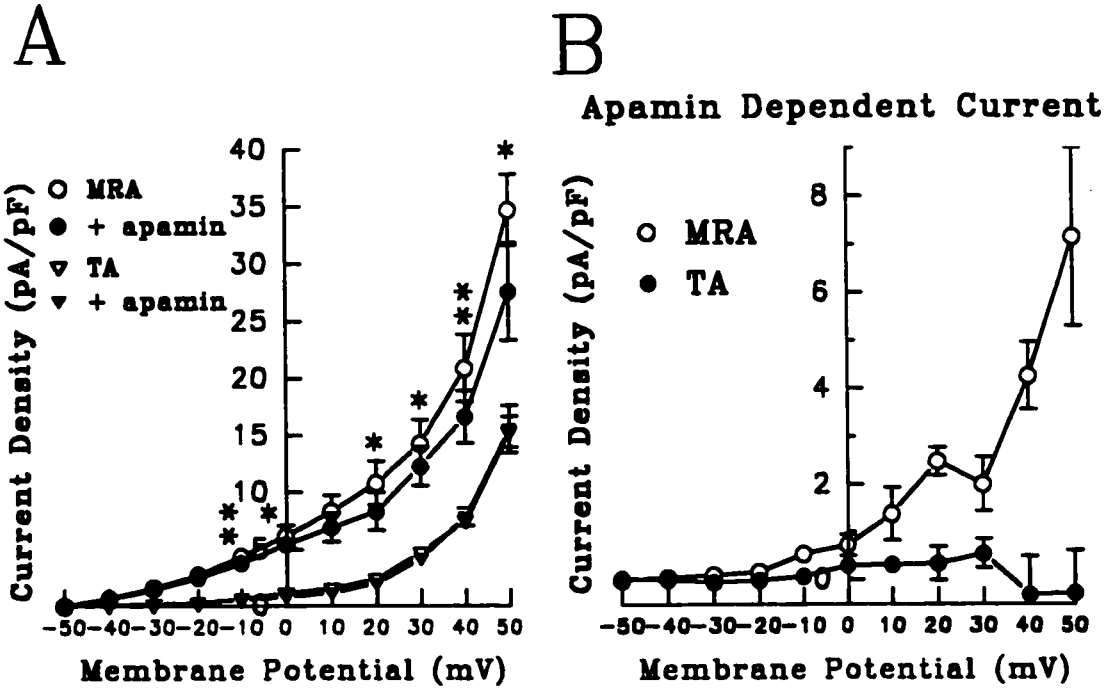

Figure RII–6. Current–voltage Relationship of Apamin on MRA and TA VSMCs.

Panel A. Apamin (300 nM) significantly inhibited whole–cell current from MRA but not TA VSMCs. Cells were held at –50 mV and step depolarized to +50 mV in 10 mV increments. The data were obtained from 4 MRA and 4 TA cells. (Paired t—test between control and apamin; *, $p<0.05$; **, $p<0.01$).

Panel B. The apamin dependent current was isolated and magnified. The difference current was obtained by subtracting the current in the presence of apamin from the control. Apamin significantly inhibited MRA but not TA VSMC whole–cell current. The data were obtained from 4 MRA and 4 TA cells.

In Figure RII–7B, the same cell was maintained at a holding potential of –40 mV. IbTX (150 nM) completely abolished the whole–cell current which was composed exclusively of the K_{Ca}–dependent current. Addition of 4–AP (2 mM) produced no further reduction in current.

Figure RII–8 is the current voltage relationship for a single MRA VSMC exposed to IbTX and 4–AP. Figure RII–8A is the current voltage relationship for the cell maintained at a holding potential of –80 mV. IbTX (150 nM) blocked the K_{Ca}–dependent current; further addition of 4–AP (2 mM) abolished the remaining K_{dr}–dependent current. In Figure RII–8B, the cell was maintained at a holding potential of –40 mV to eliminate the K_{dr}–dependent current. IbTX (150 nM) blocked the K_{Ca}–dependent current and no significant outward current remained. 4–AP (2 mM) had no additive effect. Leak currents were not subtracted and accounted for the remaining small inward currents at negative holding potentials.

Figure RII–7. Pharmacology of MRA VSMC Whole–cell Major Currents.

A MRA VSMC was held at two holding potentials in the whole–cell configuration. At –80 mV, two components of outward current were elicited by 500 ms depolarizing pulses to +60 mV (10 mV increments). The first component of outward current was elicited at –30 mV and was smooth and small. This current corresponded to the delayed rectifier potassium channel (K_{dr}) –dependent current. At voltages above +30 mV, a larger noisy current was elicited. This current corresponded to the calcium–dependent potassium channel (K_{Ca}) – dependent current. At a holding potential of –40 mV, only the K_{Ca}–dependent current was elicited by depolarizing pulses. Leak currents were not subtracted.

Panel A. A MRA VSMC was held at –80 mV and both K_{dr} and K_{Ca} –dependent currents were elicited. IbTX (150 nM) was perfused into the bath and blocked the K_{Ca}–dependent current. Further addition of 4–AP (2 mM) resulted in the block of the K_{dr}–dependent current. Leak currents were not subtracted.

Panel B. A MRA VSMC was held at –40 mV and only the K_{Ca}–dependent current was observed. IbTX (150 nM) perfusion blocked the K_{Ca}–dependent current. Further addition of 4–AP (2 mM) had no effect. Leak currents were not subtracted.

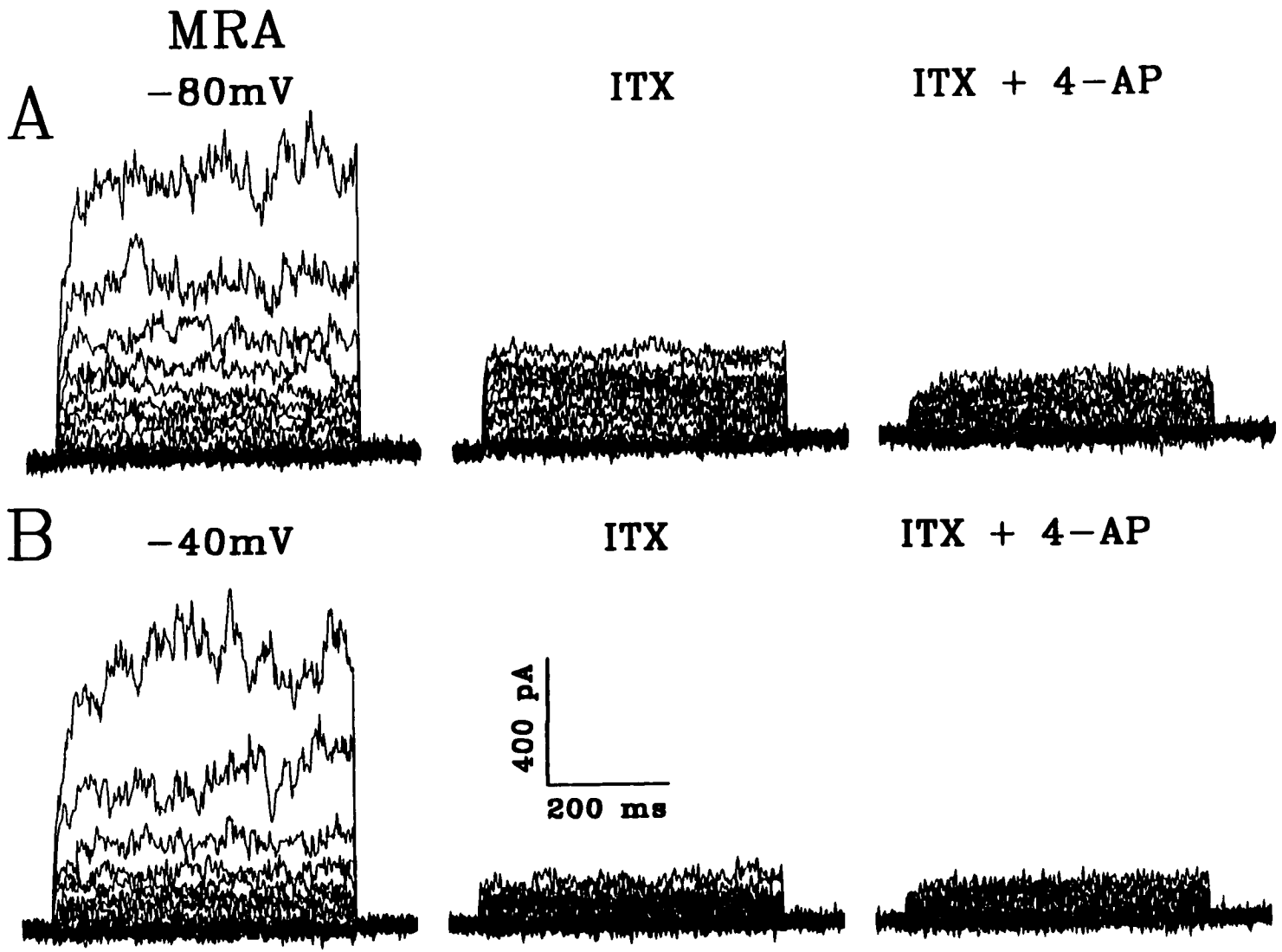
MRA
A
−80mV
ITX
ITX + 4−AP
B
−40mV
ITX
ITX + 4−AP
400 pA
200 ms

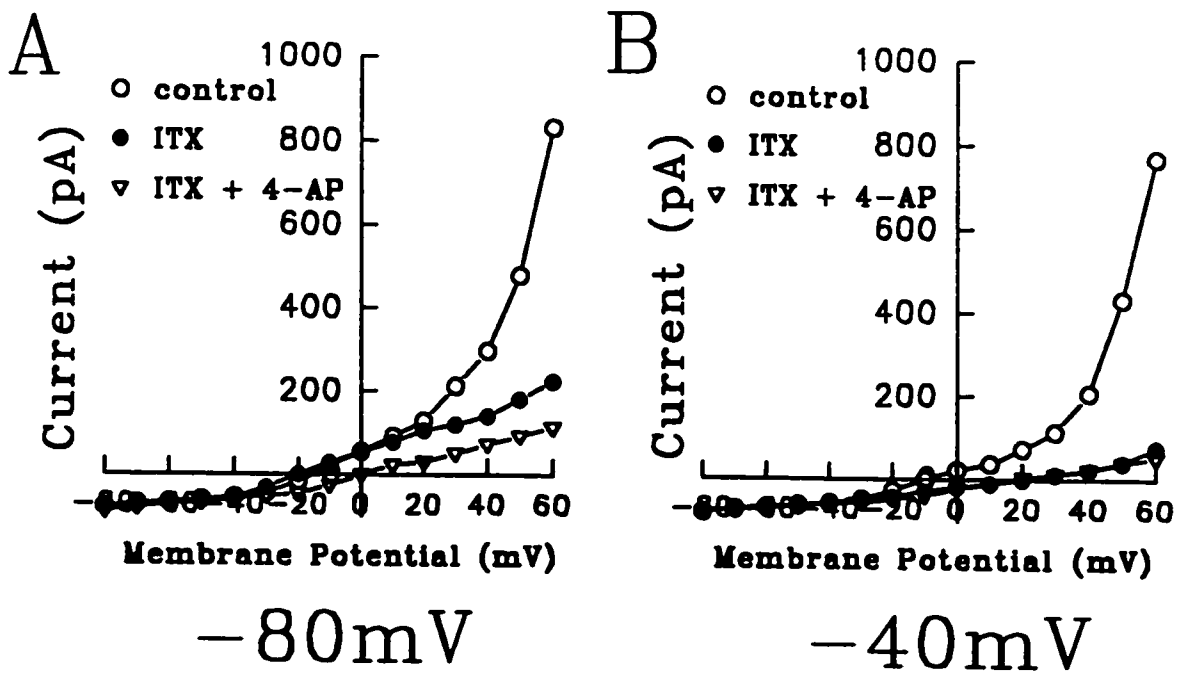

Figure RII–8. Current–voltage Relationship of IbTX and 4–AP on MRA VSMCs.

Panel A. A MRA VSMC was held at –80 mV and step depolarized to +60 mV by 10 mV increments for 500 ms. Both K_{Ca}– and K_{dr} –dependent currents were elicited. IbTX (150 nM) significantly blocked the K_{Ca}–dependent current. Further addition of 4–AP (2 mM) blocked the K_{dr}–dependent current. Leak currents were not subtracted.

Panel B. A MRA VSMC was held at –40 mV and step depolarized to +60 mV by 10 mV increments for 500 ms, and K_{Ca}–dependent current was elicited. This current was blocked by IbTX (150 nM). Further addition of 4–AP (2 mM) had no effect. Leak currents were not subtracted.

PART III. Properties of Four Types of MRA VSMC K–Channel — Linear Method

III.1 MRA VSMCs exhibited four types of K–channel

Single MRA VSMCs were patch clamped using the inside–out technique. When held at +40 mV, four distinct channel types were observed. These four types of K–channel were named according to their amplitude. Binned histograms from inside–out patches were made to measure the amplitude of the K–channels. Only very stable patches with long distinct openings were included in the amplitude histograms. The smallest K–channel was labeled the **miniK** (mini K–channel), and successively larger channels were named **SK** (small K–channel), **IK** (intermediate K–channel), and **BK** (big K–channel), respectively. Figure RIII–1 is an example of the four types of potassium channel from inside–out patches from MRA VSMCs.

TA VSMCs were patch clamped using the inside–out technique. Using the same protocol as per MRA VSMCs, four distinct K–channel types were observed. At +40 mV, they had similar amplitudes to the four types observed in MRA VSMCs and were named using the same convention (miniK, SK, IK, and BK). Figure RIII–2 is an example of the four types of K–channel observed from inside–out patches from TA VSMCs.

The similar amplitude of the four TA and MRA K–channels suggests that both VSMC types are regulated by similar K–channels. Thus it is likely that the K_{Ca} whole–cell current of both TA and MRA VSMCs is made up of BK and possibly IK channel events (Bolzon, 1992). The role of small K_{Ca} (SK and

Figure RIII–1. Examples of Four MRA VSMC K–channels.

Inside–out patches from MRA VSMCs were held at +40 mV. The bath solution, HPIS, contained 155 nM $[Ca^{2+}]_i$. The pipette solution, K–Hanks, contained 2 mM $[Ca^{2+}]_o$. Four distinct K–channels were observed and were named according to amplitude. The largest was the BK channel, with successively smaller channels named IK, SK, and miniK, respectively. The miniK channel had a small unitary current and is indicated with an asterisk (*). The record was filtered at 500 Hz to reduce noise and reveal the miniK. The closed state is marked (c).

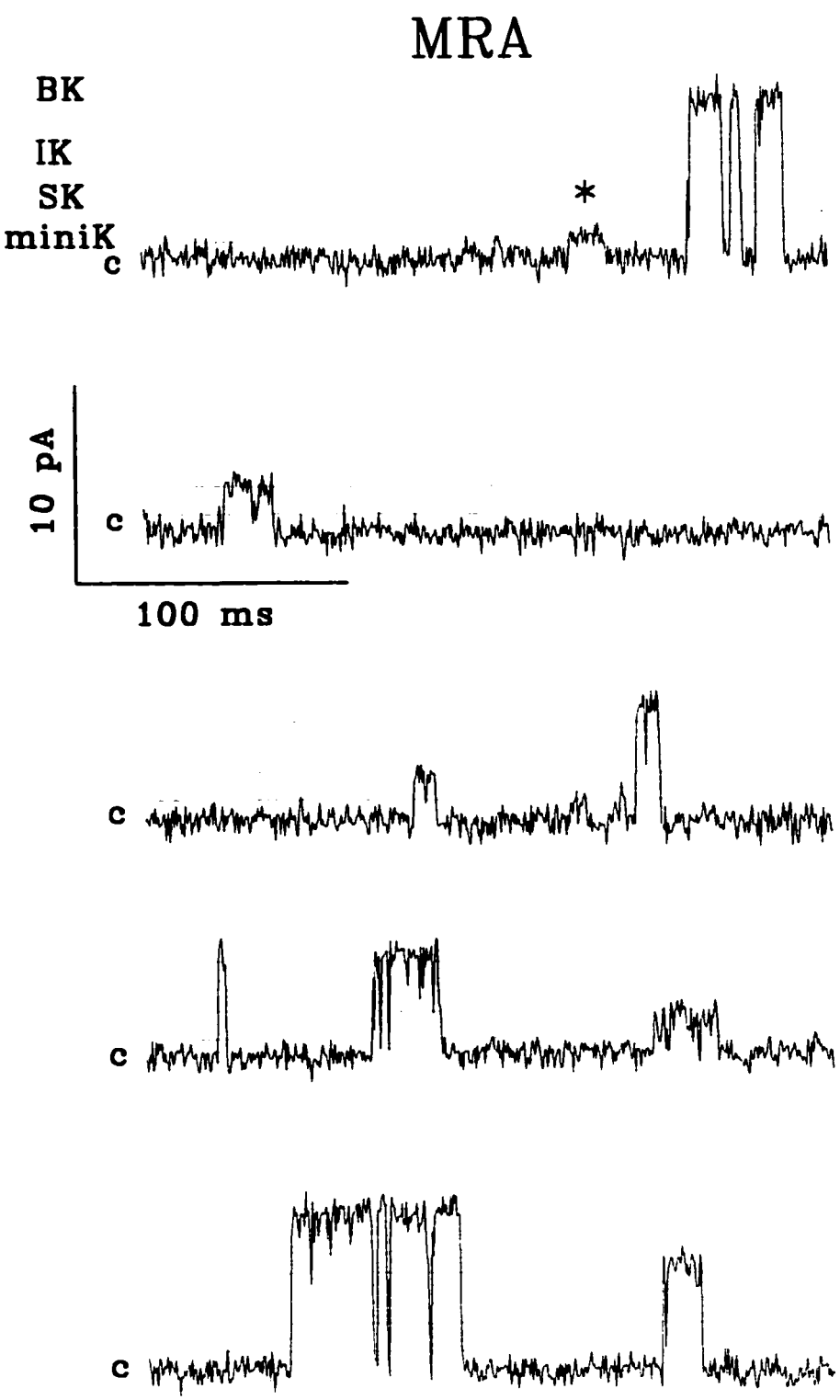
MRA
BK
IK
SK
miniK
c
*
10 pA
c
100 ms
c
c
c

Figure RIII–2. Examples of Four TA VSMC K–channels.

Inside–out patches from TA VSMCs were held at +40 mV. The bath solution, HPIS, contained 155 nM $[Ca^{2+}]_i$. The pipette solution, K–Hanks, contained 2 mM $[Ca^{2+}]_o$. Four distinct K–channels were observed and were named according to amplitude, as per MRA K–channels. The largest was the BK channel, with successively smaller channels named IK, SK, and miniK, respectively. The miniK channel had a small unitary current and is indicated with an asterisk (*). The record was filtered at 500 Hz to reduce noise and reveal the miniK. The closed state is marked (c).

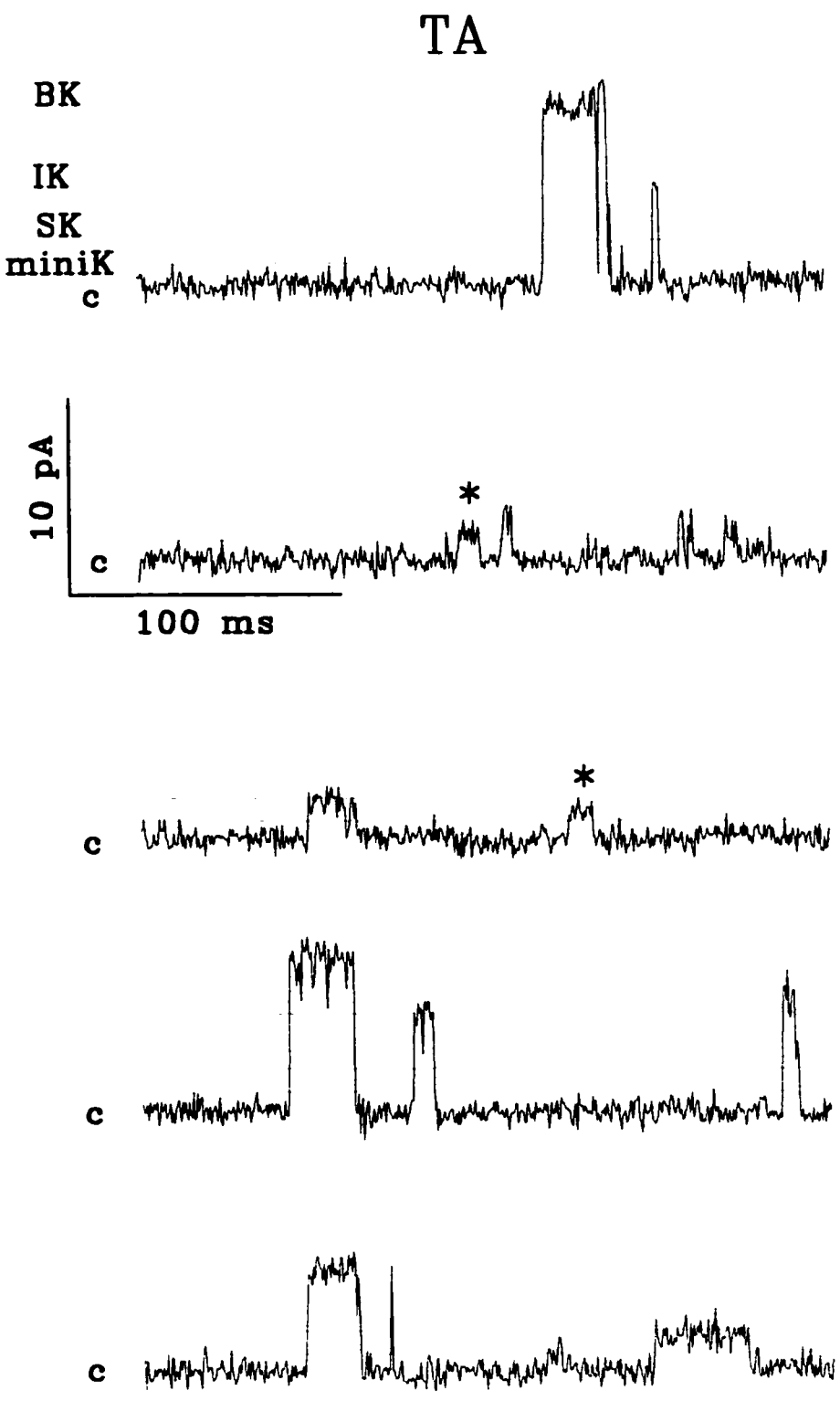
TA
BK
IK
SK
miniK
c
10 pA
c
100 ms
*
c
*
c
c

miniK) channels in VSM is unknown, but are responsible for afterhyperpolarizations in neurons and may regulate RMP (Lang and Ritchie, 1990; Leinders and Vijverberg, 1992); other functions are debatable since they were detected by apamin blockade rather than measurement of channel size.

III.2 linear method

MRA VSMCs were patch clamped using the inside–out technique under varying voltage (–60 to +60 mV) and external potassium concentration ($[K^+]_o$ = 5.5, 50, 100, 150 mM) and the unitary currents of the four K–channel types were recorded to determine the linear conductance. The unitary current–voltage data were plotted and fitted with linear functions (linear regression, least squares, pClamp6.1.1) to compare MRA data with the literature.

The reversal potential (K_{rev}) was calculated from the x–axis intercept of the function. Figures RIII–3A, 4A, 5A, and 6A are the data as analyzed by this linear function method. The conductance (g) and reversal potential (K_{rev}) of the four MRA K–channels are in the following table:

Table RIII–1. Linear Conductance of 4 MRA VSMC K–channels.

K–channel	$[K^+]_o$ (mM)	g (pS)	K_{rev} (mV)
BK	150	197	0.60
	100	179	–11
	50	137	–30
	5.5	(123)[1]	(–47)[1]
IK	150	94	0.96
	100	88	–9
	50	60	–29
	5.5	(70)[1]	(–45)[1]

SK	150	50	0.50
	100	48	−12
	50	29	−33
	5.5	(39)[1]	(−42)[1]
miniK	150	31	−1.6
	100	24	−3.8
	50	14	−51
	5.5	(11)[1]	(−58)[1]

Notes: *1.* The conductance and reversal potential are poor approximations because the K_o = 5.5 mM data were non–linear.

The conductance and reversal potential for MRA K–channels in the physiological condition ($[K^+]_o$ = 5.5 mM) are in parentheses because the data are poorly fitted with a linear function. Non–linear analysis of the data using fitted Goldman–Hodgkin–Katz (GHK) equations became more accurate than the linear technique as the $[K^+]_o$ decreased (see Results PART IV). That is, when conditions became less symmetrical, the linear approximation became less valid. However, linear approximations of conductance and reversal potential for $[K^+]_o$ = 50 and 100 mM were still valid since the data were linear within the range of voltages used to obtain channel amplitudes (0 to +60 mV). At these two external potassium concentrations, non–linear amplitudes dominate below 0 mV.

The miniK single channel amplitude was extremely difficult to measure, even when symmetrical potassium solutions ensured that channel amplitude was linear.

Figures RIII–3, 4, 5, and 6. Linear Analysis of Unitary Current.

Panel A. The unitary current of four MRA VSMC K–channels was measured at different voltages (–60 to +60 mV). The external concentration of potassium was reduced from symmetrical to physiological ($[K^+]_o$ = 150, 100, 50, and 5.5 mM). Linear regressions to the four sets of data were used to calculate the conductance (g) and reversal potential (K_{rev}). The data were obtained from 2 – 3 different membrane patches.

Panel B. The Nernst equation theoretical reversal potential at different concentrations of external potassium was plotted (solid line) as a linear function by taking the $\log_{10}$ of $[K^+]_o$. The reversal potential from linear regression in *Panel A* was plotted as symbols (filled triangle, open triangle, filled circle) and a linear regression to the data was determined (dotted line). The reversal potential calculated from linear regression deviated from the theoretical values as the $[K^+]_o$ deviated from symmetrical. The data were obtained from 2 – 3 different membrane patches.

Panel C. The unitary conductance calculated from linear regression in *Panel A* was plotted against the $[K^+]_o$. The data were fitted with a Michaelis–Menten function to determine the maximum conductance (g_{max}) and the concentration of potassium at half–maximum conductance ($K_{1/2}$). The data were obtained from 2 – 3 different membrane patches.

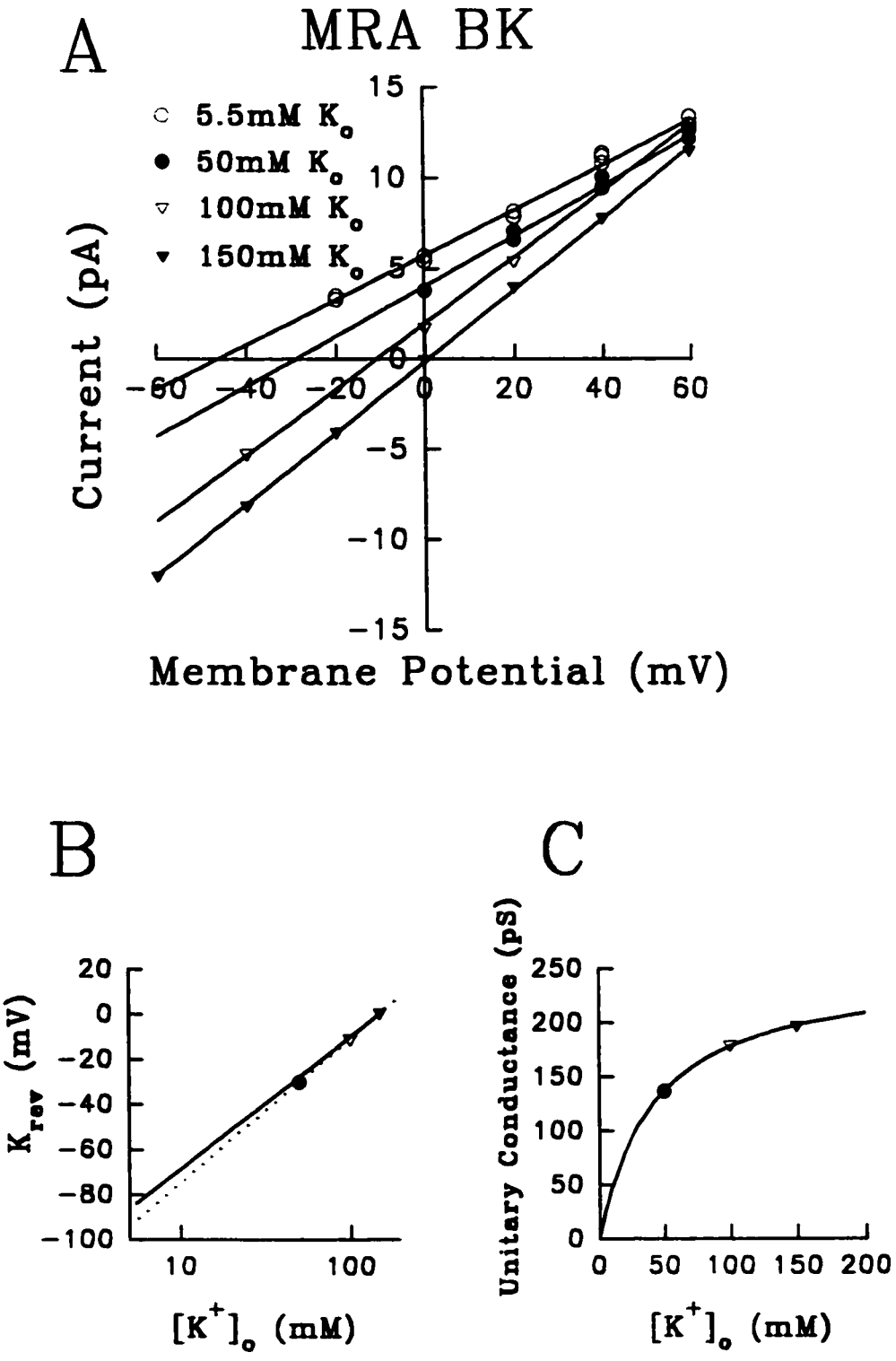
A
MRA BK
5.5mM K$_o$
50mM K$_o$
100mM K$_o$
150mM K$_o$
Current (pA)
Membrane Potential (mV)
15
10
5
0
-5
-10
-15
-60
-40
-20
0
20
40
60
B
K_{rev} (mV)
20
0
-20
-40
-60
-80
-100
10
100
$[K^+]_o$ (mM)
C
Unitary Conductance (pS)
250
200
150
100
50
0
0
50
100
150
200
$[K^+]_o$ (mM)

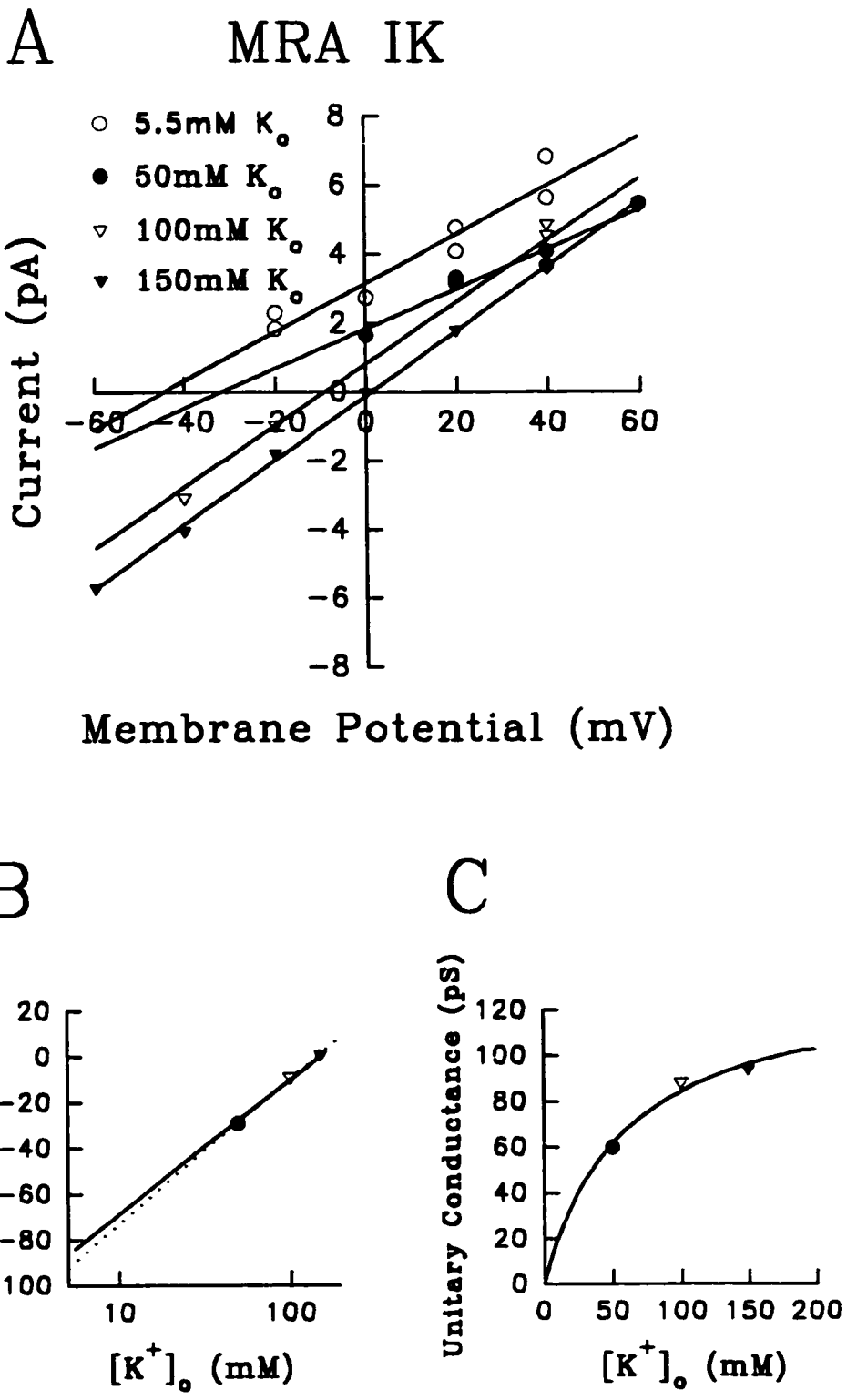
A
MRA IK
5.5mM K$_o$
50mM K$_o$
100mM K$_o$
150mM K$_o$
Current (pA)
8
6
4
2
0
-2
-4
-6
-8
-60
-40
-20
0
20
40
60
Membrane Potential (mV)
B
K_{rev} (mV)
20
0
-20
-40
-60
-80
-100
10
100
$[K^+]_o$ (mM)
C
Unitary Conductance (pS)
120
100
80
60
40
20
0
0
50
100
150
200
$[K^+]_o$ (mM)

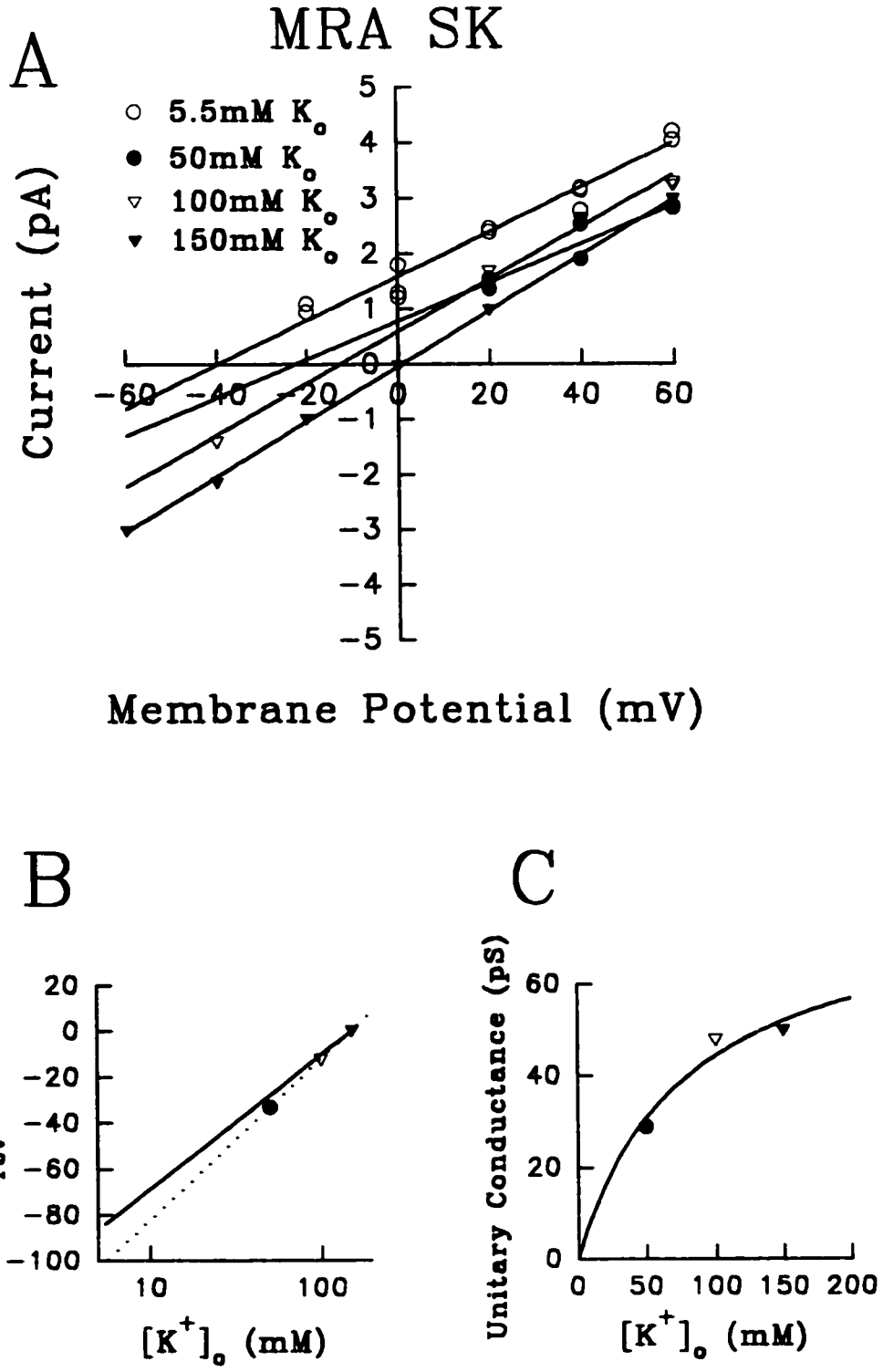
A
MRA SK
5.5mM K$_o$
50mM K$_o$
100mM K$_o$
150mM K$_o$
Current (pA)
Membrane Potential (mV)
B
K_{rev} (mV)
$[K^+]_o$ (mM)
C
Unitary Conductance (pS)
$[K^+]_o$ (mM)

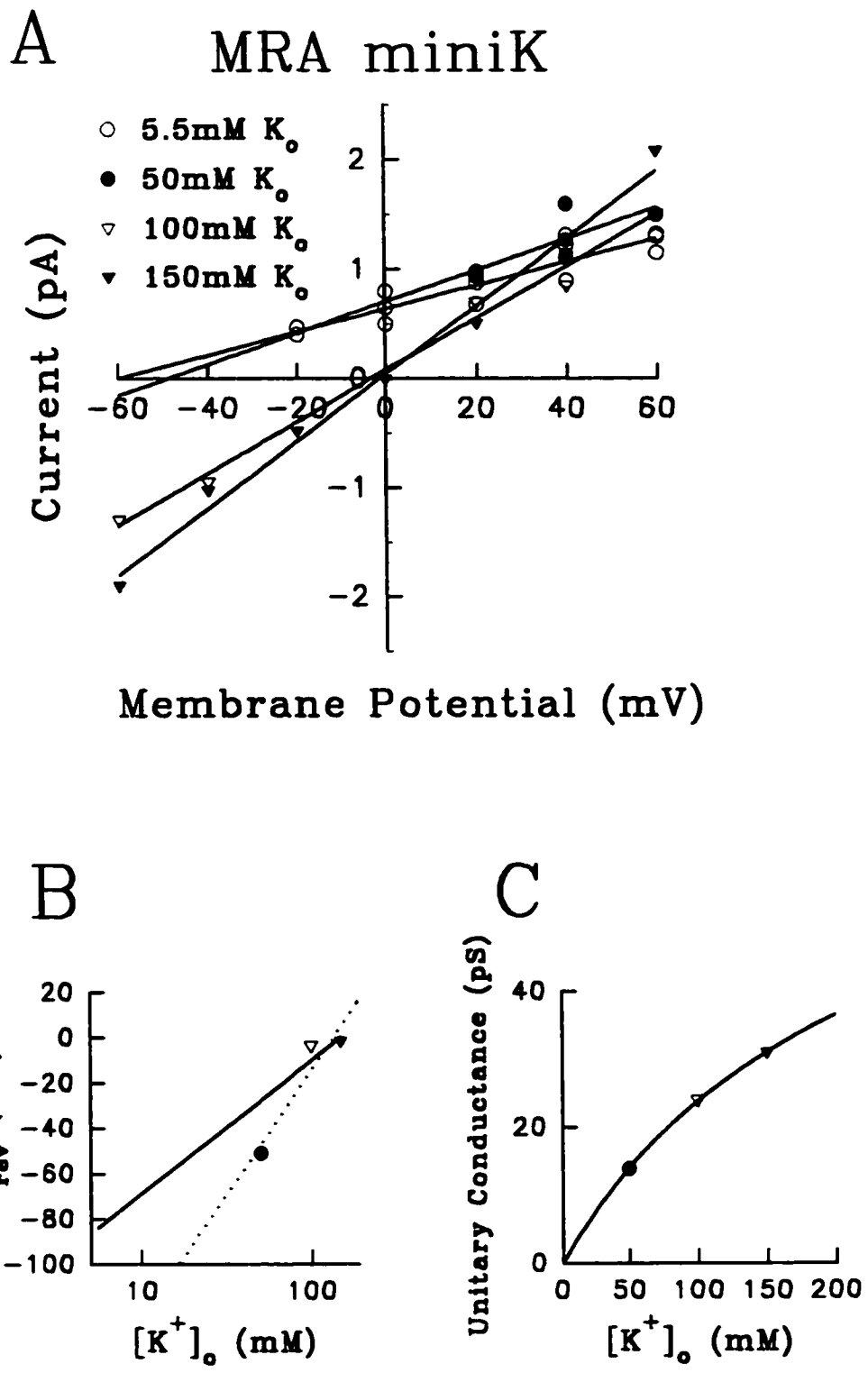
A
MRA miniK
5.5mM K$_o$
50mM K$_o$
100mM K$_o$
150mM K$_o$
Current (pA)
2
1
0
−1
−2
−60
−40
−20
0
20
40
60
Membrane Potential (mV)
B
K_{rev} (mV)
20
0
−20
−40
−60
−80
−100
10
100
$[K^+]_o$ (mM)
C
Unitary Conductance (pS)
40
20
0
0
50
100
150
200
$[K^+]_o$ (mM)

TA VSMC K–channels were also analyzed by the linear method. TA VSMCs were patch clamped using the inside–out technique using symmetrical potassium concentrations only. Figure RIII–7 is a combined plot of the amplitudes of the four major K–channel types in symmetrical solutions. The conductance and reversal potential for the four types of K–channel were determined from linear regression of the data and are displayed in the following table:

Table RIII–2. Linear Conductance of 4 TA VSMC K–channels.

K–channel	$[K^+]_o$ (mM)	g (pS)	K_{rev} (mV)
BK	150	210	–2.1
IK		115	–4.4
SK		67	–4.3
miniK		31	–2.2

III.3 reversal potential analysis (Nernst and K_{rev})

The Nernst equation was graphed as a linear function by plotting the theoretical and linear reversal potential against the logarithm (base 10) of the $[K^+]_o$. It was apparent that the approximation of the reversal potential as derived from the linear fit method diverged from the Nernst values as the $[K^+]_o$ decreased, particularly in the region below 50 mM.

At +40 mV, the miniK open amplitude was approximately 1 pA, the same size as the signal noise. The error associated with measuring such small channels resulted in poor estimations of the miniK reversal potential (Figure RIII–6B) and conductance (Table RIII–1).

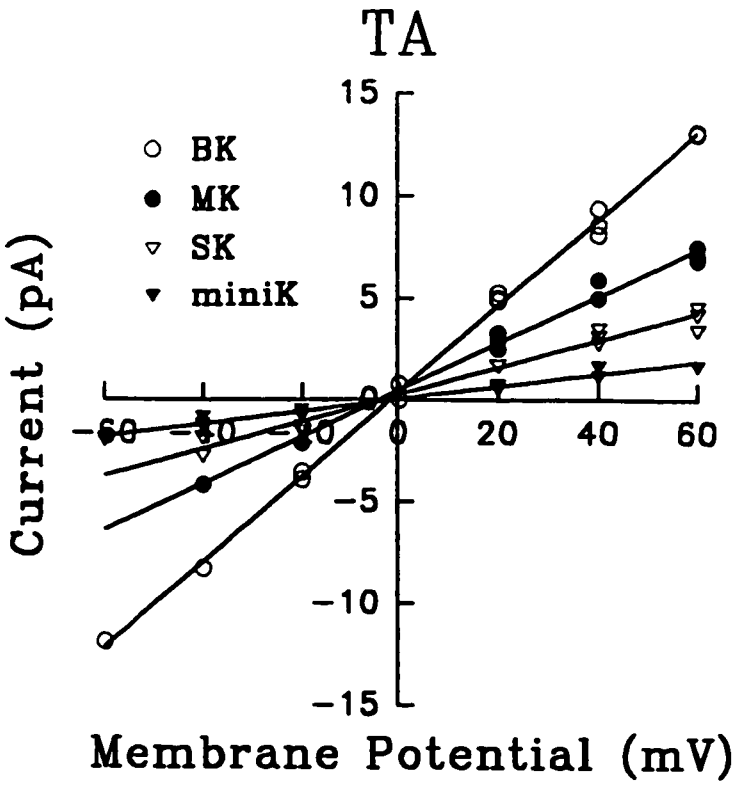

Figure RIII–7. Linear Analysis of TA VSMC K–channels.

The unitary current of TA VSMCs was recorded at different holding potentials. The bath and pipette contained symmetrical potassium solutions to maintain a linear conductance. The single channel conductance of the four TA VSMC K–channels were similar to those found in MRA VSMCs and are compared in the text. The data were obtained from 2 – 3 different membrane patches.

III.4 maximum conductance (g_{max} and $K_{1/2}$)

Figures RIII–3C, 4C, 5C, and 6C are plots of the unitary conductance of the channels as plotted against the $[K^+]_o$. The Michaelis–Menten function was fitted to the data to obtain a theoretical maximal conductance and concentration of potassium at half maximal conductance (to compare MRA K—channels with those found in the literature and to determine their functions and limits), and are presented in the following table:

Table RIII–3. Linear g_{max} and $K_{1/2}$ for MRA VSMC K–channels.

K–channel	$[K^+]_o$ (mM)	$g_{max} \pm$ SD (pS)	$K_{1/2} \pm$ SD (mM K^+_o)
BK	0, 50, 100, 150	253 ± 2.39	42.1 ± 1.28
IK		133 ± 11.9	58.0 ± 13.9
SK		79.0 ± 15.3	77.9 ± 34.9
miniK		(78.0 ± 2.04)[1]	(227 ± 8.98)[1]

Notes: *1.* These g_{max} and $K_{1/2}$ values are poor approximations.

PART IV. Properties of Four Types of MRA VSMC K–Channel — Non–Linear Method

IV.1 permeability constants

The permeability constants for the four MRA VSMC K–channels were calculated according to the equation which used the unitary conductance under symmetrical potassium solutions, and are presented in the following table:

Table RIV–1. MRA VSMC K–channel Permeability Constants.

K–channel	$[K^+]_{i/o}$ (mM)	g (pS)	P_K (cm/s)
BK	150	197	3.46×10^{-13}
IK		94	1.65×10^{-13}
SK		50	0.879×10^{-13}
miniK		31	0.545×10^{-13}

IV.2 GHK equations

The single channel amplitude data was observed to be less linear as the $[K^+]_o$ was decreased from symmetrical (150 mM) to physiological (5.5 mM). It was found that this data could be fitted with the constant field equations of Goldman–Hodgkin–Katz.

Figures RIV–1A, 2A, 3A, and 4A are plots of the unitary conductance of the MRA K–channels as fitted with GHK theoretical curves (solid lines). The curves use the data from the symmetrical condition to estimate the unitary current of the channels at different $[K^+]_o$ (100, 50, and 5.5 mM).

Figures RIV–1, 2, 3, and 4. Non–linear Analysis of Unitary Current.

Panel A. The data from 2 – 3 inside–out patches for the four MRA VSMC K–channels were analyzed by fitting the Goldman–Hodgkin–Katz equation. The conductance from the truly linear data (symmetrical 150 mM $[K^+]_{i/o}$) was used to calculate the theoretical conductance at varied external concentrations of potassium ($[K^+]_o$ = 150, 100, 50, and 5.5 mM, solid lines). Saturation of the channel at 150 mM $[K^+]_o$ resulted in errors in estimating the conductance at non–symmetrical concentrations. This deviation from unity increased as the concentrations deviated from symmetrical. A fit of the GHK equation to the 5.5 mM data (dotted line) is included to demonstrate the extreme deviation at this $[K^+]_o$. The GHK equation was fitted to all the data and the conductance of the K–channels are compared in the text. The data were obtained from 2 – 3 different membrane patches.

Panel B. The instantaneous unitary conductance at a particular set of conditions was calculated by dividing the unitary current by the driving force. The driving force was calculated by subtracting the reversal potential from the voltage. The Nernst reversal potential was used since the GHK equation fit the data well. The data were plotted as symbols at varied holding potentials. The physiological condition was approximated by the protocol using 5.5 mM $[K^+]_o$. However, only non–physiological holding potentials were used since it was very difficult to measure unitary current at –50 mV, the resting potential of MRA VSMCs in excised arteries. A linear function was plotted through the 5.5 mM data (solid line) with 95% confidence intervals (dotted lines flanking solid line) to estimate the physiological conductance of the four K–channel types. The data were obtained from 2 – 3 different membrane patches.

Panel C. The most accurate data was obtained at +40 mV since patches became unstable at higher voltages. At +60 mV, membrane patches regularly became leaky (R_s < 1 GΩ). This data (contained in vertical ellipse in *Panel B*) was plotted as instantaneous conductance versus the external concentration of potassium. Michaelis–Menten curves were fitted to the data including the 5.5 mM condition (+5.5, dotted line) and to the data excluding 5.5 mM $[K^+]_o$ (–5.5, solid line). The maximum conductance (g_{max}) and the Michaelis–Menten constant ($K_{1/2}$) were calculated for both sets of curves. The data were obtained from 2 – 3 different membrane patches.

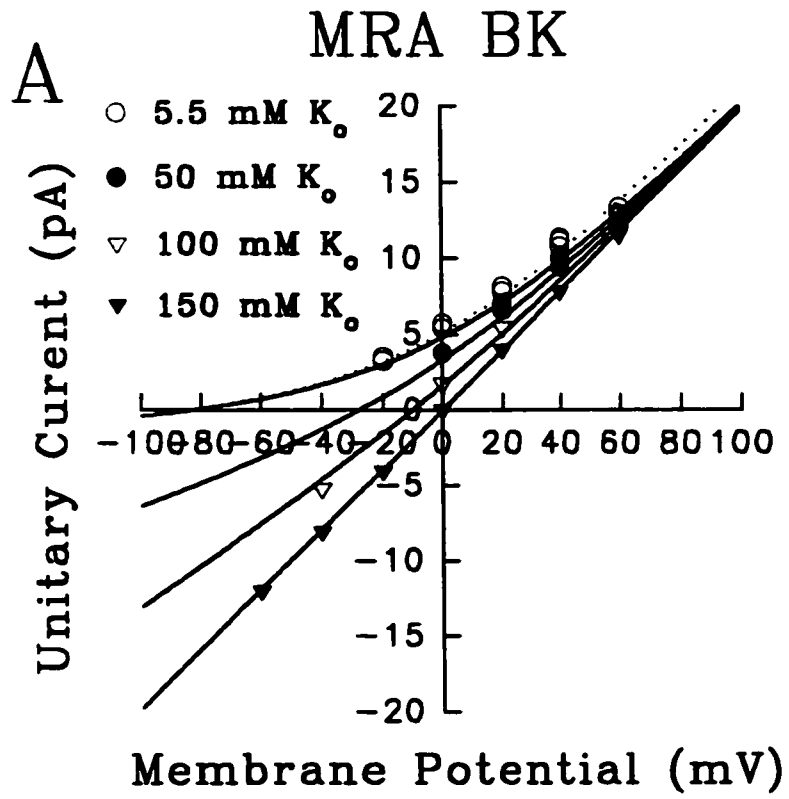
A
MRA BK
5.5 mM K$_o$
50 mM K$_o$
100 mM K$_o$
150 mM K$_o$
Unitary Curent (pA)
Membrane Potential (mV)

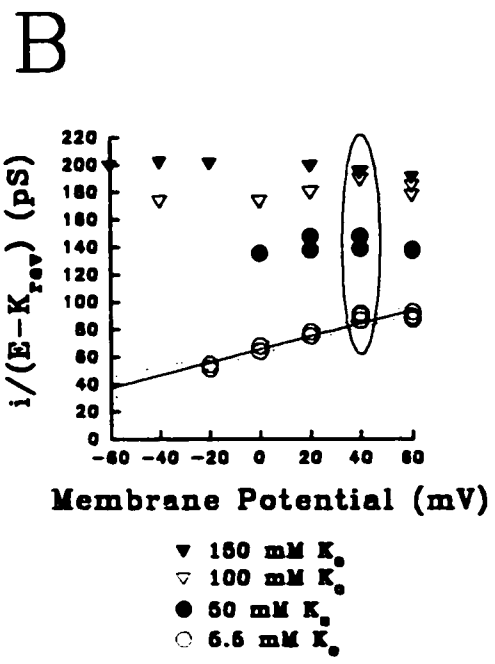
B
i/(E−K$_{rev}$) (pS)
Membrane Potential (mV)
150 mM K$_o$
100 mM K$_o$
50 mM K$_o$
5.5 mM K$_o$

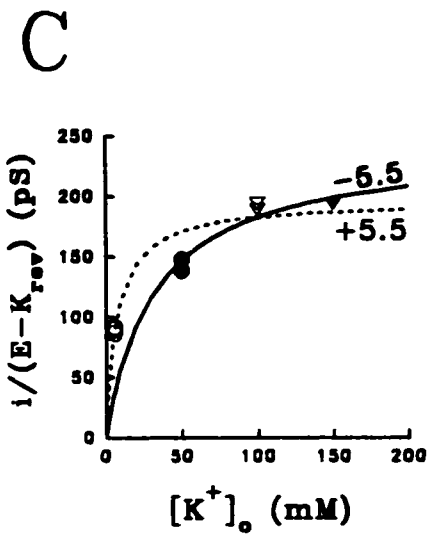
C
i/(E−K$_{rev}$) (pS)
−5.5
+5.5
[K$^+$]$_o$ (mM)

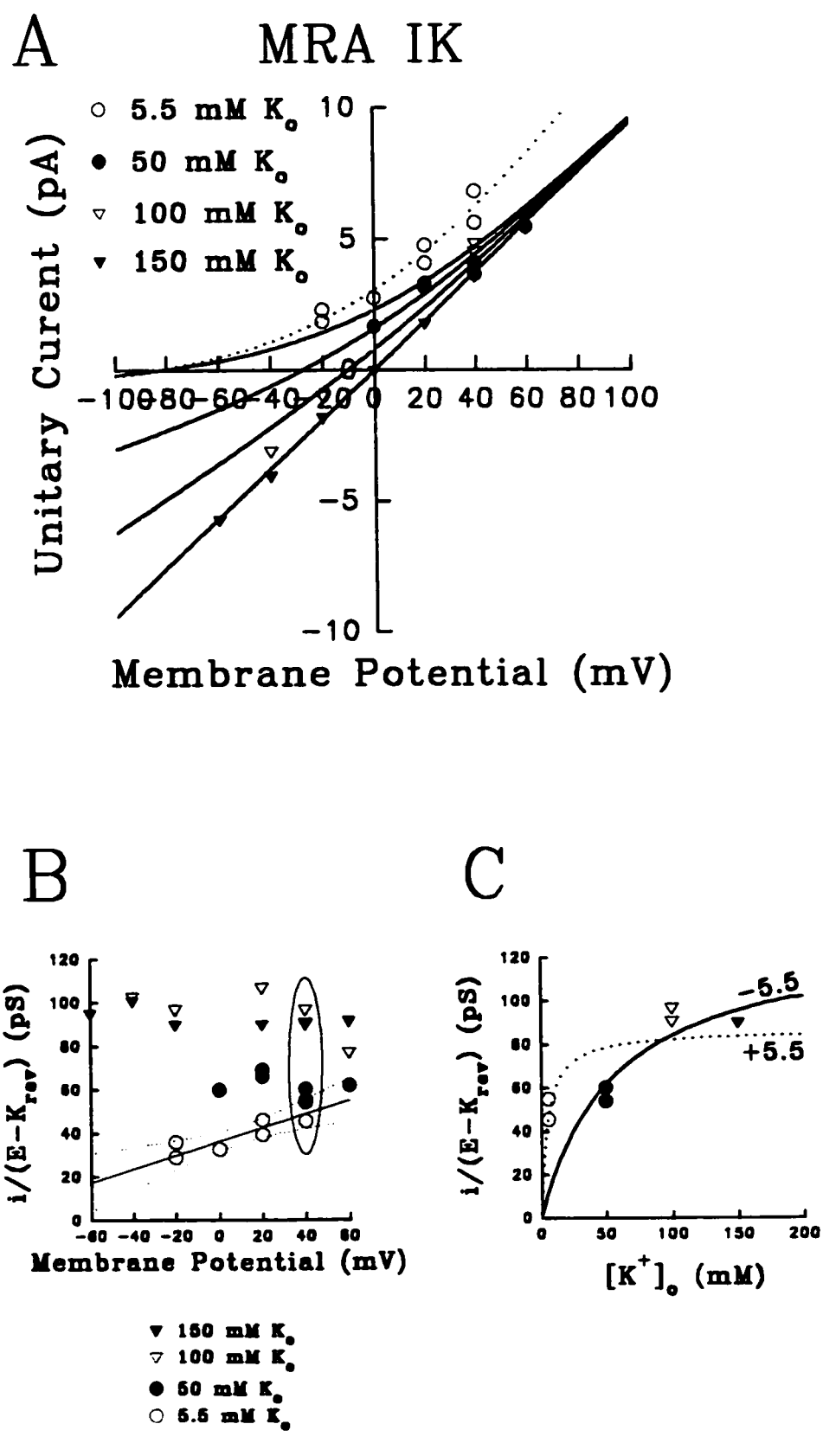
A
MRA IK
5.5 mM K$_o$
50 mM K$_o$
100 mM K$_o$
150 mM K$_o$
Unitary Curent (pA)
10
5
-5
-10
-100 -80 -60 -40 -20 0 20 40 60 80 100
Membrane Potential (mV)
B
i/(E-K$_{rev}$) (pS)
120
100
80
60
40
20
0
-60 -40 -20 0 20 40 60
Membrane Potential (mV)
150 mM K$_o$
100 mM K$_o$
50 mM K$_o$
5.5 mM K$_o$
C
i/(E-K$_{rev}$) (pS)
-5.5
+5.5
0 50 100 150 200
[K$^+$]$_o$ (mM)

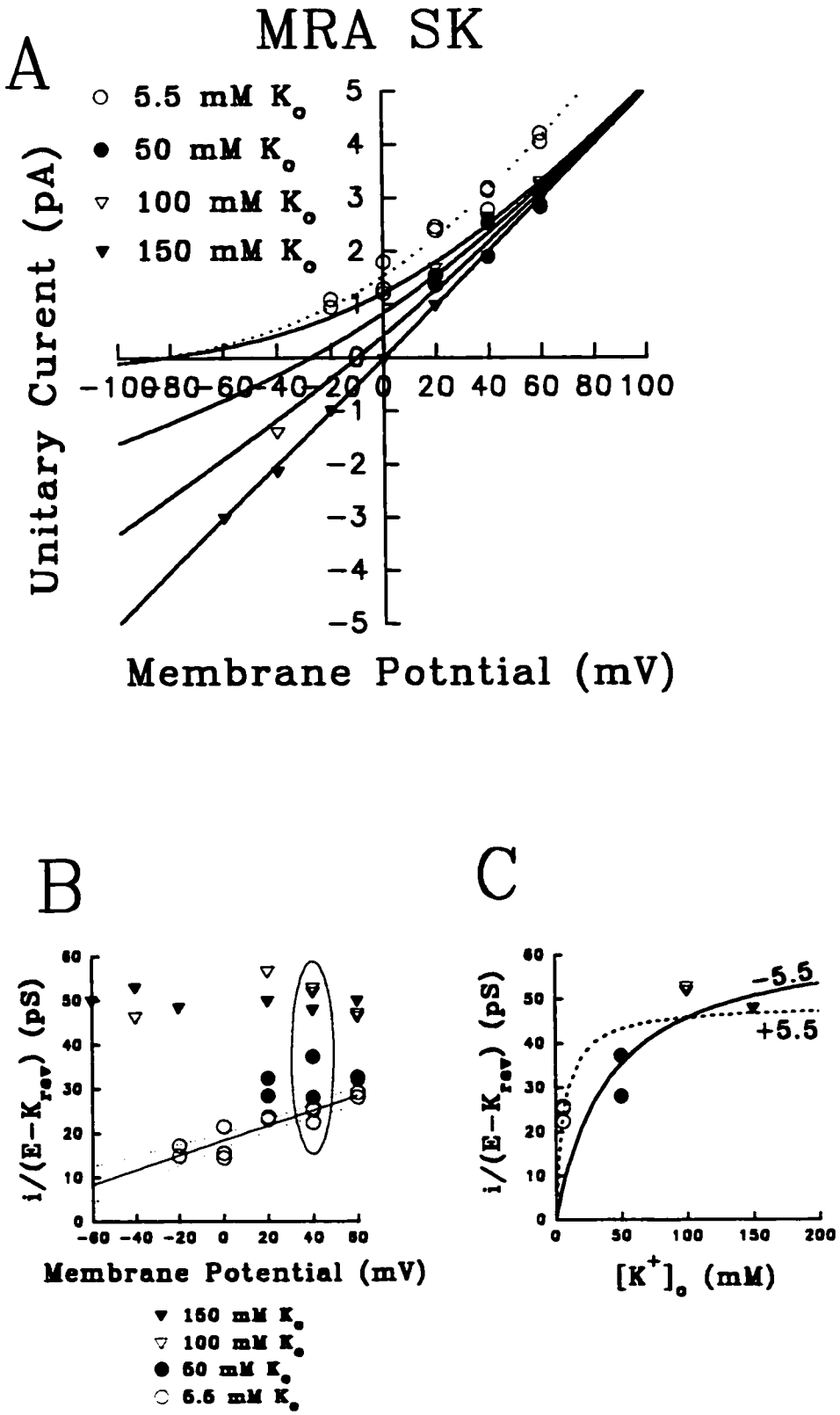
MRA SK
A
5.5 mM K$_o$
50 mM K$_o$
100 mM K$_o$
150 mM K$_o$
Unitary Curent (pA)
Membrane Potntial (mV)
B
i/(E−K$_{rev}$) (pS)
Membrane Potential (mV)
150 mM K$_o$
100 mM K$_o$
50 mM K$_o$
5.5 mM K$_o$
C
i/(E−K$_{rev}$) (pS)
−5.5
+5.5
[K$^+$]$_o$ (mM)

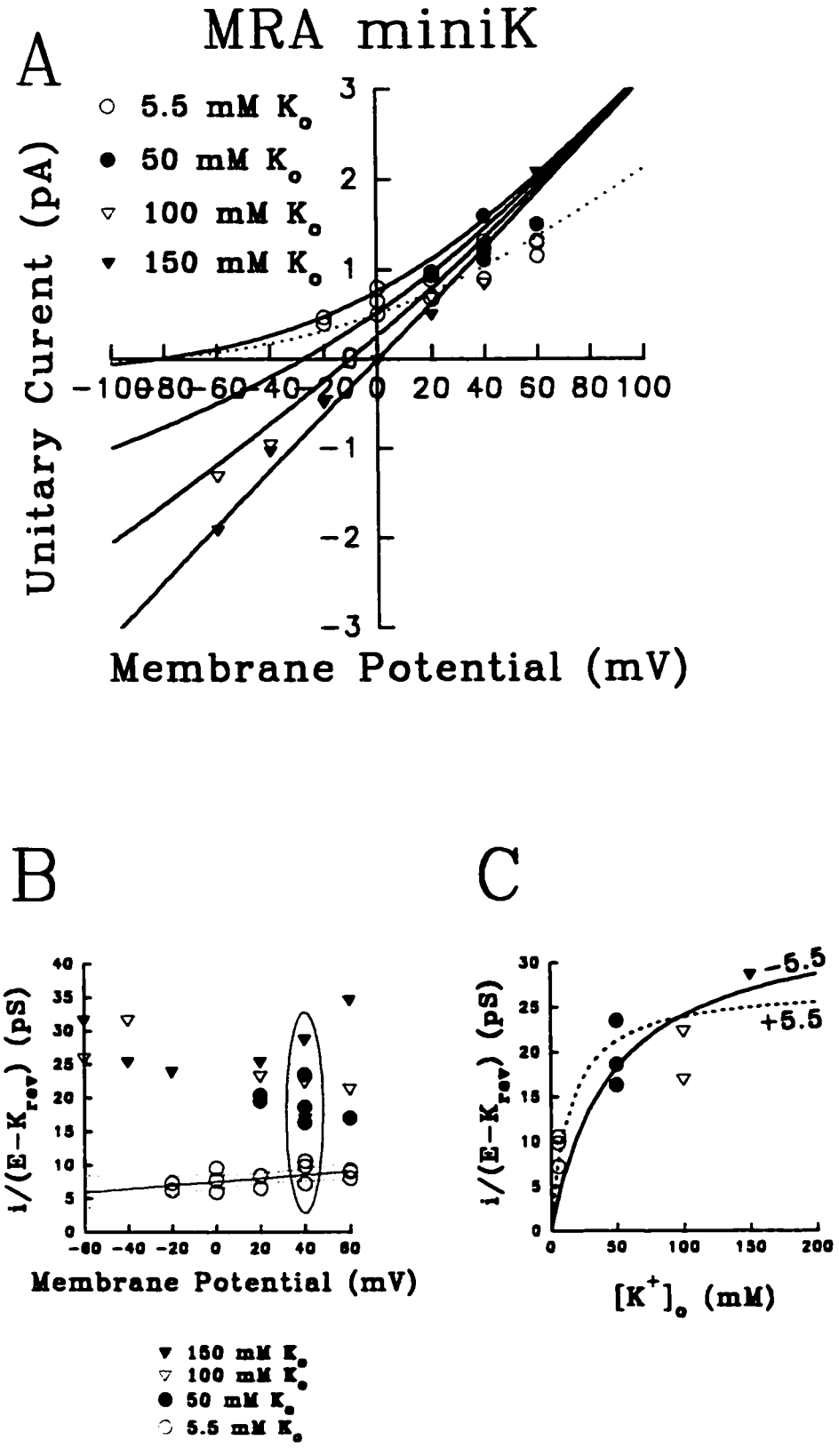
A
MRA miniK
5.5 mM K$_o$
50 mM K$_o$
100 mM K$_o$
150 mM K$_o$
Unitary Curent (pA)
Membrane Potential (mV)
B
i/(E-K$_{rev}$) (pS)
Membrane Potential (mV)
150 mM K$_o$
100 mM K$_o$
50 mM K$_o$
5.5 mM K$_o$
C
i/(E-K$_{rev}$) (pS)
-5.5
+5.5
[K$^+$]$_o$ (mM)

These curves fit the data well but shared the same fault as the linear method. The GHK functions failed to take into account the saturation of the channel at the symmetrical concentration of potassium (150 mM) when extrapolating the curve to the physiological concentration of potassium ($[K^+]_o$ = 5.5 mM). At 150 mM $[K^+]_o$, channel permeability had slowed due to slight saturation of the pore. The estimation of conductance at the physiological $[K^+]_o$ was lower than what was actually observed for the BK, IK, and SK channels. For all four K–channel types, the GHK equation was also fitted to the data. It was assumed that the reversal potential was unchanged and the conductance of the channel was extrapolated to the symmetrical ($K_{i/o}$ = 150 mM) condition.

The dotted line in Figures RIV–1A, 2A, 3A, and 4A is the GHK equation as fitted to the $[K^+]_o$ = 5.5 mM data. The equation was fitted to the 50 and 100 mM data as well, but was not plotted to prevent confusion. The extrapolated symmetrical conductance of each K–channel type as derived from the GHK equation under varying $[K^+]_o$ (150, 100, 50, and 5.5 mM) is presented in the following table:

Table RIV–2. GHK Conductance for Four MRA VSMC K–channels.

K–channel	$[K^+]_o$ (mM)	g (pS)
BK	150	197 ± 1.91
	100	211 ± 3.82
	50	199 ± 5.58
	5.5	208 ± 4.52
IK	150	93.7 ± 1.54
	100	102 ± 6.59
	50	87.8 ± 4.25
	5.5	124 ± 5.18

SK	150	50.1 ± 0.62
	100	56.0 ± 1.91
	50	45.7 ± 1.83
	5.5	62.7 ± 1.02
miniK	150	30.8 ± 1.57
	100	26.1 ± 2.47
	50	27.1 ± 1.86
	5.5	20.7 ± 1.05

Under symmetrical conditions, the GHK equation was reduced to a linear function, and the conductance results were identical to those obtained using the linear method.

IV.3 instantaneous conductance

Figures RIV–1B, 2B, 3B, and 4B are plots of the instantaneous conductance of the four MRA VSMC K–channels at different voltages under different $[K^+]_o$. For the four MRA K–channels, the instantaneous conductance under non–physiological $[K^+]_o$ (150, 100, 50 mM) was variable but was approximately linear (linear regression, least squares, pClamp 6.1.1) with a flat slope. In contrast, the instantaneous conductance under physiological $[K^+]_o$ (5.5 mM) was also linear but displayed a positive slope (linear regression, least squares, pClamp 6.1.1), which suggests that MRA K_{Ca} channels become partially saturated at elevated $[K^+]_o$ (50 mM) and are almost completely saturated at 100 mM. Thus, physiologically relevant information should be derived from data that most closely approximates the *in vivo* environment.

IV.4 physiological conductance

The actual conductance of the channels under physiological conditions was not known. The physiological condition could be approximated with the patch clamp technique at 5.5 mM $[K^+]_o$. Intact smooth muscle cells in SMA had a resting membrane potential of –50 to –51 mV (Chen and Cheung, 1997). The data for 5.5 mM $[K^+]_o$ were limited to the region between +60 mV and –20 mV.

A linear function was applied to the data to extrapolate a conductance at physiological holding potentials (–60 to –40 mV). The data appeared to be linear for all the channel types between –20 and +40 mV. However, it was not known whether it continued to be linear below –20 mV. The physiological conductance might have been significantly higher than estimated if the function approached an asymptote. With this in mind, 95% confidence intervals were applied to linear regressions of the data (linear regression, least squares, pClamp 6.1.1). Since the smallest calculated conductance was measured at –20 mV, this value and its error are also given in the following table:

Table RIV–3. Estimated Physiological Conductance of 4 MRA VSMC K–channels.

K–channel	$[K^+]_o$ (mM)	g (–20 mV) ± sem (pS)	g (–50 mV),(pS) (95% confidence interval)
BK	5.5	53.0 ± 1.48	42.3 (35.3 – 49.4)
IK		32.4 ± 3.52	20.6 (9.00 – 32.2)
SK		16.0 ± 1.17	10.1 (6.41 – 13.7)
miniK		6.80 ± 0.55	6.23 (4.05 – 8.42)

IV.5 maximum conductance (g_{max} and $K_{1/2}$)

The maximal conductance (g_{max}) and $[K^+]_o$ at half–maximal conductance ($K_{1/2}$) were calculated from the non–linear analysis of instantaneous conductance to compare the MRA K–channels with literature. The g_{max} determines the maximal, saturated conductance of the K–channel whereas the $K_{1/2}$ determines the rate at which changes in $[K^+]_o$ affect the conductance of K–channels and thus K current.

The data at +40 mV were selected because the single channel amplitudes at this holding potential were maximized. Only at +60 mV were higher amplitudes recorded. However, the membrane commonly became unstable at +60 mV and the seal was lost. This suggested that the membrane was under undue stress and could not provide accurate measurements at this high potential. The IK channel had a low open probability and no IK open channel amplitude data could be recorded at +60 mV before seal loss. The +40 mV data in Figures RIV–1B, 2B, 3B, and 4B are enclosed in an ellipse. The data was plotted as instantaneous conductance versus $[K^+]_o$ in Figures RIV–1C, 2C, 3C, and 4C.

The Michaelis–Menten equation used to calculate g_{max} and $K_{1/2}$ in the Linear Method section was applied to the non–linear derived data. The data were fitted with two curves, one which included the 5.5 mM data (+5.5, dotted line) and one which did not (–5.5, solid line). The g_{max} and $K_{1/2}$ values were calculated for both conditions and presented in the following table:

Table RIV–4. Non–linear g_{max} and $K_{1/2}$ for MRA VSMC K–channels.

K–channel	$[K^+]_o$ (mM)	$g_{max} \pm SD$ (pS)	$K_{1/2} \pm SD$ (mM K^+_o)
BK	50, 100, 150	242 ± 12.5	32.1 ± 6.65
IK		132 ± 23.2	56.6 ± 27.2
SK		64.5 ± 10.6	41.0 ± 23.1
miniK		35.6 ± 7.32	47.6 ± 29.4
BK	5.5, 50, 100, 150	196 ± 8.08	7.29 ± 1.65
IK		86.2 ± 7.80	4.78 ± 2.81
SK		48.6 ± 3.30	6.16 ± 2.35
miniK		27.4 ± 2.66	14.4 ± 6.83

The curve which includes the K_o = 5.5 mM data (+5.5, dotted line) passes through the 5.5 mM point but completely excludes the 50 mM data for the BK, IK, and SK channels. The g_{max} values calculated are only slightly higher than the values recorded at 150 mM. However, the curve which excludes the K_o = 5.5 mM data (–5.5, solid line) fits the remainder of the data well but poorly fits the physiological range of $[K^+]_o$. This discrepancy in fit is due to the high intracellular potassium (K_i = 150 mM). Channel saturation curves are accurate only when symmetrical ion concentrations are maintained (Hille, 1992). The elevated $[K^+]_i$ increases the outward driving force and thus single channel instantaneous conductance. This effect increases as the ratio of intracellular to extracellular potassium increases. However, the data can be fit with a general function that can predict the instantaneous conductance at any K_o (but only within the range tested) (Sadoshima *et al.*, 1988), of the form:

$$g([K^+]_o) = (g[K^+]_o = \text{"0"}) + n \sqrt{[K^+]_o}$$

where:

$g([K^+]_o)$ is the conductance at any $[K^+]_o$ (within tested range)

($g[K^+]_o$ = "0") is the predicted conductance at $[K^+]_o$ = 0 mM, which is the y–intercept

n is the slope factor

$[K^+]_o$ is the external potassium concentration

However, no additional information can be gained from fitting this function to the data. The only purpose of doing so would be to accurately calculate the conductance within the range of $[K^+]_o$ tested. The linear and non–linear fits used to calculate g_{max} were sufficient for channel characterization.

IV.6 MRA VSMC K–channel ion selectivity

The Goldman–Hodgkin–Katz equation used to fit the data did not take into account permeability of the channel to any ion other than the selective one. The GHK equation fit the data well and was a useful predictor of conductance and unitary current at a particular voltage at a particular external or internal potassium concentration. The small deviations from theoretical values could be accounted for by saturation theory.

The linear method of determining reversal potential was also very close to the theoretical values for 150, 100 and 50 mM $[K^+]_o$. It was not accurate for estimating the non–linear 5.5 mM $[K^+]_o$ data or the miniK reversal potential. The reversal potentials that could be compared to theoretical values were those from the BK, IK, and SK channels at 50, 100, and 150 mM $[K^+]_o$. These values were so close to theoretical that any variation was probably due to chance and not to sodium permeability. In fact, all the data at 50 mM $[K^+]_o$ for the BK, IK, and SK

channels would predict infinitely higher preference for potassium over sodium permeation since the reversal potentials were lower than the –28 mV Nernst value.

The data from linear and non–linear analysis of reversal potentials suggested that the three largest K–channel types (BK, IK, and SK) were selective K–channels. These three K–channel types had a 1000 to 10 000 times greater selectivity for potassium over sodium. The small single channel amplitude of the miniK made it was difficult to determine if this channel was as highly selective as the BK, IK, and SK were for potassium.

PART V. Single Channel Activity of Four MRA VSMC K–Channels

V.1 Ca^{2+}–dependent NP_O of 4 MRA VSMC K–channels (+40 mV)

Initial experiments indicated that the activity of all four MRA VSMC K–channels was highly calcium–dependent. The experiments performed use calcium concentrations within physiological ranges (0, 50, 155, 300, 500, and 750 nM $[Ca^{2+}]_i$). Figures RV–1, 2, 3, and 4 are 15 second traces from inside–out patches held at +40 mV. At 0 nM $[Ca^{2+}]_i$, all K–channels demonstrated low activity with only short, rare openings. As the $[Ca^{2+}]_i$ increased, the open probability of all four K–channel types increased.

Figure RV–5 is a concentration response curve of the open probability of the four MRA VSMC K–channel types for changes in calcium within the physiological range (0 to 750 nM, voltage clamped at +40 mV). Calcium concentration–dependently increased the open probability of all four K–channels from 0 to 500 nM $[Ca^{2+}]_i$. The most active K–channel at +40 mV and 500 nM $[Ca^{2+}]_i$ was the BK channel, with decreasing activity expressed by the miniK, SK, and IK channels, respectively. At +40 mV, the BK channel was very calcium sensitive, and the miniK, SK, and IK were less sensitive.

All four K–channel types were less active at 750 nM than at 500 nM $[Ca^{2+}]_i$. This may be due to "run–down" of the patch or to calcium–dependent inhibition of channel activity (see Discussion). Run–down is the slow decrease in ion channel current measured over time due to the loss of intracellular regulators leaking through the membrane, the lack of energy sources (ATP, glucose), or to changes in regulation due to damage during single VSMC isolation with enzymes

Figures RV–1, 2, 3, and 4. Examples of Calcium–dependent Activity of Four MRA VSMC K–channels (+40 mV).

The single channel activity of the four MRA VSMC K–channels was observed at +40 mV for fifteen–second sweeps from inside–out patches. The open probability of all four K–channels was concentration dependently increased (0 to 500 nM $[Ca^{2+}]_i$). BK channels appear in traces from IK, SK, and miniK examples because they were so common. The closed state is marked with a (c).

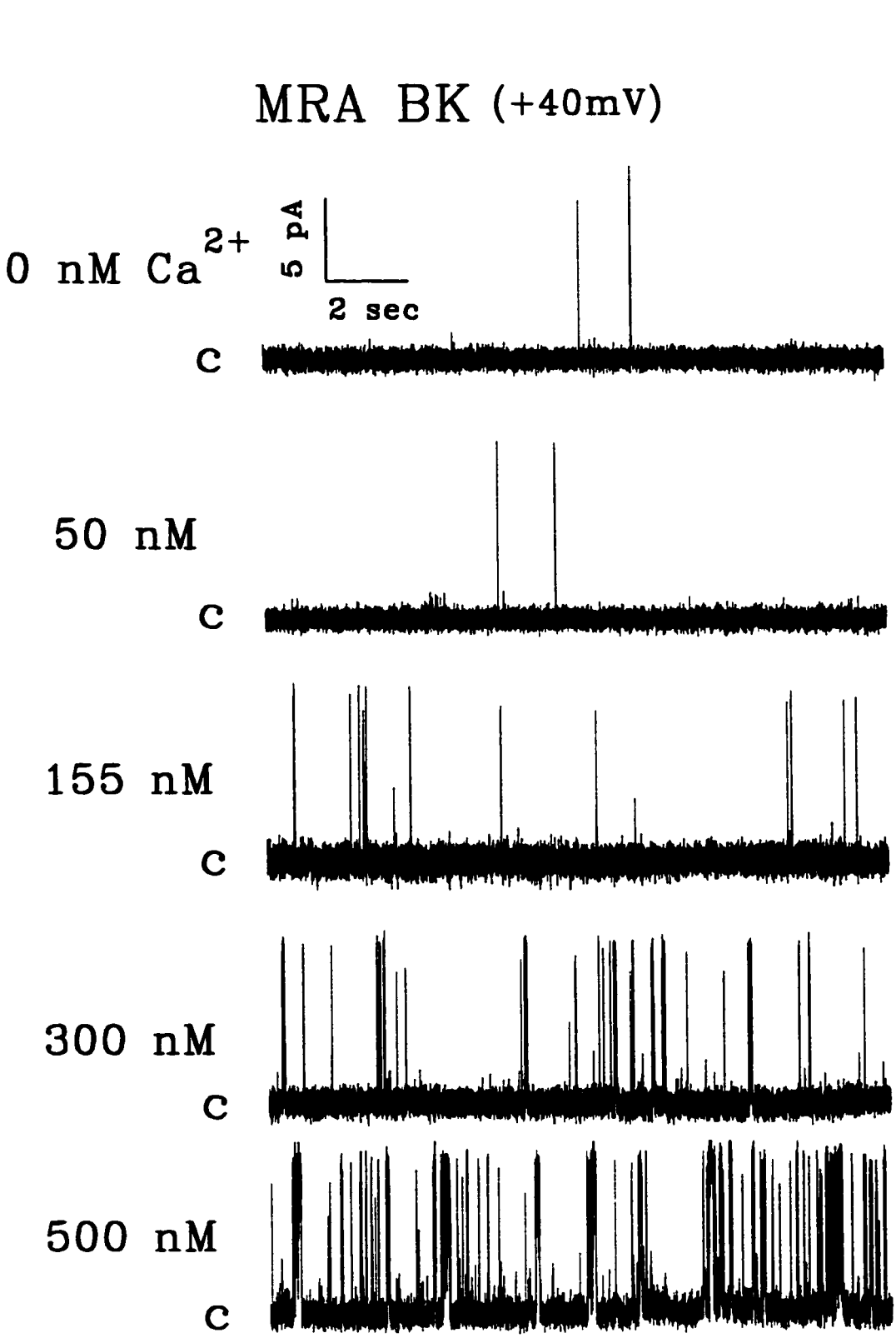
MRA BK (+40mV)
0 nM Ca2+
5 pA
2 sec
C
50 nM
C
155 nM
C
300 nM
C
500 nM
C

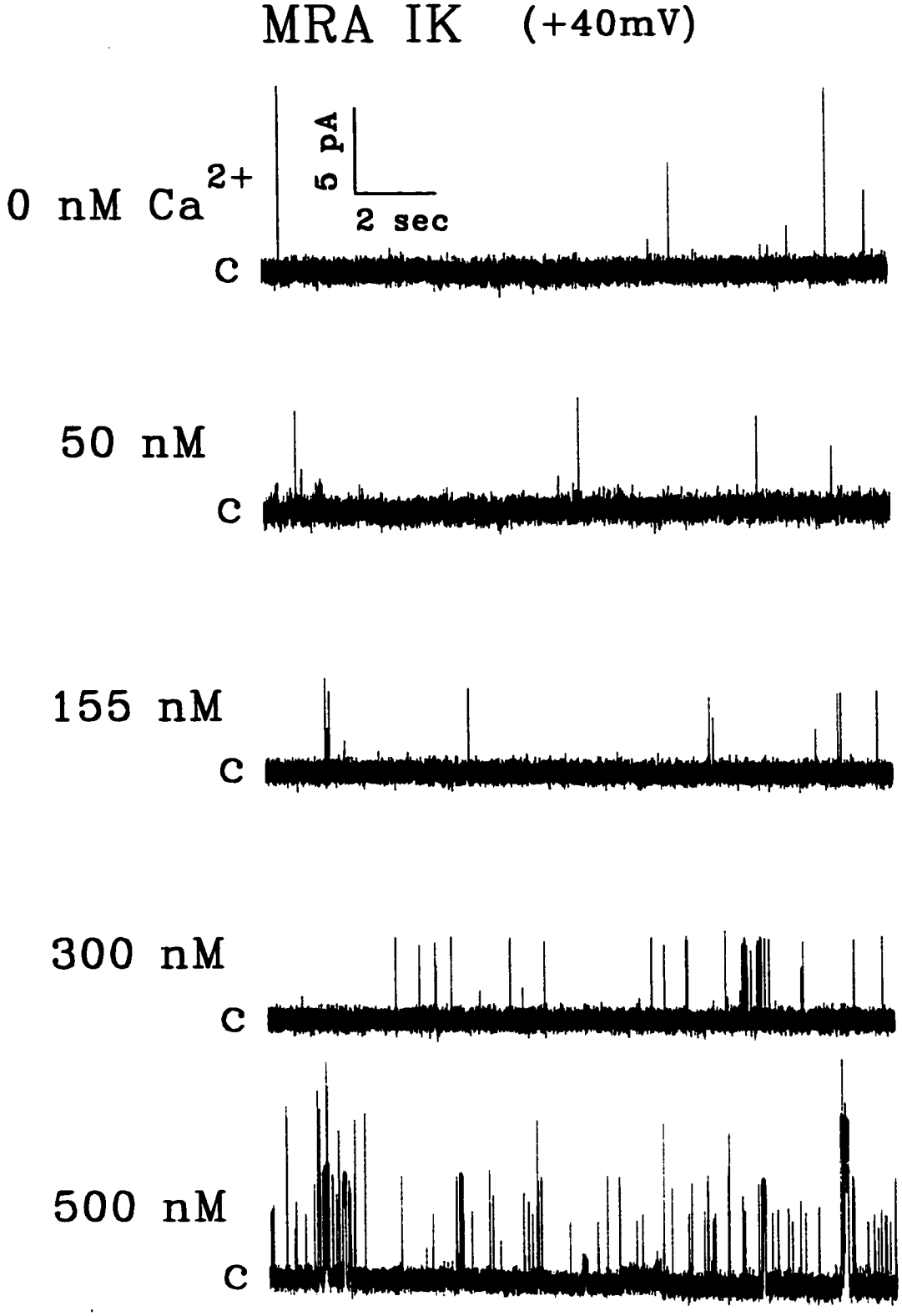
MRA IK (+40mV)
0 nM Ca2+
5 pA
2 sec
C
50 nM
C
155 nM
C
300 nM
C
500 nM
C

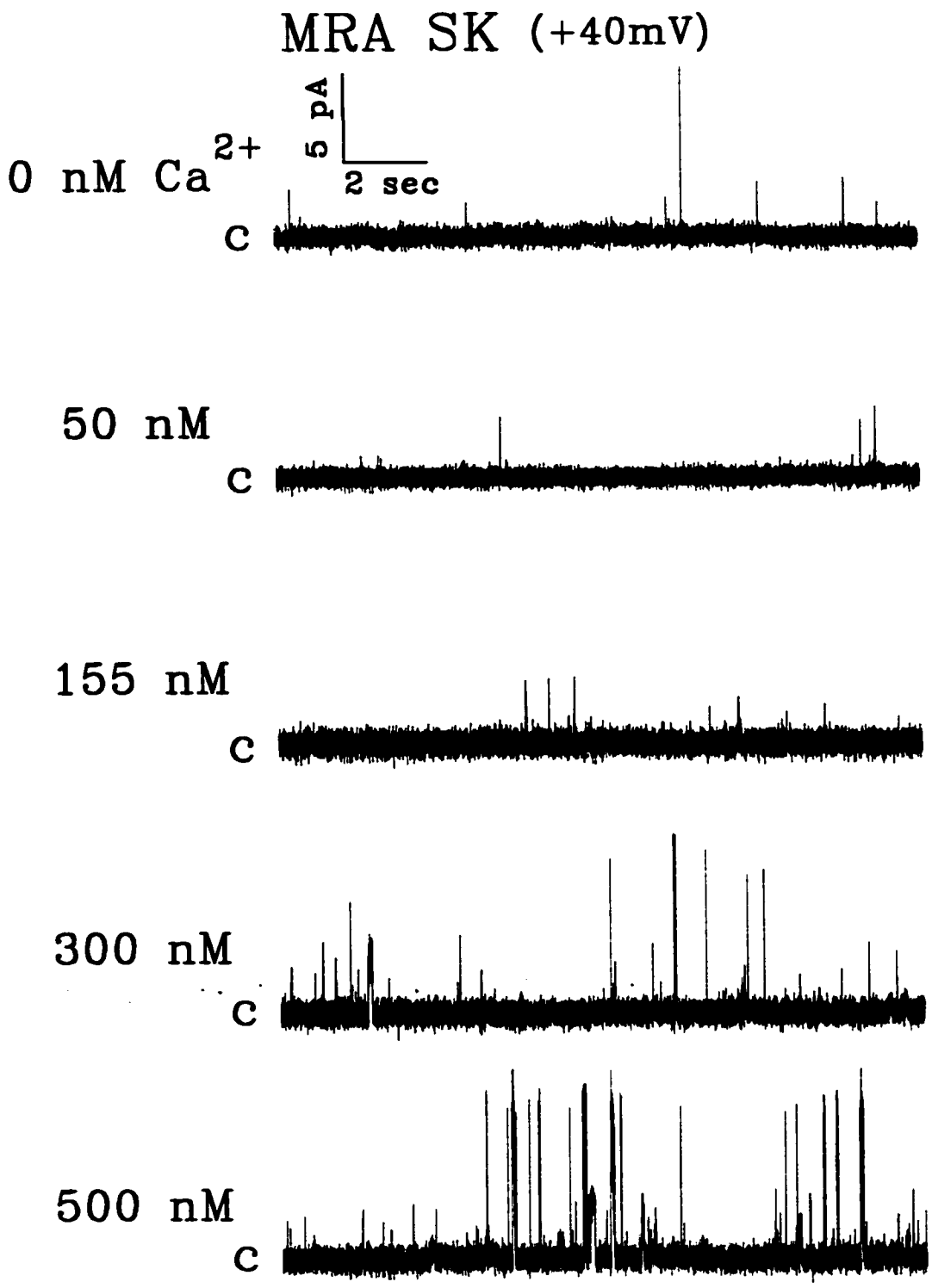
MRA SK (+40mV)
5 pA
2 sec
0 nM Ca2+
C
50 nM
C
155 nM
C
300 nM
C
500 nM
C

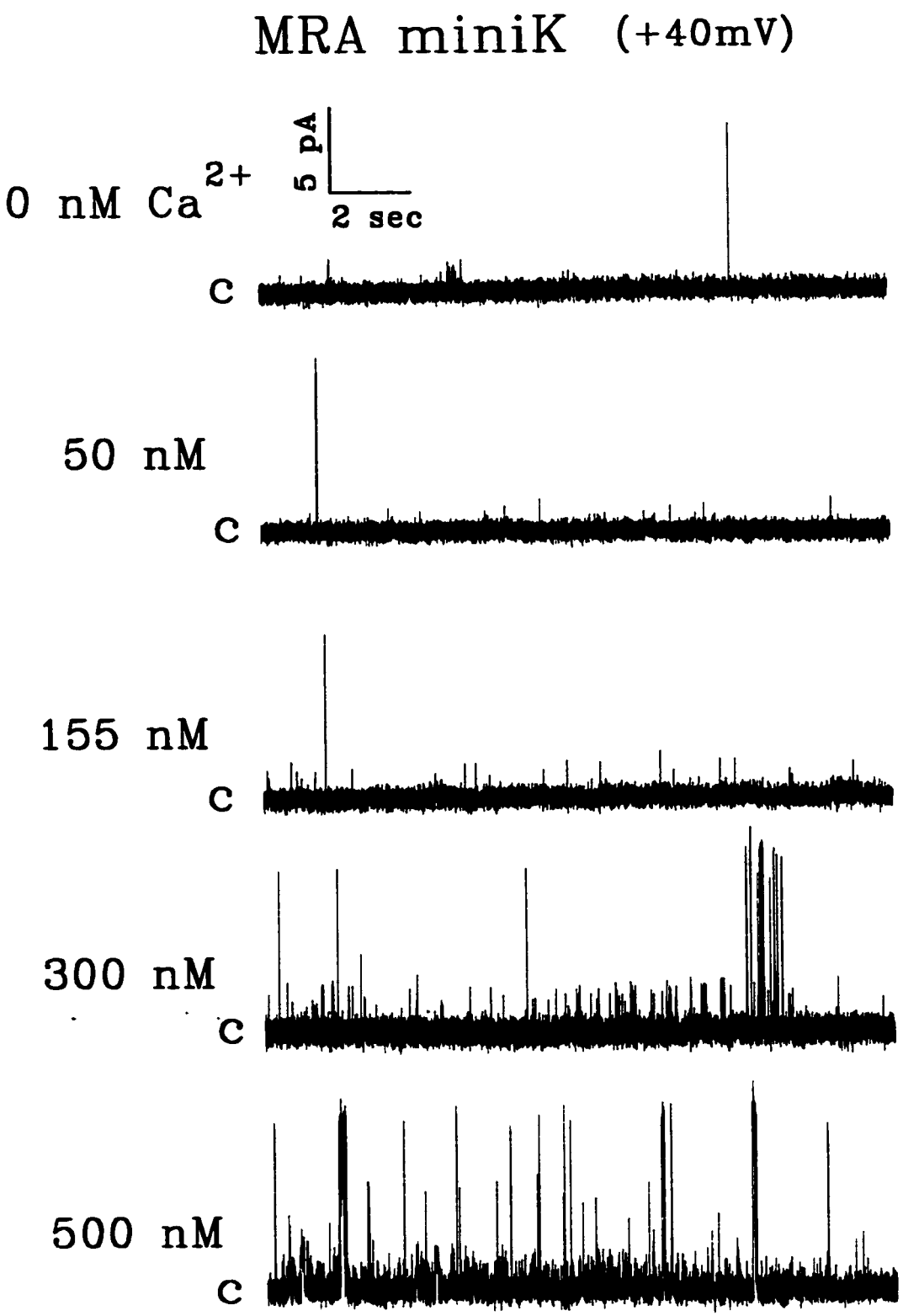
MRA miniK (+40mV)
0 nM Ca2+
5 pA
2 sec
C
50 nM
C
155 nM
C
300 nM
C
500 nM
C

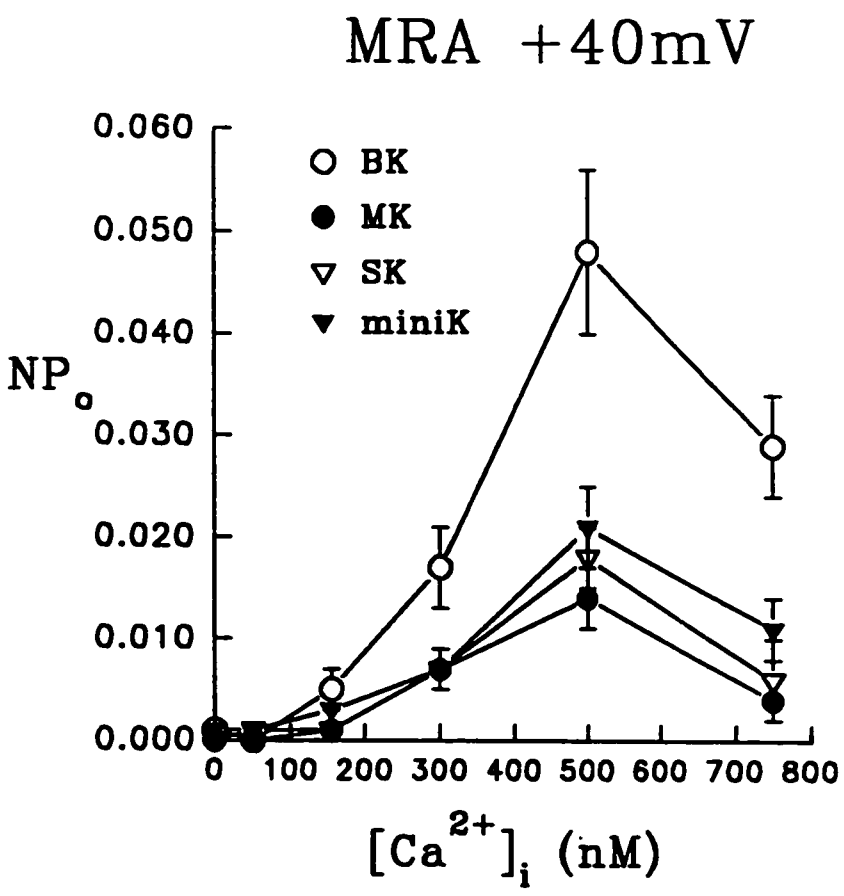

Figure RV–5. Calcium–dependent Activity of 4 MRA VSMC K–channels (+40 mV).

The single channel activity of the four MRA VSMC K–channels was calculated from long segments of inside–out data (+40 mV, ~ 5 minutes, ≥2000 events). The open probability of all four K–channels was concentration dependently increased by intracellular calcium (0 to 500 nM $[Ca^{2+}]_i$). All four K–channels had a reduced open probability at 750 nM compared to 500 nM $[Ca^{2+}]_i$. This may have been due to Ca^{2+}–dependent inhibition of the channel or to run–down. See text for comparison of open probability between MRA VSMC K–channels at –40 mV. (n ($[Ca^{2+}]_i$ = 0, 50, 155, 300, 500, and 750 nM): BK, (10, 9, 13, 8, 17, 4); IK, (8, 9, 13, 8, 20, 4); SK, (7, 10, 13, 8, 19, 4); miniK, (10, 8, 13, 6, 19, 4)).

(Clapp and Gurney, 1991). Run–down was minimized by the inclusion of energy sources, gentle digestion, and the use of the nystatin perforated patch. As well, no more than 3 concentrations of calcium were tested on a single cell.

The intracellular calcium concentration was stepped from low to high values. Membrane patches tolerated increases in calcium, and increases in activity were rapid and sustained. Decreases in calcium required long periods of time before open probability stabilized and were not used for data collection. More than half of the MRA VSMCs could be patch clamped for 45 to 80 minutes before run–down was apparent and only these cells were used for experiments.

The mean and standard error of the mean (s.e.m.) for the open probability of inside–out patches from TA and MRA VSMC patches at +40 mV and 500 nM $[Ca^{2+}]_i$ are in the following table:

Table RV–1. NP_o of 4 K–channel Types from Inside–out Patches for TA and MRA VSMCs at +40 mV.

K–channel	voltage (mV)	$[Ca^{2+}]_i$ (nM)	NP_o ± s.e.m. (n) TA	MRA
BK	+40	500	0.075 ± 0.056 (n=4)	0.048 ± 0.008 (n=17)
IK			0.018 ± 0.005 (n=4)	0.014 ± 0.003 (n=20)
SK			0.029 ± 0.005 (n=4)	0.018 ± 0.003 (n=19)
miniK			0.047 ± 0.016 (n=3)	0.021 ± 0.004 (n=19)

No statistical comparison was made since the TA VSMC data were insufficient.

V.2 Ca^{2+}–dependent NP_o of 4 MRA VSMC K–channels (–40 mV)

The single channel activity of TA and MRA VSMCs was also recorded at –40 mV while varying the concentration of calcium within physiological ranges (0, 50, 155, 500, and 750 nM $[Ca^{2+}]_i$). The activity of all four K–channel types was much lower at –40 mV than at +40 mV. Only the miniK channel showed any degree of activity at –40 mV when the concentration of calcium exceeded 155 nM. Because the open probability of the four MRA VSMC K–channel types was so low, no figure is presented with examples of single channel traces at –40 mV.

Figure RV–6 is a calcium concentration response curve of the open probability of four MRA VSMC K–channels at –40 mV. Note that the NP_o increments are the same as those in Figure RV–5 (+40 mV) for comparison of activity. TA VSMC inside–out patches were also recorded at –40 mV at 500 nM $[Ca^{2+}]_i$. The open probability of TA and MRA K–channels using inside–out patches at –40 mV and 500 nM $[Ca^{2+}]_i$ is presented in the following table:

Table RV–2. NP_o of 4 K–channel Types from Inside–out Patches for TA and MRA VSMCs at –40 mV.

K–channel	voltage (mV)	$[Ca^{2+}]_i$ (nM)	NP_o ± s.e.m. (n) TA	MRA
BK	–40	500	0.000 ± 0.000 (n=4)	0.000 ± 0.000 (n=9)
IK			0.001 ± 0.001 (n=4)	0.001 ± 0.000 (n=10)
SK			0.003 ± 0.002 (n=4)	0.003 ± 0.001 (n=8)
miniK			0.040 ± 0.028 (n=4)	0.015 ± 0.003 (n=7)

Again, no statistical comparison was made because the number of TA VSMC patches was insufficient.

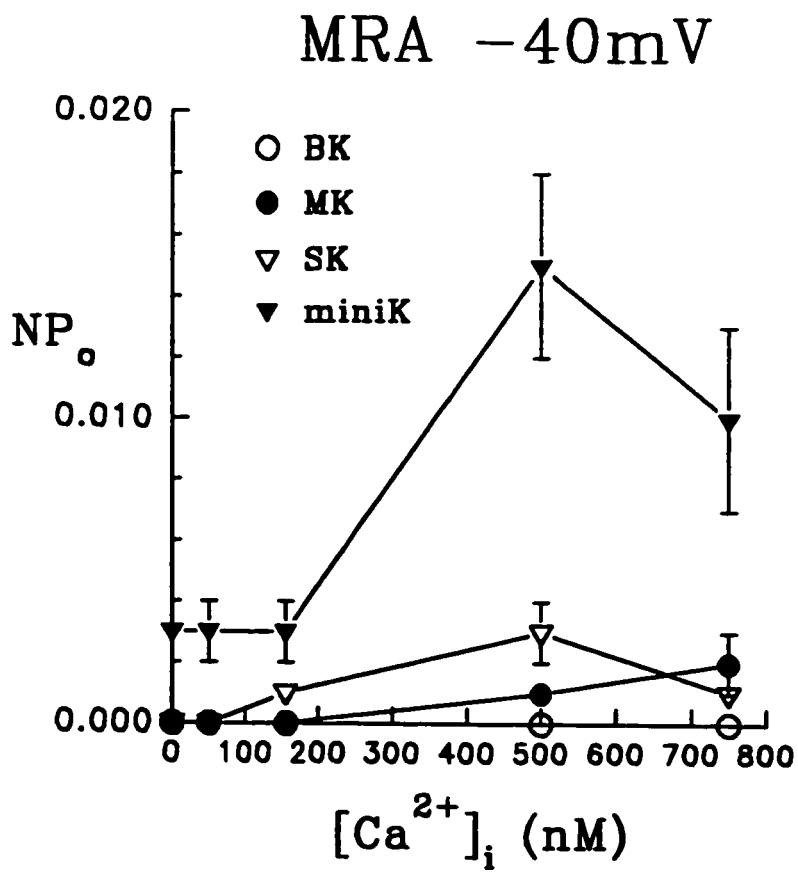

Figure RV–6. Calcium–dependent Activity of 4 MRA VSMC K–channels (–40 mV).

The single channel activity of the four MRA VSMC K–channels was calculated from long segments of inside–out data (–40 mV, ~ 5 minutes, ≥2000 events). Only the miniK channel was activated by calcium at –40 mV. See text for comparison of open probability between MRA VSMC K–channels at +40 mV. (n ($[Ca^{2+}]_i$ = 0, 50, 155, 500, and 750 nM): BK, (9, 7, 9, 9, 10); IK (9, 7, 8, 10, 10); SK, (8, 7, 9, 8, 8); miniK, (9, 7, 7, 7, 8)).

V.3 Voltage–dependent NP_o of Four MRA VSMC K–channels

The activity of the four MRA VSMC K–channel types was maximized at 500 nM $[Ca^{2+}]_i$ at both +40 mV and –40 mV. To determine the voltage dependence of single channel activity from inside–out patches, the $[Ca^{2+}]_i$ was fixed at 500 nM.

Figure RV–7 is an example of a single inside–out patch held at a range of holding potentials (–40, –20, 0, +20, +40, and +60 mV). Each segment of data is from a fifteen second recording selected from a longer (~ 5 minute) stable section. The figure includes a patch held at +60 mV. This was the only patch at which a stable section of data was recorded at this voltage. All patches became unstable at voltages greater than +40 mV and less than –40 mV, and membrane integrity was soon lost. It was found that calculations of open probability were restricted to this range of voltages (–40 mV to +40 mV).

Figure RV–8 a plot of the open probability data at different voltages for the four MRA VSMC K–channel types. The NP_o calibrations are aligned to compare the open probabilities of the four K–channel types. The miniK channel was the only K–channel that opened regularly at negative voltages, almost as much at –40 mV as at +40 mV (miniK: NP_o (–40 mV) = 0.015 ± 0.003, n=7 vs. NP_o (+40 mV) = 0.021 ± 0.004, n=19; P=0.33, not significantly different). In contrast, the SK, IK, and BK channels opened very rarely at negative voltages.

Figure RV–7. Voltage–dependent Activity of 4 MRA VSMC K–channels.

Inside–out patches from MRA VSMCs were recorded at different holding potentials with a fixed concentration of 500 nM $[Ca^{2+}]_i$ in symmetrical potassium solutions. These fifteen second sweeps demonstrated that the activity of all K–channels increased with increasing positive voltage. At negative voltages, only the miniK channel was activated. This patch was successfully recorded at +60 mV but was unique. Voltages above +40 mV and below –40 mV usually resulted in loss of seal.

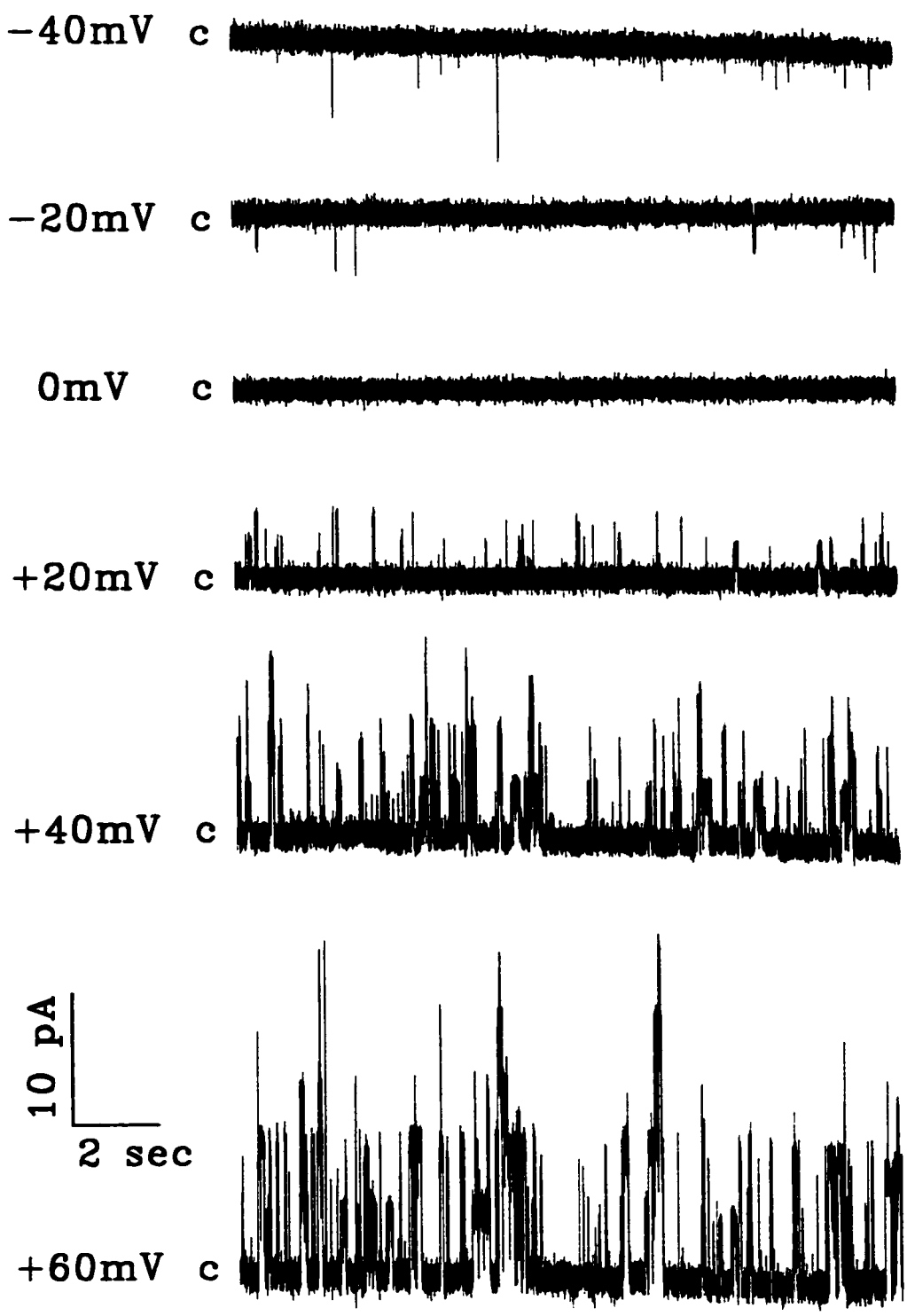
−40mV c
−20mV c
0mV c
+20mV c
+40mV c
10 pA
2 sec
+60mV c

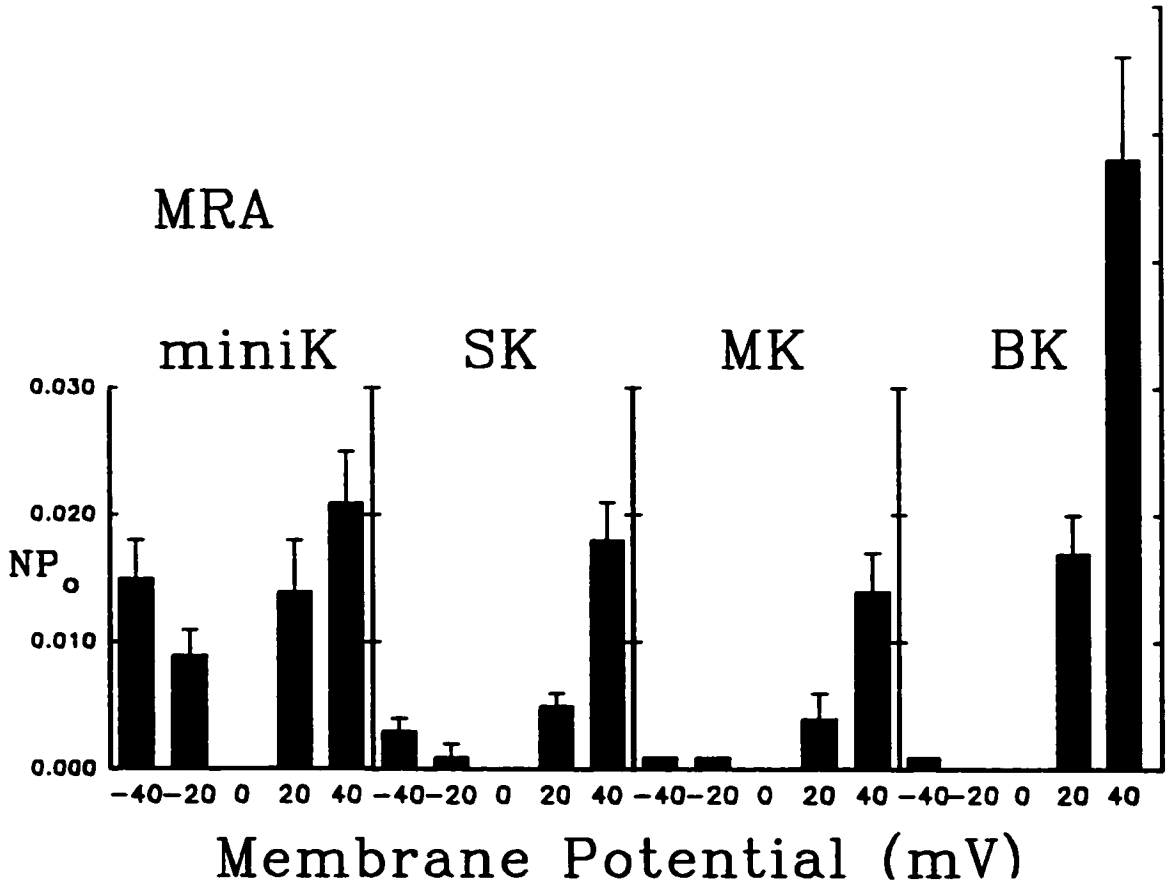

Figure RV–8. Voltage–dependent NP_o of 4 MRA VSMC K–channels (500 nM $[Ca^{2+}]_i$).

The inside–out single channel open probability of four MRA VSMC K–channels was plotted at a range of holding potentials between –40 mV and +40 mV. The BK channel had the highest open probability at +40 mV whereas the miniK channel had the highest NP_o at –40 mV. Major tick marks were aligned to compare the open probability between channels at the same voltage (see text for statistics). (n(–40, –20, 0, +20, and +40 mV): BK, (8, 6, 7, 4, 17); IK, (10, 6, 7, 5, 20); SK, (8, 6, 7, 5, 20); miniK, (7, 5, 7, 4, 19)).

This contrast between miniK and the other three K–channels is summarized in the following table:

Table RV–3. Comparison of NP_o (–40 and +40 mV) for 4 MRA VSMC K–channels.

K–channel	NP_o (–40 mV) ± s.e.m. (n)	NP_o (+40 mV) ± s.e.m. (n)	Student's t–test: P, significance
BK	0.000 ± 0.000 (n=9)	0.048 ± 0.008 (n=17)	2.75×10^{-4}, ***
IK	0.001 ± 0.000 (n=10)	0.014 ± 0.003 (n=20)	1.59×10^{-3}, **
SK	0.003 ± 0.001 (n=8)	0.018 ± 0.003 (n=19)	7.86×10^{-3}, **
miniK	0.015 ± 0.003 (n=7)	0.021 ± 0.004 (n=19)	0.33, ns

$P \leq 0.01$: **; $P \leq 0.001$: ***

At +40 mV, the BK channel was much more active than the three other K–channels. However, the three smallest K–channels had similar open probabilities at this holding potential. In contrast, at –40 mV, the miniK channel had the highest open probability. A comparison of open probability between different MRA K–channels at +40 mV and –40 mV is presented in the following table:

Table RV–4. Comparison of NP_o for 4 MRA VSMC K–channels (–40 and +40 mV).

K–channel	BK P significance	IK P significance	SK P significance	miniK P significance
BK		–40 mV: 6.42×10^{-2} ns	–40 mV: 2.28×10^{-3} **	–40 mV: 4.49×10^{-5} ***
IK	+40 mV: 6.21×10^{-5} ***		–40 mV: 6.20×10^{-3} **	–40 mV: 1.02×10^{-5} ***
SK	+40 mV: 6.48×10^{-4} ***	+40 mV: 3.27×10^{-1} ns		–40 mV: 3.92×10^{-4} ***
miniK	+40 mV: 2.33×10^{-3} **	+40 mV: 9.41×10^{-2} ns	+40 mV: 5.10×10^{-1} ns	

$P \leq 0.05$: *; $P \leq 0.01$: **; $P \leq 0.001$: ***

At +40 mV, the IK, SK, and miniK MRA VSMC K–channels had inside–out single channel activity that was not significantly different from each other. At –40 mV, the BK and IK MRA VSMC K–channels had inside–out single channel activity that was not significantly different from each other.

V.4 percentage contribution of 4 MRA VSMC K–channels

The four MRA VSMC K–channels were compared according to single channel conductance and voltage–dependent NP_o. A comparison of channel activity was made by taking the product of single channel conductance and open probability ($g*NP_o$) at each voltage step (–40, –20, 0, +20, +40 mV) at fixed calcium ($[Ca^{2+}]_i$ = 500 nM). The data are displayed in Figure RV–9. The units of

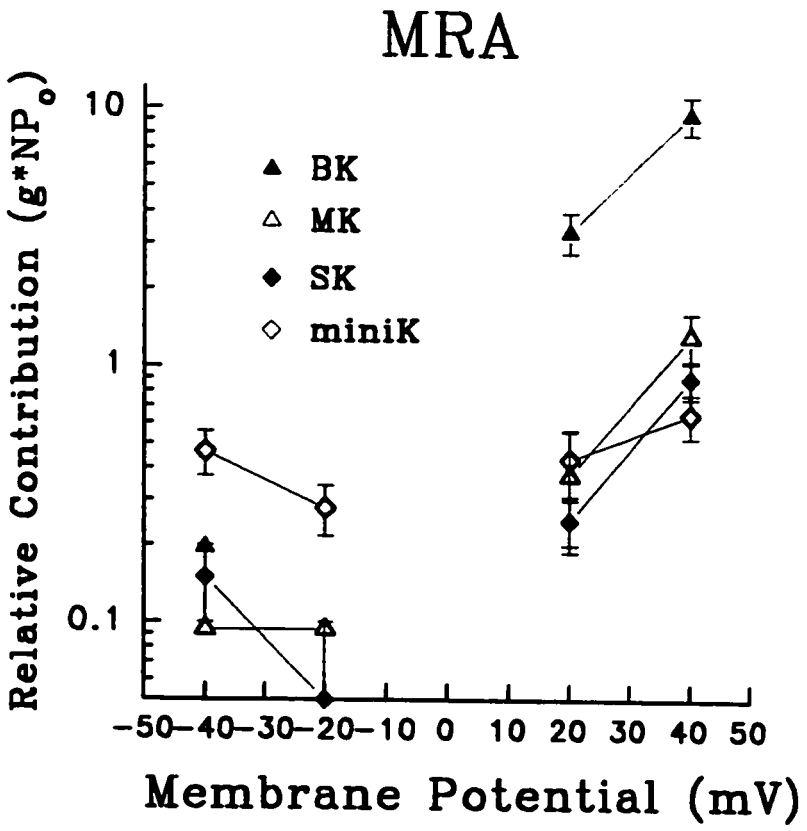

Figure RV–9. Relative Contribution of 4 MRA VSMC K–channels.

The relative contributions of the four MRA VSMC K–channels were calculated under symmetrical potassium solutions by taking the product of single channel conductance and open probability at different voltages (–40, –20, 0, +20, +40 mV) and fixed calcium ($[Ca^{2+}]_i$ = 500 nM). The units were omitted because they hold no conventional value and were used only for channel comparison. Under these conditions, miniK channels carried more current than the SK, IK, or BK channels at negative potentials. At positive potentials, BK channels carried more current than IK, SK, or miniK. (n (–40, –20, 0, +20, +40 mV) = BK: (10, 6, 7, 4, 17); IK: (10, 6, 7, 5, 20); SK: (8, 6, 7, 5, 19); miniK: (7, 5, 7, 4, 19)

relative activity are omitted because they hold no conventional value and are used only for channel comparison.

The symmetrical potassium solutions were used to calculate the open probability, which constrained the conductance to the same parameters (BK, 197 pS; IK, 94 pS; SK, 50 pS; miniK, 31 pS). This unfortunately limited the results to non–physiological conditions (K_o = 150 mM). At negative potentials, miniK channels contributed to more total current than SK, IK, or BK channels. However, at positive potentials, BK channels carried far more current than IK, SK, or miniK channels. At 0 mV with symmetrical potassium solutions, there were almost no channel events.

V.5 pharmacology of 4 MRA VSMC K–channels

Four K–channel blockers were used to determine the sensitivity of the four MRA VSMC K–channels. Inside–out patches were held at +40 mV and recorded for ~5 minutes. The K–channel blockers (ChTX, IbTX, apamin, or 4–AP) were included in the pipette solution because they were only effective from the extracellular side.

The open probability (NP_o) of MRA VSMC inside–out patches was calculated in the presence or absence of one of the four K–channel antagonists, and the results presented in the following table:

Table RV–5. Pharmacology of Four MRA VSMC K–channels.

K–channel	control	ChTX (150 nM)	IbTX (150 nM)	apamin (300 nM)	4–AP (2 mM)
BK	0.048 ± 0.008 (n=17)	0.002 ** ± 0.001(n=6)	0.000 *** ± 0.000 (n=6)	0.012 ** ± 0.008 (n=8)	0.003 ** ± 0.002 (n=6)
IK	0.014 ± 0.003 (n=20)	0.001 * ± 0.001 (n=6)	0.000 ** ± 0.000 (n=7)	0.014 ± 0.004 (n=9)	0.002 * ± 0.001 (n=7)
SK	0.018 ± 0.003 (n=19)	0.007 ± 0.004 (n=6)	0.001 ** ± 0.000 (n=6)	0.022 ± 0.008 (n=6)	0.006 * ± 0.002 (n=8)
miniK	0.021 ± 0.004 (n=19)	0.002 * ± 0.003 (n=4)	0.003 * ± 0.001 (n=6)	0.028 ± 0.012 (n=6)	0.009 ± 0.003 (n=7)

P≤0.05 : *
P≤0.01 : **
P≤0.001 : ***

key: NP_o ± sem (n)

ChTX (150 nM) completely blocked the activity of the BK, IK, and miniK channels but did not significantly reduce the NPo of the SK channel (62% reduction, P=0.088, n=6).

IbTX (150 nM) completely blocked the activity of all four MRA VSMC K–channels, even though it is selective for BK channels in some tissue (Nelson and Quayle, 1995; Brayden, 1996).

Apamin (300 nM) significantly inhibited the BK NP_o (75% reduction), but had no effect on the open probability of the other K–channels. This suggests that there is an apamin–sensitive BK_{Ca} in the MRA that is pharmacologically distinct from the apamin–resistant BK_{Ca} found in other tissues.

4–AP (2 mM) completely blocked the BK and IK channels and significantly inhibited the SK channel (66% reduction). 4–AP did not significantly reduce the NP_o of the miniK channel (57% reduction, P=0.059, n==7).

DISCUSSION

The purpose of this study was to characterize the effects of ACh–induced TA and SMA EDHF on single TA VSMC cell membrane potential, and the biophysics and pharmacology of the novel MRA VSMC K–channels and currents involved.

The K–channel inhibitors ChTX (typically BK_{Ca} selective) and especially apamin (typically SK_{Ca} selective) were effective inhibitors of EDHF–dependent smooth muscle hyperpolarization, especially in combination (Chen and Cheung, 1997). Since ACh–induced hyperpolarization and relaxation were significantly inhibited by ChTX and even more by apamin, and blocked by the combination, the MRA VSMC K–channel current was targeted by these toxins.

The SMA has lateral branches known as the mesenteric resistance arteries (MRA). Novel rat MRA VSMCs and their K–channels were selected and studied because small resistance arterioles are the primary vessels involved in blood pressure regulation (Nelson and Quayle, 1995; Brayden and Nelson, 1992; Brayden, 1996; Urakami–Harasawa *et al.*, 1997) and MRA is regulated by EDHF more than NO (Hwa *et al.*, 1994; Shimokawa *et al.*, 1996).

PART I. Endothelium–dependent Hyperpolarization

A new protocol was established to demonstrate that EDHF was an inducible and transferable factor. Rat SMA and TA sections were used as EDHF donor tissues which were exposed to L–NNA, a known nitric oxide (NO)–synthase inhibitor (Chen and Cheung, 1997). In rat SMA, a significant L–NNA–resistant component of ACh–induced hyperpolarization and relaxation was observed (Chen and Cheung, 1997; Fukao *et al.*, 1995). It has been proposed that EDHF is an inducible and transferable factor (Félétou and Vanhoutte, 1988; Chen *et al.*, 1991). However, it has been suggested that hyperpolarization and relaxation may be the result of gap junctions between the endothelium and smooth muscle (Nagao and Vanhoutte, 1993). There is also speculation that ChTX and apamin abolish ACh–induced EDHF release by acting selectively on the endothelium and not on the smooth muscle (Edwards and Weston, 1998; Doughty *et al.*, 1999). Our hypothesis was that EDHF was an inducible and transferable factor. A number of different techniques were performed using TA and SMA endothelium–intact donors and single TA VSMC targets.

The advantage of the new methodology is that donor and target tissues are separated by a measurable physical distance. Unlike the sandwich preparation in which the two tissues are very close together, in some cases in direct contact, the protocols presented (internal perfusion, SMA/TA–IP; pinned inverted tubes, SMA–PIT; and inverted rings in pipette tip, SMA–IRPT) allow the donor and target to be physically separated. This separation was used to demonstrate that EDHF is inducible and transferable.

I.1 EDHF is an inducible and transferable factor

Target TA VSMCs in current–clamp mode were contracted and depolarized by ACh (Figure RI–1A). Similarly, muscarinic stimulation contracted isolated VSMCs from guinea pig and canine trachea (Janssen and Sims, 1992; Wade and Sims, 1993), cat esophagus (Sims *et al.*, 1990), and guinea pig taenia caecum (Mita and Uchida, 1987). Janssen and Sims (guinea pig trachea, 1992) found that ACh–induced VSMC contraction and depolarization was blocked by atropine, indicating a muscarinic receptor mediated pathway.

However, when endothelium–intact donor SMA or TA were perfused with ACh, the response was reversed and the target TA VSMC was hyperpolarized (Figures RI–1B, RI–2, RI–3, RI–4, RI–5). The PIT technique (Figure RI–3), in which atropine was not used, demonstrates that the direct effect of ACh (depolarization / contraction) on VSMCs can be completely overturned by a powerful hyperpolarizing agent, EDHF.

The current work demonstrates that EDHF can also be released from the endothelium of rat conducting arteries (rat TA and SMA). In all three protocols tested, direct donor–target contact was not required, as occurs in a sandwich preparation, which strongly suggests that rat TA/SMA EDHF does not require gap junctions for transmission from endothelium to smooth muscle.

The three techniques employed to release and ACh–induced EDHF each had their own merits and weaknesses. The IP technique was slow to setup and the extended time and small impacts during manipulation were damaging to the endothelium. The inversion of the lumen in the PIT and IRPT techniques was

surprisingly less damaging to the endothelium, and a greater number of successful donor tissues were obtained compared to the IP technique (no data). There was no difference in the longevity or viability (ACh–induced EDHF) between the IRPT (more cutting) and the PIT (longer length resulted in greater friction when inverted).

EDHF is an inducible, transferable factor in the organ bath preparation (donor: canine femoral artery, target: coronary artery, Félétou and Vanhoutte, 1988), sandwich preparations (guinea pig carotid artery, coronary artery, Chen *et al.*, 1991; rabbit carotid artery, endothelium–denuded carotid artery, Dong *et al.*, 1997), and cell culture preparation (porcine coronary and human umbilical vein endothelial cells, rat aortic and coronary VSMCs, Popp *et al.*, 1996). These examples demonstrate that EDHF can be released from diverse tissues (canine femoral artery, guinea pig and rabbit carotid, porcine coronary artery, and human umbilical vein) and underscore its importance in vascular regulation.

I.2 ACh–induced EDH has a NO–independent component

In Figure RI–2, the SMA–IRPT technique was used to demonstrate that ACh–induced EDH has a NO–independent component. ACh–induced hyperpolarization in the absence of L–NNA was robust, but a significant hyperpolarization persisted even when NO synthesis was inhibited. Even though the remaining hyperpolarization was not fully characterized, previous experiments showed that 30 μM L–NNA was sufficient for NOS inhibition in SMA, and a higher concentration of L–NNA, or the combination of L–NNA and S–methyl–L–

thiocitrulline, were no more effective (Chen and Cheung, 1997). As well, glybenclamide in the extracellular solutions and ATP in the intracellular solutions prevented K_{ATP} channel activation. There does not appear to be a prostanoid component in rat SMA (Garland and McPherson, 1992; Shimokawa *et al.*, 1996; Fukao *et al.*, 1997b; McCulloch *et al.*, 1997) and rat TA iloprost–induced dilation is glybenclamide–sensitive (Schubert *et al.*, 1997). These observations suggest that rat SMA and TA ACh–induced EDHF is NO– and PGI_2–independent in the presence of L–NNA, glybenclamide, and ATP.

EDHF may be created by NOS, so the lower hyperpolarization in the presence of L–NNA compared to without may be due to inhibition of EDHF synthesis as well as NO. EDHF has been proposed to be hydrogen peroxide (H_2O_2) derived from endothelial NOS (eNOS) (Matoba *et al.*, 2000) and NOS has been implicated in EDHF synthesis (Waldron *et al.*, 1999).

In $NOS^{+/+}$ mice, ACh–induced relaxation of MRA was completely inhibited by L–NOArg plus indomethacin or 30 mM K_o, suggesting that EDH/R were mediated by NO and / or PGI_2 (Waldron *et al.*, 1999). However, in $NOS^{-/-}$ knockout mice, ACh–induced relaxation was unaffected by L–NNA plus indomethacin but was inhibited by 30 mM K_o, suggesting that the non–NO EDH/R was mediated by EDHF and not PGI_2 (Waldron *et al.*, 1999). This evidence also supports the notion that EDHF is synthesized by NOS.

$NOS^{-/-}$ mouse MRA ACh–induced hyperpolarization and relaxation were inhibited by catalase, which dismutates H_2O_2 to from water and oxygen; as well, exogenous H_2O_2 restored EDH/R in endothelium denuded MRA, and laser

confocal imaging using peroxide sensitive dye demonstrated ACh–induced endothelium H_2O_2 production which was reduced in $NOS^{-/-}$ (Matoba *et al.*, 2000).

These observations suggest that the reduced hyperpolarization in the presence of L–NNA (Results RI–2) in rat MRA may in part be due to inhibition of EDHF synthesis by eNOS, rather than solely NO. The continued EDHF response in the presence of L–NNA and in $NOS^{-/-}$ suggests that EDHF synthesis may be accomplished by multiple oxygenases (NOS, also possibly cylco–oxygenase, lipoxygenase, P–450 mono–oxygenase, NAD(P)H oxidase).

The use of different inhibitors may provide clues as to the nature of EDHF but may also lead one astray. If EDHF were H_2O_2 synthesized by multiple oxygenases, then the use of one inhibitor may suggest that EDHF is NO (L–NNA to inhibit NOS) whereas another may suggest an arachidonic acid metabolite (clotrimazole to inhibit P–450). Therefore caution must be taken when drawing conclusions since the inhibition of one synthesis pathway may result in the up–regulation of another.

I.3 ACh–induced EDH was a function of donor–target distance

The pinned inverted tubes (SMA–PIT) technique demonstrated that rat SMA releases an EDHF (Figure RI–2) which hyperpolarized target TA VSMCs close ($\leq$ 0.2 mm) to donor tissue but not target cells far ($\geq$ 1.8 mm) from donor tissue. This suggests that: *i.* EDHF is a potent factor, released in small quantities, which is diluted by the bath volume, and/or *ii.* EDHF is transiently active and is rapidly metabolized to an inactive byproduct. The nature of the EDHF released

from TA and SMA is unknown. If the EDHF is a P–450 metabolite, it is probably released in very small quanta and highly reactive, especially in the oxygenated solutions used.

RMP regulation by EDHF and K-channels

Endothelium removal in rat hepatic artery depolarizes the RMP, which suggests that EDHF may be constitutively released to modulate RMP (Zygmunt *et al.*, 1998). Endothelium–intact rat SMA RMP was depolarized by TEA and ChTX, but not by apamin (300 nM) (Chen and Cheung, 1997). However, the combination of ChTX plus apamin was more effective than either antagonist alone, which suggests that both ChTX and apamin dependent K–channels regulate rat SMA RMP (Chen and Cheung, 1997).

In contrast, apamin was an effective inhibitor of ACh–induced EDHF–mediated hyperpolarization in rat SMA (Chen and Cheung, 1997). Apamin halved EDHF–mediated hyperpolarization in NE–contracted arteries and nearly abolished it in relaxed arteries, suggesting that apamin sensitive K–channels contribute to maintaining tone in resting arteries more than contracted arteries. Similarly, ACh–induced EDHF–mediated hyperpolarization in guinea pig carotid artery was partially inhibited by apamin (500 nM) (Chataigneau *et al.*, 1998). ChTX plus apamin abolished ACh–induced EDH and depolarized RMP in rat SMA (Chen and Cheung, 1997), guinea pig carotid artery (Chataigneau *et al.*, 1998), and rat hepatic artery (Zygmunt *et al.*, 1998). These results suggest that

EDHF–mediated hyperpolarization and relaxation act via apamin and ChTX sensitive K–channels.

This prompted the investigation of novel VSMCs from the rat MRA. The morphological, biophysical, and pharmacological properties of the MRA VSMCs and their K_{Ca} channels were characterized.

PART II. Properties of Mesenteric Resistance Artery VSMC

II.1 Morphological properties

Previous studies have demonstrated the viability of single VSMCs isolated by enzymatic digestion (Bolzon and Cheung, 1989). To study rat MRA VSMCs, a modification of the Bolzon and Cheung (1989) technique was required since the vessels were too small to canulate. A **novel slow digestion protocol (~ 2 hours)** was established which gently digested small branch rings that were previously opened with forceps to allow digestion from the luminal surface. This technique provided relaxed and viable single MRA VSMCs morphologically similar to TA VSMCs, spindle shaped when relaxed and round when contracted, though significantly smaller in length and diameter (Bolzon and Cheung, 1989; Bolzon, 1992).

II.2,3,4 Properties of MRA VSMCs

The whole–cell technique was used to characterize the properties of rat MRA VSMCs. Whole–cell experiments step depolarized cells from a holding potential (~ –50 mV, close to RMP) to positive potentials to elicit outward current (Chen and Cheung, 1997; Bolzon *et al.*, 1993). Common current populations were observed, including the voltage–dependent delayed rectifier current (K_{dr} channel dependent) and the voltage– and calcium–dependent current (K_{Ca} channel dependent). MRA whole–cell outward currents were similar in amplitude to those observed in TA, even though MRA VSMCs were approximately half the size of TA VSMCs (Bolzon, 1992). Therefore, MRA current density was about double

that observed in TA, which suggests that MRA VSMCs have twice the number of K–channels per unit area of cell membrane (channel density). Another possibility is that MRA whole–cell K–channels are more readily activated than TA K–channels, which may represent differences in channel regulation through phosphorylation, calcium entry / release, or other as yet unidentified mechanisms. However, the similar NP_o of excised inside–out patches from MRA and TA (Results, Tables RV–1, RV–2) suggests that differences in whole–cell current density probably reflect channel density. The smaller cell size and higher current density of MRA VSMCs relative to TA may promote the propagation of an electrical signal from myocyte to myocyte via gap junctions. This would allow MRA VSMCs to contract / relax very rapidly in response to stimuli. As well, the smaller MRA cell size may require more outward K_{Ca} current to fully relax since the total range of contraction (~ 80% cell length *in vitro*) is smaller than TA. MRA VSMCs are compared to TA VSMCs:

Table D1. Properties of Rat TA and MRA VSMCs.

Properties	TA VSMC	MRA VSMC
Morphological Properties		
cell length (μm)	131.7 ± 4.4	72.2 ± 4.2***
cell diameter (μm)	11.0 ± 0.4	7.7 ± 0.3***
Passive Membrane Properties		
cell capacitance (pF)	31.1 ± 1.4	12.2 ± 1.0***
electrical surface area (x 10^{-5} cm^2)	3.11 ± 0.14	1.22 ± 0.10***
series resistance (R_s) (MΩ)	9.09 ± 1.60	9.35 ± 0.86
Whole–cell Current		
voltage dependence:		
holding potential: –80 mV	K_{Ca} + K_{dr}	K_{Ca} + K_{dr}
holding potential: –40 mV	K_{Ca}	K_{Ca}
current density (+50 mV) (pA/pF)	15.3 ± 1.4	34.8 ± 3.1**

Whole–cell Current Pharmacology		
apamin (300 nM)	↔	↓ K_{Ca}*
ChTX (150 nM)	↓ $K_{Ca}^{NA, 1}$	
IbTX (150 nM)	↓ K_{Ca}^{NA}	↓ K_{Ca}^{NA}
4–AP (2 mM)	↓ $K_{dr}^{NA, 1}$	↓ K_{dr}^{NA}

Notes: *1.* Bolzon, 1992.
* : significant inhibition, P≤0.05; ** : P≤0.01; *** : P≤0.001
↔ : no effect at this concentration
NA : not applicable (n < 3)

apamin sensitive K–channel current

MRA whole–cell K_{Ca} current was partially (21%) but significantly inhibited by apamin (300 nM), whereas TA VSMC whole–cell K_{Ca} current was unaffected. These results suggest that MRA whole–cell current is modulated by distinct apamin–sensitive K_{Ca}–channels.

The effects of apamin on whole–cell current are varied. Apamin (50 – 300 nM) significantly inhibited whole–cell K_{Ca} current in rat renal arteriole myocytes (Gebremedhin *et al.*, 1996), rat hepatocytes (Yamashita *et al.*, 1996), mouse colonic myocytes (Koh *et al.*, 1997), and chick ciliary ganglion neurons (Dryer *et al.*, 1991; Cetiner and Bennett, 1993), and significantly inhibited / blocked whole–cell K_{dr} current in guinea pig ventricular myocytes (Koumi *et al.*, 1994b) and hepatocytes (Koumi *et al.*, 1994a). These results confirm that apamin is not selective for SK_{Ca} channels, and genetic characterization of SK channels has determined the amino acid residues necessary for apamin binding and ion pore blockade (Ishii *et al.*, 1997a).

The cloning of MRA K–channels would determine if they contain the apamin–binding site. However, there may be tissues / species that display both apamin sensitivity and yet lack the apamin binding site of Ishii *et al.* (1997a).

This would occur if there are alternate apamin binding site configurations or alternate mechanisms of block (changes in membrane fluidity, actions on other channels, direct actions on second messengers). Since alternate splice variants result in viable SK channels with different apamin sensitivity (Ishii *et al.*, 1997), it is probable that **tissue / species differences in K–channel toxin (apamin, ChTX, IbTX) sensitivity are due to splice variants**.

ChTX / IbTX sensitive K–channel current

MRA VSMC whole–cell K_{Ca} current was blocked by IbTX (150 nM). Similarly, whole–cell K_{Ca} current was blocked by ChTX (50 – 100 nM) in rat TA VSMCs (Bolzon, 1992; Bolzon *et al.*, 1993), bovine trachea VSMCs (Green *et al.*, 1991), and chick ciliary ganglion neurons (Cetiner and Bennett, 1993), and by IbTX (50 – 100 nM) in rat cerebral (basilar) artery VSMCs (Holland *et al.*, 1996). These results suggest that the **MRA whole–cell K_{Ca} current is distinct from that found in other tissues since it is both ChTX and apamin sensitive**.

One possibility is that MRA VSMCs have two closely associated BK_{Ca} channels, one ChTX–sensitive and one apamin–sensitive. As seen from the single channel data (Results, Table RV–5), both ChTX and apamin inhibited BK channels. Therefore, ChTX or apamin alone may not inhibit agonist–induced EDHF release if a closely associated BK channel can compensate for the inhibition. In this case, the two BK channels may share similar biophysical properties and differ only in toxin binding sites due to conservation of genetic determinants (splice variants).

Alternately, BK channels may have binding sites for both ChTX and apamin (Zygmunt *et al.*, 1997). Radioligand studies have demonstrated that ChTX binding is increased in the presence of apamin, which suggests an allosteric interaction where apamin alters the conformation of the pore (Vazquez *et al.*, 1990; Zygmunt *et al.*, 1997). BK channels may be able to express multiple binding sites for one or more of ChTX, IbTX, apamin, or other antagonists, dependent upon tissue / species and function (conductance or resistance vessel, thermal regulation), or novel K–channel types may be created by combining subunits from classical K_v and K_{Ca} channels. However, the nature and extent of different K–channel subunits associating *in vivo* has not been established.

4–AP sensitive K–channel current

In rat TA VSMCs, 4–AP (2 mM), though partially selective for K_{dr} current, still significantly inhibited K_{Ca} current (Bolzon, 1992; Bolzon *et al.*, 1993). 4–AP (2 mM) reduced TA whole–cell K_{Ca} current by 15%, whereas K_{dr} current was inhibited 75% (Bolzon, 1992). When the concentration was reduced, 4–AP (1 mM) did not inhibit TA VSMC whole–cell current (Bolzon *et al.*, 1993). However, in MRA VSMCs, 4–AP (2 mM) selectively blocked the K_{dr} current, whereas the K_{Ca} current was unaffected. These results suggest that **MRA whole–cell current was modulated by 4–AP–sensitive K–channels (K_{dr} current) that are distinct from those in TA**. However, it unknown whether this is due to different channel proteins, cellular modulation via enzymes, or channel density. The insensitivity of MRA but not TA K_{Ca} current to 4–AP underscores the differences between these tissues.

4–AP (2 – 10 mM) nearly abolished whole–cell K_{dr} current in VSMCs from rat main pulmonary artery (Okabe *et al.*, 1987), guinea pig hepatocytes (Koumi *et al.*, 1994a), and ferret airway (Fleischmann *et al.*, 1993). As well, 4–AP (50 μM) significantly inhibited a K_{dr} channel ($K_v3.1$ family) in canine atrial VSMCs (36 pS, $K_{i/o}$ = 130 mM) (Yue *et al.*, 1996). Though 4–AP is considered partially selective for K_{dr} current, this selectivity is questionable since a low concentration of 4–AP (1 mM) significantly inhibited a non–specific cation current in guinea pig ileum (Chen *et al.*, 1993).

PART III, IV. Properties of Four Types of MRA VSMC K–Channel — Linear and Non–Linear Methods

TA and MRA VSMC inside–out patches demonstrated the presence of four distinct K_{Ca}–channels (BK, IK, SK, and miniK). In symmetrical potassium solutions ($K_{i/o}$ = 150 mM), TA and MRA VSMCs were found to have K_{Ca}–channels which were similar in amplitude. The novel K–channels found in MRA (BK, IK, SK, miniK) and those that haven't been well studied in TA (IK, SK, and miniK) demonstrate that the regulation and rectification of membrane potential is dependent upon many K–channels.

The conductance of the four MRA VSMC K–channels was calculated using both linear and non–linear techniques. The linear method became less accurate as the concentration of external potassium was decreased from symmetrical (150 mM) to physiological (5.5 mM). However, linear analysis of the data was a useful technique when used to calculate conductance in linear regions of data (> 0 mV). Linear analysis has often been used by other researchers and has been useful for comparing results between rat MRA VSMC K–channels and those found in rat TA (Bolzon, 1992). The non–linear analysis of the four MRA K–channels using the GHK equation proved to be more accurate than linear analysis at predicting single channel properties (Hille, 1992).

The instantaneous conductance experiments of the four MRA VSMC K–channels provided interesting insight into the properties of ion channels (Figures RIV– 1–4 *Panel B*). The instantaneous conductance was derived by dividing the unitary current by the driving force (where the driving force is the voltage minus

the reversal potential), and was a function of both voltage (membrane potential) and $[K^+]_o$.

The instantaneous conductance of the BK, IK, SK and miniK channels at elevated $[K^+]_o$ (50, 100, and 150 mM) appeared to be voltage–independent. When fitted with a linear function (linear regression, least squares, pClamp 6.1.1), the slope was approximately zero for all four MRA K–channels. The data for the miniK channel appear to be non–linear when compared to the larger channels, in all likelihood a function of the difficulty in measuring minute channel amplitude and the axis scale.

With physiological $[K^+]_o$ (5.5 mM), the instantaneous conductance of the four MRA VSMC K–channels was voltage–dependent and linear. Linear regression (least squares, pClamp 6.1.1) resulted in a positive slope factor for all four K–channels. This indicates that the MRA K_{Ca} channels are not saturated at physiological $[K^+]_o$, are partially saturated at 50 mM $[K^+]_o$, and are saturated at higher $[K^+]_o$. Thus, at higher than physiological $[K^+]_o$, MRA K_{Ca} channel conductance is limited by ion–pore binding and unbinding.

A physiological conductance was estimated (Figures RIV– 1–4B; BK, IK, SK, miniK: 42, 21, 10, 6 pS) using linear regression to the RMP of mesenteric artery VSMCs (~ –50 mV, Chen and Cheung, 1997). As well, the relative activity ($g * NP_o$) of the four MRA K–channels was compared (Figure RV–9) under physiological conditions ($V = -40$ mV, $[Ca^{2+}]_i = 500$ nM). The high activity (NP_o) of the miniK channels suggests that they are very important regulators of RMP, with three times the relative activity of the other K–channels. However, the

high conductance (g) of the BK channels suggest that they re–polarize Ca^{2+}– or agonist–depolarized / contracted cells, and possibly provide a negative feedback mechanism to prevent excessive or prolonged contraction (Wade and Sims, 1993).

PART V. Single Channel Activity of Four MRA VSMC K–Channels

The single channel activity (NP_o) of the four MRA VSMC K–Channels was studied using the inside–out technique. The calcium–dependence (+40, –40 mV), voltage–dependence ($[Ca^{2+}]_i$ = 500 nM), and conductance of the four MRA VSMC K–channels are summarized:

Table D2. Properties of Four MRA K–channel Types.

Properties	BK	IK	SK	miniK
Active Range (500 nM $[Ca^{2+}]_i$)		> 0 mV		> 0 mV < 0 mV
Calcium Dependence (0–500 nM $[Ca^{2+}]_i$)		Ca^{2+}–dependent NP_o		Ca^{2+}–dep. NP_o
+40 mV		↑ NP_o		↑ NP_o
C_{50} (nM)	345	300	335	350
–40 mV		inactive		↑ NP_o
C_{50} (nM)	—	—	—	347
Voltage Dependence (500 nM $[Ca^{2+}]_i$)		V–dependent NP_o		V–dep. NP_o
+ voltages		↑ NP_o		↑ NP_o
– voltages		inactive		↑NP_o
Permeability Constant ($\times 10^{-13}$ cm/s)	3.46	1.65	0.879	0.545
Conductance (pS)				
g_{max}				
linear (–5.5)	253 ± 2.39	133 ± 11.9	79.0 ± 15.3	(78.0 ± 2.04)[1]
GHK (–5.5)	242 ± 12.5	132 ± 23.2	64.5 ± 10.6	35.6 ± 7.32
GHK (+5.5)	196 ± 8.08	86.2 ± 7.80	48.6 ± 3.30	27.4 ± 2.66
g_{linear}				
$[K^+]_o$=150 mM	197	94	50	31
100	179	88	48	24
50	137	60	29	14
5.5	(123)[2]	(70)[2]	(39)[2]	(11)[2]
$g_{physiological}$ (–50 mV, $[K^+]_o$=5.5 mM) (95% confidence interval)	42.3 (35.3–49.4)	20.6 (9.00–32.2)	10.1 (6.41–13.7)	6.23 (4.05 – 8.42)

Notes: *1.* g_{max} (linear, miniK): poor estimation, small single channel amplitude.
2. g_{linear}($[K^+]_o$=5.5 mM): poor approximations, non linear data.

V.1.2.3 Properties of 4 MRA VSMC K–channels

All four MRA VSMC K–channels were Ca^{2+}–dependent at +40 mV. As the $[Ca^{2+}]_i$ was increased from 0 to 500 nM, the NP_o increased. At 0 nM $[Ca^{2+}]_i$ / +40 mV, all four K–channels were observed but the NP_o was extremely low. This suggests that the channels *i.* were constitutively active and did not require calcium to open, or *ii.* were activated by bound calcium, or *iii.* were activated by calcium released from membrane–bound or –associated proteins or sarcolemmal remnants. Only the miniK and SK channels were Ca^{2+}–activated at –40 mV. The miniK channel was constitutively active at 0 nM $[Ca^{2+}]_i$ / –40 mV, became much more active at 500 nM, but demonstrated reduced activity at 750 nM. Because preventive measures were employed (Results, RV–1), run–down probably does not account for the reduced activity at 750 nM.

However, calcium blockade of K–channels may account for the reduced activity (Benham *et al.*, 1986; Vergara and Latorre, 1983). Calcium ions may have multiple binding sites, including the same site as barium but with greater affinity, and thus result in blockade of activated BK_{Ca} channels (Benham *et al.*, 1986). Most K_{Ca} channels approximate GHK rectification with a single–ion single–site process when under physiological conditions. When ion concentrations are altered, such as during elevated $[K^+]_o$ or $[Ca^{2+}]_i$, then K_{Ca} channels are often best modeled as multi–ion / –site barriers to reflect the complex interactions of all species. The effect of elevated $[Ca^{2+}]_i$ to reduce NP_o may act as a negative feedback mechanism to prevent over stimulation of K_{Ca} channels, and thus prevent excessive hyperpolarization / relaxation.

The Ca^{2+}–dependence of the four MRA K–channels was within a similar range to that observed for K_{Ca} channels in other tissue and species. The $[Ca^{2+}]_i$ required to activate K_{Ca} channels (NP_o = 0.5, 0 mV) averages 500 nM (rabbit jejunum, guinea pig SMA, and anterior pituitary cells), but can range from 10 nM (mouse lacrimal glands) up to 50 μM (cultured rat muscle cells incorporated into lipid bilayers) (Wong *et al.*, 1982; Benham *et al.*, 1986). At 0 mV, 500 nM $[Ca^{2+}]_i$ was insufficient to activate MRA VSMC K–channels, but at +40 mV, half–maximal activation of K–channels ranged from 300 – 350 nM $[Ca^{2+}]_i$.

The voltage–dependent activity was determined using inside–out patches of MRA VSMCs with a fixed $[Ca^{2+}]_i$ (500 nM). All four MRA K–channels displayed voltage dependent activity when the holding potential was above 0 mV. The BK and IK channels were inactivated at and below 0 mV, in accordance with observations of most K_{Ca} channels (Hille, 1992; Nelson and Quayle, 1995; Brayden, 1996), whereas the SK and miniK channels were voltage–activated at negative holding potentials

BK

The BK channel had a large conductance (197 pS, $K_{i/o}$ = 150 mM), was Ca^{2+}– and voltage–dependent, and was only active at positive potentials, similar to BK channels observed in other tissue (Table A2–1; Brayden, 1996; Nelson and Quayle, 1995). The permeability constant of the BK channel (3.46×10^{-13} cm/s) was found to be similar to others reported in rat pulmonary artery cells (4.6×10^{-13} cm/s, 245 pS, $K_{i/o}$ = 145mM, Albarwani *et al.*, 1994) and rabbit aorta cells in

primary culture (1–7 days) (8.9 x10^{-13} cm/s, 227 pS, $K_{i/o}$ = 145mM, Pavenstädt *et al.*, 1991).

Whole–cell experiments found that MRA VSMC membrane depolarization elicited an outward current which was due in part to large conductance Ca^{2+}–activated K–channels (Results, RII–4). With the pipette [Ca^{2+}] fixed at 155 nM, outward currents developed at potentials above +30 mV. In rat TA, inward calcium current was restricted to –40 to 0 mV (Bolzon, 1992). Whole–cell MRA K_{Ca} current and BK NP_o were very low at potentials below 0 mV. Therefore **MRA BK activation was not strongly modulated by calcium influx**, as in visceral smooth muscle (Walsh and Singer, 1981; Klockner and Isenberg, 1985).

BK channels displayed Ca^{2+}– and voltage–dependence only at positive potentials. However, BK channels demonstrated infrequent openings at –40 mV, BK NP_o at –40 mV was not Ca^{2+}–dependent, and VSMC $[Ca^{2+}]_i$ at the RMP is usually low (100 – 150 nM; Sumimoto and Kuriyama, 1986; Katsuyama *et al.*, 1991; Collins *et al.*, 1992). Therefore, MRA BK channels probably do not maintain RMP. MRA BK channels are likely active only when the VSMC is depolarized or when activated by endogenous factors: BK–mediated K_{Ca} outward current probably acts as a negative feedback mechanism to oppose depolarization, inactivate voltage dependent calcium channels, and prevent excessive contraction.

IK

The MRA IK channel is an intermediate conductance (94 pS, $K_{i/o}$ = 150 mM) Ca^{2+}– and voltage–dependent K–channel which was only active at positive potentials. IK channels were the rarest MRA VSMC K–channel type, found in less than half of all preparations and only in healthy looking cells. They were far less common than BK channels at positive potentials and had a lower NP_o, similar to a K_{Ca} channel in rabbit portal vein VSMCs (92 pS, $K_{i/o}$ = 142 mM; 50 pS, $K_{i/o}$ = 142/6.2 mM) (Inoue *et al.*, 1985; Inoue *et al.*, 1986). However, the MRA IK channel was considerably more common than a rare K_{Ca} channel (91 pS, $K_{i/o}$ = 145 mM) from rat pancreatic arteriole VSMCs (Stuenkel, 1989).

The MRA IK channel differs from the K_{Ca} channel (~ 100 pS, $K_{i/o}$ = 126 mM; 50 pS, $K_{i/o}$ = 126/6 mM) found in rabbit jejunum and guinea pig mesenteric artery cells which was **more common** than the larger BK channel (Benham *et al.*, 1986). In contrast to the guinea pig mesenteric artery (Benham *et al.*, 1986), rat MRA BK channel NP_o was much higher than IK. Other intermediate–conductance K_{Ca} channels have been observed, but characterization has been less complete than for BK channels (Brayden, 1996).

The Ca^{2+}–dependence of the IK channel at –40 mV is questionable since the NP_o was very low and the changes in NP_o were too small to measure statistically, but may represent an underlying Ca^{2+}–dependence that was voltage–inactivated. Like BK channels, IK displayed Ca^{2+}– and voltage–dependence only at positive potentials and infrequent openings at –40 mV. Therefore, IK channels probably do not maintain RMP and are likely active only when the VSMC is

depolarized or when activated by endogenous factors. Though their function is debatable, IK channels probably comprise a component of outward K_{Ca} current that repolarizes and relaxes VSM.

SK

The MRA SK channel is an intermediate conductance (50 pS, $K_{i/o}$ = 150 mM) Ca^{2+}–dependent K–channel which was active at positive and negative potentials. However, activity was much higher at positive than negative potentials. SK channels were common, found in most preparations and in healthy or contracted cells. They were far less common than BK channels at positive potentials and had a lower NP_o.

Rat pancreatic arterioles had a TEA–sensitive 43 pS K–channel ($K_{i/o}$ = 145 mM) which was active at the RMP (Stuenkel, 1989), which suggests that rat MRA SK channels may be active at the RMP. The SK channel displayed Ca^{2+}– and voltage–dependence at positive and negative potentials. The SK channel had very low activity but was significantly more active at –40 mV (500 nM $[Ca^{2+}]_i$) than the BK and IK channels (Table RV–4). However, activity was insufficient to determine the $[Ca^{2+}]_i$ to reach half activation. This data suggest that the SK channel was Ca^{2+}–dependent at –40 mV but was voltage–inactivated. Therefore, SK channels probably contribute little to maintaining RMP and may become active when the VSMC is partially depolarized by transient calcium fluctuations, and thus may prevent premature depolarization and contraction. SK channels may also contribute to re–polarization but their small conductance relative to BK / IK suggests that they would contribute little to the overall current.

miniK

The MRA VSMC miniK channel had a small conductance (31 pS, $K_{i/o}$ = 150 mM) Ca^{2+}–dependent K–channel which was active at positive and negative potentials. The miniK channels were very common, and were found in all preparations and in healthy or contracted cells. They were as common as BK channels at positive potentials but had a lower open probability.

Unlike the SK channel, significant miniK activity was recorded at negative potentials, which is uncommon for K_{Ca} channels (Nelson and Quayle, 1995; Hille, 1992; Brayden, 1996). The activity of miniK channels at negative voltages suggests that these K–channels may be active at the RMP (~ –50 mV) and $[Ca^{2+}]_i$ (100 – 600 nM) of *in vivo* cells (Brayden, 1996; Chen and Cheung, 1997; Bolzon *et al.*, 1993).

The $[Ca^{2+}]_i$ required to half activate miniK channels was the same at +40 mV (350 nM) and –40 mV (347 nM), suggesting that the miniK channel would be more active at the RMP than other K_{Ca} channels. The small amplitude and voltage– and Ca^{2+}–dependent activity of the miniK channel at negative potentials suggest that miniK channels regulate RMP but probably do not contribute to re–polarization of depolarized / contracted VSMCs.

V.4 percentage contribution of 4 MRA VSMC K–channels

The four MRA VSMC K–channels were compared according to single channel conductance and voltage–dependent single channel activity. A comparison of channel activity was made by taking the product of single channel conductance and open probability ($g*NP_o$) at each voltage step (–40, –20, 0, +20, +40 mV) at fixed $[Ca^{2+}]_i$ (500 nM) (Figure RV–9). Symmetrical potassium solutions were used to calculate NP_o, which constrained the conductance to the same non–physiological parameters (BK, 197; IK, 94; SK, 50; miniK, 31 pS).

At negative potentials, miniK channels contributed to more total current than SK, IK, or BK channels. This reinforces the notion that **miniK channels may be important regulators of RMP**. However, at positive potentials, BK channels carried far more current than IK, SK, or miniK channels, which reinforces the notion that **BK channels may be the dominant outward K–current carrier when MRA VSMCs are depolarized above 0 mV**.

V.5 pharmacology of 4 MRA VSMC K–channels

Inside–out experiments were performed to determine the single channel components that comprised the macroscopic whole–cell current and to characterize the K–channels. Specific K–channel blockers were used to aid in channel characterization:

Table D3. Selectivity of Antagonists for MRA and TA K–channels.

K–channel	tissue	g[1] (pS)	ChTX (nM)		IbTX (nM)		apamin (nM)		4–AP (mM)	
BK	MRA	123	150	$\downarrow^{**}$	150	$\downarrow^{***}$	300	$\downarrow^{**}$	2	$\downarrow^{**}$
IK		70	150	$\downarrow^{*}$	150	$\downarrow^{**}$	300	$\leftrightarrow$	2	$\downarrow^{*}$
SK		39	150	$\downarrow^{NS}$	150	$\downarrow^{**}$	300	$\leftrightarrow$	2	$\downarrow^{*}$
miniK		11	150	$\downarrow^{*}$	150	$\downarrow^{*}$	300	$\leftrightarrow$	2	$\downarrow^{NS}$
K_{Ca} / BK	TA[2]	120	10-50	$\downarrow^{NA}$					2	$\downarrow^{NS}$
K_{to}		85	50	$\leftrightarrow$					1 – 2	$\downarrow^{NA}$
K_{dr}		11	50	$\leftrightarrow$					1 – 5	$\downarrow^{NA}$

Notes: *1.* g approximations are poor ($[K^+]_o$ = 5.5 mM data non–linear).
2. Bolzon, 1992.
* : significant inhibition, P≤0.05; ** : P≤0.01; *** : P≤0.001
NS : not significant
↔ : no effect at this concentration
NA : not applicable (n < 3)

Thus, only MRA and TA BK_{Ca} channels share voltage–, calcium–, and pharmacological–similarities. The other currents / channels (K_{to} / K_{dr}) isolated from TA are distinct and different from the MRA IK / SK / miniK K_{Ca} channels. The MRA and TA K–channel conductance and pharmacology can be compared to other tissue and species in the literature (Appendix II, Table A2–1).

ChTX / IbTX

The MRA BK channel inside–out NP_o was completely blocked by ChTX (150 nM) and IbTX (150 nM). Similarly, ChTX (50 – 100 nM) significantly inhibited BK_{Ca}–channels in TA VSMCs (~ 200 pS, Bolzon *et al.*, 1993). The TA VSMC BK channel was similar to the MRA BK channel (Table D2) and probably corresponds to the TA BK_{Ca} channel previously characterized (Bolzon *et al.*, 1993).

ChTX (50 – 100 nM) blocked BK_{Ca} channels in rat renal arteriole VSMCs (Gebremedhin *et al.*, 1996), rabbit aorta VSMCs in primary culture (Pavenstädt *et al.*, 1991), bovine tracheal VSMCs (Green *et al.*, 1991), ferret retinal ganglion cells (Wang *et al.*, 1998), and cultured GH_3 pituitary cells (Lang and Ritchie, 1990). IbTX (> 5 nM) blocked bovine aortic VSMCs BK_{Ca} (266 pS) (Roy–Contancin *et al.*, 1990). These similarities suggest that MRA VSMC whole–cell K_{Ca} current was primarily composed of BK channel events, and possibly IK channel events.

The MRA IK channel inside–out NP_o was completely blocked by ChTX (150 nM) and IbTX (150 nM). Similarly, ChTX (50 – 100 nM) inhibited IK channels from mouse ileum (40 pS, $K_{i/o}$ = 150/2.5 mM; Vogalis *et al.*, 1998) and rat renal arteries (68 pS, $K_{i/o}$ = 145 mM; Gebremedhin *et al.*, 1996).

The MRA SK channel inside–out NP_o was partially but not significantly blocked by ChTX (150 nM) but was completely blocked by IbTX (150 nM). Conversely, the K_{Ca} channel from human pancreas (39 pS, $K_{i/o}$ = 120 mM) was blocked by low concentrations of ChTX and minimally inhibited by IbTX (50 nM) (Ishii *et al.*, 1997b). The SK channel was the only MRA VSMC K–channel that was selectively blocked by IbTX but was not significantly blocked by ChTX. IbTX is usually selective for large conductance K_{Ca} channels, such as the bovine aortic VSMC BK_{Ca} (266 pS), which is blocked by IbTX (> 5 nM) (Roy–Contancin *et al.*, 1990). However, the concentration of IbTX (150 nM) employed may exhibit non–specific inhibition.

The MRA miniK channel inside–out NP_o was completely blocked by ChTX (150 nM) and IbTX (150 nM). Similarly, ChTX (20 – 500 nM) nearly abolished small K_{Ca} channel NP_o from rat aortic endothelial cells (18 pS, $K_{i/o}$ = 150 mM; 6.7 pS, $K_{i/o}$ = 150/3 mM; Marchenko and Sage, 1996) and cloned human brain cells (hSK4, 12 pS, $K_{i/o}$ = 130/3 mM; Joiner *et al.*, 1997).

apamin

The BK channel inside–out NP_o was significantly inhibited (75% reduction) by apamin (300 nM). MRA BK apamin–sensitivity could be due to a lack of specificity at this high concentration, but the other K_{Ca} channels were unaffected by apamin. Apamin blockade of BK channels is not common, and this concentration (300 nM) is often used to completely block the small conductance calcium–dependent K–channel (SK_{Ca}; Garcia *et al.*, 1991). The partial block of the rat MRA VSMC BK channel by apamin suggests these K–channels are distinct and different from the apamin–insensitive K_{Ca} channels in other tissues.

The genetic structure of the BK channel pore may account for apamin sensitivity. Recently, two SK channels have been cloned and expressed in *Xenopus* oocytes, one apamin–insensitive (100 nM, SK1) and one highly apamin–sensitive (IC_{50} = 60 pM, SK2) (Ishii *et al.*, 1997a). Amino acid substitution and co–expression of chimeric partial channel head and tail dimers demonstrated that apamin sensitivity was dependent upon the presence of three specific amino acids in the pore region (aspartic acid, Asp/D 330; asparagine, Asn/N 357; and partially by glutamine, Gln/Q 328) (Ishii *et al.*, 1997a). However, a cloned IK channel

from human pancreas (hIK1) expressed in *Xenopus* oocytes that did not have the apamin pore sequence was partially inhibited by a low concentration of apamin (100 nM) (Ishii *et al.*, 1997b). Cloning and sequencing of MRA channels should help determine whether there are other binding sites for apamin.

The MRA IK channel inside–out NP_o was unaffected by apamin (300 nM), nor was the intermediate K_{Ca} channel from cultured mouse neuroblastoma cells (98 pS, $K_{i/o}$ = 145 mM; Leinders and Vijverberg, 1992). Conversely, apamin–sensitive (50 – 500 nM) intermediate K_{Ca} channels were observe in rat renal artery (68 pS, $K_{i/o}$ = 145 mM; Gebremedhin *et al.*, 1996) and mouse ileum (40 pS, $K_{i/o}$ = 150/2.5 mM; Vogalis *et al.*, 1998). The apamin–sensitivity of the IK from mouse ileum VSMCs (500 nM, partial inhibition) was much lower than that of rat renal artery (50 nM, blockade), and may be due to the pore structure or conformation (Ishii *et al.*, 1997a).

The MRA SK channel inside–out NP_o was unaffected by apamin (300 nM). In contrast, apamin (1 μM) inhibited a small K_{Ca} channel from ferret retinal ganglion cells (22 pS, $K_{i/o}$ = 140/5.9 mM; Wang *et al.*, 1998), but the micromolar concentration was three–fold higher than that used in MRA patches and may represent non–specific blockade.

The MRA miniK channel inside–out NP_o was unaffected by apamin (300 nM). This observation was unexpected since apamin (300 nM) is an effective inhibitor of small K_{Ca} channels in many tissues (Garcia *et al.*, 1991). An endogenous apamin–like compound was isolated from porcine brain (Fosset *et al.*, 1984), and porcine VSM expressed mRNA for an apamin sensitive K–channel

(Sokol *et al.*, 1994), which suggests that apamin–sensitive K–channels are physiologically relevant targets. However, apamin–insensitive (100 nM) small K_{Ca} channels have been observed in cloned brain SK channels (rat SK1; Ishii *et al.*, 1997a; human hSK4; Joiner *et al.*, 1997).

Most researchers found that apamin selectively inhibited small K_{Ca} channels. Apamin (1 – 500 nM) blocked small K_{Ca} channels from mouse colonic VSMCs (5.3 pS, $K_{i/o}$ = 140 mM; 2.9 pS, $K_{i/o}$ = 140/5 mM; Koh *et al.*, 1997), rat aortic endothelial cells (9.1 pS, $K_{i/o}$ = 150 mM; 2.8 pS, $K_{i/o}$ = 150/3 mM; Marchenko and Sage, 1996), cultured GH_3 pituitary cells (9 – 14 pS, $K_{i/o}$ = 150 mM; 6 pS, $K_{i/o}$ = 150/75 mM; Lang and Ritchie, 1990), and cultured mouse neuroblastoma cells (5.4 pS, $K_{i/o}$ = 145/5 mM; Leinders and Vijverberg, 1992).

Marchenko and Sage (1996) observed two disparate small K_{Ca} channels in rat aortic endothelial cells, one selectively blocked by ChTX (50 nM) (18 pS $K_{i/o}$ = 150 mM), the other selectively blocked by apamin (10 nM) (9.1 pS). The MRA miniK channel, similar to the 18 pS small K_{Ca} channel in rat aortic endothelial cells (Marchenko and Sage, 1996), was ChTX / IbTX–sensitive and apamin–insensitive.

4–AP

In the whole–cell configuration, 4–AP (2 mM) was selective for the MRA K_{dr} current and spared the K_{Ca} current. However, in the inside–out configuration, 4–AP (2 mM) completely blocked MRA BK and IK events, and partially inhibited SK NP_o. Most researchers have found that BK channels are unaffected

by 4–AP (Brayden, 1996). The concentration of 4–AP used to block the MRA BK and IK channels (2 mM) was higher than the concentration used to half block the K_{dr} channel (0.2 – 1 mM) in canine renal artery, human mesenteric artery, and rabbit pulmonary artery (Gelband and Hume, 1992; Smirnov and Aaronson, 1992; Okabe *et al.*, 1987). The selectivity of 4–AP for K_{dr} channels is reduced above 1 mM, which suggests that the blockade of the MRA BK and IK channels may be due to non–specific inhibition. However, further investigation is required before conclusions can be drawn.

4–AP (2 mM) significantly inhibited MRA SK channel inside–out NP_o, and partially but insignificantly inhibited MRA miniK channel inside–out NP_o. The effective concentration of 4–AP for K_{dr} selectivity (1 mM) was exceeded, which suggests that inhibition of MRA SK and miniK may be due to non–selective blockade.

CONCLUSION

The present studies can be summarized by the following statements:

1. Rat tail artery (TA) and superior mesenteric artery (SMA) donor tissue released an ACh–inducible, transferable endothelium–derived hyperpolarizing factor (EDHF). In the absence of donor tissue, ACh depolarized and contracted single TA vascular smooth muscle cells (VSMCs). In the presence of donor tissue, TA VSMCs were hyperpolarized. When NO synthesis was inhibited by L–nitro–N^{ω}–arginine (L–NNA), a NO–independent hyperpolarization persisted.

2. Rat mesenteric resistance artery (MRA) VSMCs have at least four calcium–dependent potassium channels, which range in single channel conductance from small to large (miniK, SK, IK, BK: 31, 50, 94, and 197 pS, $K_{i/o}$ = 150 mM). The MRA BK channel had similar biophysical properties to ~200 pS large conductance K_{Ca} channels found in other tissue. The calcium dependence (0 to 500 nM) of the four MRA K–channels was similar to that in other tissue. All four channels were inhibited by higher $[Ca^{2+}]_i$ (750 nM), which was probably due to calcium dependent block at the barium site. IK channel had some similar properties to intermediate K_{Ca} channels. The SK and miniK channels were similar to intermediate and small conductance K_{Ca} channels in calcium dependence but had a somewhat larger conductance. At negative voltages, the MRA SK and miniK channels demonstrated voltage–dependent NP_o (500 nM $[Ca^{2+}]_i$) whereas K_{Ca} channels are usually voltage inactivated.

3. The MRA K–channels were pharmacologically distinct from those found in other tissue. BK inside–out single channel NP_o was blocked by ChTX (150 nM), IbTX (150 nM), 4–AP (2 mM), and significantly inhibited by apamin (300 nM). Large conductance K_{Ca} channels are typically inhibited by ChTX / IbTX, partially inhibited by 4–AP (2 mM), and unaffected by apamin. However, apamin is usually used in lower concentrations (< 200 nM).

4. IK inside–out single channel NP_o was completely blocked by ChTX, IbTX, and 4–AP, but unaffected by apamin. Intermediate conductance K_{Ca} channels are typically blocked by ChTX and apamin; the effects of other antagonists are poorly characterized.

5. SK inside–out single channel NP_o was completely blocked by IbTX, significantly inhibited by 4–AP, dramatically but not significantly inhibited by ChTX, but unaffected by apamin. Smaller intermediate conductance K_{Ca} channels are poorly characterized though most are TEA–sensitive.

6. MiniK inside–out single channel NP_o was completely blocked by ChTX and IbTX, dramatically but not significantly inhibited by 4–AP, but unaffected by apamin. Small conductance K_{Ca} channels are **typically** inhibited by apamin but not by ChTX / IbTX. However, **some small K_{Ca} channels are pharmacologically unique, being apamin–sensitive and ChTX / IbTX insensitive.**

The pharmacological anomalies observed suggest that the MRA VSMC K–channels are distinct from those observed in other tissues. Discretion must be exercised until characterization has been completed.

FUTURE STUDIES

1. What is the effect of ACh–induced EDHF on MRA VSMCs?

TA VSMCs were used as targets in the hyperpolarization studies. MRA VSMCs should also be used to compare donor and target tissue diversity. Matched donor–target tissue experiments would reveal physiological relevance.

2. What is the specificity of the K–channel antagonists?

Lower concentrations of the K–channel antagonists (ChTX / IbTX: 10,30,50,100 nM; apamin: 20, 60, 100, 200 nM; 4–AP: 0.1, 0.3, 1.0 mM) might prove more selective and render a greater degree of specificity. The venom from the Australian taipan snake contains a peptide, taicatoxin, which has been used to block Ca^{2+} channels. However, taicatoxin (50 nM) blocked apamin–sensitive afterhyperpolarizations in rat chromaffin cells (97%) but only partially inhibited voltage–dependent Ca^{2+} channel current (12%) (Doorty *et al.*, 1997). TsKapa, a ChTX–like scorpion toxin from *Tityus serrulatus*, had a high affinity for apamin–sensitive K_{Ca} channels (Blanc *et al.*, 1997). A non–peptide antagonist (UCL 1684) for apamin–sensitive channels is available with nanomolar affinity (Rosa *et al.*, 1998). These and other apamin–specific antagonists should be used to characterize the pharmacology of the MRA VSMC K–channels. Other researchers have used a structure based approach to mutate specific amino acids of toxins, thus increasing channel specificity. Based on channel crystal topography, ChTX Lys(32) was mutated to produce ChTX analogs with 20 fold greater selectivity for the K_{Ca} (IKCa1) versus K_v (Kv1.3) channel in T–

lymphocytes (Rauer *et al.*, 2000). Outside out experiments with MRA VSMCs would determine K–channel reversibility (washout) and specificity.

3. What physiological relevance do the MRA VSMC K–channels hold?

The relative contribution of each MRA VSMC K–channel to total potassium current in the single cell was not measured under physiological conditions:

1. The intracellular calcium concentration was fixed at 500 nM, higher than 3 – 30 nM, the concentration of mesenteric artery smooth muscle cells near the resting membrane potential (–50 mV). The intracellular calcium concentration should have been matched to the membrane potential tested.
2. The extracellular potassium concentration was elevated so as to be symmetrical with the intracellular solution (150 mM), far above physiological (5.5 mM). The extracellular potassium concentration should have been matched to physiological (5.5 mM).

The elevated, fixed $[Ca^{2+}]_i$ resulted in open probabilities which would not occur under physiological conditions. Likewise, the elevated $[K^+]_o$ altered the single channel conductance.

An alternative technique would be to current clamp single cells using the nystatin perforated patch technique (Hamill, 1992). Membrane potential would be measured under physiological calcium concentrations stepped from 0 nM to 500 – 750 nM. This would determine the calcium concentration required to depolarize cells to specific membrane potentials. Calcium exchange in the pipette

tip could be accomplished through the use of a pipette micropump (Hamill, 1992). Calcium step could be expedited through the use of the whole–cell technique, but intracellular organelles and solutions are rapidly washed out of the cell by this method. The loss of intracellular mediators of membrane potential might result in cell contraction.

The calcium–potential data could be used to measure the open probability of the four MRA VSMC K–channels under these more physiological conditions. A very low NP_o would be expected at approximate physiological conditions (–50 mV, ~ 0 nM $[Ca^{2+}]_i$) which would increase at depolarized potentials at elevated internal calcium (500 – 750 nM $[Ca^{2+}]_i$). The relative contribution of each K–channel to the total potassium current carried under physiological conditions would be the product of the conductance and NP_o.

APPENDIX I

Appendix I contains an unpublished paper which studied the effects of cytochrome P–450 inhibitors on rat TA VSMC K–channel activities. Additional material not included in the original submission appears in [square parentheses]. The additional material includes the effects of systemic cytochrome P–450 induction (3–MC / β–NF) and depletion ($CoCl_2$).

Modulation of Vascular Smooth Muscle K^+ Channel Activity

By Cytochrome P–450 Inhibitors

Ethan Burnette & Donald. W. Cheung

Department of Pharmacology and

The University of Ottawa Heart Institute

410 Ruskin Street

Ottawa K1Y 4E9

CANADA

[unpublished]

Abstract

The effects of cytochrome P–450 inhibitors on the delayed rectifier and Ca^{2+}–activated K^+ channel activities in freshly isolated single smooth muscle from the rat tail artery were studied by patch clamp recording technique. Clotrimazole (> 1 μM) and metyrapone (1 mM) increased whole–cell Ca^{2+}–activated K^+ channel currents. Clotrimazole also increased significantly the open probability and the number of openings of single Ca^{2+}–activated K^+ channels in isolated outside–out patches. Proadifen only produced inhibition of the outward currents. All three inhibitors reduced significantly the delayed rectifier currents.

[Systemic induction of cytochrome P–450 activity was accomplished through intraperitoneal injection of 3–methylcholanthrene and β–naphthoflavone (3–MC / β–NF, 80mg/kg/day, 3 days). Induction of cytochrome P–450 activity did not change basal activity of whole–cell currents from Ca^{2+}–activated K^+ channels and delayed rectifier currents. In cytochrome P–450 induction experiments, clotrimazole (30 μM) increased Ca^{2+}–activated K^+ channel currents and decreased delayed rectifier currents. Systemic depletion of cytochrome P–450 activity was accomplished through intraperitoneal injection of cobalt chloride ($CoCl_2$, 24 mg/kg/day, 2 days). Depletion of cytochrome P–450 activity did not change basal activity of whole–cell currents from Ca^{2+}–activated K^+ channels and delayed rectifier currents. In cytochrome P–450 depletion experiments, clotrimazole (30 μM) did not increase Ca^{2+}–activated K^+ channel currents but did decrease delayed rectifier currents.] Results from the present study indicate that cytochrome P–450

inhibitors[, inducers, and depletors] have a direct effect on K^+ channels in vascular smooth muscle cells.

Introduction

Recent studies suggest that cytochrome P–450 enzymes and metabolites may participate in the regulation of vascular tone (Harder *et al.*, 1995). Metabolites of arachidonic acid such as epoxyeicosatrienoic acids (EETs) and hydroxyeicosatetraenoic acids (HETEs) produced via cytochrome P–450 dependent pathways in the endothelium or vascular smooth muscle cells have potent vascular effects. EETs, in general, produced vasodilatory effect while HETE increased vascular tone. Both EETs and HETEs are known to alter K^+ channel activities in vascular smooth muscle cells. EETs increased single K^+ channel activities (Hu and Kim, 1993) while 20–HETE inhibited the activity of a large conductance K^+ channel in vascular muscle cells (Harder *et al.*, 1994).

Studies with cytochrome P–450 inhibitors also indicate that P–450 enzymes and/or metabolites may be involved in the regulation of basal K^+ channel activities in vascular smooth muscle cells. Clotrimazole and other P–450 inhibitors attenuated a steady–state component of whole–cell K^+ channel currents in cells from rat pulmonary and mesenteric arteries (Yuan *et al.*, 1995). 17–octadecynoic acid, another P–450 inhibitor, was found to increase the number of openings and the open probability of a large conductance K^+ channel in cells from cat cerebral microvessels (Harder *et al.*, 1994). In the present study, we compared the effects of clotrimazole with two other chemically different P–450 inhibitors metyrapone and proadifen on

the activities of the delayed rectifier and Ca^{2+}–activated K^+ channel currents in cells from the rat tail artery.

[P–450 induction or depletion were accomplished through the use of 3–methylcholanthrene plus β–naphthoflavone or cobalt chloride, respectively (Pinto *et al.*, 1987; Chen and Cheung, 1996). In rat SMA, P–450 induction (3–MC / β–NF, 80mg/kg/day, 3 days) enhanced ACh–induced EDHF–mediated hyperpolarization (–14 mV increased to –23 mV) but not relaxation (Chen and Cheung, 1996). P–450 depletion ($CoCl_2$, 24 mg/kg/day, 2 days) significantly reduced the hyperpolarization (–14 mV reduced to –10 mV) and relaxation responses (Chen and Cheung, 1996). In canine coronary artery rings, P–450 induction (3–MC / β–NF, 40mg/kg/day, 3 days) enhanced arachidonic acid–induced endothelium–dependent relaxation (Pinto *et al.*, 1987). In contrast, P–450 depletion ($CoCl_2$, 24 mg/kg/day, 2 days) diminished arachidonic acid–induced relaxation (Pinto *et al.*, 1987). In the present study, we compared the effects of cytochrome P–450 induction / depletion and clotrimazole on whole–cell outward currents.]

Materials and Methods

[*P–450 Induction / Depletion*

Rats were given intraperitoneal injections of 3–methylcholanthrene and β–naphthoflavone (Sigma) (3–MC / β–NF, 80mg/kg/day, 3 days) to induce cytochrome P–450 activity or with cobalt chloride (Sigma) ($CoCl_2$, 24 mg/kg/day, 2 days) to deplete cytochrome P–450 activity. Solutions of 3–MC / β–NF or $CoCl_2$

were prepared according to Pinto *et al.* (1987). Untreated (control) animals were not injected.]

Cell Isolation

Single cells were isolated from tail arteries of male Wistar rats (10 – 12 weeks old, Charles River, Wilmington, Mass., USA) according to a technique developed in our laboratory (Bolzon and Cheung, 1989). The tail artery was internally perfused with a Ca^{2+}–free 4–(2–hydroxymethyl) –1–piperazineethanesulfonic acid (HEPES) buffer containing 0.02% collagenase (150 U/ml, type II, Sigma, St. Louis, Mo., USA), 0.1% papain (BDH, Toronto, Ont., Canada), and 4 mM dithiothreitol (Sigma) for 60 min. Single cells were harvested by gentle teasing of the arteries with a pair of fine forceps following enzyme treatments. These cells contract to stimulation by NPY, noradrenaline, KCl, caffeine, and ATP (Small *et al.*, 1992).

Patch Clamp Recording and Data Analysis

Recordings from freshly isolated cells were made using both whole–cell and outside–out patch configurations of the patch clamp technique. Patch pipettes having a resistance of 2 – 4 MΩ were pulled from borosilicate glass with a Flaming–Brown P–80 puller (Sutter Instruments, Novato, Ca., USA) and recordings were made using an Axopatch 200 amplifier (Axon Instruments, Foster City, Ca., USA). Series resistance (about 3 – 5 MΩ) and cell capacitance (about 50 pF) were determined and electronically compensated. In general, about 80% compensation of

the series resistance could be achieved. The leak current was negligible and was not subtracted from the records. Nifedipine (1 μM) was included in all outside solutions to eliminate Ca^{2+}–channel currents. This concentration of nifedipine has been shown to be effective in abolishing the Ca^{2+}–channel currents in these cells (Xiong *et al.*, 1993). When studying the Ca^{2+}–activated K^+ channel activities alone, the delayed rectifier was inactivated by keeping the holding potential at –40 mV (Bolzon *et al.*, 1993). The whole–cell currents remained stable for at least 60 min and well within the time required to complete the experiments. The current amplitude was determined at the end of the test pulse of an average signal derived from three consecutive traces.

For single channel recordings, only patches with stable basal activities were used to ensure that the changes in activity were not due to run–down or random fluctuations. To study the effect of clotrimazole on open probability, a control period of 5 – 8 min to record the basal channel activity was allowed before introduction of a single concentration of the drug. A complete recovery of the activities to control level after washout was observed. Open probability (NP_o) of single channel was calculated using pClamp 6.1 program based on the ratio of time spent in the open state to the duration of the recording:

$$NP_o = (t_1 + t_2 + \ldots + t_n) / t_{tot}$$

Where t is the amount of time that n channels are open and N is the maximum number of levels observed in the patch. The effect of clotrimazole was expressed as percentage change in NP_o compared to control period. Data acquisition and analysis were performed using the pClamp 6.1 program (Axon Instruments). Figures and

curve–fitting were made using SigmaPlot 5.0 (Jandel Scientific, San Rafael, Ca., USA). Student's t–test was used for statistical comparison and $P < 0.05$ is considered to be significant. All values are presented as means ± S.E.M.

Solutions

The composition of the extracellular solution was (in mM): NaCl 137; KCl 5.5; $CaCl_2$ 1.8; $MgCl_2$ 1.0; KH_2PO_4 0.4; $NaHCO_3$ 4.2; glucose 5.6. Nifedipine (1 μM) was also included in all extracellular solutions. pH was buffered to 7.4 with 10 mM HEPES and Tris. The pipette solutions contained (in mM): KCl 150; $MgCl_2$ 1.0; Na_2–ATP 1.0; $CaCl_2$ 3.0; EGTA 5.0. pH was buffered to 7.2 with HEPES and Tris. Free Ca^{2+} in the pipette solution was estimated to be 240 nM. The final concentration of dimethyl sulfoxide in the experiments was less than 0.1% and was found to have no significant effect on the activity of the K^+ channels. The solutions were introduced into a 1 ml volume recording chamber at a constant perfusion rate of 2 ml/min. All experiments were performed at room temperature.

Results

Effects of Clotrimazole on Whole–cell K_{Ca} Currents

At a holding potential of –40 mV, outward currents previously characterized as a Ca^{2+}–activated K^+ channel currents (K_{Ca}) were elicited by depolarizing test pulses (Bolzon *et al.*, 1989; Xiong *et al.*, 1994). Clotrimazole increased the outward currents (Figure AI–1). At 30 μM clotrimazole, a 57% increase of the current density was observed at a test potential of +70 mV. Another obvious change with

clotrimazole was that the currents now became less smooth, i.e. at similar current amplitudes, there were more oscillations of the currents (Figure AI–1B). The effects of clotrimazole could be observed at concentrations above 1 μM (Figure AI–2).

Effects of Clotrimazole on Single K_{Ca} Channel Activity

In isolated outside–out patches, single K_{Ca} channel activities were recorded at a holding potential of +50 mV. Clotrimazole (30 μM) increased significantly the open probability by 51.7 ± 13.0% (n = 5) and the number of openings by 156.0 ± 47.5% (Figure AI–3). These changes in single channel activity were compatible with a 40.0 ± 16.9% (n = 5) increase in whole–cell K_{Ca} current at the same test potential (Figure AI–1). The whole–cell and single channel currents and the increases induced by clotrimazole were inhibited by TEA (5 mM) or ChTX (100 – 150 nM) (Figure AI–3B).

Effects of Metyrapone and Proadifen on Whole–cell K_{Ca} Currents

Metyrapone produced similar effects as clotrimazole on whole–cell K_{Ca} currents (Figure AI–4). However, it was much less potent than clotrimazole and significant changes were not observed unless a high concentration of 1 mM was used (Figure AI–2). Unlike clotrimazole, metyrapone did not cause an increase in in oscillations of the currents. Proadifen, a widely used cytochrome P–450 inhibitor, produced only inhibitory effects on K_{Ca} currents (Figure AI–2, Figure AI–4B). Despite the diminished amplitude of the currents by proadifen, an increase in oscillations of the currents was still evident.

Effects of P–450 Inhibitors on the Delayed Rectifier

At a holding potential of –80 mV, delayed rectifier currents were activated at test potentials positive to –40 mV before recruitment of the K_{Ca} currents at about +30 mV (Figure AI–4). The delayed rectifier currents elicited at the lower test potentials were inhibited by clotrimazole and metyrapone, in contrast to an increase in K_{Ca} currents generated at more positive potentials (Figure AI–4A). A current–voltage curve of the delayed rectifier could be generated by the difference in the currents generated at holding potentials of –80 mV and –40 mV when the delayed rectifier was inactivated (Bolzon *et al.*, 1993). All three cytochrome P–450 inhibitors were effective in attenuating the delayed rectifier currents (Figure AI–5). At a test potential of +20 mV, the delayed rectifier currents were inhibited by 88.9 ± 13.0% for clotrimazole (30 μM), 45.6 ± 19.9% for metyrapone (1 mM), and 100% for proadifen (30μM).

[*Effects of P–450 Induction with 3–MC/β–NF on Whole–cell Current*

In isolated single vascular smooth muscle cells, outward current was elicited by step depolarization from a holding potential of –80 mV. The induction of cytochrome P–450 activity with 3–MC/β–NF did not change basal outward K_{Ca} or K_{dr} currents (Figure AI–6A). Clotrimazole (30μM) significantly increased K_{Ca} current at +70 mV by 38.6 % (n=4) and significantly decreased K_{dr} –dominant current at +20 mV by 67.0 % (n=4). Note that the K_{Ca} component at +20 mV was not subtracted.]

[*Effects of P–450 Depletion with $CoCl_2$ on Whole–cell Current*

In isolated single vascular smooth muscle cells, outward current was elicited by step depolarization from a holding potential of –80 mV. The depletion of cytochrome P–450 activity with $CoCl_2$ did not change basal outward K_{Ca} or K_{dr} currents (Figure AI–6B). Clotrimazole (30μM) did not significantly increase K_{Ca} current at +70 mV (increase 9.1 %; n=4) but significantly decreased K_{dr} –dominant current at +20 mV by 77.3 % (n=4). Note that the K_{Ca} component at +20 mV was not subtracted.]

Discussion

Clotrimazole is an antimycotic which exerts its fungistatic action by inhibiting sterol 14α–demethylase, a cytochrome P–450–dependent enzyme (Yoshida and Aoyama, 1987). Clotrimazole inhibits cytochrome P–450–dependent processes by binding to the heme moiety of the enzyme. Clotrimazole is also known to modulate ion channel activities. In human red blood cells and rat thymocytes, clotrimazole was effective in inhibiting Ca^{2+} channels and ChTX–sensitive Ca^{2+}–dependent K^+ channels (Alvarez *et al.*, 1992). In the present study, we observed that clotrimazole potentiated the activity of Ca^{2+}–activated K^+ channels in vascular smooth muscle cells. In addition, clotrimazole was very effective in inhibiting the delayed rectifier currents.

Clotrimazole increased the amplitude as well as the oscillations of whole–cell Ca^{2+}–activated K^+ channel currents. The oscillations are the result of opening and closing of the large conductance Ca^{2+}–activated K^+ channels. This was

confirmed from studies of isolated patches showing significant increases in channel opening probability and the number of openings of single Ca^{2+}–activated K^+ channels. Similar increases in single Ca^{2+}–activated K^+ channel activity to 17–octadecynoic acid, a specific mechanism–based inhibitor of cytochrome P–450 mediated metabolism of arachidonic acid, have also been reported in vascular smooth muscle cells (Harder *et al.*, 1994). The increases were reversed by 20–hydroxyeicosatetraenoic acid, an arachidonic acid metabolite. These observations led to the suggestion that endogenous cytochrome P–450 metabolites contribute to the regulation of basal Ca^{2+}–activated K^+ channel activity.

Metyrapone, another inhibitor of cytochrome P–450 via type II binding, also increased whole–cell Ca^{2+}–activated K^+ channel currents but only at high concentrations. A reduced sensitivity of the Ca^{2+}–activated K^+ channel to metyrapone relative to clotrimazole was also observed in human red [blood] cells (Alvarez *et al.*, 1992). Metyrapone also differed from clotrimazole in not increasing the oscillations of the currents. Whether these differences were related to different modes of action or involvement of different subfamilies of cytochrome P–450 remain to be determined. Proadifen has a structure related to local anesthetics and has been previously shown to inhibit K^+ and other ion channels by a mechanism unrelated to cytochrome P–450 activities (Sakuta and Yoneda, 1994). Inhibition of Ca^{2+}–activated K^+ channel by proadifen in vascular smooth muscle may be attributed to this local anesthetic effect. Nevertheless, an increase in oscillations of the currents was still observed.

The delayed rectifier K^+ current was inhibited by all three cytochrome P–450 inhibitors tested, with metyrapone having the weakest effect. Similar inhibition of the delayed rectifier current by clotrimazole and other cytochrome P–450 inhibitors has been observed in cells from the pulmonary and mesenteric arteries (Yuan *et al.*, 1995).

Cytochrome P–450 inhibitors have been used to assess the contribution of cytochrome P–450 metabolites in vascular activities, including those of endothelial cells (Graier *et al.*, 1995) and endothelium–dependent responses (Singer *et al.*, 1984; Oyekan *et al.*, 1994; Bauersachs *et al.*, 1994). In the present study, we demonstrated that these inhibitors at similar concentrations caused direct modulation of K^+ (and possibly other) channel activities in vascular smooth muscle cells. Proadifen, the most widely used amongst the inhibitors, appears to be the least specific and may have non–cytochrome P–450 related influence on ion channel activities due to its local anesthetic properties. Proadifen has been used to identify the component of the endothelium–dependent relaxation mediated by the release of a hyperpolarizing factor purportedly to be a cytochrome P–450 metabolite (Bauersachs *et al.*, 1994). However, this interpretation is compromised by the potent direct inhibitory effect of proadifen on vascular K^+ channels. Therefore, proper controls must be conducted when using these inhibitors to determine the mechanism of action in vascular tissues. Results from the present study indicate that the cytochrome P–450 system or metabolites may be involved in the regulation of basal K^+ [channel] activities in vascular smooth muscle.

Acknowledgement

This work was supported by a grant from the Heart & Stroke Foundation of Ontario.

Figure AI–1. Effect of clotrimazole (30μM) on whole–cell Ca^{2+}–acivated K^+ channel currents in single vascular cell from the rat tail artery.

Panel A. Control, outward currents elicited by test pulses from –40 to +80 mV, holding potential = –40 mV.

Panel B. Increase in currents after application of clotrimazole for 6 minutes. Note the increased oscillations of the currents.

Panel C. Current–voltage plot showing the increase in Ca^{2+}–acivated K^+ channel currents with clotrimazole. (n=5; * $p<0.05$, ** $p<0.01$).

A

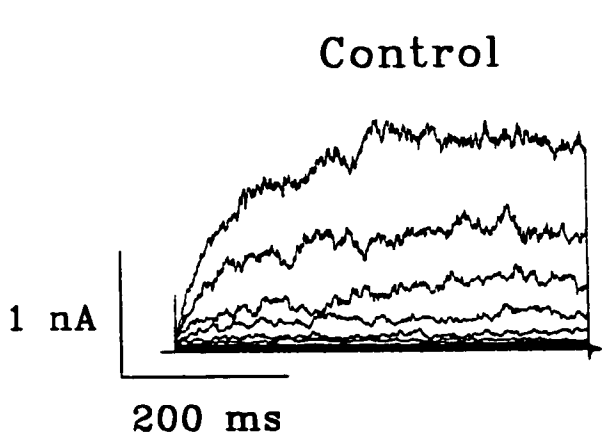
Control
1 nA
200 ms

B

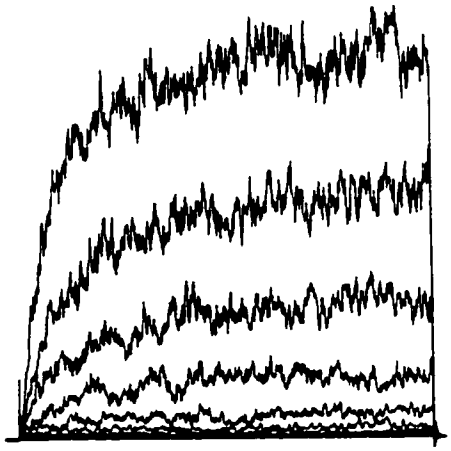
Clotrimazole 3x10 -5 M

C

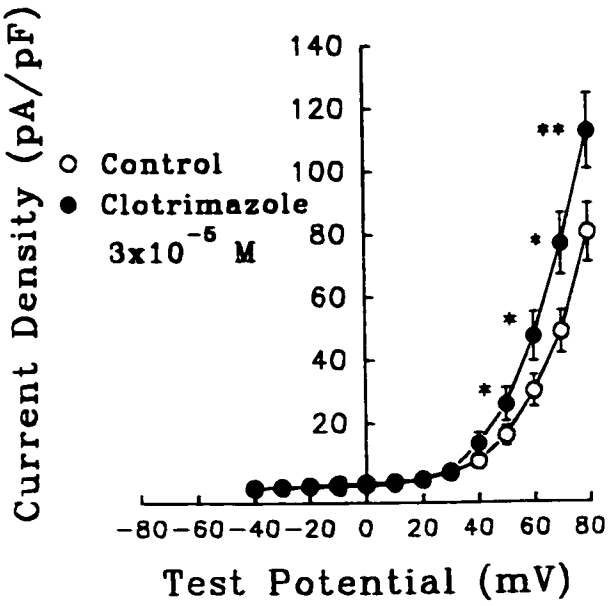
Current Density (pA/pF)
Control
Clotrimazole
3x10 -5 M
140
120
100
80
60
40
20
-80 -60 -40 -20 0 20 40 60 80
Test Potential (mV)
**
*
*
*

Figure AI–2. Modulation of whole–cell Ca^{2+}–activated K^+ channel currents by different concentrations of clotrimazole, metyrapone, and proadifen.

(n=4 – 7; * p<0.05, ** p<0.01, *** p<0.001).

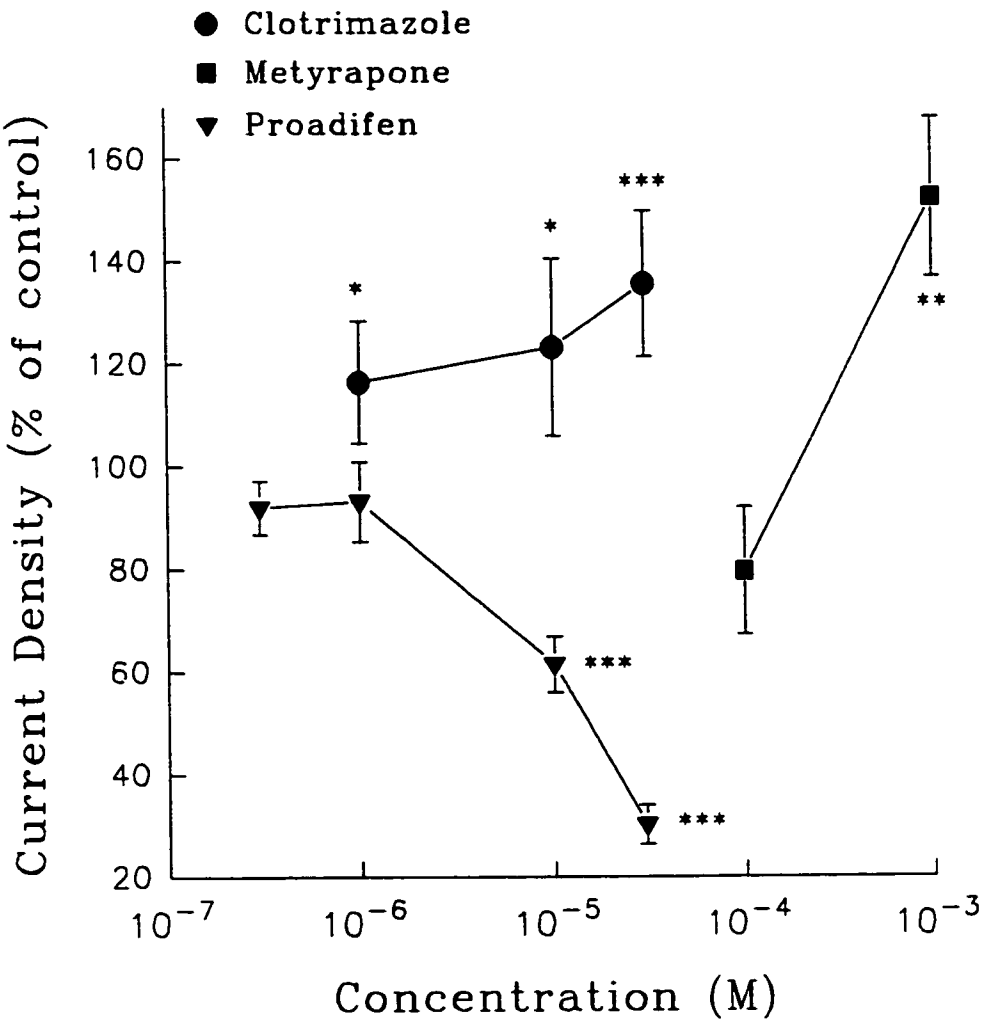
Clotrimazole
Metyrapone
Proadifen
Current Density (% of control)
160
140
120
100
80
60
40
20
*
*
***
***
***
**
10^{-7}
10^{-6}
10^{-5}
10^{-4}
10^{-3}
Concentration (M)

Figure AI–3. Single Ca^{2+}–activated K^+ channel activities recorded from an outside–out patch.

Panel A. Control activity recorded at +50 mV.

Panel B. Increase in channel activity in the presence of clotrimazole (30 μM). The channel activities were inhibited by the addition of charybdotoxin (CTX, 100 nM). C denotes the closed state of the channels.

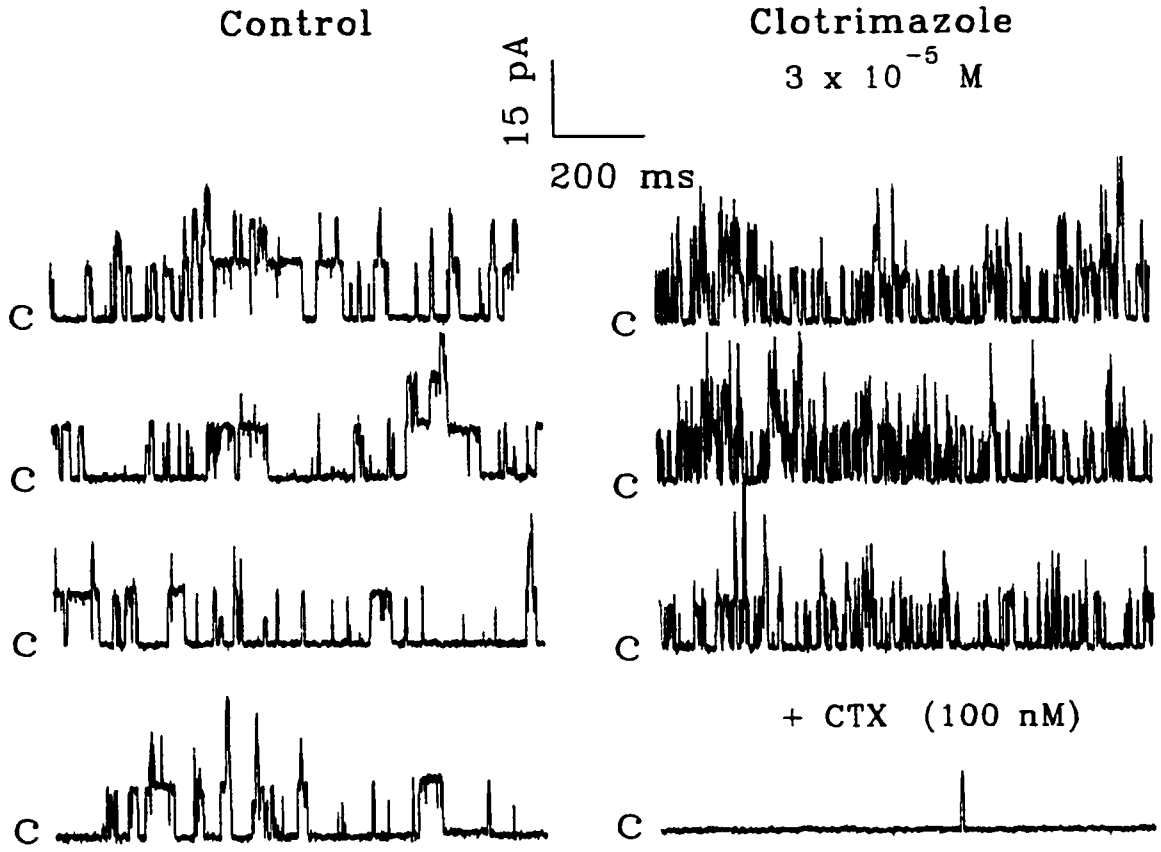
Control
Clotrimazole
3 x 10 -5 M
15 pA
200 ms
C
C
C
C
C
C
C
+ CTX (100 nM)

Figure AI–4. Effects of metyrapone and proadifen on whole–cell outward currents elicited by depolarizing pulses of –80 to +80 mV from a holding potential of –80 mV.

Panel A. At a holding [potential] of –80 mV, delayed rectifier currents were observed at test potentials positive to –40 mV. At more positive test potentials (> +20 mV), the larger oscillating Ca^{2+}–activated K^+ channel currents became dominant. The increase in Ca^{2+}–activated K^+ channel currents induced by metyrapone (1 mM) is accompanied by inhibition of the delayed rectifier current.

Panel B. Proadifen inhibits the outward currents in a concentration–dependent manner.

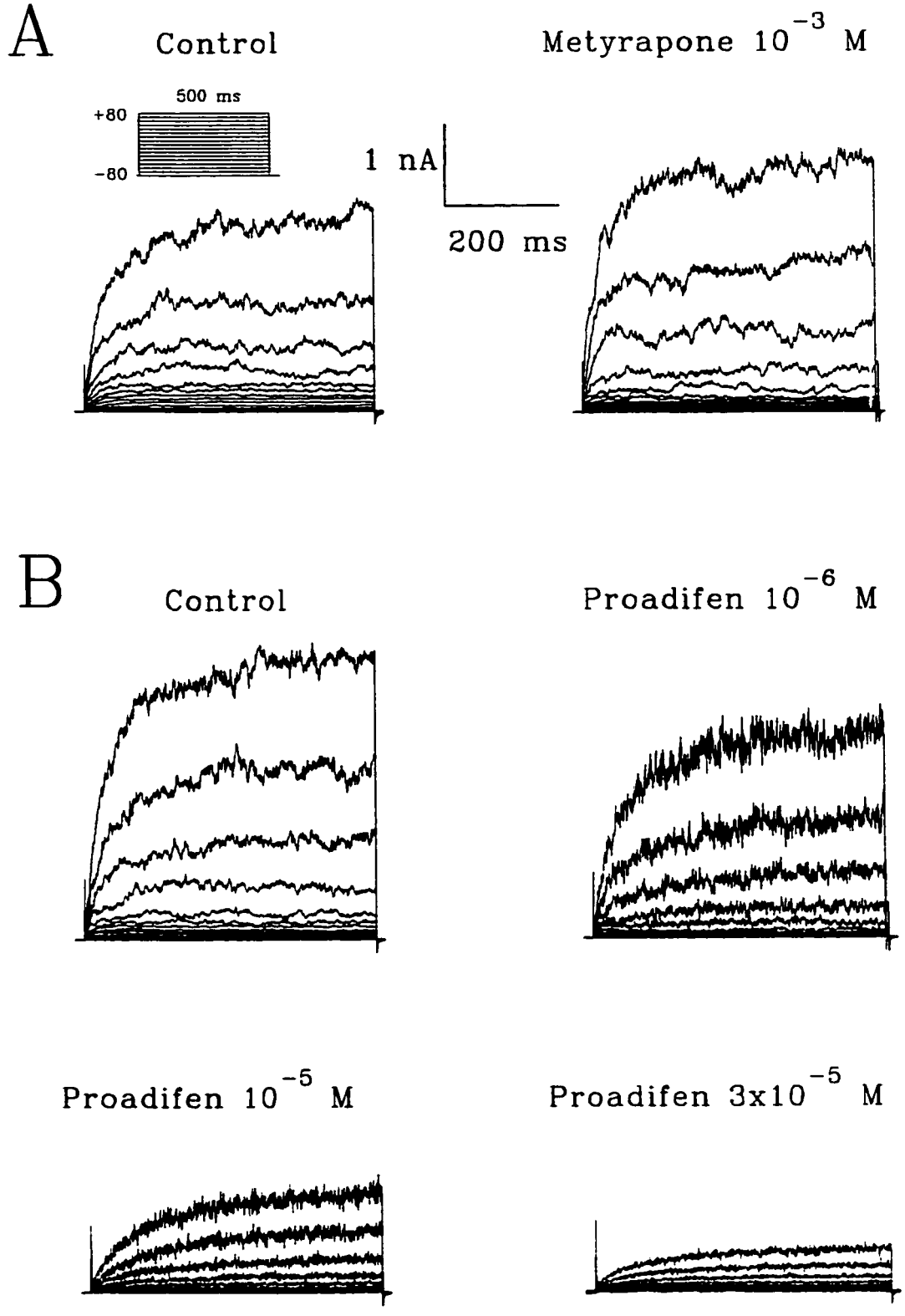
A
Control
Metyrapone 10^-3 M
500 ms
+80
-80
1 nA
200 ms
B
Control
Proadifen 10^-6 M
Proadifen 10^-5 M
Proadifen 3x10^-5 M

Figure AI–5. Effects of clotrimazole and metyrapone on whole–cell delayed rectifier currents.

Panel A. Clotrimazole inhibited the delayed rectifier currents in a concentration–dependent manner. The currents were elicited at a holding potential of –80 mV with test pulses from –40 mV to +20 mV. Some of the currents could be attributed to the Ca^{2+}–activated K^+ channel currents. The traces represented the averages from 4 consecutive recordings.

Panel B. Metyrapone (1 mM) was also effective in inhibiting the delayed rectifier currents.

Panel C. Current–voltage plot showing the effect of clotrimazole (30 μM) on the delayed rectifier currents (n=5). The pure delayed rectifier currents were derived by subtracting the currents elicited at a holding potential of –80 mV from those elicited at a holding potential of –40 mV when the Ca^{2+}–activated K^+ channels were inactivated.

Panel D. Current–voltage plot showing inhibition of the delayed rectifier currents by metyrapone (1 mM). (n=4; * $p<0.05$, ** $p<0.01$, *** $p<0.001$).

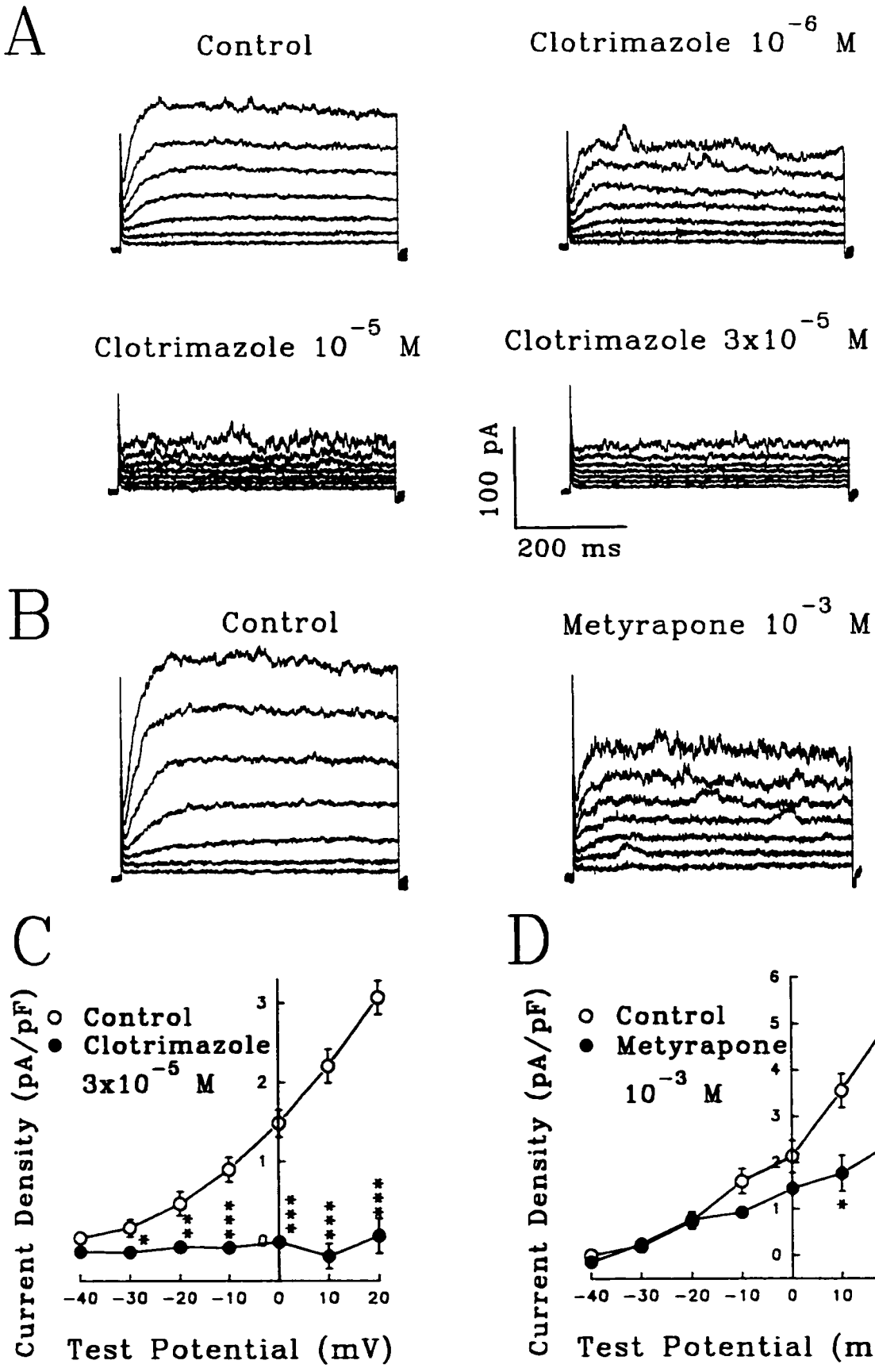
A
Control
Clotrimazole 10^-6 M
Clotrimazole 10^-5 M
Clotrimazole 3x10^-5 M
100 pA
200 ms
B
Control
Metyrapone 10^-3 M
C
Control
Clotrimazole
3x10^-5 M
Current Density (pA/pF)
Test Potential (mV)
D
Control
Metyrapone
10^-3 M
Current Density (pA/pF)
Test Potential (mV)

[**Figure AI–6. Effects of P–450 induction / depletion and clotrimazole on whole–cell current.**

Panel A. P–450 induction with 3–MC/β–NF (80mg/kg/day, 3 days) did not alter basal outward current (K_{Ca} and K_{dr}). The currents were elicited at a holding potential of –80 mV with test pulses from –80 mV to +80 mV. P–450 induction increased the K_{Ca} current and decreased the K_{dr} current. The traces represented the averages from 4 consecutive recordings.

Panel B. P–450 depletion with $CoCl_2$ (24 mg/kg/day, 2 days) did not alter basal outward current (K_{Ca} and K_{dr}). The currents were elicited at a holding potential of –80 mV with test pulses from –80 mV to +80 mV. P–450 depletion did not increase the K_{Ca} current but did decrease the K_{dr} current. The traces represented the averages from 4 consecutive recordings.

Panel C. Current–voltage plot of P–450 induction showing the statistically significant increase in the whole–cell K_{Ca} current and statistically significant decrease in the K_{dr} current by clotrimazole (30 μM) (n=4; * $p<0.05$, ** $p<0.01$, *** $p<0.001$).

Panel D. Current–voltage plot of P–450 depletion showing no change in the whole–cell K_{Ca} current and statistically significant decrease in the K_{dr} current by clotrimazole (30 μM) (n=4; * $p<0.05$, ** $p<0.01$, *** $p<0.001$).]

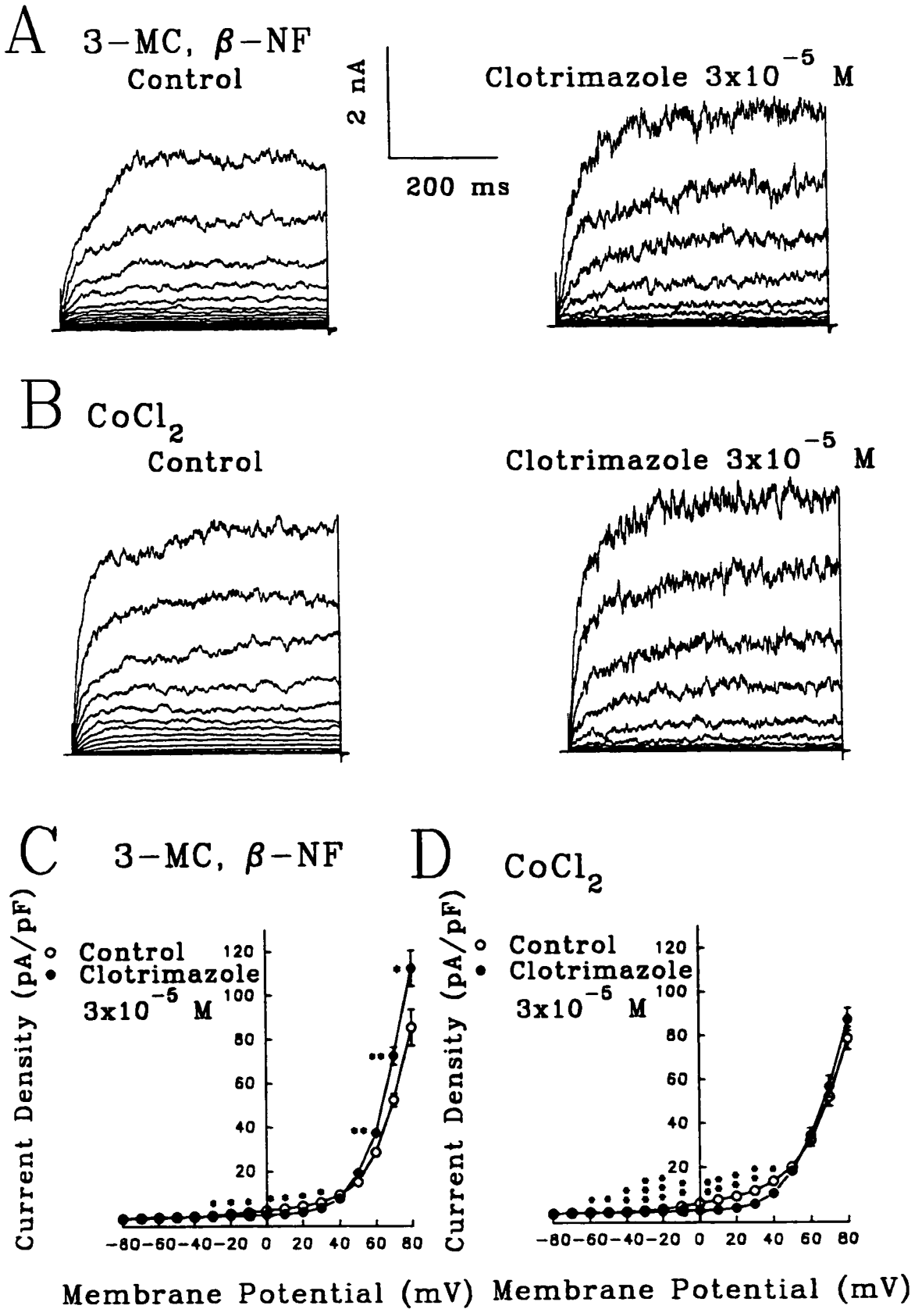
A
3−MC, β−NF
Control
2 nA
200 ms
Clotrimazole 3x10 −5 M
B
CoCl2
Control
Clotrimazole 3x10 −5 M
C
3−MC, β−NF
D
CoCl2
Current Density (pA/pF)
Control
Clotrimazole
3x10 −5 M
120
100
80
60
40
20
−80 −60 −40 −20 0 20 40 60 80
Membrane Potential (mV)
Membrane Potential (mV)

APPENDIX II

Appendix II contains Tables A2–1 (abbreviated) and A2–2 (detailed), which are literature summaries of the effects of P–450 inhibitors and K–channel inhibitors on agonist–induced EDHF release in various tissues.

Table A2–1. Summary of EDHF and P–450 in various tissues.

Notes:

EDHF ≈ P–450: evidence suggests EDHF may be a P–450 metabolite of AA

EDHF ≠ P–450: evidence suggests EDHF may not be a P–450 metabolite of AA

Table A2–2. Literature summary of EDHF and P–450 in various tissues.

Notes: *1.* AA: arachidonic acid, H: hyperpolarization, R: relaxation.
∴ EDHF ≈ P–450: EDHF may be a P–450 metabolite of AA
∴ EDHF ≠ P–450: EDHF may not be a P–450 metabolite of AA
↓↓ : significant inhibition, abolished response
↓ : significant inhibition / block.
(↓) : partial but significant inhibition.
↔ : no effect at this concentration.

Table A2–1. Summary of EDHF and P–450 in various tissues.

tissue	species		author
	EDHF ≈ P–450	EDHF ≠ P–450	
mesenteric artery	rat SMA		Chen & Cheung, 1996
	rat SMA		McCulloch *et al.*, 1997
		rat SMA	Fukao *et al.*, 1997a
	guinea pig		Triggle *et al.*, 1999
		rabbit	Fujimoto *et al.*, 1999
aorta	rabbit		Oyekan *et al.*, 1994
	rabbit		Pfister & Campbell, 1992
	rabbit		Pfister *et al.*, 1996
	rabbit		Pfister *et al.*, 1998
coronary artery	canine		Rosolowsky *et al.*, 1990
	canine		Pinto *et al.*, 1987
	rat		Bauersachs *et al.*, 1994
	bovine / porcine		Cowan & Cohen, 1991; Holzmann *et al.*, 1994; Hecker *et al.*, 1994
	bovine / porcine		Popp *et al.*, 1996
	bovine / porcine		Graier *et al.*, 1996
	guinea pig		Eckman *et al.*, 1998 Eckman *et al.*, 1994
	guinea pig		Nishiyama *et al.*, 1998
		guinea pig	Yamanaka *et al.*, 1998
carotid artery		guinea pig	Chataigneau *et al.*, 1998
		guinea pig	Corriu *et al.*, 1996a
		guinea pig	Corriu *et al.* 1996b
	rabbit		Dong *et al.*, 1997
middle cerebral artery (MCA)	guinea pig		Petersson *et al.*, 1997
	guinea pig		Triggle *et al.* 1999
	cat		Gebremedhin *et al.*, 1992
	cat		Ellis *et al.*, 1990
		rabbit	Ellis *et al.*, 1990
		rabbit	Dong *et al.*, 1998;
		rabbit	Triggle *et al.*, 1999
hepatic artery		rat	Zygmunt *et al.*, 1996
		rat	Zygmunt & Högestätt, 1996
renal artery	rat		Mieyal *et al.*, 1998
	rat		Rapacon *et al.*, 1996
	rat		Zou *et al.*, 1994

Table A2–2. Literature summary of EDHF and P–450 in various tissues.

mesenteric artery

tissue	agonist	R	H	antagonist	R	H	author
rat SMA	ACh	R	H	clotrimazole 10 μM	↓	↓	Chen & Cheung, 1996
rat SMA	carbachol	R		clotrimazole 1–10 μM	↓		McCulloch *et al.*, 1997
∴ EDHF ≈ P–450 in rat SMA							
guinea pig	ACh	R		clotrimazole 1, 3 μM	↔		Triggle *et al.*, 1999
∴ EDHF ≠ P–450 in guinea pig mesenteric artery							

aorta

tissue	agonist	R	H	antagonist	R	H	author
rabbit	ACh	R		clotrimazole 2.5–10 μM	↓		Oyekan *et al.*, 1994
				proadifen 50–200 μM	↓		
				7–ER	↓		
				17–ODYA 2.5–5 μM	↔		
				ETYA	↔		
rabbit	ACh	R		lipoxygenase inhibitors	↓		Pfister & Campbell, 1992
				11,14,15–THETA	↓		Pfister *et al.*, 1996; Pfister *et al.*, 1998
				11,12,15–THETA	↓		
∴ EDHF ≈ P–450 in rabbit aorta							

coronary artery					
tissue	agonist	R H	antagonist	R H	author
canine	ACh	R			Rosolowsky *et al.*, 1990
	EET	R			
canine	AA	R	proadifen	↓	Pinto *et al.*, 1987
			proadifen + indomethacin	↓↓	
∴ EDHF ≈ P–450 in canine coronary artery					
rat	bradykinin	R	proadifen 3 μM	↓	Bauersachs *et al.*, 1994
			TBA 0.3 mM	↓	
∴ EDHF ≈ P–450 in rat coronary artery					
bovine / porcine	bradykinin	R	clotrimazole 100 μM	↓	Cowan & Cohen, 1991; Holzmann *et al.*, 1994; Hecker *et al.*, 1994
			proadifen 30–100 μM	↓	
			TBA 3 mM	↓	
			apamin 1 μM	↓	
			7–ER	↔	
bovine / porcine	bradykinin	R	clotrimazole 3 μM	↓↓	Popp *et al.*, 1996
			17–ODYA 3 μM	↓↓	
	5,6–EET	R			ibid.
bovine / porcine	ACh	R	proadifen 10–100 μM		Graier *et al.*, 1996
	11,12–EET	R			ibid.
bovine	A23187	R	PTX	↓	ibid.
			apamin 1 μM	↓	
∴ EDHF ≈ P–450 in bovine / porcine coronary artery					

coronary artery						
tissue	agonist	R	H	antagonist	R	H	author
guinea pig	ACh	R	H	proadifen	↓	↓	Eckman *et al.*, 1998
				clotrimazole	↓	↓	
				17–ODYA	↔	↔	
				7–ER	↔	↔	
				IbTX 100 nM	↔	↔	
				4–AP 5 mM	↓	↓	
	AA	R		proadifen	↓		ibid.
				clotrimazole	↓		
				17–ODYA	↔		
				7–ER	↔		
				IbTX	↓		
				4–AP	↔		
	11,12-EET	R		IbTX	↓		ibid.
				4–AP	↔		
guinea pig	ACh (hyperpol.: initial rapid, delayed sustained)	H		clotrimazole	↓,↓		Nishiyama *et al.*, 1998
				proadifen	↓,↓		
				ChTX 50 nM	↓,↔		
				apamin 100 nM	(↓),↔		
				indomethacin	↔,↓		
				4–AP 0.1–1 mM	↔,↓		
∴ EDHF ≈ P–450 in guinea pig coronary artery							
guinea pig	ACh	R		proadifen	↓		Yamanaka *et al.*, 1998
				17–ODYA	↔		
				4–AP 1 mM	↓		
				ChTX 100 nM + apamin 100 nM	↓		
				IbTX 100 nM + apamin	↔		
	5,6–EET	≠R					ibid.
	11,12–EET	≠R					
	14,15–EET	≠R					
∴ EDHF ≠ P–450 in guinea pig coronary artery							

carotid artery

tissue	agonist	R	H	antagonist	R	H	author
guinea pig	ACh		H	ChTX 100 nM + apamin 500 nM		↓↓	Chataigneau *et al.*, 1998
				apamin		(↓)	
				apamin + IbTX 30 nM		(↓)	
				ChTX / IbTX		↔	
				17-ODYA 10μM		(↓)	
				17–ODYA + apamin		(↓)	
				17–ODYA + ChTX / IbTX		↔	
	5,6–EET		≠H				ibid.
	8,9–EET		≠H				
	11,12–EET		≠H				
	14,15–EET		≠H				
guinea pig	ACh		H	L–NNA 100 μM		↔	Corriu *et al.*, 1996a
				indomethacin		↔	
				clotrimazole 100 μM		↔	
				proadifen 100μM		↔	
				metyrapone 100 μM		↔	
				17–ODYA 5 μM		↔	
guinea pig	ACh		H	ChTX 100 nM + apamin 500 nM		↓↓	Corriu *et al.* 1996b
				ChTX		↔	
				apamin		↔	
				glybenclamide		↔	
∴ EDHF ≠ P–450 in guinea pig carotid artery							
rabbit	ACh		R	proadifen 10 μM		(↓)	Dong *et al.*, 1997
				clotrimazole 100 μM		(↓)	
				17–ODYA		(↓)	
	ACh		R	ChTX 100 nM		↓↓	ibid.
				IbTX 100 nM		(↓)	
				apamin 3 μM		(↓)	
∴ EDHF ≈ P–450 in rabbit carotid artery							

middle cerebral artery (MCA)

tissue	agonist	R	H	antagonist	R	H	author
guinea pig	ACh	R		ChTX 100 nM + apamin 100 nM	↓↓		Petersson *et al.*, 1997
				ChTX	(↓)		
				IbTX 100 nM	↔		
				apamin	↔		
				IbTX + apamin	↔		
				4-AP 1 mM	↔		
				ciclazindol (K_v)	↓		
				ciclazindol + apamin	↓↓		
				glybenclamide	↔		
				dendrotoxin	↔		
guinea pig	ACh	R		clotrimazole	↓		Triggle *et al.* 1999
∴ EDHF ≈ P–450 in guinea pig cerebral artery							
cat	5,6–EET 8,9–EET 11,12–EET	R					Gebremedhin *et al.*, 1992
cat	5,6–EET	R		indomethacin	↓↓		Ellis *et al.*, 1990
	AA	R		indomethacin	↓↓		
∴ EDHF ≈ P–450 in cat cerebral artery							
rabbit	5,6–EET	R		indomethacin	↓↓		Ellis *et al.*, 1990
	AA	R		indomethacin	↓↓		
rabbit	ACh	R		L–NNA + indomethacin	↓↓		Dong *et al.*, 1998; Triggle *et al.*, 1999
rabbit	ACh	R		ChTX	↓		Dong *et al.*, 1998
				IbTX	↓		
				4–AP	↓		
				apamin	↓		
				clotrimazole	↔		
∴ EDHF ≠ P–450 in rabbit cerebral artery							

hepatic artery

tissue	agonist	R	H	antagonist	R	H	author
rat	ACh	R	H	proadifen	↓	↓	Zygmunt *et al.*, 1996
				clotrimazole	↓	↔	
				17–ODYA	↔	↔	
	EETs	≠R	≠H				
rat	ACh		R	TBA 1 mM	↓		Zygmunt & Högestätt, 1996
				4–AP 1 mM	↓		
				ChTX + apamin	↓		
				ChTX 300 nM	↔		
				IbTX 100 nM	↔		
				apamin 300 nM	↔		

∴ EDHF ≠ P–450 in rat hepatic artery

renal artery

tissue	agonist	R	H	antagonist	R	H	author
rat	ACh		R	clotrimazole 1 μM	↓		Mieyal *et al.*, 1998
				ChTX 10 nM	↓		
				IbTX 50 nM	↔		
				apamin 250 nM	↔		
rat	bradykinin		R	TBA	↓		Rapacon *et al.*, 1996
				TEA	↓		
				ChTX	↓		
				IbTX	↔		
rat	antagonist: 17–ODYA	↑ kidney perfusion; ↓ 20–HETE, 11,12–EET, and 14,15–EET synthesis					Zou *et al.*, 1994

∴ EDHF ≈ P–450 in rat renal artery and kidney

APPENDIX III

Appendix III contains Table A3–1 which is a literature summary of the properties of K_{Ca} channels observed in mammalian tissue. The table is arranged from largest conductance to smallest. The table is divided into three areas by double lines. The top third are examples of BK; the middle third, of IK; and the last portion contain the SK/miniK channels.

Notes: *1.* Voltage–dependent, Ca–dependence NOT proven but implied.
↓ : significant inhibition / block.
(↓) : partial but significant inhibition.
↔ : no effect at this concentration.

Table A3–1. Properties of K–channels in the Literature.

g (pS)	$K_{i/o}$ (mM)	species	tissue	TEA (mM)
251	145	rat	renal artery SMC	↓ (0.1–0.3)
278	145	*rat*	pancreatic cells	
245	145	rat	pulmonary artery SMC	
218		rat	myotube cells	
227	145	rabbit	aortic SMC	↓ (1 – 10)
180	142	rabbit	portal vein cells	↓ (1 – 10)
~200	126	rabbit	jejunum	
~100	126/6	guinea pig	mesenteric artery SMC	
200	150/50	guinea pig	portal vein cells	
118	140/5.9	ferret	retinal ganglion cells	
240 (110)	140 (140/5)	mouse	motoneurons	
98	145/5	*mouse*	neuroblastoma cells	↓ (1 – 2)
266		cow	aortic SMC	↓ (< 5)
229	140	cow	tracheal SMC	↓ (1)
240	140	cow	microglia	
150	150	cow	nonpigmented ciliary epithelial cells	
250–300	150	GH_3	pituitary cells	↓ (0.03 – 3)
135	142	rat	aortic cultured SMC	↓ (10 – 30)
68	145	rat	renal artery SMC	↓ (0.1– 0.3)
91	145	rat	pancreatic artery SMC	
~100[2]	126	rabbit	jejunum	
(50)	(126/6)	guinea pig	mesenteric artery SMC	
43[2]	145	rat	pancreatic artery SMC	↓ (10)
12	130/3	human	hSK4 in CHO	(↓)(5)
22	140/5.9	ferret	retinal ganglion cells	
18 (6.7)	150 (150/3)	rat	endothelial cells	↓ (50–1000)
9.1 (2.8)	150 (150/3)	rat	endothelial cell	
9 – 14 (6)	150 (150/75)	GH_3	pituitary cells	
5.3 (2.9)	140 (140/5)	mouse	colonic SMC	
5.4	145/5	mouse	neuroblastoma cells	↔ (20)

ChTX (nM)	IbTX (nM)	Apamin (nM)	4–AP (mM)	author
↓ (50)		↔ (50)		Gebremedhin *et al.*, 1996
				Stuenkel, 1989
				Albarwani *et al.*, 1994[1]
				Barrett *et al.*, 1982
↓ (0.5 – 5)				Pavenstädt *et al.*, 1991
				Inoue *et al.*, 1986
				Benham *et al.*, 1986
				ibid.
				Pfründer and Kreye, 1991
↓ (20)				Wang *et al.*, 1998
				McLarnon *et al.*, 1995a
		↔ (100)		Leinders and Vijverberg, 1992
				Roy–Contancin *et al.*, 1990
↓ (100)			↔ (1)	Green *et al.*, 1991
				McLarnon *et al.*, 1995b
				Edelman *et al.*, 1995
↓ (50)		↔ (5000)		Lang and Ritchie, 1990
				Sadoshima, *et al.* 1988
↓ (50)		↓ (50)		Gebremedhin *et al.*, 1996
				Stuenkel, 1989
				Benham *et al.*, 1986
				ibid.
				Stuenkel, 1989
↓ (20)		↔ (100)		Joiner *et al.*, 1997
		↓(1000)		Wang *et al.*, 1998
				Marchenko and Sage, 1996
		↓ (1 – 10)		*ibid.*
		↓ (500)		Lang and Ritchie, 1990
		(↓)(300)		Koh *et al.*, 1997
		↓ (3)		Leinders and Vijverberg, 1992

REFERENCES

Aaronson, P.I., C.D. Benham, T.B. Bolton, P. Hess, R.J. Lang, and R.W. Tsien. (1986). Two types of single channel and whole–cell calcium and barium currents in single smooth muscle cells of rabbit ear artery and the effects of noradrenaline. *Journal of Physiology* **377:**36p.

Adeagbo, A.S.O., and C.R. Triggle. (1993). Varying extracellular [K^+]: a functional approach to separating EDHF– and EDNO–related mechanisms in perfused rat mesenteric arterial bed. *Journal of Cardiovascular Pharmacology* **21(3):**423–429.

Adelman, J.P., K.–Z. Shen, M.P. Kavanaugh, R.A. Warren, Y.–N. Wu, A. Lagrutta, C.T. Bond, and R.A. North. (1992). Calcium–activated potassium channels expressed from cloned complementary DNAs. *Neuron* **9:**209–216.

Albarwani, S., B.E. Robertson, P.C.G. Nye, and R.Z. Kozlowski. (1994). Biophysical properties of Ca^{2+}– and Mg–ATP–activated K^+ channels in pulmonary arterial smooth muscle cells isolated from the rat. *Pflügers Archives* **428:**446–454.

Alvarez, J., M. Montero, and J. Garcia–Sancho. (1992). High affinity inhibition of Ca^{2+}–dependent K^+ channels by cytochrome P–450 inhibitors. *Journal of Biological Chemistry* **267(17):**11789–11793.

Amedee, T., W.A. Large, and Q. Wang. (1990). Characteristics of chloride currents activated by noradrenaline in rabbit ear artery cells. *Journal of Physiology* **428:**501–516.

Atkinson, N.S., G.A. Robertson, and B. Ganetzky. (1991). A component of calcium–activated potassium channels encoded by the *Drosophila slo* locus. *Science* **253:**551–555.

Barrett, J.N., K.L. Magleby, and B.S. Pallotta. (1982). Properties of single calcium–activated potassium channels in cultured rat muscle. *Journal of Physiology* **331:**211–230.

Bauersachs, J., M. Hecker, and R. Busse. (1994). Display of the characteristics of endothelium–derived hyperpolarizing factor by a cytochrome P450–derived arachidonic acid metabolite in the coronary microcirculation. *British Journal of Pharmacology* **113:**1548–1553.

Beam, K.G., and C.M. Knudson. (1988). Calcium currents in embryonic and neonatal mammalian skeletal muscle. *Journal of General Physiology* **91:**781–798.

Bean, P.B. (1989). Classes of calcium channels in vertebrate cells. *Annual Review of Physiology* **51:**367–384.

Beech, D.J., and T.B. Bolton. (1989a). Properties of cromakalim–induced potassium conductance in smooth muscle cells isolated from the rabbit portal vein. *Journal of Physiology* **98:**851–864.

Beech, D.J., and T.B. Bolton. (1989b). A voltage–dependent outward current with fast kinetics in single smooth muscle cells isolated from the rabbit portal vein. *Journal of Physiology* **412:**397–414.

Beech, D.J., and T.B. Bolton. (1989c). Two components of potassium current activated by depolarization of single smooth muscle cells from the rabbit portal vein. *Journal of Physiology* **418:**293–309.

Beech, D.J., H. Zhang, K. Nakao, and T.B. Bolton. (1993). K channel activation by nucleotide diphosphates and its inhibition by glibenclamide in vascular smooth muscle cells. *British Journal of Pharmacology* **110:**573–582.

Benham, C.D., T.B. Bolton, R.J. Lang, and T. Takewaki. (1985). The mechanism of action of Ba^{2+} and TEA^{+} on single Ca^{2+}–activated K^{+} channels in arterial and intestinal smooth muscle cell membranes. *Pflügers Archives* **403:**120–127.

Benham, C.D., T.B. Bolton, R.J. Lang, and T. Takewaki. (1986). Calcium–activated potassium channels in single smooth muscle cells of rabbit jejunum and guinea–pig mesenteric artery. *Journal of Physiology* **371**:45–67.

Benham, C.D., P. Hess, and R.W. Tsien. (1987). Two types of calcium channels in single smooth muscle cells of rabbit artery studied with whole–cell and single channel recording. *Circulation Research* **61(1)**:110–116.

Biel, M., R. Hullin, S. Freundner, D. Singer, N. Dascal, V. Flockerzi, and F. Hofmann. (1991). Tissue specific expression of high voltage dihydropyridine sensitive L–type calcium channels. *European Journal of Biochemistry* **200**:81–88.

Bkaily, G. (1991). Receptors and second messenger modulation of Ca^{2+} and K^{+} channels activity in vascular smooth muscle cells. Ion Channels of Vascular Smooth Muscle Cells and Endothelial Cells, *Ed.:* N. Sperelakis and H. Kuriyama. Elsevier Sci. Pub. Co., Inc., USA, p. 374.

Blanc, E., C. Lecomte, J.V. Rietschoten, J.M. Sabatier, and H. Darbon. (1997). Solution structure of TsKapa, a charybdotoxin–like scorpion toxin from Tityus serrulatus with high affinity for apamin–sensitive Ca^{2+}–activated K^{+} channels. *Proteins* **29(3)**:359–369.

Blatz, A.L. and K.L. Magleby. (1983). Single voltage–dependent chloride–selective channels of large conductance in cultured rat muscle. *Biophysical Journal* **43:**237–241.

Blatz, A.L. and K.L. Magleby. (1986). Single apamin blocked Ca^{2+}–activated K^{+} channels of small conductance in cultured rat skeletal muscle. *Nature* **323:**718–720.

Bogle, R.G., A.R. Baydoun, J.D. Pearson, and G.E. Mann. (1996). Regulation of L–arginine transport and nitric oxide release in superfused porcine aortic endothelial cells. *Journal of Physiology* **490(1):**229–241.

Bolotina, V.M., S. Najibi, J.J. Palacino, P.J. Pagano, and R.A. Cohen. (1994). Nitric oxide directly activates potassium channels in vascular smooth muscle. *Nature* **368:**850–853.

Bolton, T.B., R.J. Lang, and T. Takewaki. (1984). Mechanism of action of noradrenaline and carbachol on smooth muscle of guinea pig anterior mesenteric artery. *Journal of Physiology* **351:**549–572.

Bolzon, B.J. (1992). Identification of the major ionic currents in vascular smooth muscle cells. Ph.D. thesis (AOQ–7183), University of Toronto. 229 pages.

Bolzon, B.J. and D.W. Cheung. (1989). Isolation and characterization of single vascular smooth muscle cells from spontaneously hypertensive rats. *Hypertension* **14:**137–144.

Bolzon, B.J., Z. Xiong, and D.W. Cheung. (1993). Membrane rectification in single smooth muscle cells from rat tail artery. *Pflügers Archives* **425:**482–490.

Bonev, A.D., and M.T. Nelson. (1993). ATP–sensitive potassium channels in smooth muscle cells from guinea pig urinary bladder. *American Journal of Physiology* **264(33):**C1190–C1200.

Bonnet, P., N.J. Rusch, and D.R. Harder. (1991). Characterisation of an outward K^+ current in freshly dispersed cerebral arterial muscle cells. *Pflügers Archives* **418:**292–296.

Bosse, E., R. Bottlender, T. Kleppisch, J. Hescheler, A. Welling, F. Hofmann, and V. Flockerzi. (1992). Stable and functional expression of the calcium channel α_1 subunit from smooth muscle in somatic cell lines. *EMBO Journal* **11:**2033–2038.

Boulanger, C.M., and P.M. Vanhoutte. (1997). G proteins and endothelium–dependent relaxations. *Journal of Vascular Research* **34(3):**175–185.

Brayden, J.E. (1996). Potassium channels in vascular smooth muscle. *Clinical and Experimental Pharmacology and Physiology* **23:**1069–1076.

Brayden, J.E., and M.T. Nelson. (1992). Regulation of arterial tone by activation of calcium–dependent potassium channels. *Science* **256:**532–535.

Butler, A., S. Tsunoda, D.P. McCobb, A. Wei, and L. Salkoff. (1993). *mSlo*, a complex mouse gene encoding "maxi" calcium–activated potassium channels. *Science* **261:**221–224.

Byrne, N.G., and W.A. Large. (1988). Membrane ionic mechanisms activated by noradrenaline in cells isolated from the rabbit portal vein. *Journal of Physiology* **404:**557–573.

Cabell, F., D.S. Weiss, and J.M. Price. (1994). Inhibition of adenosine–induced coronary vasodilation by block of large–conductance calcium–activated K^+ channels. *American Journal of Physiology* **267:**H1455–H1460.

Caffrey, J.M., I.R. Josephson, and A.M. Brown. (1986). Calcium channels of amphibian stomach and mammalian aorta smooth muscle. *Biophysical Journal* **49:**1237–1242.

Campbell, W.B., D. Gebremedhin, P.F. Pratt, and D.R. Harder. (1996). Identification of epoxyeicosatrienoic acids as endothelium–derived hyperpolarizing factors. *Circulation Research* **78:**415–423.

Catteral, W.A. (1988). Structure and function of voltage–sensitive ion channels. *Science* **242:**50–61.

Cetiner, M., and M.R. Bennett. (1993). Nitric oxide modulation of calcium–activated potassium channels in postganglionic neurones of avian cultured ciliary ganglia. *British Journal of Pharmacology* **110:**995–1002.

Cetkovic–Cvrlje, M., S. Sandler, and D.L. Eizirik. (1993). Nicotinamide and dexamethasone inhibit interleukin–1–induced nitric oxide production by RINm5F cells without decreasing messenger ribonucleic acid expression for nitric oxide synthase. *Endocrinology* **133(4):**1739–1743.

Chataigneau, T., M. Félétou, J. Duhault, and P.M. Vanhoutte. (1998). Epoxyeicosatrienoic acids, potassium channel blockers and endothelium–dependent hyperpolarization in the guinea–pig carotid artery. *British Journal of Pharmacology* **123:**574–580.

Chaytor, A.T., W.H. Evans, and T.M. Griffith. (1998). Central role of heterocellular gap junctional communication in endothelium–dependent relaxations of rabbit arteries. *Journal of Physiology* **508(2):**561–573.

Chen, G., and D.W. Cheung. (1996). Modulation of endothelium–dependent hyperpolarization and relaxation to acetylcholine in rat mesenteric artery by cytochrome P450 enzyme activity. *Circulation Research* **79:**827–833.

Chen, G., and D.W. Cheung. (1997). Effect of K^+–channel blockers on ACh–induced hyperpolarization and relaxation in mesenteric arteries. *American Journal of Physiology* **272 (41):**H2306–H2312.

Chen, G., H. Suzuki, and A.H. Weston. (1988). Acetylcholine releases endothelium–derived hyperpolarizing factor and EDRF from rat blood vessels. *British Journal of Pharmacology* **96:**1165–1174.

Chen, G., Y. Yamamoto, K. Miwa, and H. Suzuki. (1991). Hyperpolarization of arterial smooth muscle induced by endothelial humoral substances. *American Journal of Physiology* **260:**H1888–H1892.

Chen, S., R. Inoue, and Y. Ito. (1993). Pharmacological characterization of muscarinic receptor–activated cation channels in guinea–pig ileum. *British Journal of Pharmacology* **109:**793–801.

Cheung, D.W. (1984). Neural regulation of electrical and mechanical activities of the rat tail artery. *Pflügers Archives* **400:**335–337.

Cheung, D.W., G. Chen, M.J. MacKay, and E. Burnette. (1999). Regulation of vascular tone by endothelium–derived hyperpolarizing factor. *Clinical and Experimental Pharmacology and Physiology* **26(2):**172–175.

Clapp, L.H., and A.M. Gurney. (1991). Outward currents in rabbit pulmonary artery cells dissociated with a new technique. *Experimental Physiology* **76:**677–693.

Clark, S.G., and L.C. Fuchs. (1997). Role of nitric oxide and Ca^{2++}–dependent K^+ channels in mediating heterogeneous microvascular responses to acetylcholine in different vascular beds. *Journal of Pharmacology and Experimental Therapeutics* **282(3):**1473–1479.

Collins, E.M., M.P. Walsh, and K.G. Morgan. (1992). Contraction of single vascular smooth muscle cells by phenylephrine at constant $[Ca^{2+}]_i$. *American Journal of Physiology* **262(31):**H754–H762.

Connor, J.A., and C.F. Stevens. (1971). Voltage–clamp studies of a transient outward membrane current in gastropod neural somata. *Journal of Physiology* **213**:21–30.

Corriu, C., M. Félétou, E. Canet, and P.M. Vanhoutte. (1996a). Inhibitors of the cytochrome P450–mono–oxygenase and endothelium–dependent hyperpolarizations in the guinea–pig isolated carotid artery. *British Journal of Pharmacology* **117**:607–610.

Corriu, C., M. Félétou, E. Canet, and P.M. Vanhoutte. (1996b). Endothelium–derived factors and hyperpolarization of the carotid artery of the guinea–pig. *British Journal of Pharmacology* **119**:959–964.

Coulombe, A., H. Duclohier, E. Coraboeuf, and N. Touzet. (1987). Single chloride permeable channels of large conductance in cultured cardiac cells of newborn rats. *European Biophysical Journal* **14**:155–162.

Cowan, C.L., and R.A. Cohen. (1991). Two mechanisms mediate relaxation by bradykinin of pig coronary artery: NO–dependent and –independent responses. *American Journal of Physiology* **261**:H830–H835.

Croci, T., L. Manara, G. Aureggi, F. Guagnini, M. Rinaldi–Carmona, J.P. Maffrand, G. Le Fur, S. Mukenge, and G. Ferla. (1998). In vitro functional

evidence of neuronal cannabinoid CB_1 receptors in human ileum. *British Journal of Pharmacology* **125(7):**1393–5.

Dart, C., and N.B. Standen. (1993). Adenosine–activated potassium current in smooth muscle cells isolated from the pig coronary artery. *Journal of Physiology* **471:**767–786.

DiChiara, T.J., and P.H. Reinhart. (1995). Distinct effects of Ca^{2+} and voltage on the activation and deactivation of cloned Ca^{2+}–activated K^+ channels. *Journal of Physiology* **489(2):**403–418.

Dong, H., G.J. Waldron, W.C. Cole, and C.R. Triggle. (1998). Roles of calcium–activated and voltage–gated delayed rectifier potassium channels in endothelium–dependent vasorelaxation of the rabbit middle cerebral artery. *British Journal of Pharmacology* **123:**821–832.

Dong, H., G.J. Waldron, D. Galipeau, W.C. Cole, and C.R. Triggle. (1997). NO/PGI_2–independent vasorelaxation and the cytochrome P–450 pathway in rabbit carotid artery. *British Journal of Pharmacology* **120:**695–701.

Doorty, K.B., S. Bevan, J.D. Wadsworth, and P.N. Strong. (1997). A novel small conductance Ca^{2+}–activated K^+ channel blocker from Oxyuranus scutellatus

taipan venom. Re–evaluation of taicatoxin as a selective Ca^{2+} channel probe. *Journal of Biological Chemistry* **272(32):**19925–19930.

Doughty, J.M., F. Plane, and P.D. Langton. (1999). Charybdotoxin and apamin block EDHF in rat mesenteric artery if selectively applied to the endothelium. *American Journal of Physiology* **276:**H1107–H1112.

Douglas, S.A., and E.H. Ohlstein. (1997). Signal transduction mechanisms mediating the vascular actions of endothelin. *Journal of Vascular Research* **34(3):**152–164.

Droogmans, G., L. Raeymaekers, and R. Casteels. (1977). Electro– and pharmacomechanical coupling in the smooth muscle cells of the rabbit ear artery. *Journal of General Physiology* **70:**129–148.

Drummond, G.R., and T.M. Cocks. (1996). Evidence for mediation by endothelium–derived hyperpolarizing factor of relaxation to bradykinin in the bovine isolated coronary artery independently of voltage–operated Ca^{2+} channels. *British Journal of Pharmacology* **117:**1035–1040.

Dryer, S.E., M.M. Dourado, and M.E. Wisgirda. (1991). Characteristics of multiple Ca^{2+}–activated K^+ channels in acutely dissociated chick ciliary–ganglion neurones. *Journal of Physiology* **443:**601–627.

Dubois, J.M. (1981). Evidence for the existence of three types of potassium channels in the frog Ranvier node membrane. *Journal of Physiology* **318:**297–316.

Eckman, D.M., N. Hopkins, C. McBride, and K.D. Keef. (1998). Endothelium–dependent relaxation and hyperpolarization in guinea–pig carotid artery: role of epoxyeicosatrienoic acid. *British Journal of Pharmacology* **124:**181–189.

Eckman, D.M., J.S. Weinert, I.L.O. Buxton, and K.D. Keef. (1994). Cyclic GMP–independent relaxation and hyperpolarization with acetylcholine in guinea–pig coronary artery. *British Journal of Pharmacology* **111:**1053–1060.

Edelman, J.L., D.D. Loo, and G. Sachs. (1995). Characterization of potassium and chloride channels in the basolateral membrane of bovine nonpigmented ciliary epithelial cells. *Investigative Ophthalmology and Visual Science* **36(13)**:2706–2716.

Edwards, F.R., and G.D.S. Hirst. (1988). Inward rectification in submucosal arterioles of guinea–pig ileum. *Journal of Physiology* **404**:437–454.

Edwards, F.R., G.D.S. Hirst, and G.D. Silverberg. (1988). Inward rectification in rat cerebral arterioles: involvement of potassium ion in autoregulation. *Journal of Physiology* **404**:455–466.

Edwards, G., P.M. Zygmunt, E.D. Högestätt, and A.H. Weston. (1996). Effects of cytochrome P450 inhibitors on potassium currents and mechanical activity in rat portal vein. *British Journal of Pharmacology* **119**:691–701.

Edwards, G., and A.H. Weston. (1998). Endothelium–derived hyperpolarizing–factor – a critical appraisal. *Progress in Drug Research* **50**:107–133.

Ellis, E.F., R.J. Police, L. Yancey, J.S. McKinney, and S.C. Amruthesh. (1990). Dilation of cerebral arterioles by cytochrome P–450 metabolites of arachidonic acid. *American Journal of Physiology* **259**:H1171–H1177.

Fabiato, A. (1988). Computer programs for calculating total from specified free or free from specified total ionic concentrations in aqueous solutions containing multiple metals and ligands. *Methods in Enzymology* **7**:378–417.

Felder, C.C., K.E. Joyce, E.M. Briley, J. Mansouri, K. Mackie, O. Blond, Y. Lai, A.L. Ma, and R.L. Mitchell. (1995). Comparison of the pharmacology and signal transduction of the human cannabinoid CB_1 and CB_2 receptors. *Molecular Pharmacology* **48**:443–450.

Félétou, M., and P.M. Vanhoutte. (1988). Endothelium–dependent hyperpolarization of canine coronary artery smooth muscle. *British Journal of Pharmacology* **93:**515–524.

Félétou, M., and P.M. Vanhoutte. (1996). Endothelium–derived hyperpolarizing factor. *Clinical and Experimental Pharmacology and Physiology* **23:**1082–1090.

Félétou, M., and P.M. Vanhoutte. (1999). The alternative: EDHF. *Journal of Molecular and Cellular Cardiology* **31(1):**15–22.

Fleischmann, B.K., R.J. Washabau, and M.I. Kotlikoff. (1993). Control of resting membrane potential by delayed rectifier potassium currents in ferret airway smooth muscle cells. *Journal of Physiology* **469:**625–638.

Fosset, M., H. Schmid–Antomarchi, M. Hugues, G. Romey, and M. Lazdunski. (1984). The presence in pig brain of an endogenous equivalent of apamin, the bee venom peptide that specifically blocks Ca^{2+}–dependent K^+ channels. *Proceedings of the National Academy of Sciences* **81(22):**7228–7232.

Fujii, K., S. Ohmori, M. Tominaga, I. Abe, Y. Takata, Y. Ohya, K. Kobayashi, and M. Fujishima. (1993). Age–related changes in endothelium–dependent

hyperpolarization in the rat mesenteric artery. *American Journal of Physiology* **265(34):**H509–H516.

Fujii, K., M. Tominaga, S. Ohmori, K. Kobayashi, T. Koga, Y. Takata, and M. Fujishima. (1992). Decreased endothelium–dependent hyperpolarization to acetylcholine in smooth muscle of the mesenteric artery of spontaneously hypertensive rats. *Circulation Research* **70:**660–669.

Fujimoto, S., Y. Ikegama, M. Isaka, T. Kato, K. Nishimura, and T. Itoh. (1999). K^+ channel blockers and cytochrome P450 inhibitors on acetylcholine–induced, endothelium–dependent relaxation in rabbit mesenteric artery. *European Journal of Pharmacology* **384(1):**7–15.

Fukao, M., Y. Hattori, M. Kanno, I. Sakuma, and A. Kitabatake. (1995). Evidence for selective inhibition by lysophosphatidylcholine of acetylcholine–induced endothelium–dependent hyperpolarization and relaxation in rat mesenteric artery. *British Journal of Pharmacology* **116:**1541–1544.

Fukao, M., Y. Hattori, M. Kanno, I. Sakuma, and A. Kitabatake. (1997a). Evidence against a role of cytochrome P450–derived arachidonic acid metabolites in endothelium–dependent hyperpolarization by acetylcholine in rat isolated mesenteric artery. *British Journal of Pharmacology* **120:**439–436.

Fukao, M., Y. Hattori, M. Kanno, I. Sakuma, and A. Kitabatake. (1997b). Sources of Ca^{2+} in relation to generation of acetylcholine–induced endothelium–dependent hyperpolarization in rat mesenteric artery. *British Journal of Pharmacology* **120:**1328–1334.

Furchott, R.F., and J.V. Zawadski. (1980). The obligatory role of endothelial cells in the relaxation of the arterial smooth muscle by acetylcholine. *Nature* **286:**373–376.

Gaboury, J., R.C. Woodman, D.N. Granger, P. Reinhardt, and P. Kubes. (1993). Nitric oxide prevents leukocyte adherence: role of superoxide. *American Journal of Physiology* **265:**H862–H867.

Galvez, A., G. Gimenez–Gallego, J.P. Reuben, L. Roy–Contancin, P. Feigenbaum, G.J. Kaczorowski, and M.L. Garcia. (1990). Purification and characterization of a unique, potent, peptidyl probe for the high conductance calcium–activated potassium channel from venom of the scorpion *Buthus tamulus*. *Journal of Biological Chemistry* **265:**11083–11090.

Garcia, M.L., A. Galvez, M. Garcia–Calvo, V.F. King, J. Vazquez, and G.J. Kaczorowski. (1991). Use of toxins to study potassium channels. *Journal of Bioenergetics and Biomembranes* **23:**615–646.

García–Pascual, A., A. Labadía, E. Jimenez, and G. Costa. (1995). Endothelium–dependent relaxation to acetylcholine in bovine oviductal arteries: mediation by nitric oxide and changes in apamin–sensitive K^+ conductance. *British Journal of Pharmacology* **115:**1221–1230.

Garg, U.C., and A. Hassid. (1989). Nitric oxide–generating vasodilators and 8–bromo–cyclic guanosine monophosphate inhibit mitogenesis and proliferation of cultured rat vascular smooth muscle cells. *Journal of Clinical Investigation* **83(5):**1774–1777.

Garland, C.J., and G.A. McPherson. (1992). Evidence that nitric oxide does not mediate the hyperpolarization and relaxation to acetylcholine in the rat small mesenteric artery. *British Journal of Pharmacology* **105:**429–435.

Garland, C.J., F. Plane, B.K. Kemp., and T.M. Cocks. (1995). Endothelium–dependent hyperpolarization: a role in the control of vascular tone. *Trends in Pharmacological Sciences* **16:**23–30.

Ge, Z.D., X.H. Zhang, P.C. Fung, and G.W. He. (2000). Endothelium–dependent hyperpolarization and relaxation resistance to N(G)–nitro–L–arginine and indomethacin in coronary circulation. *Cardiovascular Research* **46(3):**547–556.

Gebremedhin, D., M. Kaldunski, E.R. Jacobs, D.R. Harder, and R.J. Roman. (1996). Coexistence of two types of Ca^{2+}–activated K^+ channels in rat renal arteries. *American Journal of Physiology* **270(39):**F69–F81.

Gebremedhin, D., Y.–H. Ma, J.R. Falck, R.J. Roman, M. VanRollins, D.R. and Harder. (1992). Mechanism of action of cerebral epoxyeicosatrienoic acids on cerebral arterial smooth muscle. *American Journal of Physiology* **263(32):**H519–H525.

Gelband, C.H. and J.R. Hume. (1992). Ionic currents in single smooth muscle cells of the canine renal artery. *Circulation Research* **71:**745–758.

Geng, Y.J., Q. Wu, amd G.K. Hansson. (1994). Protein kinase C activation inhibits cytokine–induced nitric oxide synthesis in vascular smooth muscle cells. *Biochimica et Biophysica Acta* **1223(1):**125–132.

Giangiacomo, K.M., M.L. Garcia, and O.B. McManus. (1992). Mechanism of iberiotoxin block of the large–conductance calcium–activated potassium channel from bovine aortic smooth muscle. *Biochemistry* **31:**6719–6727.

Graier, W.F., S. Holzmann, B.G. Hoebel, W.R. Kukovetz, and G.M. Kostner. (1996). Mechanisms of L–N^G nitroarginine/indomethacin–resistant relaxation in

bovine and porcine coronary arteries. *British Journal of Pharmacology* **119:**1177–1186.

Graier, W., S. Simecek, and M. Sturek. (1995). Cytochrome P–450 mono–oxygenase–regulated signalling of Ca^{2+} entry in human and bovine endothelial cells. *Journal of Physiology*. **482(2):**259–274.

Green, K.A., R.W. Foster, and R.C. Small. (1991). A patch–clamp study of K^+–channel activity in bovine isolated tracheal smooth muscle cells. *British Journal of Pharmacology* **102:**871–878.

Gruetter, C.A., and S.M. Lemke. (1986). Comparison of endothelium–dependent relaxation in bovine intrapulmonary artery and vein by acetylcholine and A23187. *Journal of Pharmacology and Experimental Therapeutics* **238(3):**1055–1062.

Hagiwara, N., H. Irisawa, and M. Kameyama. (1988). Contribution of two types of calcium currents to the pacemaker potentials of rabbit sino–atrial node cells. *Journal of Physiology* **359:**233–253.

Hagiwara, S., S. Ozawa, and O. Sand. (1975). Voltage clamp analysis of two inward current mechanisms in the egg cell membrane of a starfish. *Journal of General Physiology* **65(5):**617–644.

Hamill, O.P., A. Marty, E. Neher, B. Sakmann, and F.J. Sigworth. (1981). Improved patch clamp techniques for high–resolution recordings from cells and cell–free membrane patches. *Pflügers Archives* **391:**85–100.

Hara, Y., K. Kitamura, and H. Kuriyama. (1980). Actions of 4–aminopyridine on vascular smooth muscle tissues of the guinea pig. *British Journal of Pharmacology* **68:**99–106.

Harder, D.R., W.B. Campbell, and R. Roman. (1995). Role of cytochrome P–450 enzymes and metabolites of arachidonic acid in the control of vascular tone. *Journal of Vascular Research.* **32:**79–92.

Harder, D.R., D. Gebremedhin, J. Narayanan, C. Jefcoat, J.R. Falck, W.B. Campbell, and R. Roman. (1994). Formation and action of a P–450 4A metabolite of arachidonic acid in cat cerebral microvessels. *American Journal of Physiology* **266(35):**H2098–H2107.

Hashitani, H., and H. Suzuki. (1997). K^+ channels which contribute to the acetylcholine–induced hyperpolarization in smooth muscle of the guinea–pig submucosal arteriole. *Journal of Physiology* **501(2):**319–329.

He, G.–W., C.–Q. Yang, W.F. Graier, and J.–A. Yang. (1996). Hyperkalemia alters EDHF–mediated hyperpolarization and relaxation in coronary arteries. *American Journal of Physiology* **271(40):**H760–H767.

Hecker, M., A.T. Bara, J. Bauersachs, and R. Busse. (1994). Characterization of endothelium–derived hyperpolarizing factor as a cytochrome P450–derived arachidonic acid metabolite in mammals. *Journal of Physiology* **481(2):**407–414.

Hille, B. (1992). Ionic channels of excitable membranes, second edition. Sunderland, MA: Sinauer Associates, Inc. 607pp.

Hirst, G.D.S., G.D. Silverberg, and D.F. van Helden. (1986). The action potential and underlying ionic currents in proximal rat middle cerebral arteries. *Journal of Physiology* **371:**289–304.

Hodgkin, A.L., and A.F. Huxley. (1952). A quantitative description of membrane current and its application to conduction and excitation in nerve. *Journal of Physiology* **117:**500–544.

Holland, M., P.D. Langton, N.B. Standen, and J.P. Boyle. (1996). Effects of the BK_{Ca} channel activator, NS1619, on rat cerebral artery smooth muscle. *British Journal of Pharmacology* **117:**119–129.

Holzmann, S., W.R. Kukovetz, W. Windischhofer, E. Paschke, and W.F. Graier. (1994). Pharmacologic differentiation between endothelium–dependent relaxations sensitive and resistant to nitro–L–arginine in coronary arteries. *Journal of Cardiovascular Pharmacology* **23(5):**747–756.

Hosey, M.M., and M. Lazdunski. (1988). Calcium channels: molecular pharmacology, structure, and regulation. *Journal of Membrane Biology* **104:**81–105.

Hu, S., and H.S. Kim. (1993). Activation of K^+ channel in vascular smooth muscles by cytochrome P450 metabolites of arachidonic acid. *European Journal of Pharmacology* **230**:215–221.

Hume, J.R., and N. Leblanc. (1989). Macroscopic K^+ currents in single smooth muscle cells of the rabbit portal vein. *Journal of Physiology* **413:**49–73.

Hutcheson, I.R., A.T. Chaytor, W.H. Evans, and T.M. Griffith. (1999). Nitric oxide–independent relaxations to acetylcholine and A23187 involve different routes of heterocellular communication. Role of gap junctions and phospholipase A_2. *Circulation Research* **84(1):**53–63.

Hwa, J.J., L. Ghibaudi, P. Williams, and M. Chatterjee. (1994). Comparison of acetylcholine–dependent relaxation in large and small arteries of rat mesenteric vascular bed. *American Journal of Physiology* **266(35):**H952–H958.

Ignarro, L.J. (1990). Nitric oxide: A novel signal transduction mechanism for transcellular communication. *Hypertension* **16(5):**477–483.

Ignarro, L.J., G.M. Buga, K.S. Wood, R.E. Byrns, and G. Chaudhuri. (1987). Endothelium–derived relaxing factor produced and released from artery and vein is nitric oxide. *Proceedings of the National Academy of Sciences* **84:**9265–9269.

Inagaki, N., T. Gonoi, J.P. Clement, C.Z. Wang, L. Aguilar–Bryan, J. Bryan, and S. Seino. (1996). A family of sulfonylurea receptors determines the pharmacological properties of ATP–sensitive K^+ channels. *Neuron* **16(5):**1011–1017.

Inagaki, N, T. Gonoi, and S. Seino. (1997). Subunit stoichiometry of the pancreatic beta–cell ATP–sensitive K^+ channel. *FEBS Letters* **409(2):**232–236.

Inoue, I., Y. Nakaya, S. Nakaya, and H. Mori. (1989). Extracellular Ca^{2+}–activated K channel in coronary artery smooth muscle cells and its role in vasodilation. *FEBS Letters* **255:**281–284.

Inoue, R., K. Kitamura, and H. Kuriyama. (1985). Two Ca–dependent K–channels classified by the application of tetraethylammonium distribute to smooth muscle membranes of the rabbit portal vein. *Pflügers Archives* **405:**173–179.

Inoue, R., K. Okabe, K. Kitamura, and H. Kuriyama. (1986). A newly identified Ca^{2+} dependent K^+ channel in the smooth muscle membrane of single cells dispersed from rabbit portal vein. *Pflügers Archives* **406:**138–143.

Ishihara, K., T. Mitsuiye, A. Noma, and M. Takano. (1989). The Mg^{2+} block and intrinsic gating underlying inward rectification of the K^+ current in guinea–pig cardiac myocytes. *Journal of Physiology* **419:**297–320.

Ishii, T.M., J. Maylie, and J.P. Adelman. (1997a). Determinants of apamin and *d*–tubocurarine block in SK potassium channels. *Journal of Biological Chemistry* **272(37):**23195–23200.

Ishii, T.M., C. Silva, B. Hirschberg, C.T. Bond, J.P. Adelman, and J. Maylie. (1997b). A human intermediate conductance calcium–activated potassium channel. *Proceedings of the National Academy of Sciences* **94:**11651–11656.

Ishikawa, T., J.R. Hume, and K.D. Keef. (1993). Modulation of K^+ and Ca^{2+} channels by histamine H_1–receptor stimulation in rabbit coronary artery cells. *Journal of Physiology* **468:**379–400.

Jacobs, M., F. Plane, and K.R. Bruckdorfer. (1990). Native and oxidized low–density lipoproteins have different inhibitory effects on endothelium–derived relaxing factor in the rabbit aorta. *British Journal of Pharmacology* **100(1):**21–26.

Jain, V., Y.P. Vedernikov, G.R. Saade, K. Chwalisz, and R.E. Garfield. (1999). Endothelium–dependent and –independent mechanisms of vasorelaxation by corticotropin–releasing factor in pregnant rat uterine artery. *Journal of Pharmacology and Experimental Therapeutics* **288(2):**407–413.

Janssen, L.J., and S.M. Sims. (1992). Acetylcholine activates non–selective cation and chloride conductances in canine and guinea–pig tracheal myocytes. *Journal of Physiology* **453:**197–218.

Joiner, W.J., L.–Y. Wang, M.D. Tang, and L.K. Kaczmarek. (1997). hSK4, a member of a novel subfamily of calcium–activated potassium channels. *Proceedings of the National Academy of Sciences* **94:**11013–11018.

Jovanović, A., L. Grbović, and S. Jovanović. (1995). K^+ channel blockers do not modify relaxation of guinea–pig uterine artery evoked by acetylcholine. *European Journal of Pharmacology* **280:**95–100.

Jovanović, A., S. Jovanović, I. Tulic, and L. Grbović. (1998). Predominant role for nitric oxide in the relaxation induced by vasoactive intestinal peptide in human uterine artery. *Molecular Human Reproduction* **4(1):**71–76.

Kaczorowski, G.J., H.G. Knaus, R.J. Leonard, O.B. McManus, and M.L. Garcia. (1996). High–conductance calcium–activated potassium channels; structure, pharmacology, and function. *Journal of Bioenergetics and Biomembranes* **28(3):**255–67.

Katsuyama, H., S. Ito, T. Itoh, and H. Kuriyama. (1991). Effects of ryanodine on acetylcholine–induced Ca^{2+} mobilization in single smooth muscle cells of the porcine coronary artery. *Pflügers Archives* **419:**460–466.

Kauser, K., and G.M. Rubanyi. (1996). The N^G–nitro–L–arginine insensitive endothelium–dependent relaxation of porcine coronary arteries is not mediated by a transferable relaxing substance. Endothelium–derived Hyperpolarizing Factor, *Ed.:* P.M. Vanhoutte. Harwood Acad. Pub., OPA, Netherlands, p. 338.

Kemp, B.K., and T.M. Cocks. (1997). Evidence that mechanisms dependent and independent of nitric oxide mediate endothelium–dependent relaxation to bradykinin in human small resistance–like coronary arteries. *British Journal of Pharmacology* **120:**757–762.

Kemp, B.K., J.J. Smolich, B.C. Ritchie, and T.M. Cocks. (1995). Endothelium–dependent relaxations in sheep pulmonary arteries and veins: resistance to block by N^G–nitro–L–arginine in pulmonary hypertension. *British Journal of Pharmacology* **116:**2457–2467.

Khan, S.A., W.R. Mathews, and K.D. Meisheri. (1993). Role of calcium–activated K^+ channels in vasodilation induced by nitroglycerine, acetylcholine, and nitric oxide. *Journal of Pharmacology and Experimental Therapeutics* **267(3):**1327–1335.

Kitagawa, S., Y. Yamaguchi, M. Kunitomo, E. Sameshima, and M. Fujiwara. (1994). N^G–nitro–L–arginine–resistant endothelium–dependent relaxation induced by acetylcholine in the rabbit renal artery. *Life Sciences* **55(7):**491–498.

Kitazono, T., S. Ibayashi, T. Nagao, K. Fujii, and M. Fujishima. (1997). Role of Ca^{2+}–activated K^+ channels in acetylcholine–induced dilatation of the basilar artery *in vivo*. *British Journal of Pharmacology* **120:**102–106.

Klockner, U., and G. Isenberg. (1985). Action potentials and net membrane currents of isolated smooth muscle cells (urinary bladder of the guinea pig). *Pflügers Archives* **405:**329–339.

Knot, H.J., and M.T. Nelson. (1995). Regulation of membrane potential and diameter by voltage–dependent K^+ channels in rabbit myogenic cerebral arteries. *American Journal of Physiology* **269:**H348–H355.

Knot, H.J., P.A. Zimmerman, and M.T. Nelson. (1996). Extracellular K^+–induced hyperpolarizations and dilatations of rat coronary and cerebral arteries involve inward rectifier K^+ channels. *American Journal of Physiology* **492(2):**419–430.

Koh, S.D., G.M. Dick, and K.M. Sanders. (1997). Small–conductance Ca^{2+}–dependent K^+ channels activated by ATP in murine colonic smooth muscle. *American Journal of Physiology* **273(42):**C2010–C2021.

Kokubun, S., A. Saigusa, and T. Tamura. (1991). Blockade of Cl channels by organic and inorganic blockers in vascular smooth muscle cells. *Pflügers Archives* **18:**204–213.

Koumi, S.–I., R. Sato, and H. Hayakawa. (1994a). Modulation of the delayed rectifier K^+ current by apamin in guinea–pig heart. *European Journal of Pharmacology* **261:**213–216.

Koumi, S–I., R. Sato, T. Horikawa, T. Aramaki, and H. Okumura. (1994b). Characterization of the calcium–sensitive voltage–gated delayed rectifier

potassium channel in isolated guinea pig hepatocytes. *Journal of General Physiology* **104:**147–171.

Krapivinsky, G., E.A. Gordon, K. Wickman, B. Velimirovic, L. Krapivinsky, and D.E. Clapham. (1995). The G–protein–gated atrial K^+ channel IKACh is a heteromultimer of two inwardly rectifying K^+–channel proteins. *Nature* **374:**135–141.

Krishnan, S.N., T. Desai, D.C. Ward, and G.G. Haddad. (1995). Isolation and chromosomal localization of a human ATP–regulated potassium channel. *Human Genetics* **96(2):**155–160.

Kubo, Y., T.J. Baldwin, Y.N. Jan, and L.Y. Jan. (1993a). Primary structure and functional expression of a mouse inward rectifier potassium channel. *Nature* **362:**127–133.

Kubo, Y., E. Reuveny, P.A., Slesinger, Y.N. Jan, and, L.Y. Jan. (1993b). Primary structure and functional expression of a rat G–protein–coupled muscarinic potassium channel. *Nature* **364:**802–806.

Kuriyama, H., K. Ohshima, and Y. Sakamoto. (1971). The membrane properties of the smooth muscle of the guinea pig portal vein in isotonic and hypertonic solutions. *Journal of Physiology* **217:**179–199.

Lang, D.G. (1989). Identification of the major membrane currents in freshly dispersed single smooth muscle cells of guinea–pig ureter. *Journal of Physiology* **412:**375–395.

Lang, D.G. and A.K. Ritchie. (1990). Tetraethylammonium blockade of apamin–sensitive and insensitive Ca^{2+}–activated K^+ channels in a pituitary cell line. *Journal of Physiology* **425:**117–132.

LeBlanc, N., X. Wan, and P.M. Leung. (1994). Physiological role of Ca^{2+}–activated and voltage–dependent K^+ currents in rabbit coronary myocytes. *American Journal of Physiology* **266(35):**C1523–C1537.

Lefer, D.J., K. Nakanishi, W.E. Johnston, and J. Vinten–Johansen. (1993). Antineutrophil and myocardial protecting actions of a novel nitric oxide donor after acute myocardial ischemia and reperfusion of dogs. *Circulation* **88:**2337–2350.

Leinders, T. and H.P.M. Vijverberg. (1992). Ca^{2+} dependence of small Ca^{2+}–activated K^+ channels in cultured N1E–115 mouse neuroblastoma cells. *Pflügers Archives* **422:**223–232.

Liu, S., I.M. Adcock, R.W. Old, P.J. Barnes, and T.W. Evans. (1993). Lipopolysaccharide treatment in vivo induces widespread tissue expression of inducible nitric oxide synthase mRNA. *Biochemical and Biophysical Research Communications* **196(3):**1208–1213.

Llinas, R., M. Sugimori, J.W. Lin, and B. Chertsey. (1989). Blocking and isolation of a calcium channel from neurons in mammals and cephalopods utilizing a toxin fraction (FTX) from funnel–web spider poison. *Proceedings of the National Academy of Sciences* **86:**1689–1693.

Lorenz, J.N., J. Schnermann, F.C. Brosius, J.P. Briggs, and P.E. Furspan. (1992). Intracellular ATP can regulate afferent arteriolar tone via ATP–sensitive K^+ channels in the rabbit. *Journal of Clinical Investigation* **90:**733–740.

Lüscher, T.F., Y. Dohi, and M. Tschudi. (1992). Endothelium–dependent regulation of resistance arteries: alterations with aging and hypertension. *Journal of Cardiovascular Pharmacology* **19(5):**S34–S42.

Marchenko, S.M., and S.O. Sage. (1996). Calcium–activated potassium channels in the endothelium of intact rat aorta. *Journal of Physiology* **492(1):**53–60.

Marrion, N.V., and S.J. Tavalin. (1998). Selective activation of Ca^{2+}–activated K^+ channels by co–localized Ca^{2+} channels in hippocampal neurons. *Nature* **395(6705):**900–905.

Matoba, T., H. Shimokawa, M. Nakashima, Y. Hirakawa, Y. Mukai, K. Hirano, H. Kanaide, and A. Takeshita. (2000). Hydrogen peroxide is an endothelium–derived hyperpolarizing factor in mice. *Journal of Clinical Investigation* **106(12):**1521–1530.

McCulloch, A.I., F.E. Botrill, M.D. Randall, and R.C. Hiley. (1997). Characterization and modulation of EDHF–mediated relaxations in the rat isolated superior mesenteric arterial bed. *British Journal of Pharmacology* **120:**1431–1438.

McGiff, J.C. (1991). Cytochrome P–450 metabolism of arachidonic acid. *Annual Review of Pharmacology and Toxicology* **31**:339–369.

McLarnon, J.G., S.U. Kim, M. Michikawa, and R. Xu. (1995a). Properties of inward and outward potassium currents in cultured mouse motoneurons. *Neuroscience* **64(1):**139–151.

McLarnon ,J.G., D. Sawyer, and S.U. Kim. (1995b). Cation and anion unitary ion channel currents in cultured bovine microglia. *Brain Research* **693(1–2):**8–20.

Michelakis, E.D., H.L. Reeve, J.M. Huang, S. Tolarova, D.P. Nelson, E.K. Weir, and S.L. Archer. (1997). Potassium channel diversity in vascular smooth muscle cells. *Canadian Journal of Physiology and Pharmacology* **75(7):**889–897.

Mieyal, P., D. Fulton, J.C. McGiff, and J. Quilley. (1998). NO–independent vasodilation to acetylcholine in the rat isolated kidney utilizes a charybdotoxin–sensitive, intermediate–conductance Ca^{++}–activated K^+ channel. *Journal of Pharmacology and Experimental Therapeutics* **285(2):**659–664.

Miller, R.J., and A.P. Fox. (1990). Voltage–sensitive calcium channels. In *Intracellular calcium regulation*, pp97–138, Alan R. Liss, Inc.

Miller, C., E. Moczydowski, R. Latorre, and M. Phillips. (1985). Charybdotoxin, a protein inhibitor of single Ca^{2+}–activated K^+ channels from skeletal muscle. *Nature* **313:**316–318.

Mita, M., and M.K. Uchida. (1987). Desensitization of isolated smooth muscle cells from guinea pig taenia caecum to acetylcholine. *Canadian Journal of Physiology and Pharmacology* **65(3):**293–297.

Miyoshi, H., and Y. Nakaya. (1994). Endotoxin–induced nonendothelial nitric oxide activates the Ca^{2+}–activated K^+ channel in cultured vascular smooth muscle cells. *Journal of Molecular and Cellular Cardiology* **26:**1487–1495.

Mombouli, J.–V., and P.M. Vanhoutte. (1997). Endothelium–derived hyperpolarizing factor(s): updating the unknown. *Trends in Pharmacological Sciences* **18(7):**252–256.

Moncada, S., and A. Higgs. (1993). The L–arginine–nitric oxide pathway. *New England Journal of Medicine* **329:**2002–2012.

Murphy, M.E., and J.E. Brayden. (1995). Apamin–sensitive K^+ channels mediate an endothelium–dependent hyperpolarization in rabbit mesenteric arteries. *Journal of Physiology* **489:**723–734.

Nagao, T., S. Illiano, and P.M. Vanhoutte. (1992). Heterogeneous distribution of endothelium–dependent relaxations resistant to N^G–nitro–L–arginine in rats. *American Journal of Physiology* **263(32):**H1090–H1094.

Nagao, T., and P.M. Vanhoutte. (1992a). Hyperpolarization as a mechanism for endothelium–dependent relaxations in the porcine coronary artery. *Journal of Physiology* **445:**355–367.

Nagao, T., and P.M. Vanhoutte. (1992b). Characterization of endothelium–dependent relaxations resistant to nitro–L–arginine in the porcine coronary artery. *British Journal of Pharmacology* **107:**1102–1107.

Nagao, T., and P.M. Vanhoutte. (1993). Endothelium–derived hyperpolarizing factor and endothelium–dependent relaxations. *American Journal of Respiratory Cell and Molecular Biology* **8:**1–6.

Nastainczyk, N., A. Rohrkasten, M. Sieber, and F. Hofmann. (1987). Phosphorylation of the purified receptor for calcium channel blockers by cAMP kinase and protein kinase C. *European Journal of Biochemistry* **169:**137–142.

Nelson, M.T. and J.M. Quayle. (1995). Physiological roles and properties of potassium channels in arterial smooth muscle. *American Journal of Physiology* **268(37):**C799–C822.

Neylon, C.B. (1999). Vascular biology of endothelin signal transduction. *Clinical and Experimental Pharmacology and Physiology* **26(2):**149–153.

Nilius, B. (1991). Ion channels and regulation of transmembrane Ca^{2+} influx in endothelium. Ion Channels of Vascular Smooth Muscle Cells and Endothelial Cells, *Ed.:* N. Sperelakis and H. Kuriyama. Elsevier Sci. Pub. Co., Inc., USA, p. 374.

Nishiyama, M., H. Hashitani, H. Fukuta, Y. Yamamoto, and H. Suzuki. (1998). Potassium channels activated in the endothelium–dependent hyperpolarization in guinea–pig coronary artery. *Journal of Physiology* **510(2):**455–465.

Noack, T., P. Deitmer, G. Edwards, and A.H. Weston. (1992). Characterization of potassium currents modulated by BRL 38227 in rat portal vein. *British Journal of Pharmacology* **106:**717–726.

Noma, A. (1983). ATP–regulated K^+ channels in cardiac muscle. *Nature* **305:**147–148.

Nowycky, M.C., A.P. Fox, and R.W. Tsien. (1985). Three types of neuronal calcium channels with different calcium agonist sensitivity. *Nature* **316:**440–443.

Ohmori, H. (1978). Inactivation kinetics and steady–state current noise in the anomalous rectifier of tunicate egg cell membranes. *Journal of Physiology* **281:**77–99.

Okabe, K., K. Kitamura, and H. Kuriyami. (1987). Features of 4–aminopyridine sensitive outward current observed in single smooth muscle cells from the rabbit pulmonary artery. *Pflügers Archives* **409:**561–568.

Overturf, K.E., S.N. Russell, A. Carl, F. Vogalis, P.J. Hart, J.R. Hume, K.M. Sanders, and B. Horowitz. (1994). Cloning and characterization of a $K_v1.5$ delayed rectifier K^+ channel from vascular and visceral smooth muscles. *American Journal of Physiology* **267(36):**C1231–C1238.

Oyekan, A.O., J.C. McGiff, P. Rosencrantz–Weiss, and J. Quilley. (1994). Relaxant responses of rabbit aorta: influence of cytochrome P450 inhibitors. *Journal of Pharmacology and Experimental Therapeutics* **268:**262–269.

Pacaud, P., G. Loirand, J.L. Lavie, C. Mironneau, and J. Mironneau. (1989). Calcium activated chloride current in rat vascular smooth muscle cells in short term primary culture. *Pflügers Archives* **413:**629–636.

Palmer, R.M.J., A.G. Ferrige, and S. Moncada. (1987). Nitric oxide release accounts for the biological activity of endothelium–derived relaxing factor. *Nature* **327:**524–526.

Pavenstädt, H., S. Lindeman, V. Lindeman, M. Späth, K. Kunzelmann, and R. Greger. (1991). Potassium conductance of smooth muscle cells from rabbit aorta in primary culture. *Pflügers Archives* **419:**57–68.

Perrella, M.A., M. Yoshizumi, Z. Fen, J.C. Tsai, C.M. Hsieh, S. Kourembanas, and M.E. Lee. (1994). Transforming growth factor–beta 1, but not dexamethasone, down–regulates nitric–oxide synthase mRNA after its induction by interleukin–1 beta in rat smooth muscle cells. *Journal of Biological Chemistry* **269(20):**14595–14600.

Petersson, J., P.M. Zygmunt, L. Brandt, and E.D. Högestätt. (1996). Role of hyperpolarization in endothelium–dependent relaxations of human cerebral arteries. Endothelium–dependent Hyperpolarizing Factor, *Ed.:* P.M. Vanhoutte. Harwood Acad. Pub., OPA, Netherlands, p. 338.

Petersson, J., P.M. Zygmunt, and E.D. Högestätt. (1997). Characterization of the potassium channels involved in EDHF mediated relaxation in cerebral arteries. *British Journal of Pharmacology* **120:**1344–1350.

Pfister, S.L., and W.B. Campbell. (1992). Arachidonic acid– and acetylcholine–induced relaxations of rabbit aorta. *Hypertension* **20(5):**682–689.

Pfister, S.L., N. Spitzbarth, W. Edgemond, and W.B. Campbell. (1996). Vasorelaxation by an endothelium–derived metabolite of arachidonic acid. *Am. Journal of Physiology* **270:**H1021–H1030.

Pfister, S.L., N. Spitzbarth, K. Nithipatikom, W.S. Edgemond, J.R. Falck, and W.B. Campbell. (1998). Identification of the 11,14,15– and 11,12,15–trihydroxyeicosatrienoic acids as endothelium–derived relaxing factors in rabbit aorta. *Journal of Biological Chemistry* **273(47)**:30879–30887.

Pfründer, D., I. Anghelescu, and V.A.W. Kreye. (1993). Intracellular ADP activates ATP–sensitive K^+ channels in vascular smooth muscle cells of the guinea pig portal vein. *Pflügers Archives* **423**:149–151.

Pfründer, D., and V.A.W. Kreye. (1991). Tedisamil blocks single large–conductance Ca^{2+}–activated K^+ channels in membrane patches from smooth muscle cells of the guinea–pig portal vein. *Pflügers Archives* **418**:308–312.

Pfründer, D., and V.A.W. Kreye. (1992). Tedisamil inhibits the delayed rectifier K^+ current in single smooth muscle cells of the guinea–pig portal vein. *Pflügers Archives* **421**:22–25.

Pinto, A., N.G. Abraham, and K.M. Mullane. (1987). Arachidonic acid–induced endothelial–dependent relaxations of canine coronary arteries: contribution of a cytochrome P–450–dependent pathway. *Journal of Pharmacology and Experimental Therapeutics* **240(3)**:856–863.

Plane, F., M. Holland, G.J. Waldron, C.J. Garland, and J.P. Boyle. (1997). Evidence that anandamide and EDHF act via different mechanisms in rat isolated mesenteric arteries. *British Journal of Pharmacology* **121:**1509–1511.

Popp, R., J. Bauersachs, M. Hecker, I. Fleming, and R. Busse. (1996). A transferable, β–naphthoflavone–inducible, hyperpolarizing factor is synthesized by native and cultured porcine coronary endothelial cells. *Journal of Physiology* **497(3):**699–709.

Portier, M., M. Rinaldi–Carmona, F. Pecceu, T. Combes, C. Poinot–Chazel, B. Calandra, F. Barth, G. Le Fur, and P. Casellas. (1999). SR 144528, an antagonist for the peripheral cannabinoid receptor that behaves as an inverse agonist. *Journal of Pharmacology and Experimental Therapeutics* **288(2):**582–589.

Quayle, J.M., A.D. Bonev, J.E. Brayden, and M.T. Nelson. (1994). Calcitonin gene–related peptide activated ATP–sensitive K^+ currents in rabbit arterial smooth muscle via protein kinase A. *Journal of Physiology* **475:**9–13.

Quayle, J.M., J.G. McCarron, J.E. Brayden, and M.T. Nelson. (1993). Inward rectifier K^+ currents in smooth muscle cells from rat resistance–sized cerebral arteries. *American Journal of Physiology* **265(34):**C1363–C1370.

Randall, M.D., S.P.H. Alexander, T. Bennett, E.A. Boyd, J.R. Fry, S.M. Gardiner, P.A. Kemp, A.I. McCulloch, and D.A. Kendall. (1996). An endogenous cannabinoid as an endothelium–derived vasorelaxant. *Biochemical and Biophysical Research Communications* **229:**114–120.

Randall, M.D., and D.A. Kendall. (1997). Involvement of a cannabinoid in endothelium–derived hyperpolarizing factor–mediated coronary vasorelaxation. *European Journal of Pharmacology* **335:**205–209.

Randall, M.D., and D.A. Kendall. (1998). Anandamide and endothelium–derived hyperpolarizing factor act via a common vasorelaxant mechanism in rat mesentery. *European Journal of Pharmacology* **346:**51–53.

Randall, M.D., A.I. McCulloch, and D.A. Kendall (1997). Comparative pharmacology of endothelium–derived hyperpolarizing factor and anandamide in rat isolated mesentery. *European Journal of Pharmacology* **333**:191–197.

Ranjan, V., Z. Xiao, and S.L. Diamond. (1995). Constitutive NOS expression in cultured endothelial cells is elevated by fluid shear stress. *American Journal of Physiology* **269**:H550–H555.

Rapacon, M., P. Mieyal, J.C. McGiff, D. Fulton, J. Quilley. (1996). Contribution of calcium–activated potassium channels to the vasodilator effect of bradykinin in

the isolated, perfused kidney of the rat. *British Journal of Pharmacology* **118(6)**:1504–1508.

Rauer, H., M.D. Lanigan, M.W. Pennington, J. Aiyar, S. Ghanshani, M.D. Cahalan, R.S. Norton, and K.G. Chandy. (2000). Structure–guided transformation of charybdotoxin yields an analog that selectively targets Ca^{2+}–activated over voltage–gated K^+ channels. *Journal of Biological Chemistry* **275(2)**:1201–1208.

Resende, A.C., G. Ballejo, and M.C. Salgado. (1998). Role of non–nitric oxide non–prostaglandin endothelium–derived relaxing factor(s) in bradykinin vasodilation. *Brazilian Journal of Medical and Biological Research* **31(9)**:1229–1235.

Reuter, H., C.F. Stevens, R.W. Tsien, and G. Yellen. (1982). Properties of single calcium channels in cultured cardiac cells. *Nature* **297**:501–504.

Rinaldi–Carmona, M., F. Barth, M. Heaulme, R. Alonso, D. Shire, C. Congy, P. Soubrie, J.C. Breliere, G. Le Fur. (1995). Biochemical and pharmacological characterisation of SR141716A, the first potent and selective brain cannabinoid receptor antagonist. *Life Sciences* **56(23–24)**:1941–1947.

Rinaldi–Carmona, M., F. Barth, M. Heaulme, D. Shire, B. Calandra, C. Congy, S. Martinez, J. Maruana, G. Neliat, D. Caput, P. Ferrara, P. Soubrie, J.C. Breliere, and G. Le Fur. (1994). SR 141716A, a potent and selective antagonist of the brain cannabinoid receptor. *FEBS Letters* **350(2–3)**:240–244.

Rinaldi–Carmona, M., F. Barth, J. Millan, J.M. Derocq, P. Casellas, C. Congy, D. Oustric, M. Sarran, M. Bouaboula, B. Calandra, M. Portier, D. Shire, J.C. Breliere, G.L. Le Fur. (1998a). SR 144528, the first potent and selective antagonist of the CB_2 cannabinoid receptor. *Journal of Pharmacology and Experimental Therapeutics* **284(2)**:644–650.

Rinaldi–Carmona, M., B. Calandra, D. Shire, M. Bouaboula, D. Oustric, F. Barth, P. Casellas, P. Ferrara, and G. Le Fur. (1996a). Characterization of two cloned human cannabinoid receptor isoforms. *Journal of Pharmacology and Experimental Therapeutics* **278(2)**:871–878.

Rinaldi–Carmona, M., A. Le Duigou, D. Oustric, F. Barth, M. Bouaboula, P. Carayon, P. Casellas, G. Le Fur. (1998b). Modulation of CB_1 cannabinoid receptor functions after a long–term exposure to agonist or inverse agonist in the Chinese hamster ovary cell expression system. *Journal of Pharmacology and Experimental Therapeutics* **287(3)**:1038–1047.

Rinaldi–Carmona, M., F. Pialot, C. Congy, E. Redon, F. Barth, A. Bachy, J.C. Breliere, P. Soubrie, G. Le Fur. (1996b). Characterization and distribution of binding sites for [3H]–SR 141716A, a selective brain (CB_1) cannabinoid receptor antagonist, in rodent brain. *Life Sciences* **58(15):**1239–1247.

Roberds, S.L., K.M. Knoth, S. Po, T.A. Blair, P.B. Bennet, R.P. Hartshorne, D.J. Snyders, and M.M. Tamkun. (1993). Molecular biology of voltage–gated potassium channels of the cardiovascular system. *Journal of Cardiovascular Electrophysiology* **4:**68–80.

Roberds, S.L., and M.M. Tamkun. (1991). Cloning and tissue–specific expression of five voltage–gated potassium channel cDNAs expressed in rat heart. *Proceedings of the National Academy of Sciences* **88:**1798–1802.

Robertson, B.E., and M.T. Nelson. (1994). Aminopyridine inhibition and voltage dependence of K^+ currents in smooth muscle cells from cerebral arteries. *American Journal of Physiology* **267(36):**C1589–C1597.

Robertson, B.E., R. Schubert, J. Hescheler, and M.T. Nelson. (1993). cGMP–dependent protein kinase activates Ca–activated K channels in cerebral artery smooth muscle cells. *American Journal of Physiology* **265:**C299–C303.

Rohrkasten, A., H. Meyer, W. Nastainczyk, M. Sieler, and F. Hofmann. (1988). cAMP–dependent protein kinase rapidly phosphorylates Serine–687 of the skeletal muscle receptor for calcium channel blockers. *Journal of Biological Chemistry* **263:**15325–15329.

Rosa, J.C., D. Galanakis, C.R. Ganellin, P.M. Dunn, and D.H. Jenkinson. (1998). Bis–quinolinium cyclophanes: 6,10–diaza– 3(1,3),8(1,4)–dibenzena– 1,5(1,4)–diquinolinacyclodecaphane (UCL 1684), the first nanomolar, non–peptidic blocker of the apamin–sensitive Ca^{2+}–activated K^+ channel. *Journal of Medicinal Chemistry* **41(1):**2–5.

Rosolowsky, M., J.R. Falck, J.T. Willerson, and W.B. Campbell. (1990). Synthesis of lipoxygenase and epoxygenase products of arachidonic acid by normal and stenosed canine coronary arteries. *Circulation Research* **66:**608–621.

Roy–Contancin, L., M.L. Garcia, A. Galvez, G.J. Kaczorowski, G.M. Katz, D. Williams, and J.P. Reuben. (1990). Ca^{2+}–activated K^+ channels in bovine aortic smooth muscle and GH3 cells: properties and regulation by guanine nucleotides. *Progress in Clinical and Biological Research* **334:**145–170.

Rusch, N.J., Y. Liu, and K.A. Pleyte. (1996). Mechanism for regulation of arterial tone by Ca^{2+}–dependent K^+ channels in hypertension. *Clinical and Experimental Pharmacology and Physiology* **23:**1077–1082.

Ruth, P., M. Rohrkasten, M. Biel, E. Bosse, S. Regulla, H.E. Meyer, V. Flockerzi, and F. Hofmann. (1989). Primary structure of the β subunit of the dihydropyridine sensitive calcium channel from skeletal muscle. *Science* **245:**1115–1117.

Sadoshima, J–I., N. Akaike, H. Tomoike, H. Kanaide, and M. Nakamura. (1988). Ca–activated K channel in cultured smooth muscle cells of rat aortic media. *American Journal of Physiology* **255 (24):**H410–H418.

Sah, P. (1996). Ca^{2+}–activated K^{+} currents in neurones: types, physiological roles and modulation. *Trends in Neurosciences* **19(4):**150–154.

Saito, S., Y. Hirata, T. Emori, T. Imai, and F. Marumo. (1996). Angiotensin II activates endothelial constitutive nitric oxide synthase via AT1 receptors. *Hypertension Research* **19(3):**201–206.

Sakura, H., C. Ammala, P.A. Smith, F.M. Gribble, and F.M. Ashcroft. (1995). Cloning and functional expression of the cDNA encoding a novel ATP–sensitive potassium channel subunit expressed in pancreatic beta–cells, brain, heart and skeletal muscle. *FEBS Letters* **377(3):**338–344.

Sakuta, H, and I. Yoneda. (1994). Inhibition by SKF 525A and quinacrine of endogenous glibenclamide–sensitive K^+ channels in follicle–enclosed Xenopus oocytes. *European Journal of Pharmacology* **252:**117-121.

Salkoff, L., K. Butler, A. Butler, M. Covarrubias, M.D. Pak, and A. Wei. (1992). An essential 'set' of K^+ channels conserved in flies, mice and humans. *Trends in Neurosciences* **15(5):**161–168.

Schubert, R., V.N. Serebryakov, H. Mewes, and H.H. Hopp. (1997). Iloprost dilates rat small arteries: role of K_{ATP}– and K_{Ca}–channel activation by cAMP–dependent protein kinase. *American Journal of Pharmacology* **272:**H1147–H1156.

Schwartzman, M.L. (1990). Modification of arachidonic acid metabolism via the cytochrome P–450–related monooxygenase system. *Advances in Prostaglandin, Thromboxane, and Leukotriene Research* **20**:241–249.

Scornik, F.S., J. Codina, L. Birnbaumer, and L. Toro. (1993). Modulation of coronary smooth muscle K_{Ca} channels by $G_S\alpha$ independent of phosphorylation by protein kinase A. *American Journal of Physiology* **265:**H1460–H1465.

Shimokawa, H., H. Yasutake, K. Fujii, M.K. Owada, R. Nakaike, Y. Fukumoto, T. Takayanagi, T. Nagao, K. Egashira, M. Fujishima, and A. Takeshita. (1996). The

importance of the hyperpolarizing mechanism increases as the vessel size decreases in endothelium–dependent relaxations in rat mesenteric circulation. *Journal of Cardiovascular Pharmacology* **28(5):**703–711.

Shyng, S., and C.G. Nichols. (1997). Octameric stoichiometry of the K_{ATP} channel complex. *Journal of General Physiology* **110(6):**655–664.

Silberberg, S.D., and C. van Breemen. (1992). A potassium current activated by lemakalim and metabolic inhibition in rabbit mesenteric artery. *Pflügers Archives* **420:**118–120.

Silverman, S.K., H.A. Lester, and D.A. Dougherty. (1996). Subunit stoichiometry of a heteromultimeric G protein–coupled inward–rectifier K^+ channel. *Journal of Biological Chemistry* **271(48):**30524–30528.

Sims, S.M., M.B. Vivaudou, C. Hillemeier, P. Biancani, J.V. Walsh Jr., J.J. Singer. (1990). Membrane currents and cholinergic regulation of K^+ current in esophageal smooth muscle cells. *American Journal of Physiology* **258:**G794–G802.

Siney, L., and M.J. Lewis. (1992). Endothelium–derived relaxing factor inhibits platelet adhesion to cultured porcine endocardial endothelium. *European Journal of Pharmacology* **229(2–3):**223–226.

Singer, D., M. Biel, I. Lotan, V. Flockerzi, F. Hofmann, and N. Dascal. (1991). The role of the subunits in the function of the calcium channel. *Science* **253:**1553–1557.

Singer, H., J. Saye, and J. Peach. (1984). Effects of cytochrome P–450 inhibitors on endothelium–dependent relaxation in rabbit aorta. *Blood Vessels* **21:**223–230.

Singer, J.J., and J.V. Walsh, Jr. (1986). Large–conductance Ca^{2+}–activated K^+ channels in freshly dissociated smooth muscle cells. *Membrane Biochemistry* **6(2):**83–110.

Small, D., B. Bolzon, and D.W. Cheung. (1992). Endothelium–independent potentiating effects of neuropeptide Y in the rat tail artery. *European Journal of Pharmacology* **210:**131–136.

Smirnov, S.V., and P.I. Aaronson. (1992). Ca^{2+}–activated and voltage–gated K^+ currents in smooth muscle cells isolated from human mesenteric arteries. *Journal of Physiology* **457:**431–454.

Sokol, P.T., W. Hu, L. Yi, J. Toral, M. Chandra, M.R. Ziai. (1994). Cloning of an apamin binding protein of vascular smooth muscle. *Journal of Protein Chemistry* **13(1):**117–128.

Spedding, M., and R. Paoletti. (1992). Classification of calcium channels and calcium antagonists: progress report. *Cardiovascular Drugs and Therapy* **6:**35–39.

Standen, N.B., J.M. Quayle, N.W. Davies, J.E. Brayden, Y. Huang, and M.T. Nelson. (1989). Hyperpolarizing vasodilators activate ATP–sensitive K^+ channels in arterial smooth muscle. *Science* **245:**177–180.

Stoffel, M., Y. Tokuyama, J.B. Trabb, M.S. German, M.L. Tsaar, L.Y. Jan, K.S. Polonsky, and G.I. Bell. (1995). Cloning of rat KATP–2 channel and decreased expression in pancreatic islets of male Zucker diabetic fatty rats. *Biochemical and Biophysical Research Communications* **212(3):**894–899.

Stuenkel, E.L. (1989). Single potassium channels recorded from vascular smooth muscle cells. *American Journal of Physiology* **257(26):**H760–H769.

Sturek, M., and K.Hermsmeyer. (1986). Calcium and sodium channels in spontaneously contracting vascular smooth muscle. *Science* **233:**475–478.

Sumimoto, K., and H. Kuriyama. (1986). Mobilization of free Ca^{2+} measured during contraction–relaxation cycles in smooth muscle cells of the porcine coronary artery using quin2. *Pflügers Archives* **406:**173–180.

Tang, W., and X.C. Yang. (1994). Cloning a novel human brain inward rectifier potassium channel and its functional expression in *Xenopus* oocytes. *FEBS Letters* **348(3):**239–243.

Taniguchi, K., K.–I. Furukawa, and M. Shigekawa. (1993). Maxi K^+ channels are stimulated by cyclic guanosine monophosphate–dependent protein kinase in canine coronary artery smooth muscle. *Pflügers Archives* **463:**167–172.

Tare, M., H.C. Parkington, and H.A. Coleman. (2000). EDHF, NO and a prostanoid: hyperpolarization–dependent and –independent relaxation in guinea–pig arteries. *British Journal of Pharmacology* **130(3):**605–618.

Taylor, H.J., A.T. Chaytor, W.H. Evans, and T.M. Griffith. (1998). Inhibition of the gap junctional component of endothelium–dependent relaxations in rabbit iliac artery by 18–alpha glycyrrhetinic acid. *British Journal of Pharmacology* **125(1):**1–3.

Taylor, S.G., and A.H. Weston. (1988). Endothelium–derived hyperpolarizing factor: a new endogenous inhibitor from the vascular endothelium. *Trends in Pharmacological Sciences* **9:**272–274.

Toro, L., and E. Stefani. (1987). Ca^{2+} and K^+ currents in cultured vascular smooth muscle. *Pflügers Archives* **408:**417–419.

Triggle, C.R., H. Dong, G.J. Waldron, and W.C. Cole. (1999). Endothelium–derived hyperpolarizing factor(s): species and tissue heterogeneity. *Clinical and Experimental Pharmacology and Physiology* **26(2):**176–179.

Tuana, B.S., and B.J. Murphy. (1990). Biochemical analysis of L–type calcium channels from skeletal and cardiac muscle. *Canadian Journal of Physiology and Pharmacology* **68:**1482–1488.

Urakami–Harasawa, L., H. Shimokawa, M. Nakashima, K. Egashira, and A. Takeshita. (1997). Importance of endothelium–derived hyperpolarizing factor in human arteries. *Journal of Clinical Investigation* **100:**2793–2799.

Vane, J.R., S. Bunting, and S. Moncada. (1982). Prostacyclin in physiology and pathophysiology. *International Review of Experimental Pathology* **23:**161–207.

Vane, J.R., J.A. Mitchell, I. Appleton, A. Tomlinson, D. Bishop–Bailey, J. Croxtall, and D.A. Willoughby. (1994). Inducible isoforms of cyclooxygenase and nitric–oxide synthase in inflammation. *Proceedings of the National Academy of Sciences* **91(6):**2046–2050.

Van Helden, D.F. (1988). An α–adrenoceptor–mediated chloride conductance in mesenteric veins of the guinea–pig. *Journal of Physiology* **401:**489–501.

Vanhoutte, P.M. (1997). Endothelium dysfunction and atherosclerosis. *European Heart Journal.* **18:**E19–E29.

Vanhoutte, P.M., and J.–V. Mombouli. (1996). Vascular endothelium: vasoactive mediators. *Progress in Cardiovascular Diseases* **39(3):**229–238.

Varadi, G., P. Lory, D. Schultz, M. Varadi, and A. Schwartz. (1991). Acceleration of activation by the β subunit of the skeletal muscle calcium channel. *Nature* **352:**159–162.

Vazquez, J., P. Feigenbaum, V.F. King, G.J. Kaczorowski, and M.L. Garcia. (1990). Characterization of high affinity binding sites for charybdotoxin in synaptic plasma membranes from brain. *Journal of Biological Chemistry* **265:**15564–15571.

Velimirovic, B.M., E.A. Gordon, N.F. Lim, B. Navarro, and D.E. Clapham. (1996). The K^+ channel inward rectifier subunits form a channel similar to neuronal G protein–gated K^+ channel. *FEBS Letters* **379(1):**31–37.

Vergara, C., and R. Latorre. (1983). Kinetics of Ca^{2+}–activated K^+ channels from rabbit muscle incorporated into planar bilayers. Evidence for a Ca^{2+} and Ba^{2+} blockade. *Journal of General Physiology* **82(4):**543–568.

Vergara, C., R. Latorre, N.V. Marrion, and J.P. Adelman. (1998). Calcium–activated potassium channels. *Current Opinion in Neurobiology* **8(3):**321–329.

Vodovotz, Y., C. Bogdan, J. Paik, Q.W. Xie, and C. Nathan. (1993). Mechanisms of suppression of macrophage nitric oxide release by transforming growth factor beta. *Journal of Experimental Medicine* **178(2):**605–613.

Vogalis F., Y. Zhang, and R.K. Goyal. (1998). An intermediate conductance K^+ channel in the cell membrane of mouse intestinal smooth muscle. *Biochimica et Biophysica Acta* **1371(2):**309–316.

Volk, K., J.J. Matsuda, and E.F. Shibata. (1991). A voltage–dependent potassium current in rabbit coronary artery smooth muscle cells. *Journal of Physiology* **439:**751–768.

Volk, K., and E.F. Shibata. (1993). Single delayed rectifier potassium channels from rabbit coronary artery myocytes. *American Journal of Physiology* **264 (33):**H1146–H1153.

Wade, G.R., and S.M. Sims. (1993). Muscarinic stimulation of tracheal smooth muscle cells activates large–conductance Ca^{2+}–dependent K^+–channnel. *American Journal of Physiology* **265(34):**C658–C665.

Waldron, G.J., and W.C. Cole. (1999). Activation of vascular smooth muscle K^+ channels by endothelium–derived relaxing factors. *Clinical and Experimental Pharmacology and Physiology* **26(2):**180–184.

Waldron, G.J., H. Ding, F. Lovren, P. Kubes, and C.R. Triggle. (1999). Acetylcholine–induced relaxation of peripheral arteries isolated from mice lacking endothelial nitric oxide synthase. *British Journal of Pharmacology* **128(3):**653–658.

Waldron, G.J., and C.J. Garland. (1994). Contribution of both nitric oxide and a change in membrane potential to acetylcholine–induced relaxation in the rat small mesenteric artery. *British Journal of Pharmacology* **112:**831–836.

Walsh, J.V., and J.J. Singer. (1981). Voltage clamp of single freshly dissociated smooth muscle cells: current–voltage relationships for three currents. *Pflügers Archives* **390:**207–210.

Wang, Q., and W.A. Large. (1991). Modulation of noradrenaline–induced membrane currents by papaverine in rabbit vascular smooth muscle cells. *Journal of Physiology* **439:**501–512.

Wang, G–Y., D.W. Robinson, and L.M. Chalupa. (1998). Calcium–activated potassium conductances in retinal ganglion cells of the ferret. *Journal of Neurophysiology* **79:**151–158.

Wei, A., M. Covarrubias, A. Butler, K. Baker, M. Pak, and L. Salkoff. (1990). K^+ current diversity is produced by an extended gene family conserved in *Drosophila* and mouse. *Science* **248(4955):**599–603.

Wei, A., C. Solaro, C. Lingle, and L. Salkoff. (1994). Calcium sensitivity of BK–type K_{Ca} channels determined by a separable domain. *Neuron* **13:**671–681.

Wei, X., E. Perez–Reyes, A.E. Lacerda, G. Shuster, A.M. Brown, and L. Birnbaumer. (1991). Heterologous regulation of the cardiac Ca^{2+} channel alpha 1 subunit by skeletal muscle beta and gamma subunits. Implications for the structure of cardiac L–type Ca^{2+}–channels. *Journal of Biological Chemistry* **266:**21943–21947.

White, R. and C.R. Hiley. (1997). A comparison of EDHF–mediated and anandamide–induced relaxations in the rat isolated mesenteric artery. *British Journal of Pharmacology* **122:**1573–1584.

Wilde, D.W., and K.S. Lee. (1989). Outward potassium currents in freshly isolated smooth muscle cells of dog coronary artery. *Circulation Research* **65:**1718–1734.

Wong, B.S., H. Lecar, and M. Adler. (1982). Single calcium dependent potassium channels in clonal anterior pituitary cells. *Biophysical Journal* **39:**313–317.

Wu, Y., L.M. Jiji, D.E. Lemons, and S. Weinbaum. (1995). A non–uniform three–dimensional perfusion model of rat tail heat transfer. *Phys. Med. Biol.* **40(5):**789–806.

Xiong, Z., B. Bolzon, and D.W. Cheung. (1993). Neuropeptide Y potentiates calcium–channel currents in single vascular smooth muscle cells. *Pflügers Archives* **423:**504–510.

Xiong, Z., E. Burnette, and D.W. Cheung. (1995). Modulation of Ca^{2+}–activated K^+ channel activity by tyrosine kinase inhibitors in vascular smooth muscle cell. *European Journal of Pharmacology* **290:**117–123.

Xu, X., and K.S. Lee. (1994). Characterization of the ATP–inhibited K^+ current in canine coronary smooth muscle cells. *Pflügers Archives* **427:**110–120.

Yamakawa, N., M. Ohhashi, S. Waga, and T. Itoh. (1997). Role of endothelium in regulation of smooth muscle membrane potential and tone in the rabbit middle cerebral artery. *British Journal of Pharmacology* **121:**1315–1322.

Yamanaka, A., T. Ishikawa, and K. Goto. (1998). Characterization of endothelium–dependent relaxation independent of NO and prostaglandins in guinea pig coronary artery. *Journal of Pharmacology and Experimental Therapeutics* **285:**480–489.

Yamashita, Y., H. Ogawa, and N. Akaike. (1996). ATP–induced rise in apamin–sensitive Ca^{2+}–dependent K^+ conductance in adult rat hepatocytes. *American Journal of Physiology* **270(33):**G307–G313.

Yatani, A., C.L. Seidel, J. Allen, and A.M. Brown. (1987). Whole–cell and single channel currents of isolated smooth muscle cells from saphenous vein. *Circulation Research* **60:**523–533.

Yoshida, Y., and Y. Aoyama. (1987). Interaction of azole antifungal agents with cytochrome P–450 14DM purified from saccharomyces cerevisiae microsomes. *Biochemical Pharmacology* **36:**229–235.

Yuan, X., M. Tod, L. Rubin, and M. Blaustein. (1995). Inhibition of cytochrome P–450 reduces voltage–gated K^+ currents in pulmonary arterial myocytes. *American Journal of Physiology* **268:**C259–270.

Yue, L., J. Feng, G.R. Li, and S. Nattel. (1996). Characterization of an ultrarapid delayed rectifier potassium channel involved in canine atrial repolarization. *Journal of Physiology* **496(3):**647–662.

Zhang, H.L., and T.B. Bolton. (1996). Two types of ATP–sensitive potassium channels in rat portal vein smooth cells. *British Journal of Pharmacology* **118(1):**105–114.

Zhang, L., A. Bonev, M.T. Nelson, and G. Mawe. (1994). Activation of ATP–sensitive K^+ channels in guinea pig gallbladder smooth muscle by lemakalim and the neuropeptide, CGRP. *Journal of Physiology* **478:**483–491.

Zou, A.P., J.D. Imig, M. Kaldunski, P.R. Oritz de Montellano, Z. Sui, and R.J. Roman. (1994). Inhibition of renal vascular 20–HETE production impairs autoregulation of renal blood flow. *American Journal of Physiology* **266:**F275–F282.

Zygmunt, P.M., G. Edwards, A.H. Weston, S.C. Davis, and E.D. Högestätt. (1996). Effects of cytochrome P450 inhibitors on EDHF–mediated relaxation in the rat hepatic artery. *British Journal of Pharmacology* **118:**1147–1152.

Zygmunt, P.M., G. Edwards, A.H. Weston, B. Larsson, and E.D. Högestätt. (1997). Involvement of voltage–dependent potassium channels in the EDHF–mediated relaxation of rat hepatic artery. *British Journal of Pharmacology* **121:**141–149.

Zygmunt, P.M., and E.D. Högestätt. (1996). Role of potassium channels in endothelium–dependent relaxation resistant to nitroarginine in the rat hepatic artery. *British Journal of Pharmacology* **117:**1600–1606.

Zygmunt, P.M., F. Plane, M. Paulsson, C.J. Garland, and E.D. Högestätt. (1998). Interactions between endothelium–derived relaxing factors in the rat hepatic artery: focus on regulation of EDHF. *British Journal of Pharmacology* **124:**992–1000.

Zygmunt, P.M., T. Ryman, and E.D. Högestätt. (1995). Regional differences in endothelium–dependent relaxation in the rat: contribution of nitric oxide and nitric oxide–independent mechanisms. *Acta Physiol. Scand.* **155(3):**257–266.